ABSTRACT

RANDOM SEARCH CONFORMATIONAL ANALYSIS OF PIPERAZINE AND PIPERADINE ANALOGS OF GBR12909: IMPLICIT AQUEOUS SOLVATION EFFECTS

by
William A. Roosma

The object of this work was to study the effect of solvent on the conformational potential energy surface (PES) of GBR12909 analogs. Local minima on the PES's were found by the Random Search algorithm using the Sybyl molecular modeling package from Tripos, Inc., and an implicit solvent model. Two force-field/charge models were employed in the analysis: the Tripos force field with Gasteiger-Hückel charges and the MMFF94 force field with MMFF94 charges.

The effect of solvent on the location of minima in multi-dimensional torsional angle space was studied by comparison to the vacuum phase results. Minima were plotted in torsional angle space using successive pairs of torsional angles. The results showed that, at least for the simple implicit solvent model used here, solvation does not significantly affect the location of the conformational minima for either of the two analogs investigated. With the MMFF94 model, some of the conformational energy minima were found in a narrower range of torsional angle space in the solvent compared to the vacuum phase, while there were no consistent differences with the Tripos model. One notable exception was the Tripos solvent phase results for the piperadine analog where a cluster of minima was found in a region of torsional angle space where no minima were present in the original vacuum phase results. This is believed to be an anomaly arising from incomplete searching of the conformational PES of the molecule. This was supported by the results of a second vacuum phase random

search, which were similar to those of the solvation case. Further study remains to be performed employing other more sophisticated solvation models and conformational search techniques.

RANDOM SEARCH CONFORMATIONAL ANALYSIS OF PIPERAZINE AND PIPERADINE ANALOGS OF GBR12909: IMPLICIT AQUEOUS SOLVATION EFFECTS

by
William A. Roosma

A Thesis
Submitted to the Faculty of
New Jersey Institute of Technology
in Partial Fulfillment of the Requirements for the Degree of
Master of Science in Computational Biology

Department of Computer Science

May 2004

APPROVAL PAGE

RANDOM SEARCH CONFORMATIONAL ANALYSIS OF PIPERAZINE AND PIPERADINE ANALOGS OF GBR12909: IMPLICIT AQUEOUS SOLVATION EFFECTS

William A. Roosma

Dr. Carol Venanzi, Thesis Advisor — Date
Distinguished Professor of Chemistry, NJIT

Dr. Qun Ma, Committee Member — Date
Assistant Professor of Computer Science, NJIT

Dr. Tamara Gund, Committee Member — Date
Professor of Chemistry, NJIT

BIOGRAPHICAL SKETCH

Author: William Andrew Roosma

Degree: Master of Science

Date: May 2004

Undergraduate and Graduate Education:

- Master of Science in Computational Biology,
  New Jersey Institute of Technology, Newark, NJ, 2004

- Bachelor of Science in Electrical Engineering,
  Stevens Institute of Technology, Hoboken, NJ, 1982

Major: Computational Biology

To my parents

ACKNOWLEDGMENT

I would like to express my appreciation to Dr. Carol Venanzi, who not only served as my research supervisor, providing valuable advice, resources, and insight, but also gave me support, encouragement, guidance, and numerous opportunities to meet leaders in the field. Dr. Venanzi was the primary person to suggest the writing of this thesis. Special thanks are also due Dr. Tamara Gund and Dr. Qun Ma for reading and advising on this thesis.

My fellow graduate students in the Dr. Venanzi's Computational Chemistry Laboratory, especially Deepangi Pandit and Milind Misra, and including Kathleen Gilbert and Deepa Pai, are deserving of recognition for their support.

Additionally, I would like to thank Andy Malato, David Perel, and Gedaliah Wolosch of Engineering Computing for their hardware and network support.

TABLE OF CONTENTS

TABLE OF CONTENTS
(Continued)

Chapter **Page**

TABLE OF CONTENTS
(Continued)

LIST OF TABLES

LIST OF FIGURES

LIST OF FIGURES
(Continued)

LIST OF FIGURES
(Continued)

LIST OF FIGURES
(Continued)

LIST OF FIGURES
(Continued)

LIST OF FIGURES
(Continued)

LIST OF FIGURES
(Continued)

LIST OF FIGURES
(Continued)

CHAPTER 1

INTRODUCTION

1.1 Objective

The objective of this thesis is to present the implications of water solvation on molecular conformations of two analogs of GBR12909 (designated DM324 and TP250), employing the implicit solvation model of the Sybyl molecular modeling program supplied by Tripos, Inc.

This was accomplished by comparison of scatter plots for the aqueous solvation case versus the vacuum phase case over multiple pairings of rotatable bond torsion angles for the lowest-energy conformers of DM324 and TP250, as found by the Random Search function of Sybyl. Two force field models included in Sybyl were used: Tripos with Gasteiger-Hückel charges and MMFF94 with MMFF94 charges.

1.2 Background Information

1.2.1 Problems Related to Cocaine Abuse

The allure of cocaine is the nearly instant (when smoked in the "crack" form) onset of the desired stimulant effect of euphoria. In the short term, heart rate, blood pressure and temperature increase while the vascular system contracts. Large doses can cause volatile, possibly violent, conduct as well as paranoia, involuntary muscle movements, anxiety and/or agitation. Rarely, death due to cardiac and respiratory arrest can occur[1].

Long-term use can increase the prevalence of the symptoms noted. Additionally, tolerance may develop, requiring larger doses for the same effect, and sensitivity to

anesthetic and spasmodic effects may increase, becoming a hazard even at small doses. Cocaine may disturb heart rhythms, and cause medical problems depending on the route of ingestion. Often, due to the suppression of appetite, malnourishment can result[1].

Sensitization to the stimulant effects of cocaine and associated stimuli may also occur. In this scenario, the dopaminergic system adapts and helps generate the addictive behavior in spite of lowered expectations of enjoyment, as well as threats to economic and social well-being[2].

The effects do not end with the abuser; cocaine addiction continues to be a serious problem for the nation. A major part of the problem is a strong tendency towards continued use and abuse[2,3]. There are serious implications for society as well as the individuals involved in usage – crime, financial losses, reduced productivity, and contribution to the spread of HIV/AIDS[3,4]. One estimate of the cost to the nation is above $100 billion for 1995 alone[4].

1.2.2 Dopamine Hypothesis

The dopamine hypothesis, which has significant support in the research literature[5-8], is that cocaine acts indirectly by binding to the dopamine transporter (DAT) of neurons, reducing reuptake of extracellular dopamine by the DATs. The resulting excess of dopamine causes the pleasurable sensation that is the object of substance use, and produces the reinforcement of the usage[2,3]. The structures can be seen below.

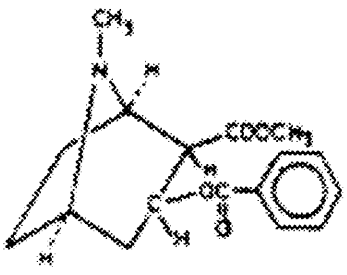

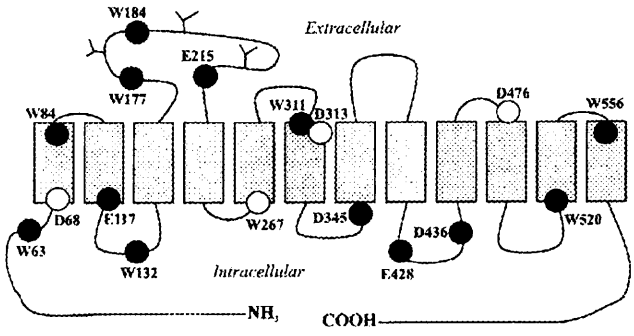

Figure 1.1 Cocaine structure. **Figure 1.2** Drawing of DAT[9].

1.2.3 Candidate Substances for Treating Cocaine Addiction

No effective medication, analogous to methadone in the case of heroin, currently exists for treatment of cocaine addiction. Desired characteristics for such a substitute are: slow entry into the brain, long duration of its effects (relating to its binding affinity), selectivity for its target and minimal side effects[10]. A likely possibility is a compound that blocks cocaine from binding to the DAT, permitting dopamine (re)uptake. A number of dopamine reuptake inhibitors have been proposed as possible drug candidates to ameliorate the addiction; several representative structures can be viewed below:

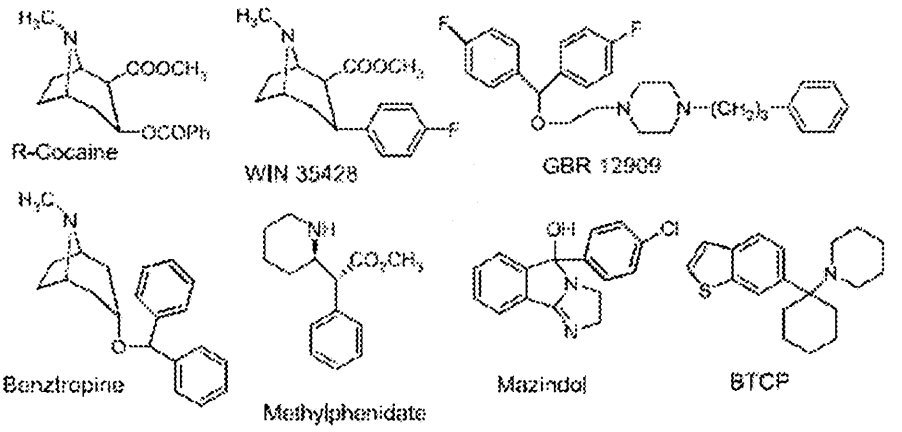

Figure 1.3 Examples of dopamine reuptake inhibitors[3]. Note that several do not resemble cocaine.

The first two are derived from tropane, the third from the GBR class, the last (BTCP) is a phencyclidine analog, and the others are from classes as labeled[3]. Another, much different, possibility is an anti-cocaine antibody. Such a molecule binds to cocaine and then breaks it down[2].

1.2.4 GBR 12909 and the Analogs Investigated

The dopamine reuptake inhibitor GBR 12909 is one of the most promising compounds for treatment of cocaine addiction, as it has successfully passed the first phase of clinical trials. GBR 12909 showed some affinity for the human DAT *in vivo*, and was found to be safe and tolerable in those trials[11]. Several surveys indicate desirable characteristics of GBR 12909: high affinity for the DAT and selectivity for DAT over the serotonin transporter (SERT) [12] and lowered cocaine self-dosage in monkeys along with little suppression of food-seeking behavior[13].

In its structure, shown below, the "A side" (with respect to the central piperazine ring) contains the single phenyl ring, while the "B side" is the bisphenyl side:

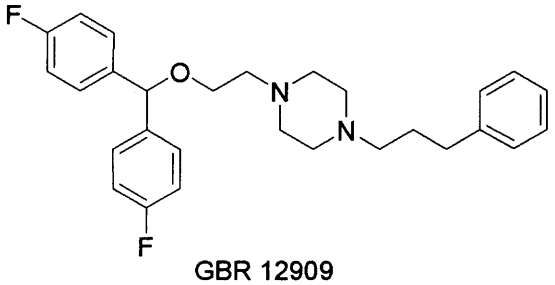

GBR 12909

Figure 1.4 GBR 12909 structure. Note the dissimilarity to cocaine. The "A Side" is on the right; the "B side" is on the left.

In concert with medicinal chemists and pharmacologists at the National Institutes of Health (NIH), the Venanzi group is investigating the behavior of analogs of GBR12909 with hypothesized pharmacophore elements similar to those of methylphenidate, previously studied by the group. Two of the most important characteristics, binding and selectivity, are outlined in the table below.

Table 1.1 Binding Affinities of GBR 12909 and Analogs at DAT and SERT Labeled with [125I]RTI-55

Analog	DAT[a]	SERT[a]	SERT/DAT[b]
GBR12909[12]	3.7 (±0.4)	126 (±5)	34
DM324[12]	8.0 (±0.3)	312 (±15)	39
TP250[14]	0.71 (±0.6)	229 (±21)	323

[a]IC_{50} in nanomolar concentration (nM), standard deviation in parentheses.
[b]SERT/DAT = ratio of DAT binding affinity to SERT binding affinity.

While these aspects alone do not determine efficacy, they may indicate the utility of these analogs in understanding GBR12909 behavior.

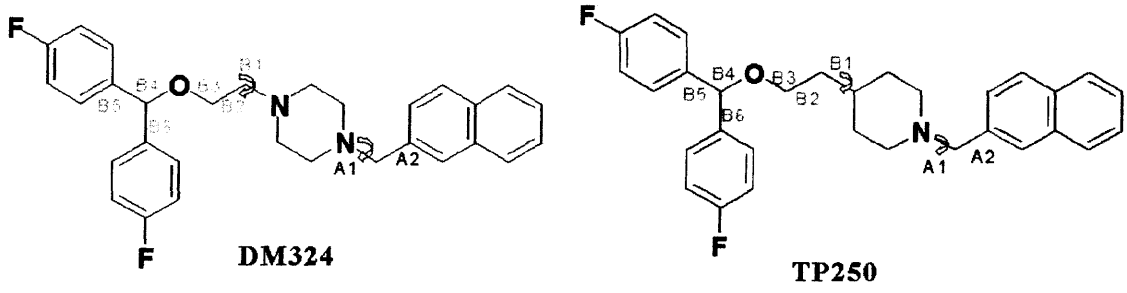

Figure 1.5 Analogs of GBR12909 investigated in this study. Note that for both analogs, the chain on the naphthalene "A" side is shorter than that for GBR12909. The analogs differ only by a nitrogen substitution for the central ring carbon closest to the bisphenyl side of the molecule. The rotatable bonds are labeled in blue on the A side and red on the B side.

The analogs exhibit greater rigidity due to reduction in the number of rotatable bonds as compared to GBR12909, facilitating the modeling process. The TP250 analog includes a central piperadine ring that incorporates the nitrogen which Dutta et al[15] have shown is required for binding. The DM324 analog differs from TP250 only by having a central piperazine ring in place of piperadine.

1.2.5 Long-Range Goal

As was carried out previously for the vacuum phase, Comparative Molecular Field Analysis (CoMFA) will be performed using representative conformations from the results of random searches done for the solvation phase. Several clustering and multivariate analysis methods are to be employed for the selection of conformations prospectively representative of the bioactive conformation (i.e., the one in which the drug binds to the

DAT). The bioactive conformation describes the pharmacophore, which is the set of spatial orientations of the important chemical features that are required for biological activity[16]. The ultimate goal is to aid in interpreting biological activity in terms of molecular structure and properties such as binding affinity and selectivity, with implications for more efficient drug design.

1.2.6 Focus of Current Study in Context

This study is part of an ongoing investigation by a group led by Dr. Carol Venanzi at NJIT, in pursuit of medications for effective treatment of cocaine. The group employs computational chemistry techniques to model drug characteristics. In particular, strong binding to the DAT (dopamine transporter) and selectivity for the DAT over the SERT (serotonin transporter) are the major characteristics desired[10].

While a solvent has important effects on the potential energy and conformation of a molecule, it is often disregarded for the sake of expediency. If the solute contains polar functional groups, a polar solvent can significantly affect conformational energy. Since most experiments are carried out in solvents (most often water, a polar solvent), and the case in vivo is an aqueous environment, it is desirable to investigate such effects on a drug candidate. The current pilot study employs the implicit solvation capability (i.e., resetting the dielectric constant) of the Sybyl modeling program as a simplified preliminary method of observing the effects of aqueous solvation on the potential representative conformations of the GBR12909 analogs.

CHAPTER 2

THEORETICAL BASIS OF SOLVENT MODELING AND RANDOM CONFORMATIONAL SEARCHING

2.1 Modeling the Effects of Solvents

Solvation tends to reduce electrostatic interactions as compared to the vacuum phase. This can be modeled in several ways. One is to change the permittivity ε (ε_0 is the permittivity of a vacuum) in the equation for Coulomb's Law:

$$F = \frac{kq_1q_2}{r^2} = \frac{q_1q_2}{4\pi\varepsilon_0 r^2}$$

The related equation for potential energy (PE) is:

$$PE = \frac{kq_1q_2}{r} = \frac{q_1q_2}{4\pi\varepsilon_0 r} \qquad \textbf{(2.1)}$$

The charges are referred to as q_1 and q_2, while r is the distance separating them, and k is a proportionality constant. The solvent permittivity $\varepsilon = \varepsilon_0 D$, where D is a constant dielectric value (usually designated "dielectric constant", changed here to avoid confusion) of the solvent, can be substituted for ε_0. This is the simplest solvent-modeling method[17-19].

Another method is to use a distance-dependent dielectric value, in which the relative permittivity value (εr in this case) is proportional to the distance between the charges. Substituting for ε_0, the following distance-dependent expression for potential energy is obtained:

$$PE = \frac{q_1 q_2}{4\pi\varepsilon r^2} \qquad (2.2)$$

This method has no physical basis, but can provide approximate information[17]. More sophisticated models use a more complex non-linear distance dependency, such as a sigmoid curve rising towards a bulk solvent value at larger distances[20]. Some add a term to the total potential energy (PE) equation to account for solvent effects. The most precise models include solvent molecules explicitly in the computation of the PE equation terms. However, the cost of the added complexity is a greater computational cost[21].

2.2 General Modeling of Potential Energy in Solvent Phase

The potential energy for a molecule is the summation of the various components, including electrostatic effects. Since energy information is empirically obtained, there exist several formulas for modeling its value. One relatively simple possible equation (from Leach[22]) is shown below:

$$PE(r^N) = \sum_{bonds}(k_i/2)*(l_i - l_{i,0})^2 + \sum_{angles}(k_i/2)*(\theta_i - \theta_{i,0})^2 + \sum_{torsions}(V_n/2)*(1+\cos(n\omega - \gamma)) + \sum_{i=1}^{N}\sum_{j=i+1}^{N} 4\varepsilon_{ij}\left[(\sigma_{ij}/r_{ij})^{12} - (\sigma_{ij}/r_{ij})^{6}\right] + \sum_{i=1}^{N}\sum_{j=i+1}^{N}(q_i q_j / 4\pi\varepsilon_0 r_{ij})$$

The first three terms refer to energy associated with stretching, bending and torsions of bonds, respectively. The last two terms refer to energies not associated with bonding interactions, which are summed over all atom pairs that either are separated by at least three bonds or are in different molecules. The fourth term accounts for van der Waals interactions using a Lennard-Jones model. The final term comprises the electrostatic energy effects[22].

The potential energy for the solvation case can be modeled in a simple fashion by adjusting the electrostatic term as noted above. Note that the ε_{ij} term in the van der Waals term refers to the depth of an energy well[23], not permittivity.

2.3 Force Fields (Molecular Mechanics) and Charges

Force field models are empirically derived. There is a tradeoff between computational efficiency and accuracy. An important consideration is "transferablility", or "generalizability", at least between similar molecules, to avoid re-inventing the wheel for each molecule studied[24].

In the current study, the grouped bonding terms are considered approximately equivalent from one force field to the other (generally, terms cannot be compared on a one-to-one basis). The main consideration is given to the non-bonding terms accounting for van der Waals and electrostatic interactions. Only atoms separated by at least three bonds are included in the non-bonding terms.

2.3.1 Tripos Force Field

The potential energy for the Tripos force field is represented using the following general equation[25]:

$$PE = \sum E_{str} + \sum E_{bend} + \sum E_{oop} + \sum E_{tors} + \sum E_{vdw} + \left[\sum E_{ele} + \sum E_{dist\_c} + \sum E_{ang\_c} + \sum E_{tors\_c} + \sum E_{range\_c} + \sum E_{multi} + \sum E_{fieldfit} \right]$$

The first four terms refer to energies due to bond stretching, bending, out-of-plane bending of atoms, and torsion. The fifth accounts for van der Waals interactions:

$$\sum E_{vdw} = \sum_{i=1}^{N_{atoms}} \sum_{j>1} E_{ij} \left[1.0 \left(\frac{R_i + R_j}{r_{ij}} \right)^{12} - 2.0 \left(\frac{R_i + R_j}{r_{ij}} \right)^{6} \right]$$

E_{ij} is the van der Waals constant in kcal/mol, equaling $\sqrt{E_i E_j}$, R_i is the van der Waals radius (in Å) of the i^{th} atom, and r_{ij} is the distance between atoms i and j[25].

The remaining terms are optional. The sixth term involves electrostatic interactions, while the others deal with energies due to constraints (distance, angle, torsion, and range), multifit and field fit. The torsion constraint term is employed only in the initial minimizations. The only one included in this study is the electrostatic term, shown below:

$$\sum E_{ele} = 332.17 \sum_{i=1}^{N_{atoms}} \sum_{j>i} \frac{Q_i Q_j}{D_{ij} r_{ij}}$$

D_{ij} is the value of dielectric function for atoms i and j, Q_i is the resultant atomic charge at the i^{th} atom, and r_{ij} is the distance between atoms i and j. 332.17 is a conversion factor for the units[25].

Several charge computation methods are available when using the Tripos force field. The Gasteiger-Hückel method uses the Gasteiger-Marsili method for calculations of the σ component and the Hückel method for the π component, and then sums them to obtain the total charge. The Hückel method, a basic quantum mechanical approach, is performed first; the Gasteiger-Marsili computation is partially based on the Hückel results. In the Gasteiger-Marsili process, charges from all bonds including an atom are iteratively computed, beginning with the formal charge, and the charges are summed over all the atoms[26].

2.3.2 MMFF94 Force Field

The general equation describing the potential energy for the MMFF94 force field[27] is given as:

$$E_{MMFF} = \sum_{bonds} EB_{ij} + \sum_{angles} EA_{ijk} + \sum_{bend-str} EBA_{ijk} + \sum_{out-of-pln} EOOP_{ijk;l} \sum_{torsions} ET_{ijkl} + \sum EvdW_{ij} + \sum EQ_{ij}$$

The first five terms refer to energies due to bond stretching, bending, bending-stretching interactions, out-of-plane bending of atoms, and torsion. The sixth accounts for van der Waals interactions:

$$\sum EvdW_{ij} = \sum_{i=1}^{N} \sum_{j=i+1}^{N} \varepsilon_{ij} \left[\left(\frac{1.07 R^*_{ij}}{R_{ij} + 0.07 R^*_{ij}} \right)^7 \left(\frac{1.12 R^{*\,7}_{ij}}{R_{ij}^{\,7} + 0.12 R^{*\,7}_{ij}} - 2 \right) \right]$$

ε_{ij} is the potential energy well depth in kcal/mol, R^*_{ij} is a buffering constant. This is referred to as the buffered-14-7 form, due to the use of buffering constants and the 14th and 7th power terms[27]. Compare to the Tripos term, which employs 12th and 6th power terms.

The seventh term involves electrostatic interactions as shown below:

$$\sum EQ_{ij} = \sum_{i=1}^{N} \sum_{j=i+1}^{N} 332.07 \left(\frac{q_i q_j}{D(R_{ij} + \delta)^n} \right)$$

D is the dielectric value ("constant"), q_i is the partial atomic charge at the i^{th} atom, and R_{ij} represents the distance between the atoms (in Å). 332.07 is a conversion factor for the units. The exponent n is set to 1 or 2, depending on whether a constant or distance-dependent dielectric function is used. A buffer represented by δ (δ >0, 0.05Å here) prevents the electrostatic term from overpowering the repulsive part of the van der Waals term at very short range[27]. Note that buffering is not included in the Tripos electrostatic term.

The MMFF94 charges are computed using the formula

$$q_i = q_1^0 + \sum(-\omega_{ki})$$

where q_1^0 is the formal charge, usually zero, and ω_{ki} is the bond charge increment of partial charge at atom i due to the i-k bond (between atom i and attached atoms k)[26,27]. Note that MMFF94 charges are considerably larger than Gasteiger charges (typically twice as large)[28].

2.4 Potential Energy Surfaces

A potential energy surface (PES) is a multidimensional surface describing potential energies for all possible molecular conformations[29]. Minima on the surface correspond to energetically favorable arrangements. For non-trivial molecules, the amount of computation required becomes large very quickly. Various approaches such as systematic and random search methods have been employed to surmount this problem.

2.5 Random Searches

A random search changes either the torsion angles of rotatable bonds or the spatial orientation of the atoms in a molecule in a random rather than systematic fashion. In such as search, a given conformation is changed (e.g., the torsion angles of the specified rotatable bonds are randomly modified), then energetically minimized, and then compared to previously-found conformations to see if it is unique[30]. The definition of uniqueness is an RMS fit value greater than the chosen RMS threshold for the heavy (i.e., non-hydrogen) atoms between the current and previously found conformers[31]. This process is repeated a specified number of times. Figure 3.1 shows a flow diagram of the process for torsion angles.

The random search procedure by its nature is not guaranteed to find all conformations[30]. An approximate formula for the probability that all conformations have been found that meet specified conditions has been given as $(1-(^1/_2)^n)$, with n representing the minimum number of times any conformer has been found[32]. For example, if each conformation was found at least twice, but not all were found three or more times, n = 2 and therefore, the probability is 0.75 that all conformations have been found.

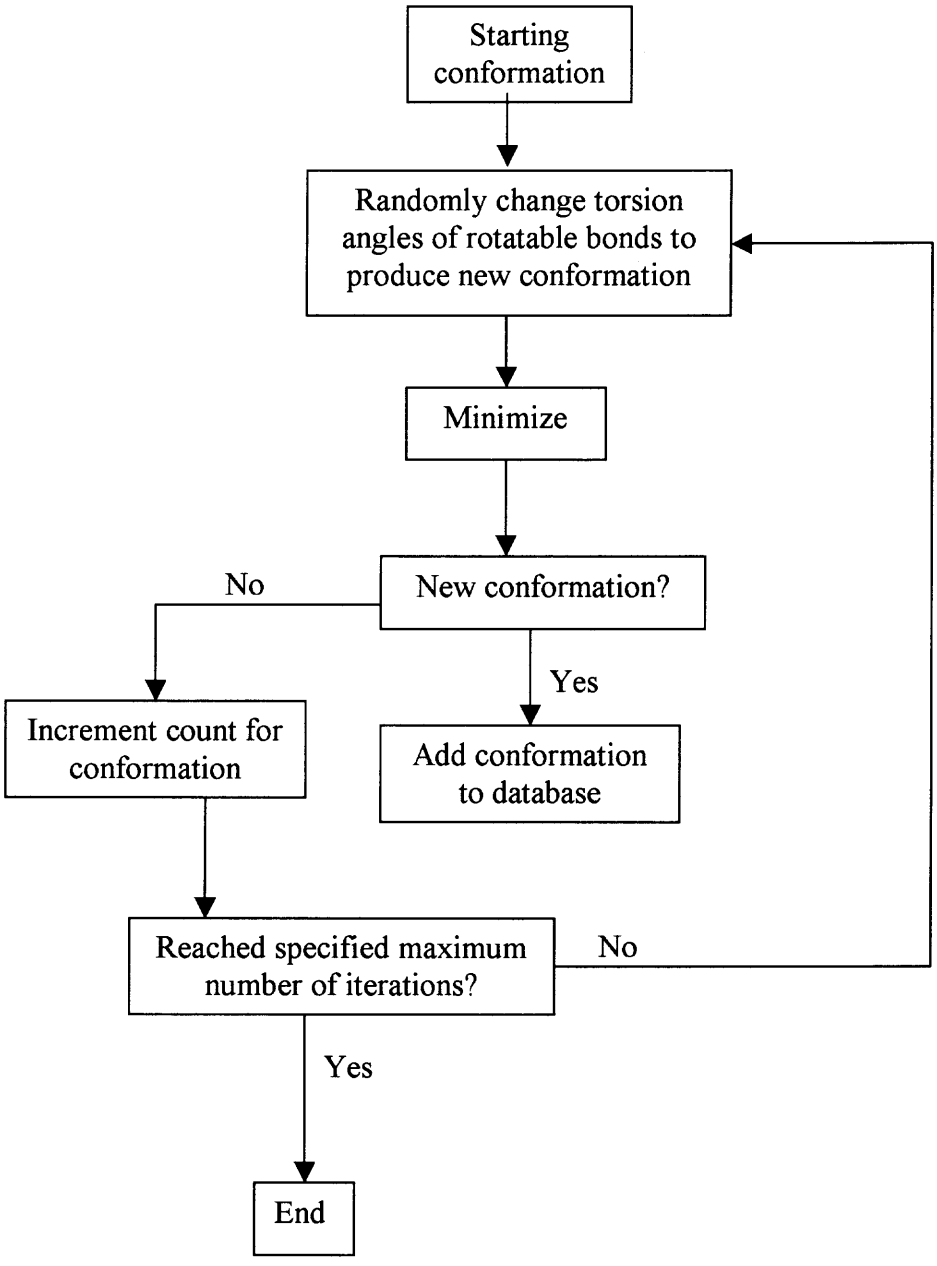

Figure 2.1 Random search process. (Adapted from Leach[30].)

CHAPTER 3

METHODS USED FOR RANDOM CONFORMATIONAL SEARCHING

3.1 Hardware and Software

The minimizations and random searches were performed using Sybyl version 6.9, a molecular modeling package from Tripos, Inc. Sybyl was run on dedicated Silicon Graphics workstations using the Unix operating system in the Venanzi laboratory at New Jersey Institute of Technology. PCs utilizing Microsoft Windows operating systems and Microsoft Excel were used to produce the graphical displays of the data obtained from the random searches.

3.2 Choice of GBR12909 Analogs

DM324 is an analog of GBR12909 that differs in two respects: the substitution of a naphthyl fused ring pair for the single phenyl ring on the so-called "A" side of the molecule, and the deletion of two rotatable C-C bonds, also on the A side. The "B" (bisphenyl) side is identical to that of GBR12909. This results in a molecule with very nearly the same extended length as GBR12909, but with more rigidity supplied by the extra fused ring of the naphthalene substituent. TP250 differs from DM324 only in replacement of the B-side nitrogen by a -CH group, producing a piperadine ring in place of the piperazine ring.

3.3 State of Protonation of Analogs

The literature indicates that dopamine probably binds to the DAT in protonated form[33], but that a cocaine analog (WIN 35,428) shows little difference in binding between the neutral and protonated cases[34]. The Venanzi group pharmacophore modeling of methylphenidate and a rigid analog (see figure below) found fewer conformations in the

Methylphenidate (MP)

Rigid Analog (R-MP)

Figure 3.1 Structures of methylphenidate and a rigid analog.

protonated state as compared with the neutral state, although they were in approximately the same conformational space[35]. This indicated that the computational load might be reduced by investigating the protonated state only.

It is not known in which state the GBR analogs exist upon binding. Quantum mechanical calculations done by the Venanzi group found that in GBR12909, protonation is favored at the A-side nitrogen[36] (i.e., closer to the naphthalene). For this reason, and for purposes of comparison between the DM324 and TP250, which lacks the B-side nitrogen of DM324, protonation at the A-side nitrogen was chosen for modeling.

3.4 Random Searches

The minimization/random search process was performed for the cases indicated in bold type in Table 3.1, in order to compare to the vacuum phase results of Deepangi Pandit and Milind Misra, other Venanzi group members.

Table 3.1 Investigation in Context of Related Studies

Analog	**DM324**				**TP250**			
Force Field	Tripos		MMFF94		Tripos		MMFF94	
Charges	Gasteiger-Hückel		MMFF94		Gasteiger-Hückel		MMFF94	
Dielectric Function	Distance- Dependent		Constant†		Distance- Dependent		Constant†	
State	vacuum phase	**aqueous solvation**	vacuum phase	**aqueous solvation**	vacuum phase	**aqueous solvation**	vacuum phase	**aqueous solvation**
Further Analysis	Macromodel, multivariate and/or clustering methods, CoMFA				Macromodel, multivariate and/or clustering methods, CoMFA			

† Default setting for MMFF94.

The phenyl rings and the naphthalene moiety were treated as active aggregates in all cases to simplify computation and prevent undesirable ring opening[37]. The molecular description (".mol2") files pertaining to the analogs were obtained from previous work done by Milind Misra. Details can be found in Appendix C. Prior to doing random searches, the molecular configuration was set to a local energy minimum by using the

Maximin2 function of Sybyl. For the minimization process, the piperadine or piperazine ring was not treated as an aggregate, but torsion angle constraints were included (refer to Appendix A for details).

Random searches were then run using the RandomSearch function of the Sybyl program. For the random searches, torsion constraints were inactivated, and the piperadine or piperazine ring was treated as an aggregate to maintain rigidity and avoid ring inversion from the energetically favorable chair/equatorial configuration. The simplification and ring-opening considerations noted above for the other rings also apply. Random searches were performed by the implicit solvation method, using a distance-dependent dielectric value of 80 to represent more closely the aqueous environment that a medication would encounter in vivo, in place of the default dielectric value of 1 associated with a vacuum.

The RandomSearch function randomly alters the torsion angles of all eight (selected) rotatable bonds, minimizes the structure via Maximin2, and saves the conformation in a database if it is unique. The definition of uniqueness is an RMS fit value greater than the chosen RMS threshold (in these studies, the Sybyl default value: 0.2Å) for the heavy (i.e., non-hydrogen) atoms between the current and previously-found conformers[31]. In the case of a duplicate, RandomSearch increments the count (i.e., the number of times the conformer was encountered) for the previously found conformation. Only conformations that had energies less than a 20 kcal/mol cutoff over the energy corresponding to the result of the original minimization were recorded. A maximum of 1000 iterations was set. The chirality function of RandomSearch was activated to ensure the energetically-favorable equatorial positions of the naphthyl and phenyl rings with

respect to the central piperazine or piperadine ring. The symmetry function was activated to account for the symmetry of the two phenyl rings on the B side of the each analog. Other parameters used in minimization and random searches can be found in Appendix A.

All the searches in this study were performed for solvent phase, with one exception. Due to discrepancies found between vacuum and solvent phase random search results for DM324 using the Tripos force field, a second random search was carried out for the vacuum phase as a check

3.5 Processing of Random Search Results

3.5.1 Scatterplots

The information produced by RandomSearch was used to construct a text file containing the torsion angles (specifics can be found in Appendix A) of rotatable bonds associated with each conformation found. The count (as described previously) and energy for each conformation were also included. The text files were exported to a PC for processing with the Microsoft Excel spreadsheet program. The conformations were sorted according to energy level, and relative energies were computed as compared to the minimum energy of all conformation energies found. The conformations were sorted into bins of relative energy (RE) $0 \leq RE < 4$, $4 \leq RE < 8$, $8 \leq RE < 12$, $12 \leq RE < 16$, and $16 \leq RE \leq 20$ kcal/mol.

Since the potential energy surface was multi-dimensional, a method of analysis was needed. One way of analyzing results is to plot conformational minima in torsional angle space. Scatterplots of conformational minima were created for selected torsion

angle pairs that were considered likely to give indications of the pharmacophore characteristics of the analogs, and therefore of GBR12909. The relative energies of the conformational minima were indicated by color-coding according to bin. The pairings included adjacent bonds as well as A-to-B-side interrelationships (refer to Figure 1.5 for locations of rotatable bonds). Particularly considered were bonds at the likely pharmacophore elements (A1, A2), substituents required for GBR12909 binding (B5, B6) and those of interest in hydrogen bonding considerations (A1, B1 (in the case of DM324), B3, B4)

Since the phenyl rings are symmetrical about the axis of B5 or B6, a second, 180-degree opposite side torsion angle, was obtained from Sybyl. The smaller (negative) value was chosen for representation in the relevant scatterplots. The results were compared on a qualitative visual basis to those from random searches conducted under the same conditions excepting the dielectric value, to determine the effect of the solvent on the locations of energy minima.

3.5.2 Shape Analysis

Conformations were classified into shape categories according to the smallest distance between the A and B sides of the molecules. Centroids were defined for each ring of the naphthalene substituent as well as both phenyl rings. Distances from each of the phenyl (B-side) centroids to each of the naphthyl ring (A-side) centroids were computed using Sybyl. The smallest of these four measurements was used to classify the conformation into the categories shown in the table below:

Table 3.2 Conformation Shape Category

Shape	**D (Distance in Å)**
C (Cup)	$0 < D < 4.5$
I (Intermediate)*	$4.5 \leq D < 5.0$
V (V-shaped)	$5.0 \leq D < 7.0$
E (Extended)	$7.0 \leq D$

* Intermediate between C and V shapes

Additionally, a virtual torsion angle was defined by four points (refer to Figure 3.2 below): 1) the centroid of the naphthalene ring which is closer to the nearer phenyl ring (as defined previously) 2) the nitrogen of the piperazine or piperadine ring that is nearer the naphthalene moiety; 3) the nitrogen (for DM324) or carbon (for TP250) which is attached to the alkyl chain linked to the phenyl rings; and 4) the centroid of the phenyl ring which is closer to the nearer naphthalene ring centroid. The virtual torsion angle refers to how far (in degrees) the A side is rotated away from the B side for the given conformation.

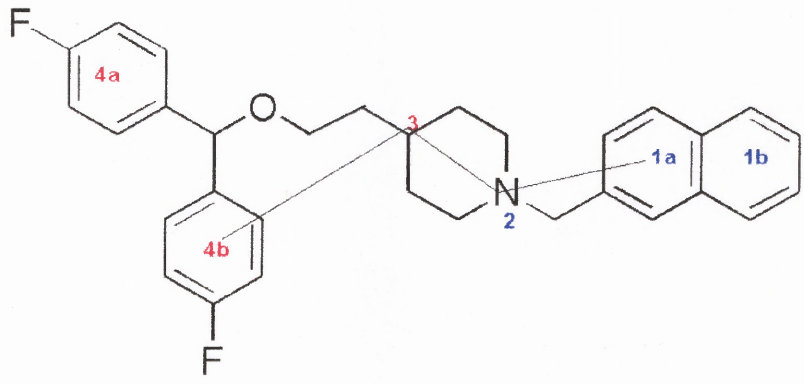

Figure 3.2 Points defining virtual torsion angle. (TP250 is shown.) A-side reference points are in blue, B-side points are in red. Torsion angle is indicated by the light lines connecting the reference points – 4b and 1a are included here since they would be used to classify the shape of the conformation.

CHAPTER 4

RESULTS OF RANDOM CONFORMATIONAL SEARCHES AND DISCUSSION

4.1 Overview

There were considerable differences in the numbers of conformations found in the various random searches (refer to the table below). The conformations all met the requirement of having relative energies of no greater than a cutoff of 20 kcal/mol compared to the initial local minimum for each search.

Table 4.1 Number of Conformations Found by Set of Conditions

Analog	**DM324**				**TP250**			
Force Field	Tripos		MMFF94		Tripos		MMFF94	
State	vacuum	**solvent**	vacuum	**solvent**	vacuum	**solvent**	vacuum	**solvent**
Number of conformers	728	**735**	643	**791**	718	**733**	632	**780**

The reasons for this are not clear, although the type of force field may be relevant, since the MMFF94 force field tended to produce a larger number of conformers than the Tripos force field for the solvent phase. The state (vacuum or solvent) made little difference for the Tripos results, but a large difference was observed in the MMFF94 results. The numbers for the vacuum state were significantly lower than for the Tripos results, but

significantly higher for the solvent state. There was no significant difference found in comparing DM324 to TP250.

Histograms that display the distribution of conformations among the relative energy (RE) bins ($0 \leq RE < 4$, $4 \leq RE < 8$, $8 \leq RE < 12$, $12 \leq RE < 16$, and $16 \leq RE \leq 20$ kcal/mol) are shown below. Each histogram represents the results of one random search. Vacuum phase is represented in the left column; solvent phase is on the right. Tripos force field cases are in the first two rows – first DM324, then TP250; similarly, MMFF94 cases are shown in the lower two rows.

Note that in every instance, there is a shift to the lower relative energy bins for the solvent cases compared to vacuum cases. The effect is more prominent in the MMFF94 situations. In the Tripos instances, TP250 relative energy results were significantly less spread out (i.e., more concentrated in the lower relative energy bins) compared to the DM324 results. Little difference between the analogs was observed for the MMFF94 cases. Comparing between force fields, an inverted relationship was seen between the analogs. DM324 showed little difference for the vacuum phase, but a large shift to lower energy bins for the MMFF94 force field relative to Tripos. Meanwhile, for TP250, the vacuum cases showed a large shift to higher energy bins for the MMFF94 force field relative to Tripos, but little difference existed in the solvation cases.

The following sections include some of the more detailed results shown graphically in scatterplots. Full sets of scatterplots can be found in Appendix D.

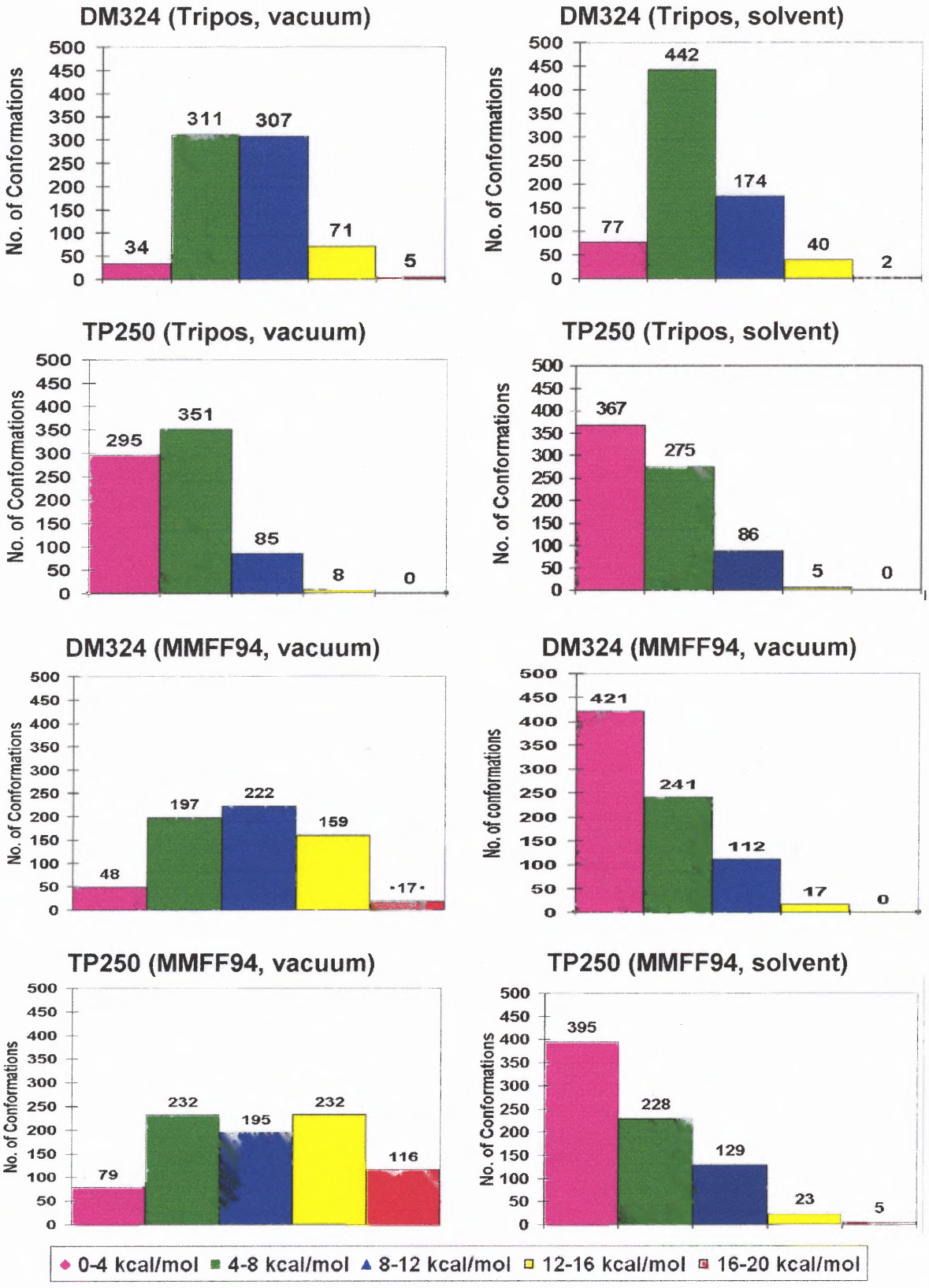

Figure 4.1 Histograms for the eight cases considered.

4.2 Tripos to Tripos Force Field Comparison

For the most part, there were few differences in the Tripos results. Typical results, demonstrating a moderate amount of clustering, are shown below.

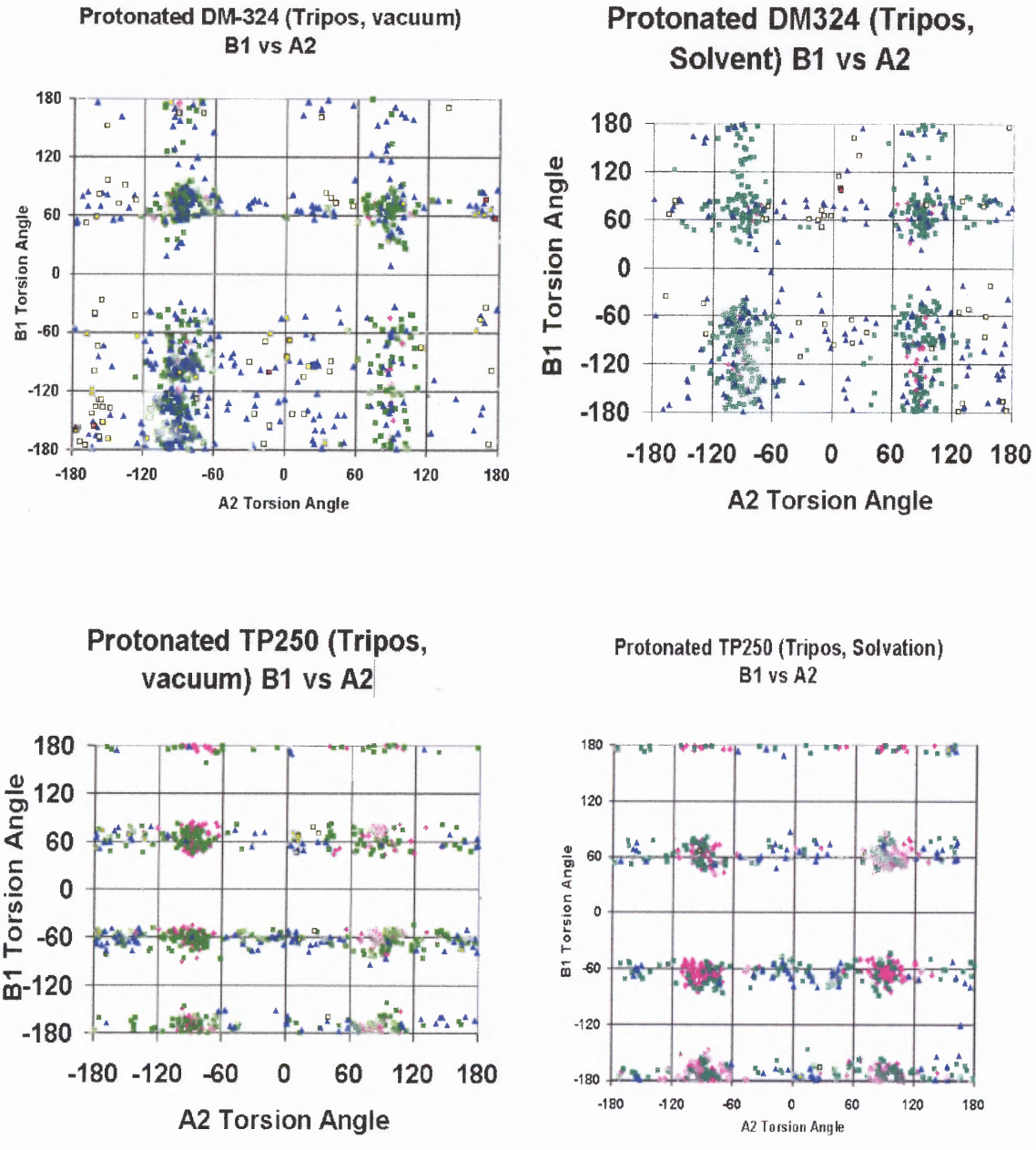

Figure 4.2 Typical Tripos scatterplot results.

The major discrepancy found, involving the presence or absence of relatively large clusters of data points representing conformations found, is noted below. Comparison of Figure 4.2 (a) and (b) shows a cluster of data points around the +60 degree line of B4, and between −180 and −140 degrees on the B5 axis, which appear in (b) but not in (a). A second random search was performed, with the result shown in (c). Note that the cluster of (b) previously discussed appears in (c), but is less dense, representing a smaller number of conformations found in that section of torsional angle space.

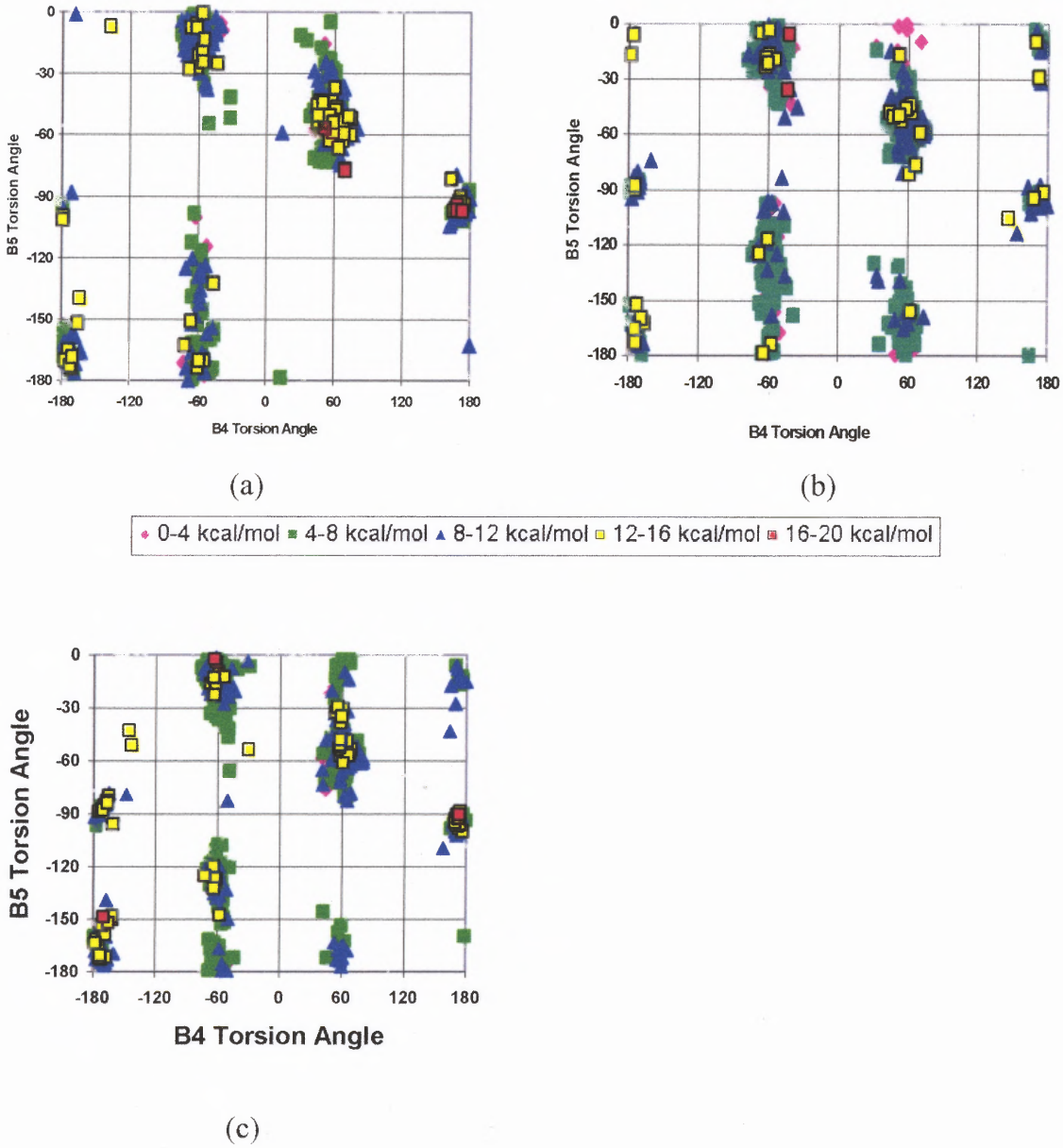

Figure 4.3 Results of random searches for torsion angles B4 and B5 of DM324 using the Tripos force field. Plot (a) includes the initial vacuum phase results; (b) shows the results for aqueous solvation; (c) shows the results of a second vacuum phase search.

4.3 MMFF94 to MMFF94 Force Field Comparison

Very few differences were found between the MMFF94 results (refer to the figure below). The solvent phase tended to produce more compact clusters of data points (conformations) compared to the vacuum phase.

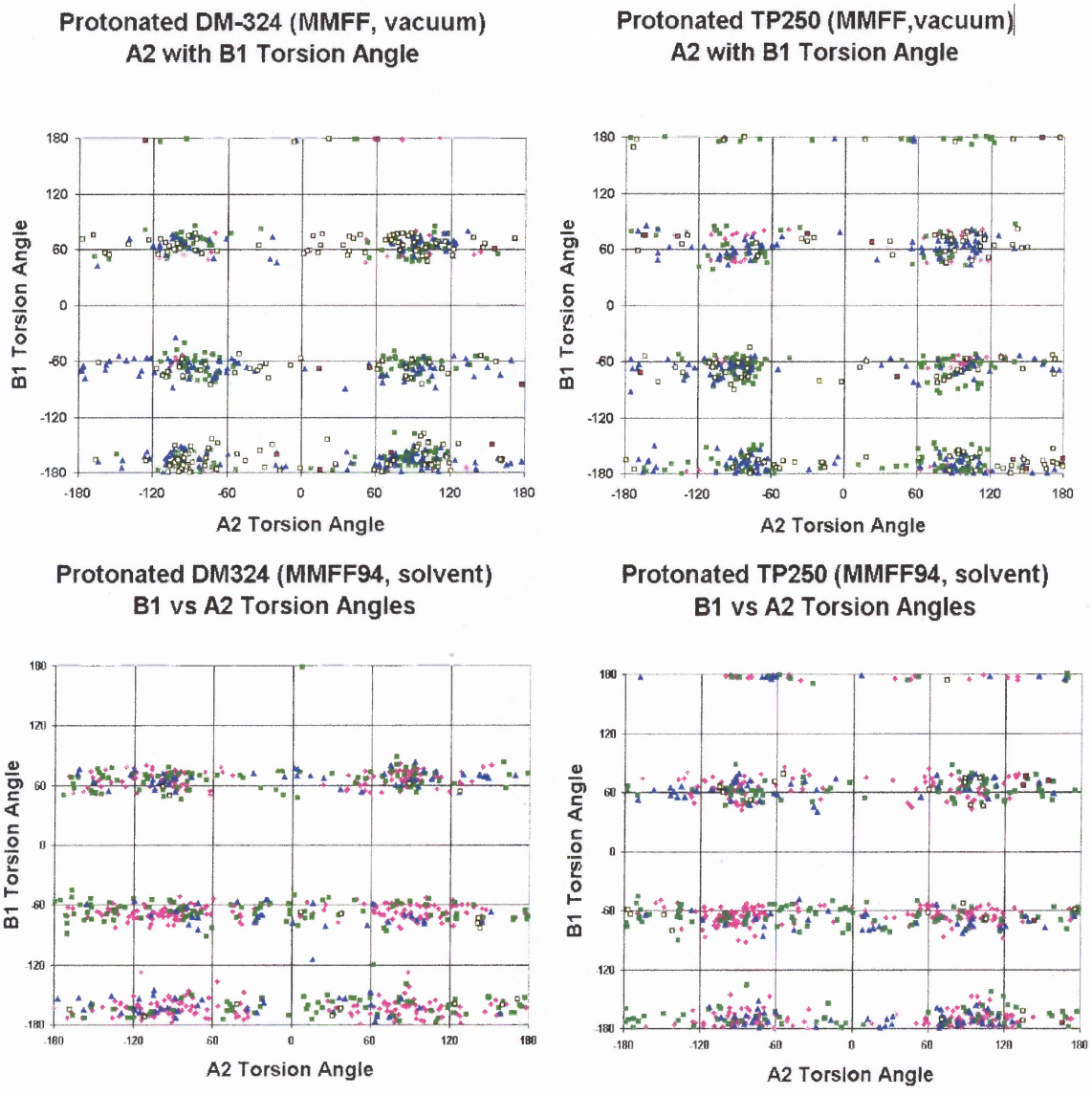

Figure 4.4 Typical MMFF94 scatterplot results.

4.4 Tripos to MMFF94 Force Field Comparison

In general, there were no large differences between the Tripos and MMFF94 results. The typical examples previously noted can be compared to demonstrate this.

One anomalous result was observed for the B4 torsion angle. This was particularly clear for the B5 vs. B4 scatterplots, as shown below.

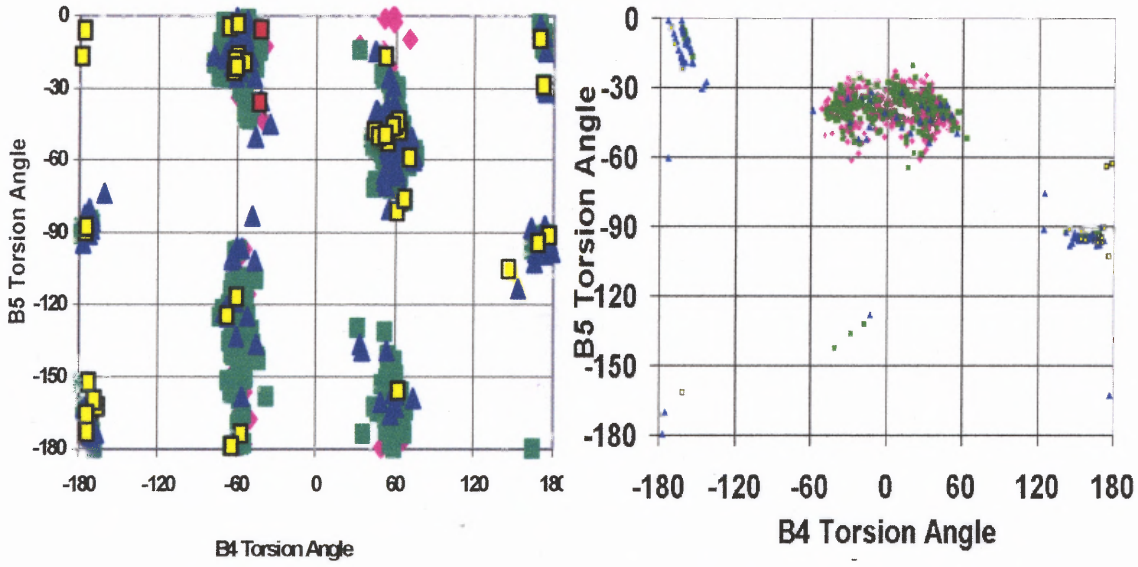

(a) (b)

Figure 4.5 Comparison of B5 vs. B4 scatterplots. On left are Tripos results (a) and on right are MMFF94 results (b). Both are for DM324 and solvent phase.

The graphical representations of the B4 distributions are shown below.

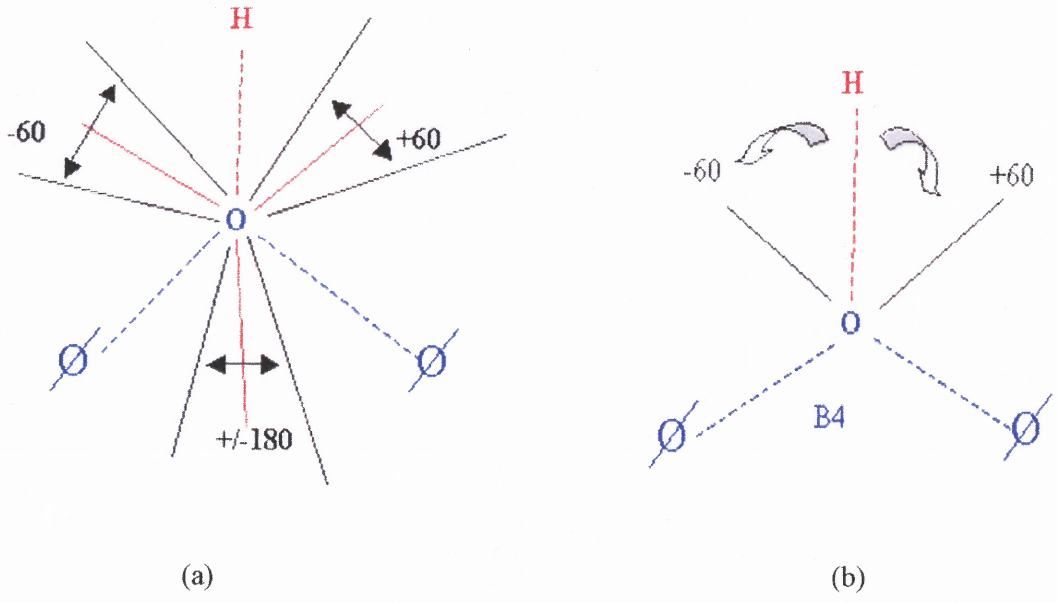

(a) (b)

Figure 4.6 Graphical representations of B4 torsion angle ranges. The view is along the B4 bond axis (into the plane of the paper). Each Ø stands for a phenyl group in the bisphenyl fragment. Tripos case is on left (a), MMFF94 case is on right (b). Zero position, defined by the hydrogen atom, is shown by red dashed lines.

4.5 Shape Analysis Results

The table below shows the distribution of conformational minima among the four shapes: The large majority of conformations were found in the extended ("E") shape for all combinations of variables. The V-shaped ("V") category was the second most populated, with few instances in the cup-shaped ("C") and intermediate ("I") configurations. This was less so for the DM324 analog in the Tripos force field, since it exhibited moderately more conformations in the C and V shapes compared to the other cases. In all cases, there were significant shifts to the lower energy bins for the solvent state relative to the vacuum state

The MMFF94 force field exhibited a shift away from the 0-4 kcal/mol relative energy bin relative to the Tripos force field for the TP250 analog. The shift was larger for the vacuum case than the solvation case. The trend was the opposite for DM324 in the solvent case, with little difference seen in the vacuum case.

There were substantially more conformational minima in the 0-4 kcal/mol energy bin for TP250 than for DM324 using the Tripos force field. Also in the Tripos case, there were a moderately smaller number of conformational minima in the "C" and "I" shapes for TP250 as compared to DM324. Regarding the MMFF94 force field, there were no significant differences between the analogs.

Table 4.2 Energy Distributions of Shapes

	0-4	4-8	8-12	12-16	16-20	Total/shape
DM324 (Tripos, vacuum)						
C ($0 < D < 4.5$)	15	6	0	0	0	21
I ($4.5 \leq D < 5.0$)	5	10	1	0	0	16
V ($5.0 \leq D < 7.0$)	4	38	9	4	0	55
E ($7.0 \leq D$)	10	257	297	67	5	636
Total/bin	34	311	307	71	5	**TOTAL**: 728
DM324 (Tripos, solvent)						
C ($0 < D < 4.5$)	22	2	0	0	0	24
I ($4.5 \leq D < 5.0$)	7	10	0	0	0	17
V ($5.0 \leq D < 7.0$)	21	25	9	2	0	57
E ($7.0 \leq D$)	27	405	165	38	2	637
Total/bin	77	442	174	40	2	**TOTAL**: 735
DM324 (MMFF94, vacuum)						
C ($0 < D < 4.5$)	0	0	0	0	0	0
I ($4.5 \leq D < 5.0$)	0	3	0	0	0	3
V ($5.0 \leq D < 7.0$)	22	32	12	8	0	74
E ($7.0 \leq D$)	26	162	210	150	18	566
Total/bin	48	197	222	158	18	**TOTAL**: 643
DM324 (MMFF94, solvent)						
C ($0 < D < 4.5$)	0	0	0	0	0	0
I ($4.5 \leq D < 5.0$)	0	0	0	0	0	0
V ($5.0 \leq D < 7.0$)	15	25	3	6	1	50
E ($7.0 \leq D$)	213	292	172	63	1	741
Total/bin	228	317	175	69	2	**TOTAL**: 791

Table 4.2 Energy Distributions of Shapes (continued)

	0-4	4-8	8-12	12-16	16-20	Total/shape
TP250 (Tripos, vacuum)						
C ($0 < D < 4.5$)	2	0	0	0	0	2
I ($4.5 \leq D < 5.0$)	1	0	0	0	0	1
V ($5.0 \leq D < 7.0$)	30	6	3	1	0	40
E ($7.0 \leq D$)	214	329	118	14	0	675
Total/bin	247	335	121	15	0	**TOTAL**: 718
TP250 (Tripos, solvent)						
C ($0 < D < 4.5$)	0	0	0	0	0	0
I ($4.5 \leq D < 5.0$)	1	2	0	0	0	3
V ($5.0 \leq D < 7.0$)	31	9	3	0	0	43
E ($7.0 \leq D$)	335	264	83	5	0	687
Total/bin	367	275	86	5	0	**TOTAL**: 735
TP250 (MMFF94, vacuum)						
C ($0 < D < 4.5$)	0	0	0	0	0	0
I ($4.5 \leq D < 5.0$)	0	0	0	0	0	0
V ($5.0 \leq D < 7.0$)	30	22	6	2	0	60
E ($7.0 \leq D$)	49	209	190	114	10	572
Total/bin	79	231	196	116	10	**TOTAL**: 632
TP250 (MMFF94, solvent)						
C ($0 < D < 4.5$)	0	0	0	0	0	0
I ($4.5 \leq D < 5.0$)	0	0	0	0	0	0
V ($5.0 \leq D < 7.0$)	26	22	5	1	0	54
E ($7.0 \leq D$)	203	295	184	33	11	726
Total/bin	229	317	189	34	11	**TOTAL**: 780

In the figure below, the virtual torsion angles are plotted versus the minimum distances. No significant differences were noted among the various cases.

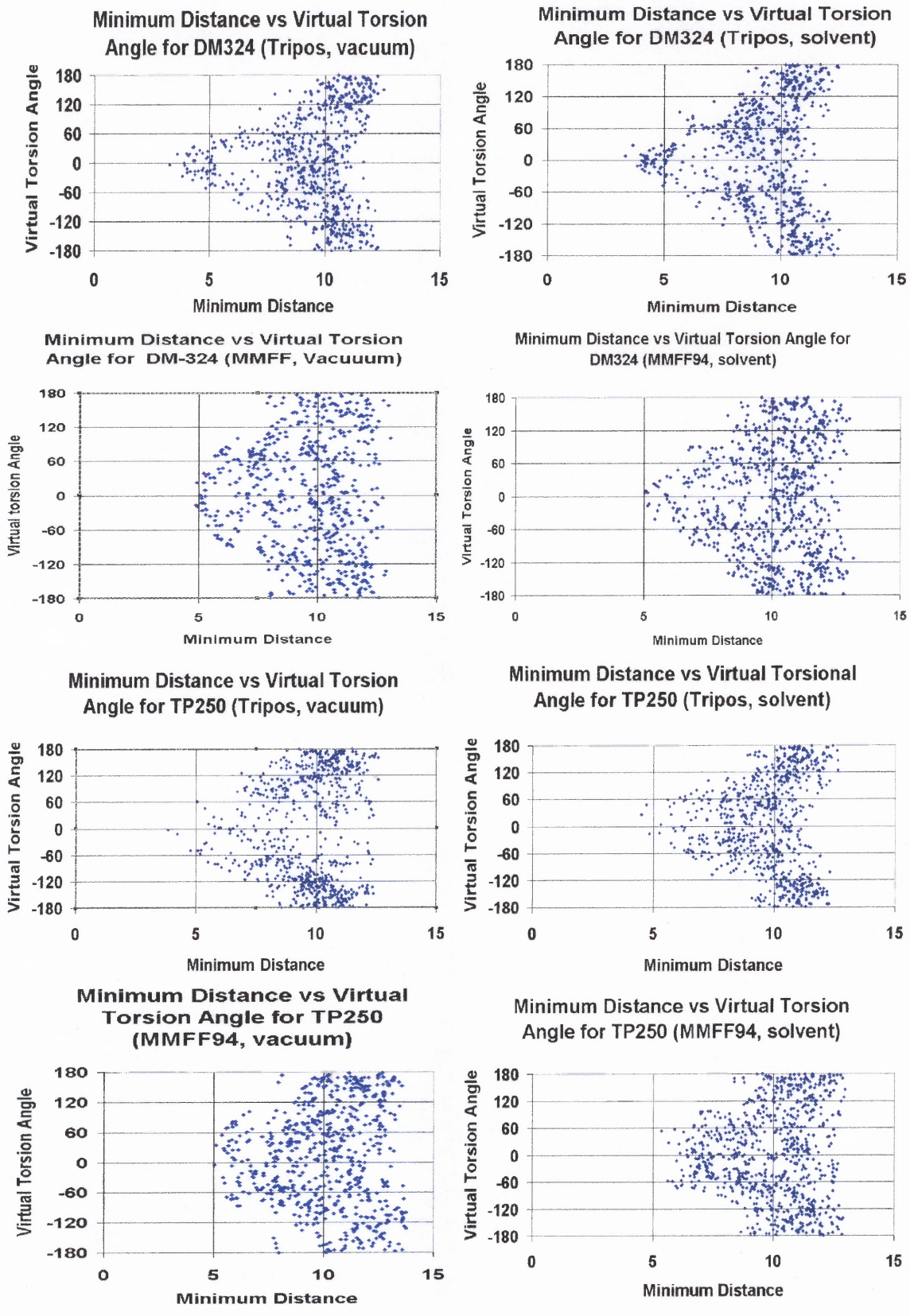

Figure 4.7 Minimum distance versus virtual torsion angle for the various cases.

4.6 Discussion

Several factors may have contributed to discrepancies: the relatively small number of iterations performed during the Sybyl random searches; the use of multiple aggregates; use of a constant vs. distance-dependent dielectric values between Tripos and MMFF94 force fields; omission of Hückel π charges in the Tripos searches; and differences in the van der Waals and electrostatic terms between the two force fields.

The considerations involved with the number of iterations performed in Sybyl RandomSearch have been discussed previously in this chapter (Section 4.2). Refer also to section 2.5 in Chapter 2.

The Tripos user manuals note that errors may be induced by using more than one aggregate simultaneously[38]. No description was provided, but such errors may explain some of the differences found, since four aggregates were present in the random searches conducted for both vacuum and solvent phases.

The default dielectric function settings that were employed in the vacuum phase random searches were also used for the solvent-phase searches, since comparability was desired between phases. The difficulty arises from the differences in the dielectric function – constant for MMFF94, distance-dependent for Tripos. The distance dependency appears in the denominator of the electrostatic term (refer to section 2.1). This would produce reductions in the size of the electrostatic term, as the distances were greater than unity. This would tend to favor the closed over the extended conformations to a greater degree in the Tripos force field model than in MMFF94.

The secondary purpose of this study was to compare the two force fields. Since both force field models are empirical, it is difficult to decide which is more "correct". In

the validation article for the Tripos force field[39], it was noted that electrostatic considerations were omitted due to variability. Nevertheless, the electrostatic effects make up a large part of the absolute energy values. Although absolute energies have no physical meaning, variations in them will likely have a proportional effect on the relative energies. Additionally, the electrostatic and van der Waals terms were computed differently between the models. For instance, in the MMFF94 electrostatic term, the use of a buffer effectively increases the distances, if only slightly, reducing the size of that term. The difference in dielectric function, as previously noted, makes comparison more difficult.

Despite these considerations, some tendencies can be noted and explained. As previously noted, TP250 relative energy results were typically less spread out (i.e., more concentrated in the lower relative energy bins) compared to the DM324 results. This is likely due to the restriction of energetically favorable conformations to a smaller PES due to steric effects owing to the hydrogen at the carbon atom at position 1 (on the piperadine ring) for TP250 in place of the lone pair of the DM324 nitrogen atom (on the piperadine ring).

The cause of the ("missing cluster") discrepancy in the Tripos-Tripos comparisons is believed to be due to the relatively small number of iterations of the Sybyl RandomSearch procedure. This is supported by the variability of the results noted. In both the vacuum and solvent phase cases conducted (in which the minimum number of occurrences of any conformer was one) there was a 50% likelihood that all conformers had been found (refer to section 2.5)[32].

The difference between Tripos and MMFF94 results at the B4 bond may be due to differences in the handling of the lone pairs of the oxygen at one end of the rotatable bond. Using the MMFF94 model, conformations were found at and near the 0-degree B4 torsion angle, despite poor steric interactions for the eclipsed (rather than staggered) configuration. The difference can be seen in the relevant B3-B4, B4-B6, and A2-B4 scatterplots in Appendix D, as they are all based on the same B4 data as the corresponding B4-B5 plots. However, no such effect occurs for rotatable bond B3, which also includes the same oxygen. The major difference is the presence of the phenyl rings one bond away from B4 but not B3. How steric effects between the phenyl rings and the lone pairs of the oxygen can occur is unclear.

Overall, the previous considerations aside, the solvent modeling done in this study shows no significant difference in the distribution of locations of conformational minima in comparison to the vacuum phase.

CHAPTER 5

CONCLUSION

The results leave a number of questions unanswered, as well as raising others. However, the purpose of the current project was to provide preliminary guidelines only, pending more rigorous modeling using more sophisticated software packages. The importance of the final applications would justify the effort expended. In addition, the methods may be applied to studies other than ones concerned with finding a medication to treat cocaine addiction. The primary purpose of the investigation - observing gross qualitative differences between vacuum and solvent phases – showed that there were no major differences.

Future investigators employing the Sybyl RandomSearch software would be well advised to note the limitations previously cited in order to produce more accurate results, or at least to keep the concerns noted in the discussion section (4.6) in mind. In this study, the purpose was primarily comparison between the previously accomplished vacuum phase results and the current implicit solvent phase results. Therefore, these issues were not as relevant as they might be in other situations. In fact, they were more necessary for facilitating such comparisons. It may be the case that Sybyl is better suited to such preliminary qualitative investigations than more explicit or quantitative ones, producing useful gross qualitative results. There exist more rigorous solvation models; however, time and efficiency are often considerations. This is especially true in the case of large molecules, which have considerable potential energy spaces, requiring a large

amount of search effort. A slightly more rigorous model may be the best choice based on those considerations.

APPENDIX A

SPECIFICATIONS FOR RANDOM SEARCHES

This Appendix provides details used for the Sybyl Random Search procedures.

Minimization details:

Method: Powell	Termination: Gradient
Max. Iterations: 1000	Non-bonded reset: 10
Max. Displacement: 0.01	RMS Displacement: 0.001
Min Energy Change: 0.05	Gradient: 0.05
Simplex threshold: 1000	Simplex Iterations: On; 20
LS Accuracy: 0.001	Derivative Reset: 100
LS Step Size: 0.001	Color Option: Potential
Status Update: 1	Checkpoint Interval: 0
Graphics Update: 1	List Terms: Off
Initial Optimization: Simplex	

Energy setup details:

Force field: Tripos or MMFF94

Charges: Gasteiger-Hückel or MMFF94

Force Field Details:

One-Four Scaling: 1

H-Bond Radius Scaling: 0.7

Boundary Conditions [...]:

PBC's (current): 0 A (all 3 cases)

Dielectric function: Distance (Tripos) or Constant (MMFF94)

Dielectric Constant: 1.0 (vacuum) or 80.0 (solvent)

NB Cutoff: 8.0

Aggregates: On

Constraints: Off

Ignore Atoms: Off

Random Search Details:

Maximum cycles: 1000

Energy cutoff: 20 kcal/mol

RMS Threshold: 0.2 A

Convergence threshold: 0.05

Maximum hits: 6

Check chirality: On

Check Symmetry: On

Table A.1 Torsion Constraints for TP250

Atoms (of piperadine ring)	**Constant (Penalty) Kcal/mol $^{o}K^{2}$**	**Default Torsions**	**Violation Pwr**
1 2 3 4	15.00	56.637	0.009
2 3 4 5	15.00	-58.920	0.006
3 4 5 6	15.00	58.924	0.008
4 5 6 1	15.00	-56.654	0.004
5 6 1 2	15.00	56.660	0.008
6 1 2 3	15.00	56.649	0.009

Table A.2 Torsion Constraints for DM324

Atoms (of piperadine ring)	**Constant (Penalty) Kcal/mol $^{o}K^{2}$**	**Default Torsions**	**Violation Pwr**
1 2 3 4	15.00	56.002	0.014
2 3 4 5	15.00	-58.122	0.000
3 4 5 6	15.00	58.023	0.005
4 5 6 1	15.00	-55.793	0.017
5 6 1 2	15.00	57.945	0.003
6 1 2 3	15.00	58.054	0.002

Table A.3 Atoms Defining Torsion Angles of Rotatable Bonds

Rotatable bond	**Atoms**
A1	3 4 23 2 4
A2	4 23 24 33
B1	2 1 7 8
B2	1 7 8 9
B3	7 8 9 10
B4	8 9 10 47
B5	9 10 11 12
B5 DASH*	9 10 11 16
B6	9 10 17 18
B6 DASH*	9 10 17 22

* 180° opposite of B5 or B6 respectively

APPENDIX B

SYBYL RANDOMSEARCH INSTRUCTIONS

This appendix provides instructions on running a random search using the Random Search function of the Sybyl software on the Unix system. Tripos Bookshelf sections Sybyl Basics p.7, Force Field pp.63-64, and Conformational Analysis pp.58-59 were used to prepare this appendix. The example shown applies to the molecules used in this study. Other applications may require different settings. Sybyl dialog boxes, parameters, and settings are indicated in **bold Arial** typeface.

B.1 Initial steps

1. Log into the computer. The system prompt ">" should be visible. If necessary, navigate to your assigned research area.

2. To start the Sybyl program, enter "Sybyl" at the prompt. In a minute or so, the **Sybyl** window will open. The **Sybyl** menubar (at the top of the window) appears as shown below:

Figure B.1 Sybyl menubar.

Graphic manipulation tools are represented by icons along the left edge of the **Sybyl** window. The **textport** window usually appears at the bottom of the terminal screen (below the **Sybyl** window):

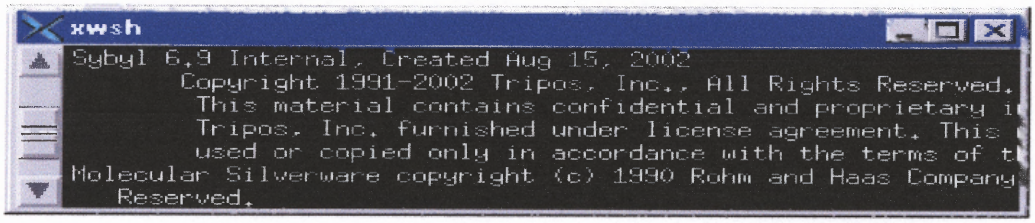

Figure B.2 Sybyl textport window.

3. To open the desired molecular description file "… **.mol2**" for reading, select **File >>> Read...** and select the appropriate file. (If necessary, select a molecular area (i.e., work area) - **m1** is the default). Click on **OK**.

NOTES:

a) If the desired molecule is not in your research area, you can open another console window to copy the molecule file to your area.

b) Help is available by using the **Help** menu at the right of the Sybyl **menubar** and clicking on **Start Bookshelf**.

c) To eliminate an onscreen molecule, select **Build/Edit >>> Zap (Delete) Molecule...** .

d) To undo an operation on a molecule, select Build/Edit >>> Undo... .

B.2 Minimization

1. Click on **Compute >>> Minimize... .** The **Minimize** dialog box as shown below will appear.

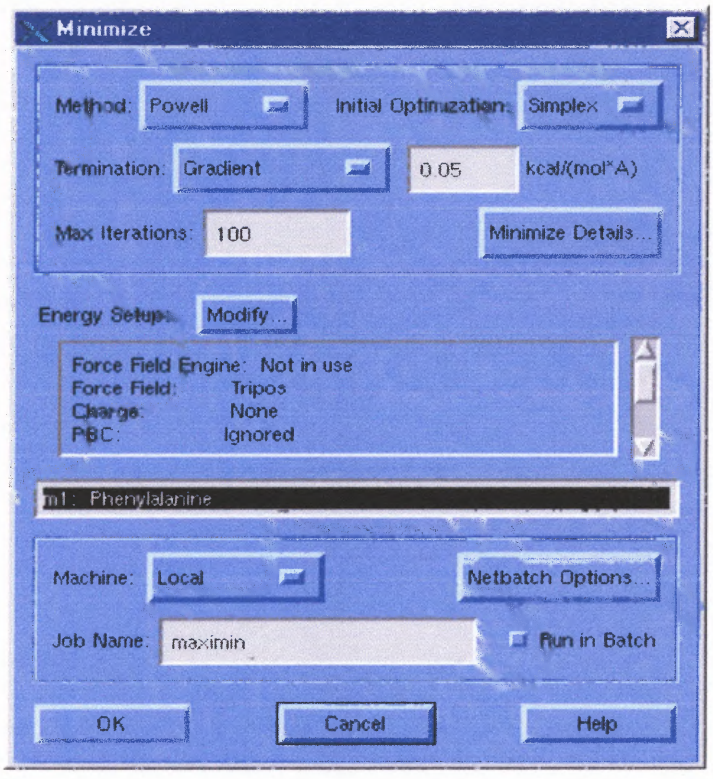

Figure B.3 Minimization dialog box.

2. Set **Max Iterations** to **1000**.

3. The other settings should be as specified in Appendix A.

4. Select **Energy Setup >>> Modify.** An **Energy** dialog box like the one shown below will appear.

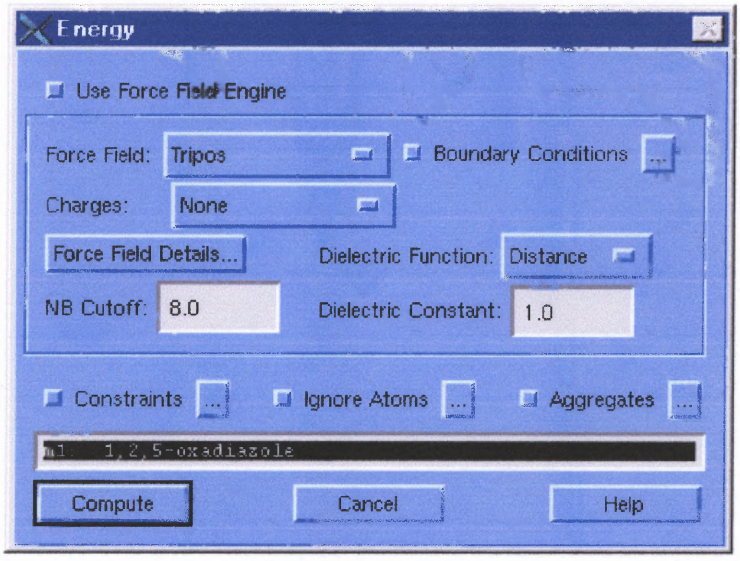

Figure B.4 Energy dialog box.

5. Select desired **Dielectric Function** (**Distance** [-dependent] or **Constant**) and **Dielectric Constant** (1.0 for air or vacuum, 80.0 for water).

6. Click on **Constraints [...].** Select **Torsion Constraints.** Set them according to the details specified in Appendix A.

7. Click on **Aggregates [...].** Make certain that there are only 3 aggregates (2 phenyl rings and a naphthalene fused ring pair), and that their **Status** is **Active**.

8. Select the **Constraints** and **Aggregates** boxes. (They will appear red when selected.)

9. Click on **OK**.

10. Click on **OK** in the **Minimize** dialog box. (The **Job Name** can be left at the default: **maximin**.)

11. Messages will appear in the **textport** window. If "**Optimization completed**" does not appear when Sybyl stops, return to the **Minimize** dialog box and click on **OK**

again. Repeat until "**Optimization completed**" is seen in the **textport** window – this may require several iterations.

B.3 Random Search

1. Click on **Compute >>> Search >>> Random Search.** The **Random Search** dialog box will appear.

Figure B.5 Random search dialog box.

2. The molecule should be displayed on the screen. Click on **Bonds to Search [...]**. For each bond to be searched, select the atoms at both ends. The default is a search of all bonds. Then click on **OK**.

3. Click on **Minimize Details** and review the settings. They should be the same as for the minimization.

4. Click on **Energy Setup**. In the resulting **Energy** dialog, de-select **Constraints** (the box to its left should not appear colored).

5. Click on **Aggregates [...]**. Then click on **New**. On the displayed molecule, highlight the 6 heavy atoms of the piperazine or piperadine ring. Click on **OK**, and name the new aggregate. Make certain the **Status** of all 4 aggregates is **Active**. Then click on **OK**.

6. Make certain that the **Aggregates** box is selected. Then click on **OK** in the **Energy** dialog.

7. Click on **Randomsearch Details**. The dialog box shown below will appear.

Figure B.6 Random search details dialog box.

8. Set **Maximum Cycles** to **1000**.

9. Set **Energy Cutoff** to **20.0**.

10. Select the **Chirality** and **Symmetry** boxes.

11. The other settings should be as specified in Appendix A. Click on **OK**.

12. Choose a unique **Job Name** and click on **Search** to start the random search. (It takes several hours to complete.) The results are stored in a molecular database in the directory in which the search is run.

APPENDIX C

RANDOM SEARCH SOURCE DATA INFORMATION

The source data for Sybyl random searches conducted in this study is located in a subdirectory of Dr. Carol Venanzi's research area on the AFS system: /afs/cad/research/chem/venanzi/14/searches_used. The original molecular description files, prt_tp_2_50.mol2 for TP250 and M_dm324_rs2.mol2 for DM324, are in the directory /afs/cad/research/chem/venanzi/2/eq_eq/.

The file designations are as follows:

RS1000.....Random Search of 1000 maximum cycles

DE80..... Dielectric constant of 80, simulating water

DE1..... Dielectric constant of 1, simulating vacuum

DM324..... the DM324 (piperazine) analog of GBR12909

TP250.....the TP250 (piperadine) analog of GBR 12909

M or trgh..... minimization with torsion constraints on (non-aggregated) piperazine or piperadine followed by random search with torsion constraints inactivated and piperazine or piperadine treated as an aggregate; Tripos force field and Gasteiger-Hückel charges

DP..... minimization performed as above, followed by random search with torsion constraints deleted and piperazine or piperadine treated as an aggregate; Tripos force field and Gasteiger-Hückel charges

MMFF94..... same as M, but with MMFF94 force field and charges

APPENDIX D

SCATTERPLOTS

The following pages include full-size sets (each containing 14 torsion angle pairs) of scatterplots for nine cases, in the following order:

Tripos force field:

DM324:

Vacuum*

Solvation

Second vacuum

TP250:

Vacuum*

Solvation

MMFF94 force field:

DM324:

Vacuum*

Solvation

TP250

Vacuum*

Solvation

* These scatterplots are courtesy of Deepangi Pandit of the Venanzi group, included for the purposes of comparison.

D.1 Tripos for DM324 and Vacuum

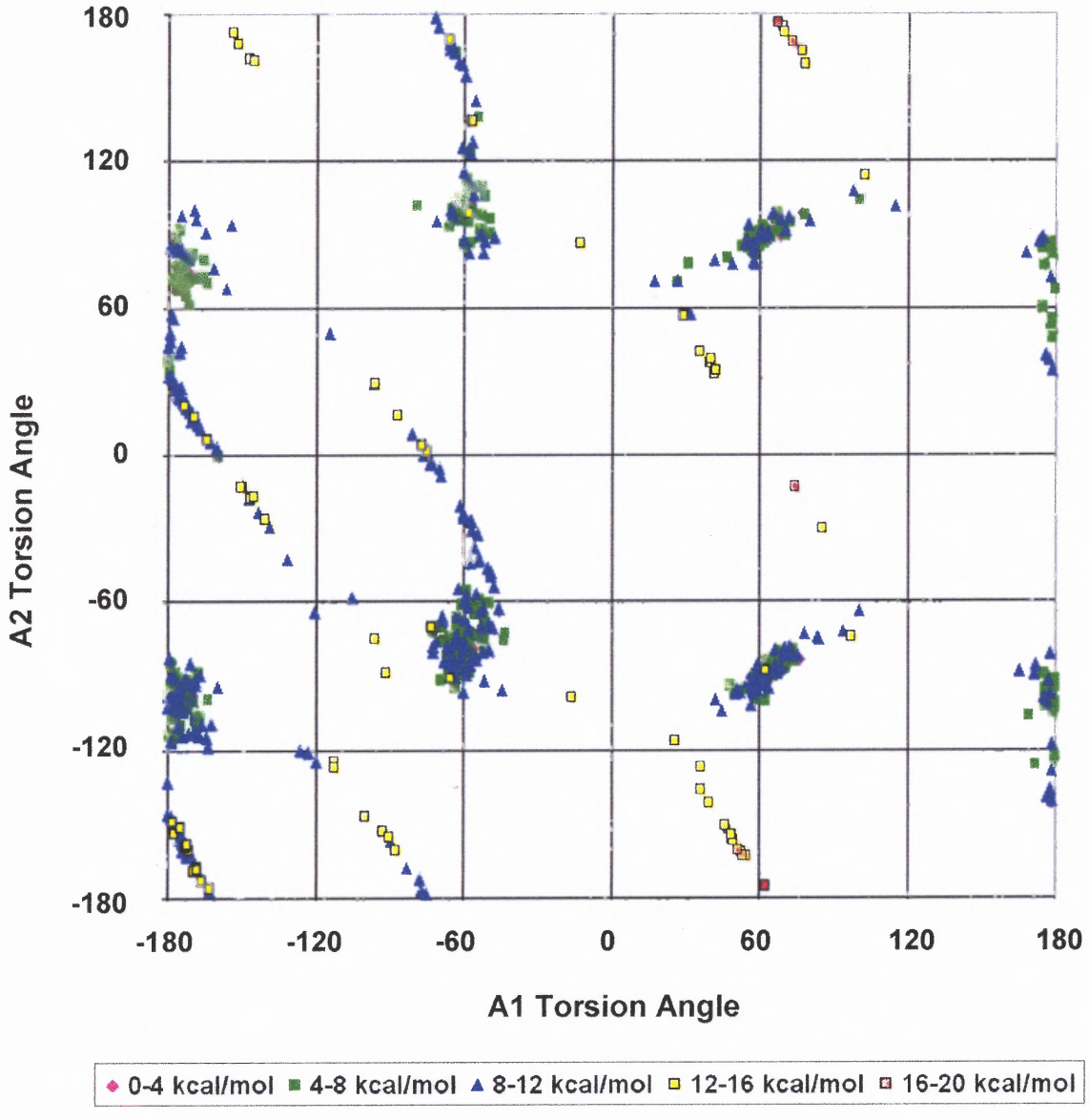

Figure D.1 Protonated DM324 (Tripos, vacuum) A2 vs A1 torsion angles.

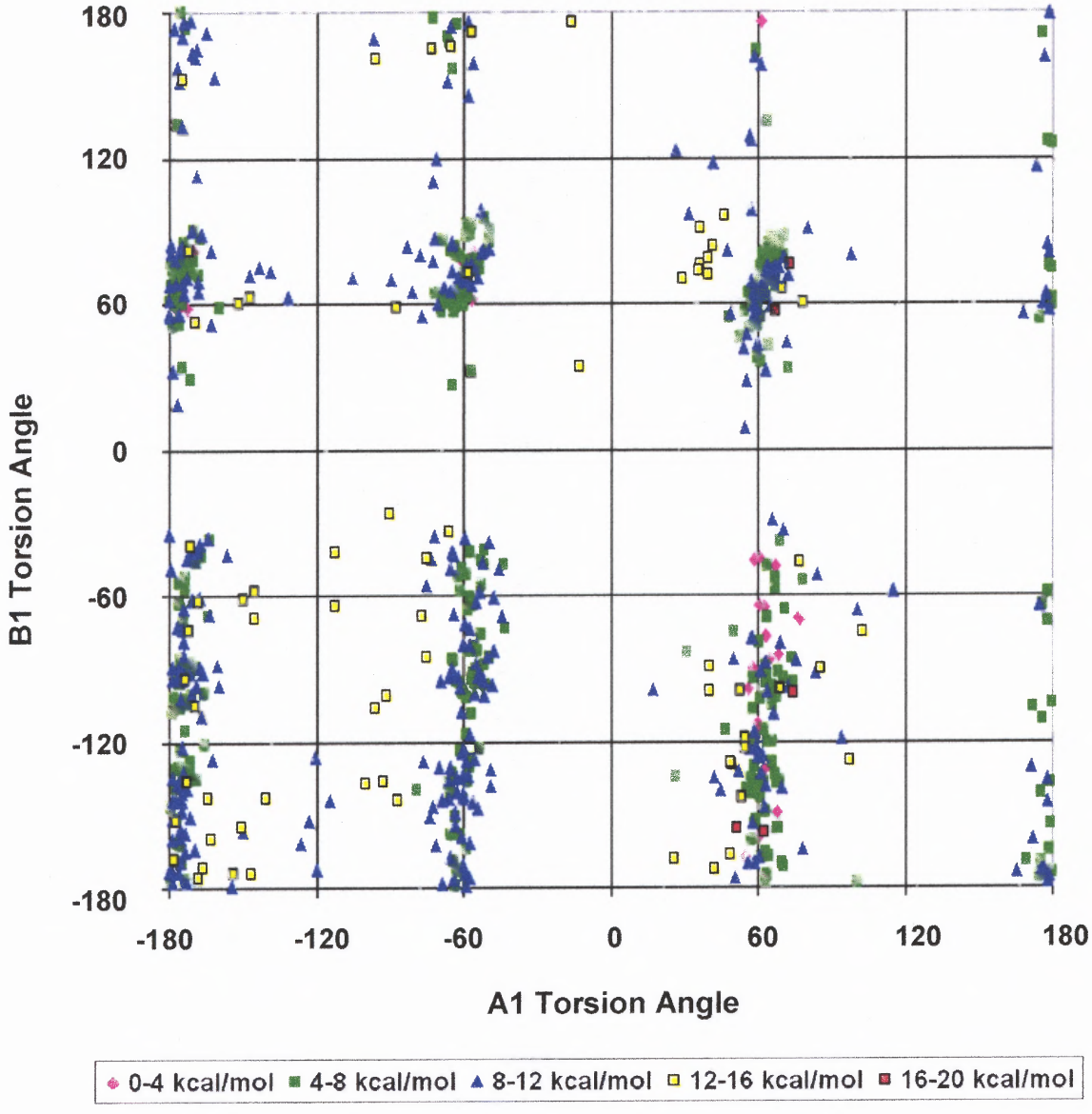

Figure D.2 Protonated DM324 (Tripos, vacuum) B1 vs A1 torsion angles.

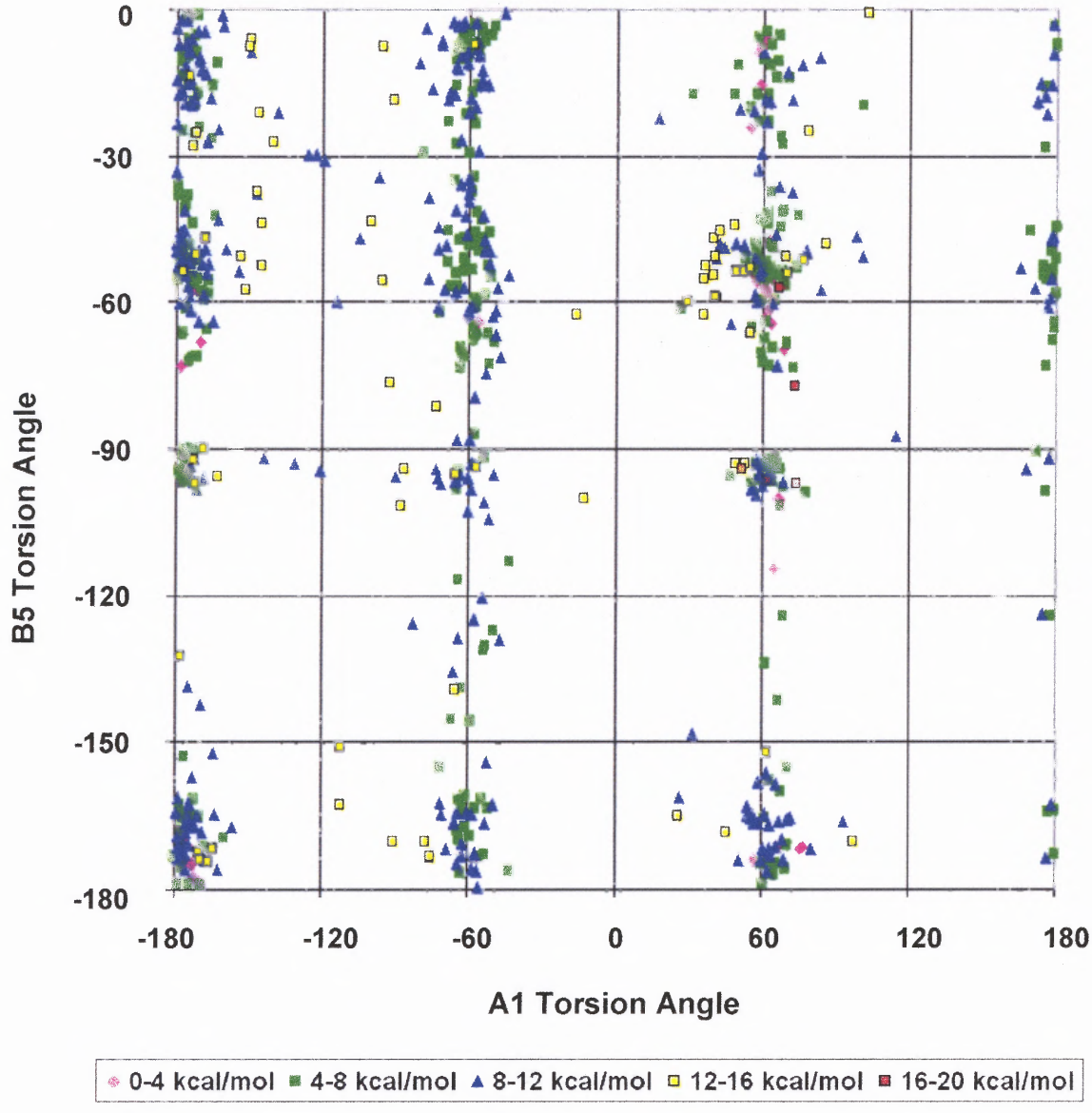

Figure D.3 Protonated DM324 (Tripos, vacuum) B5 vs A1 torsion angles.

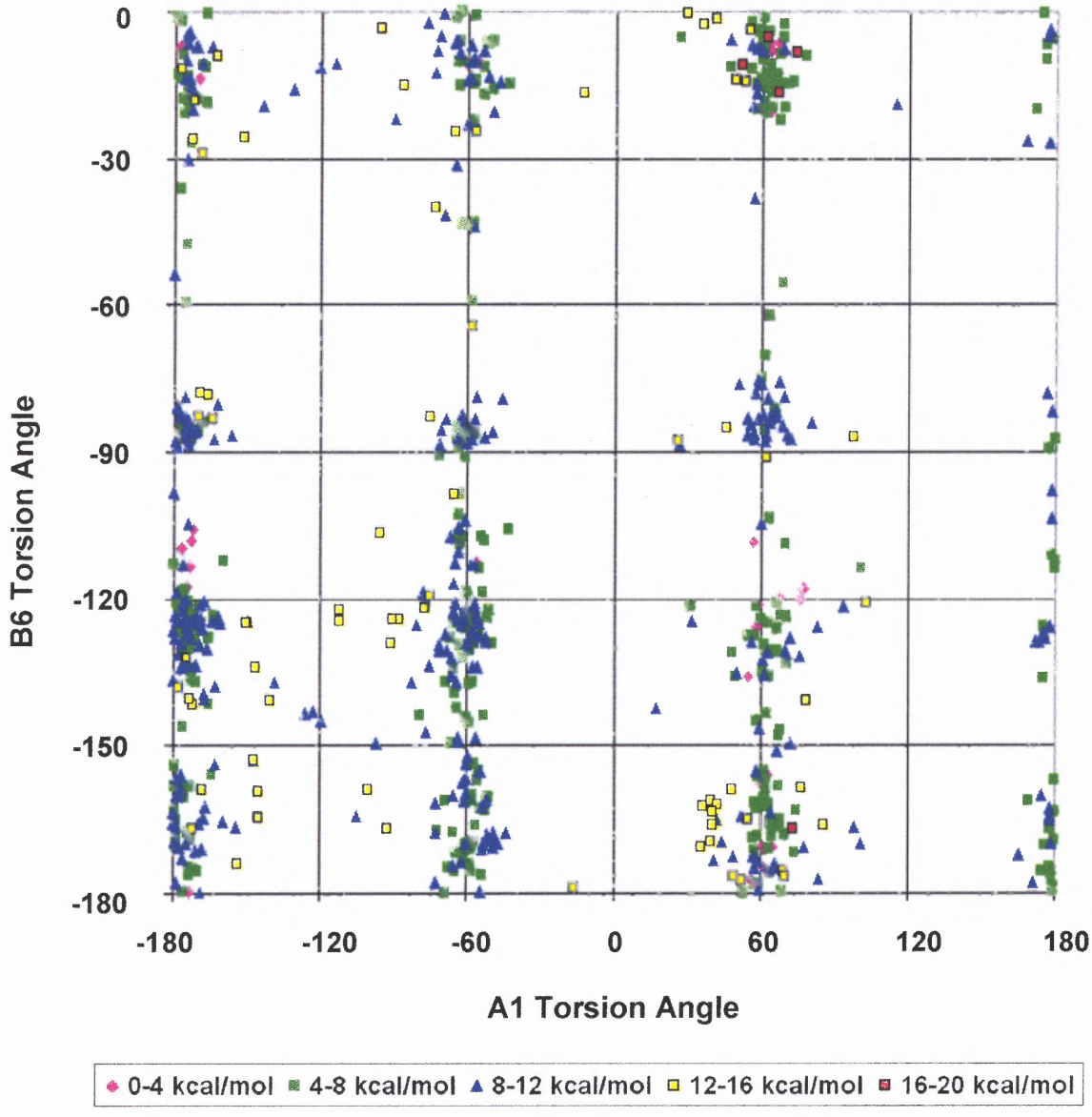

Figure D.4 Protonated DM324 (Tripos, vacuum) B6 vs A1 torsion angles.

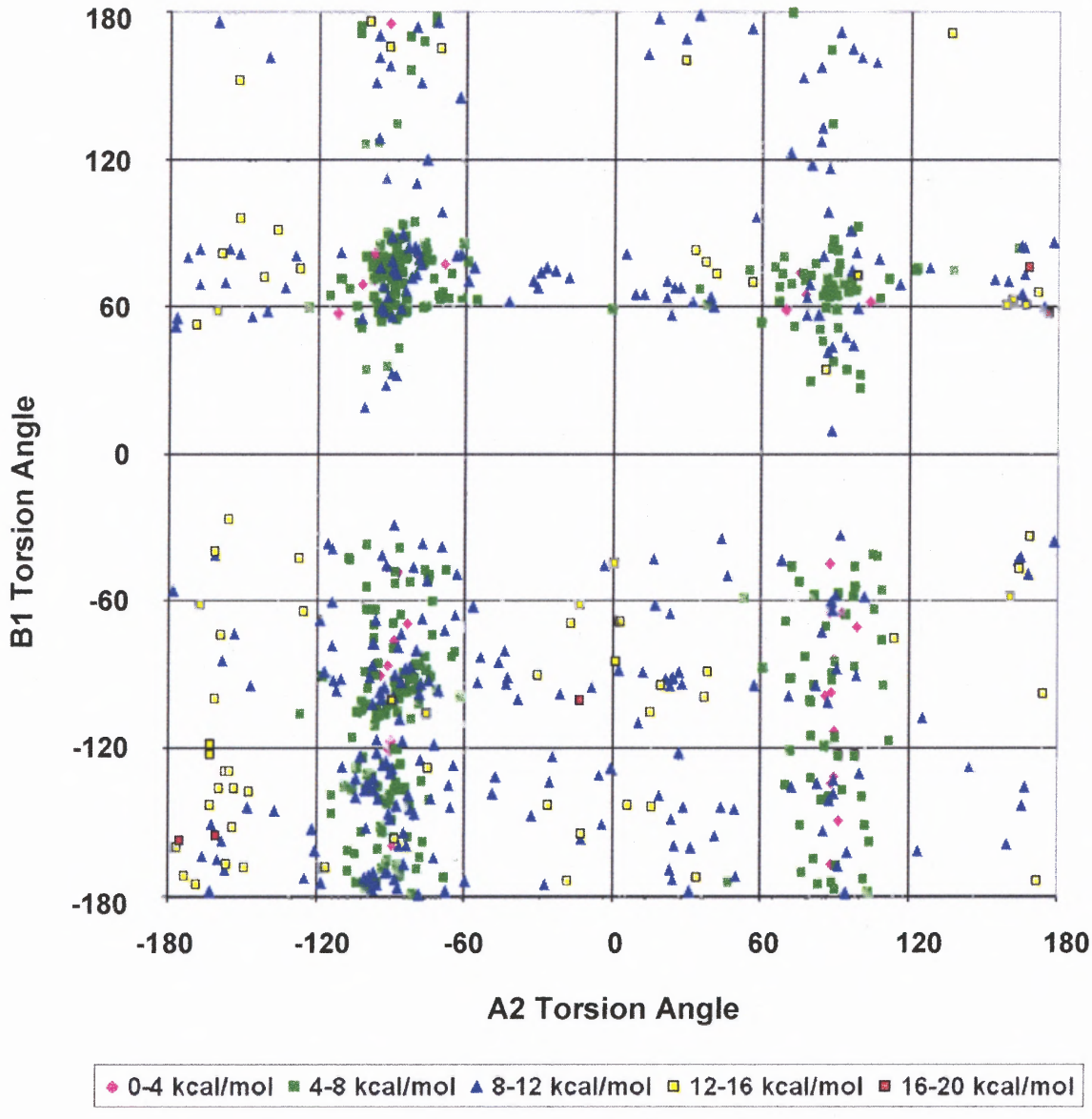

Figure D.5 Protonated DM324 (Tripos, vacuum) B1 vs A2 torsion angles.

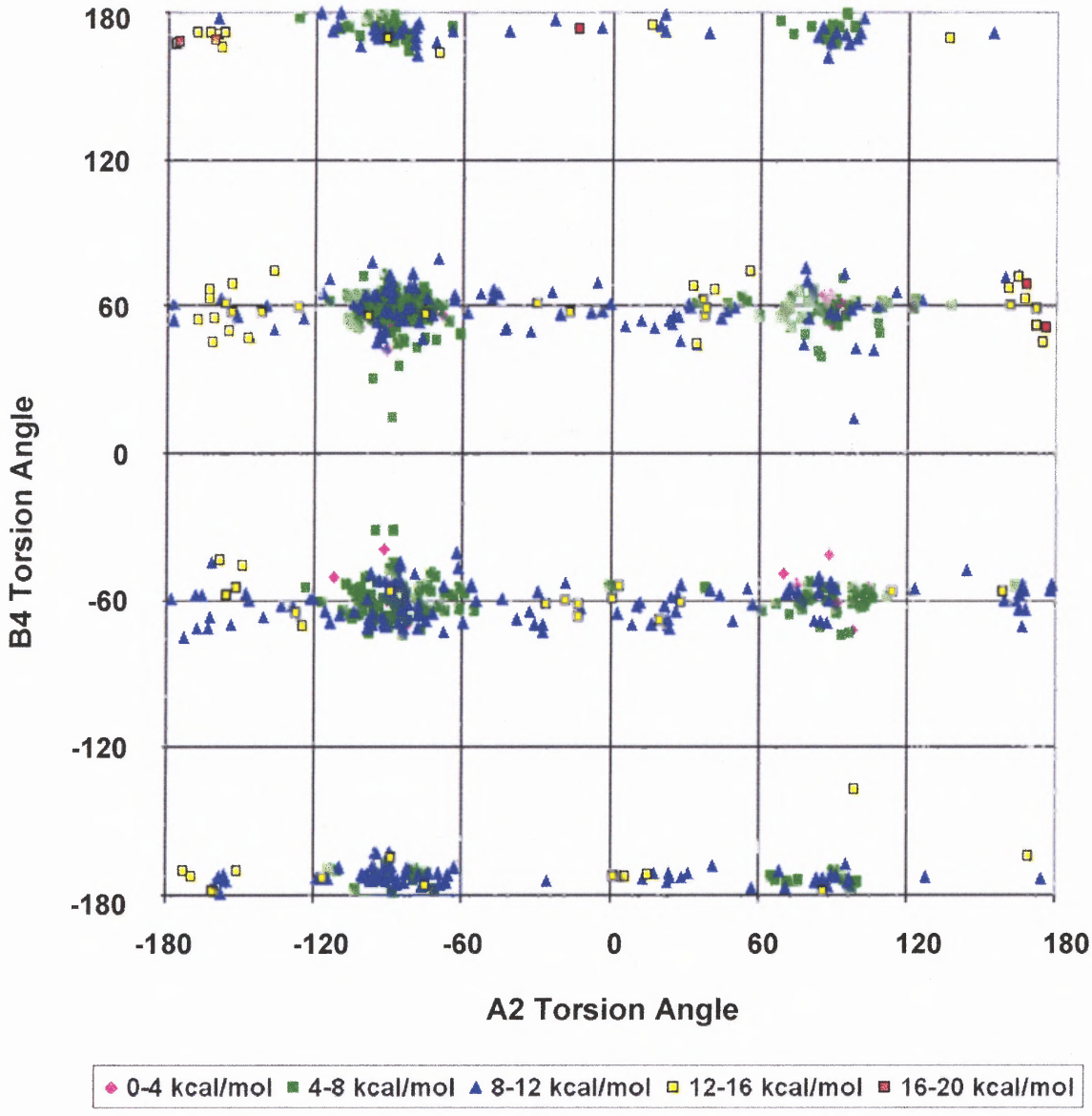

Figure D.6 Protonated DM324 (Tripos, vacuum) B4 vs A2 torsion angles.

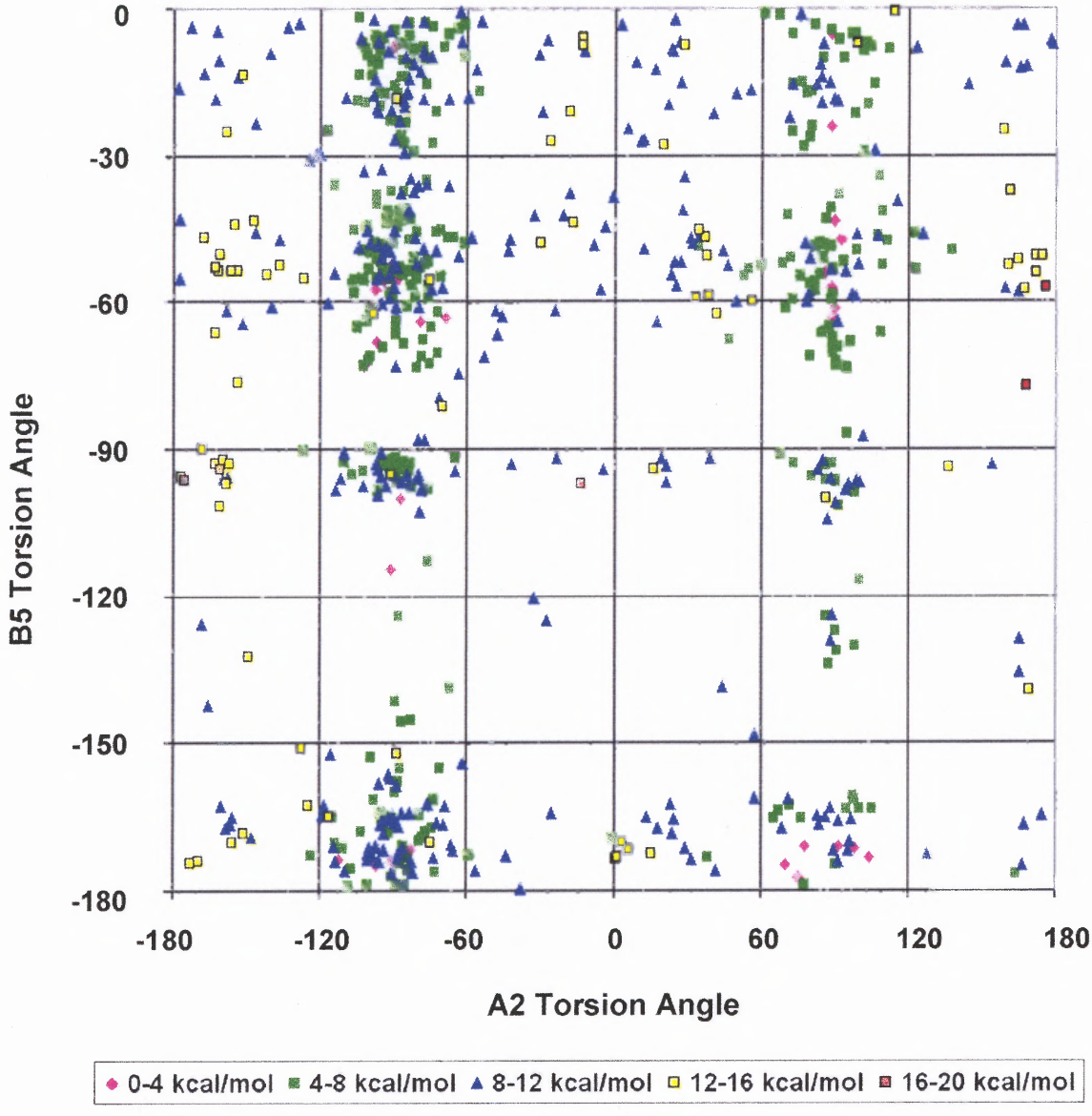

Figure D.7 Protonated DM324 (Tripos, vacuum) B5 vs A2 torsion angles.

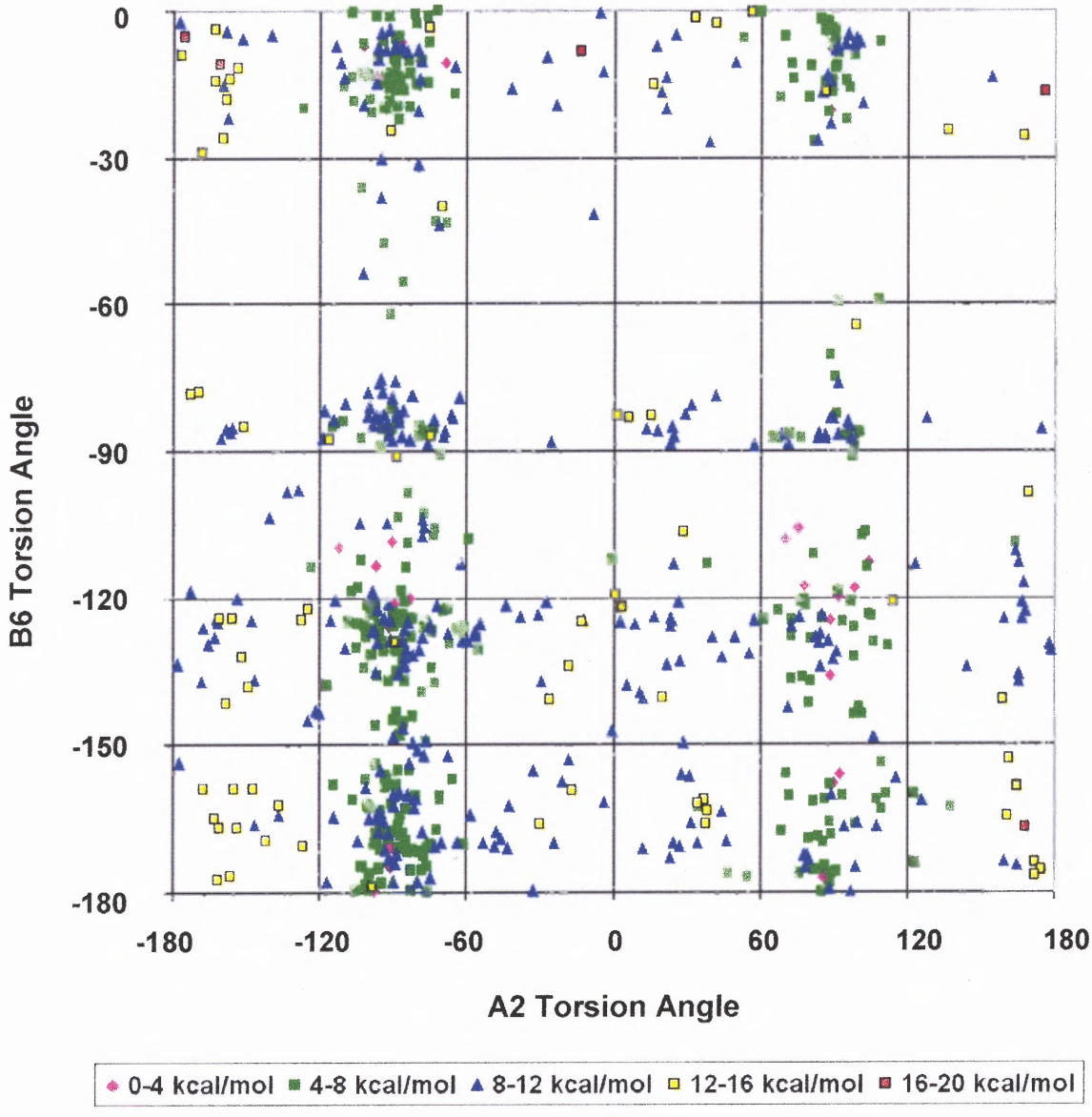

Figure D.8 Protonated DM324 (Tripos, vacuum) B6 vs A2 torsion angles.

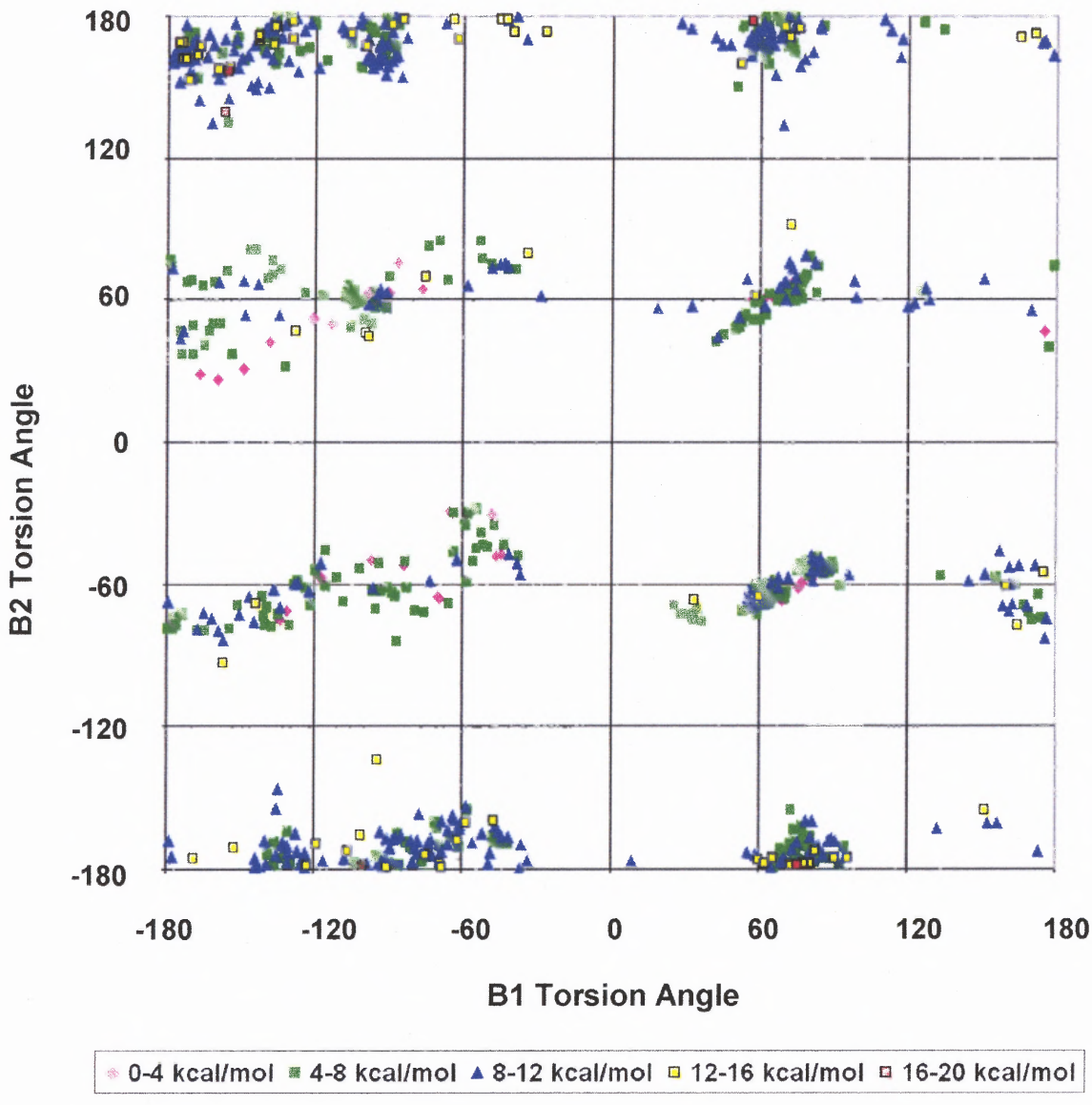

Figure D.9 Protonated DM324 (Tripos, vacuum) B2 vs B1 torsion angles.

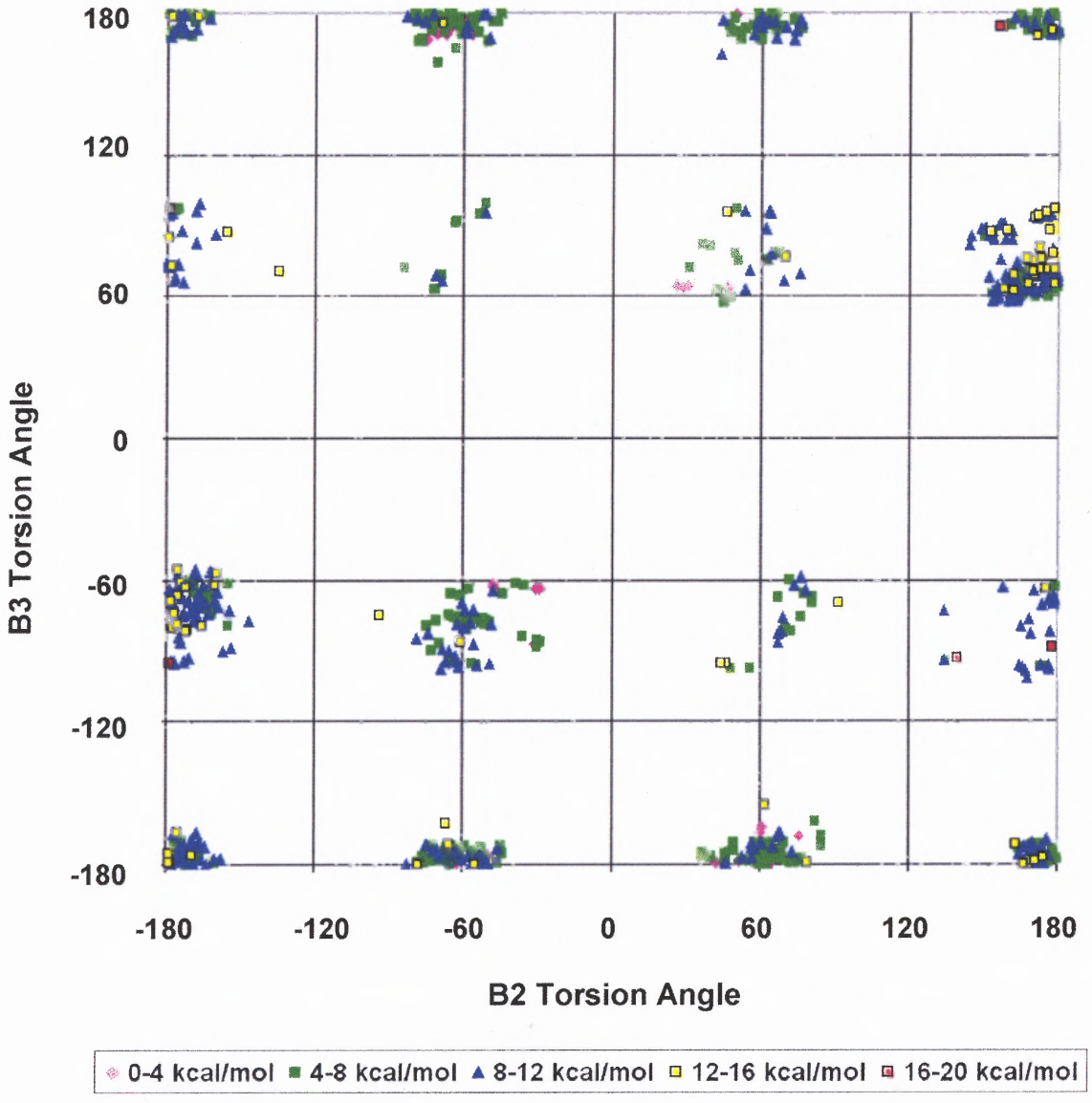

Figure D.10 Protonated DM324 (Tripos, vacuum) B3 vs B2 torsion angles.

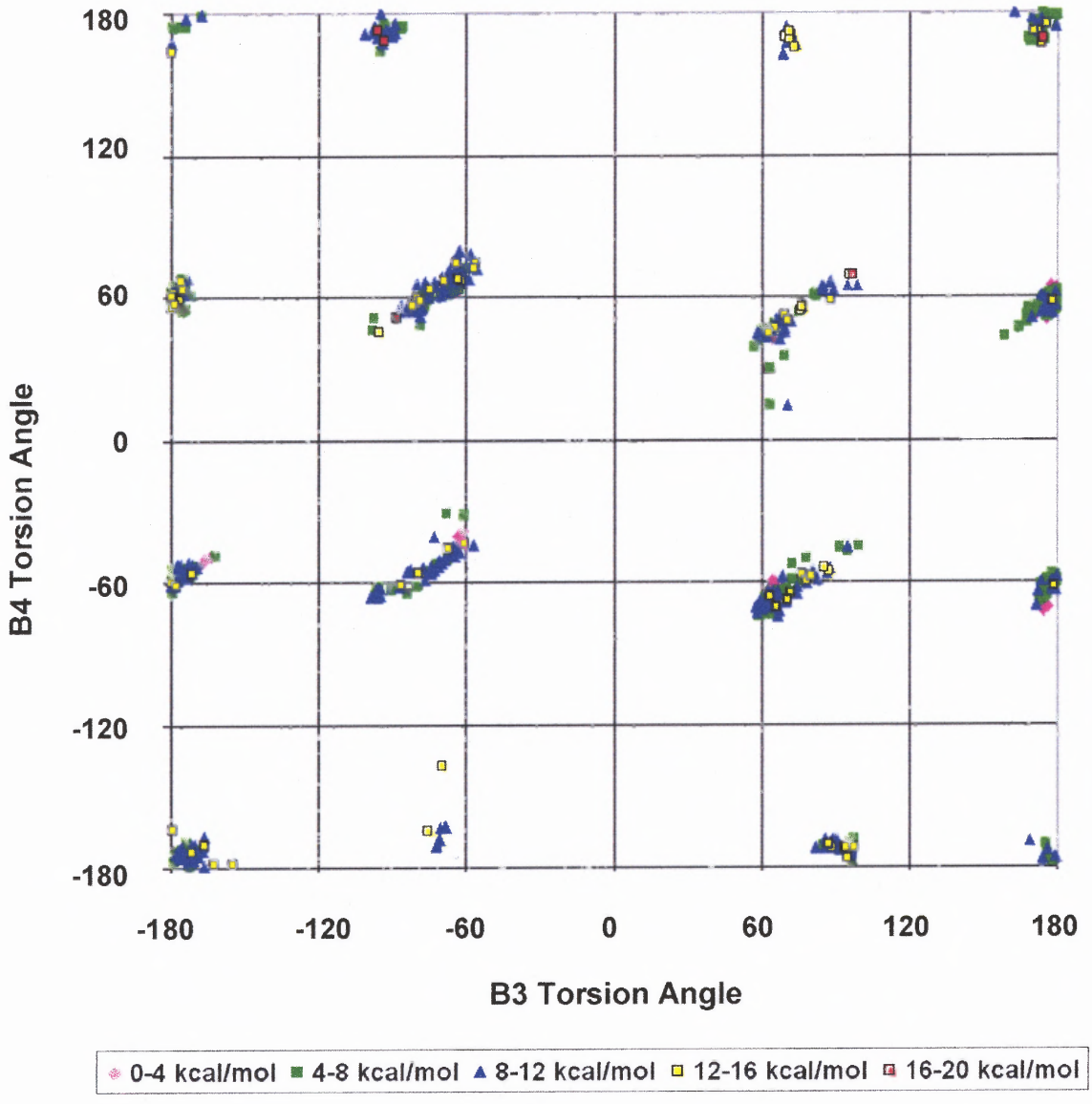

Figure D.11 Protonated DM324 (Tripos, vacuum) B4 vs B3 torsion angles.

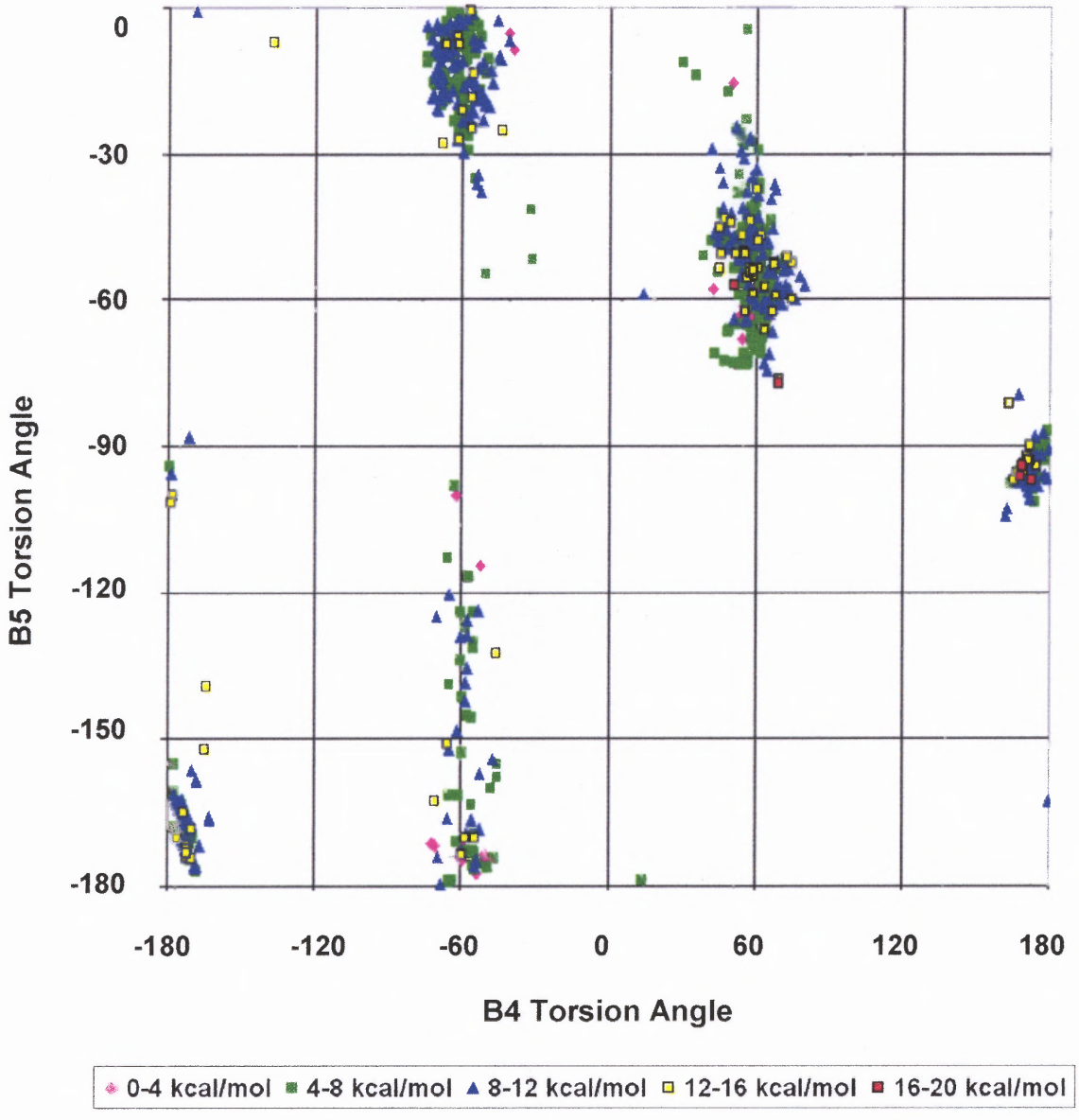

Figure D.82 Protonated DM324 (Tripos, vacuum) B5 vs B4 torsion angles.

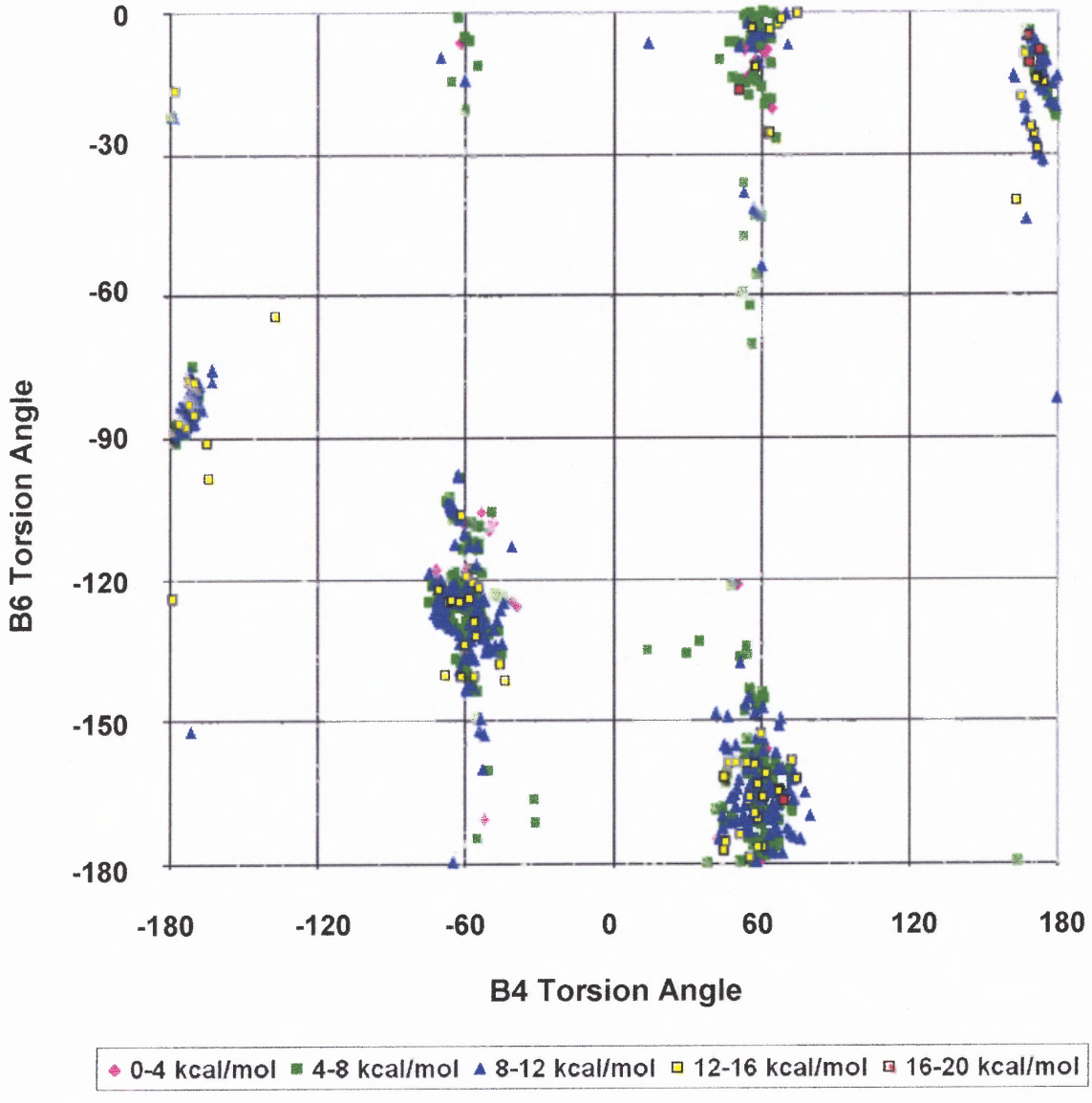

Figure D.83 Protonated DM324 (Tripos, vacuum) B6 vs B4 torsion angles.

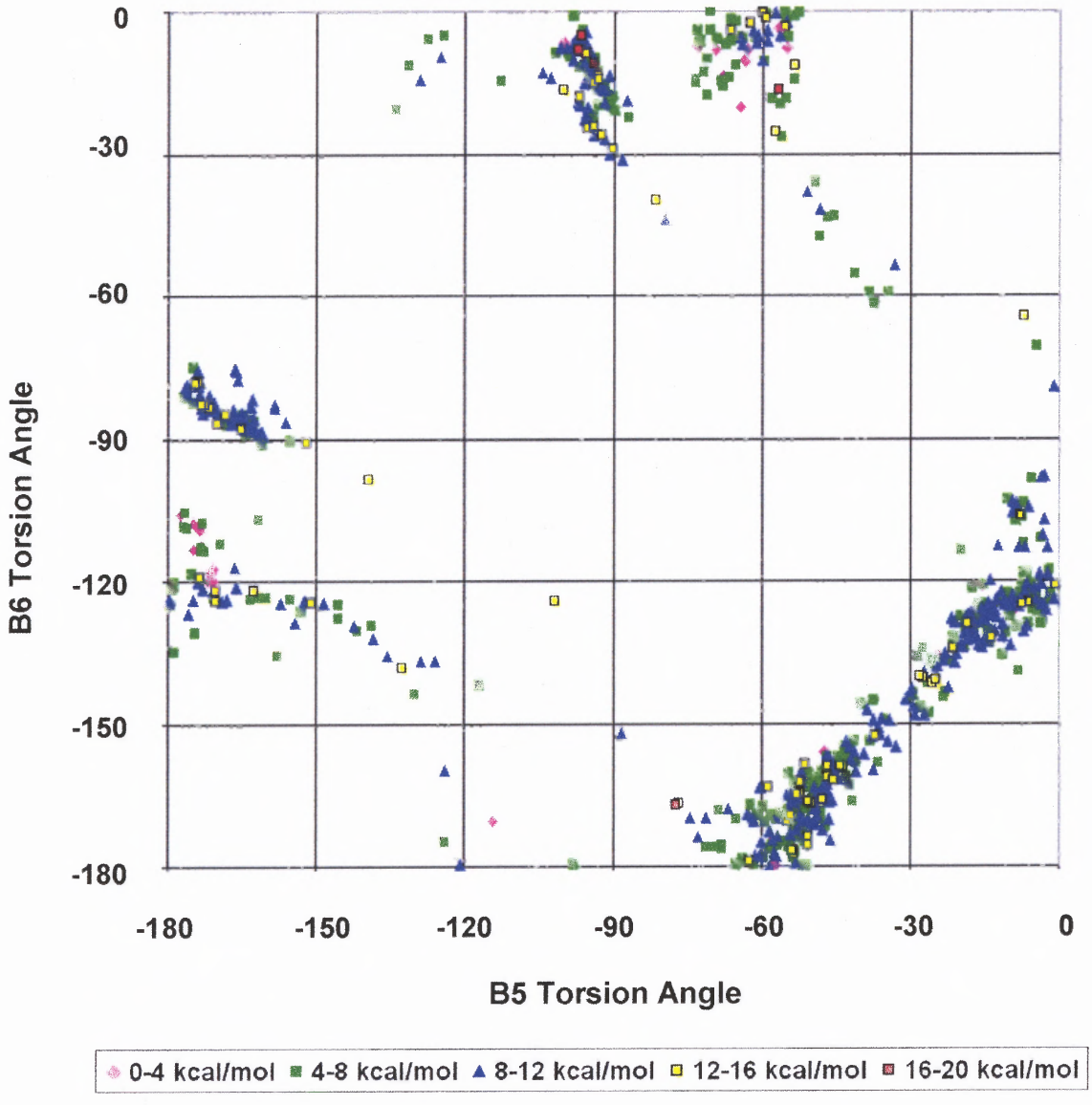

Figure D.84 Protonated DM324 (Tripos, vacuum) B6 vs B5 torsion angles.

D.2 Tripos for DM324 and Solvent

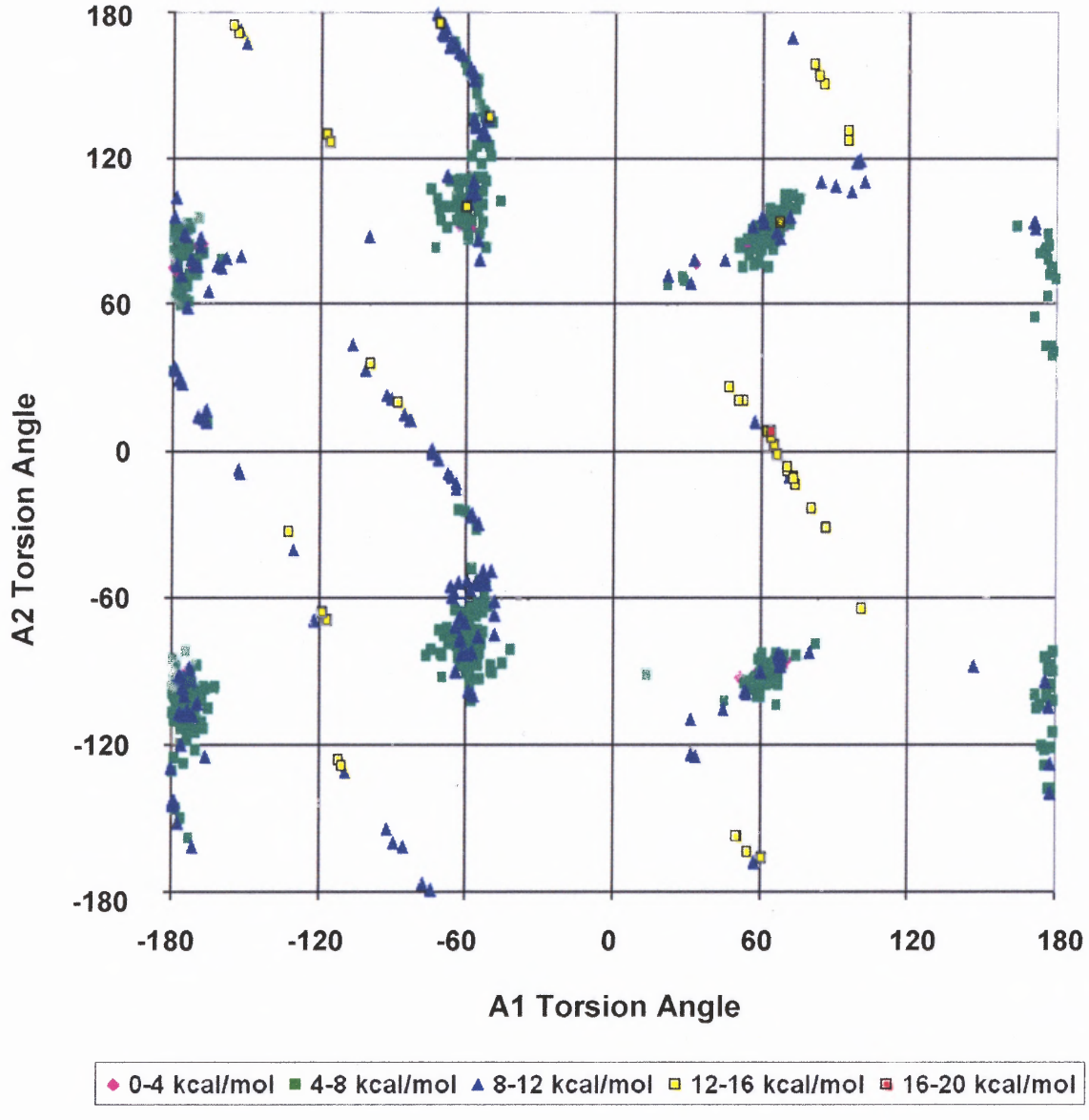

Figure D.15 Protonated DM324 (Tripos, solvent) A2 vs A1 torsion angles.

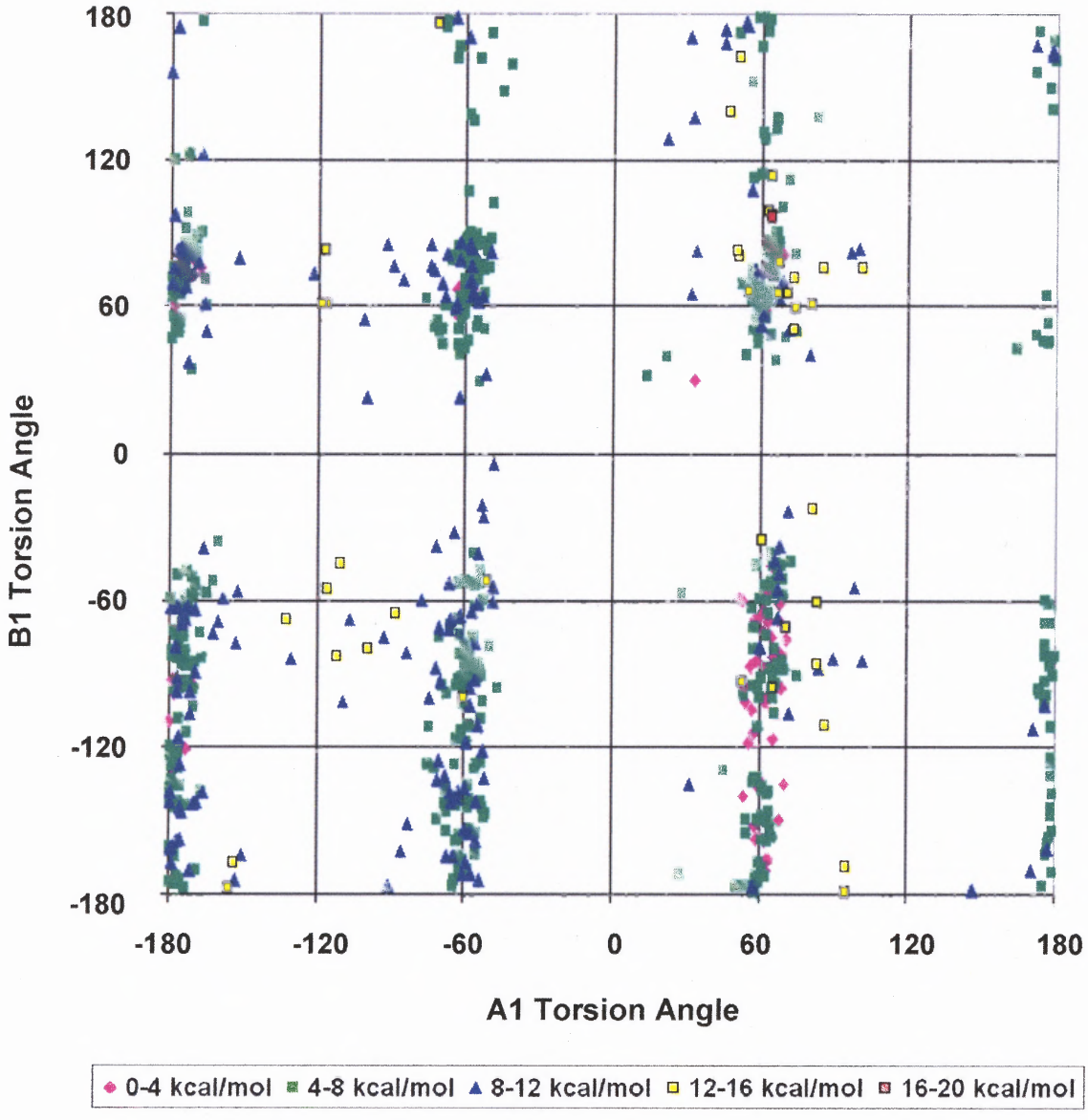

Figure D.16 Protonated DM324 (Tripos, solvent) B1 vs A1 torsion angles.

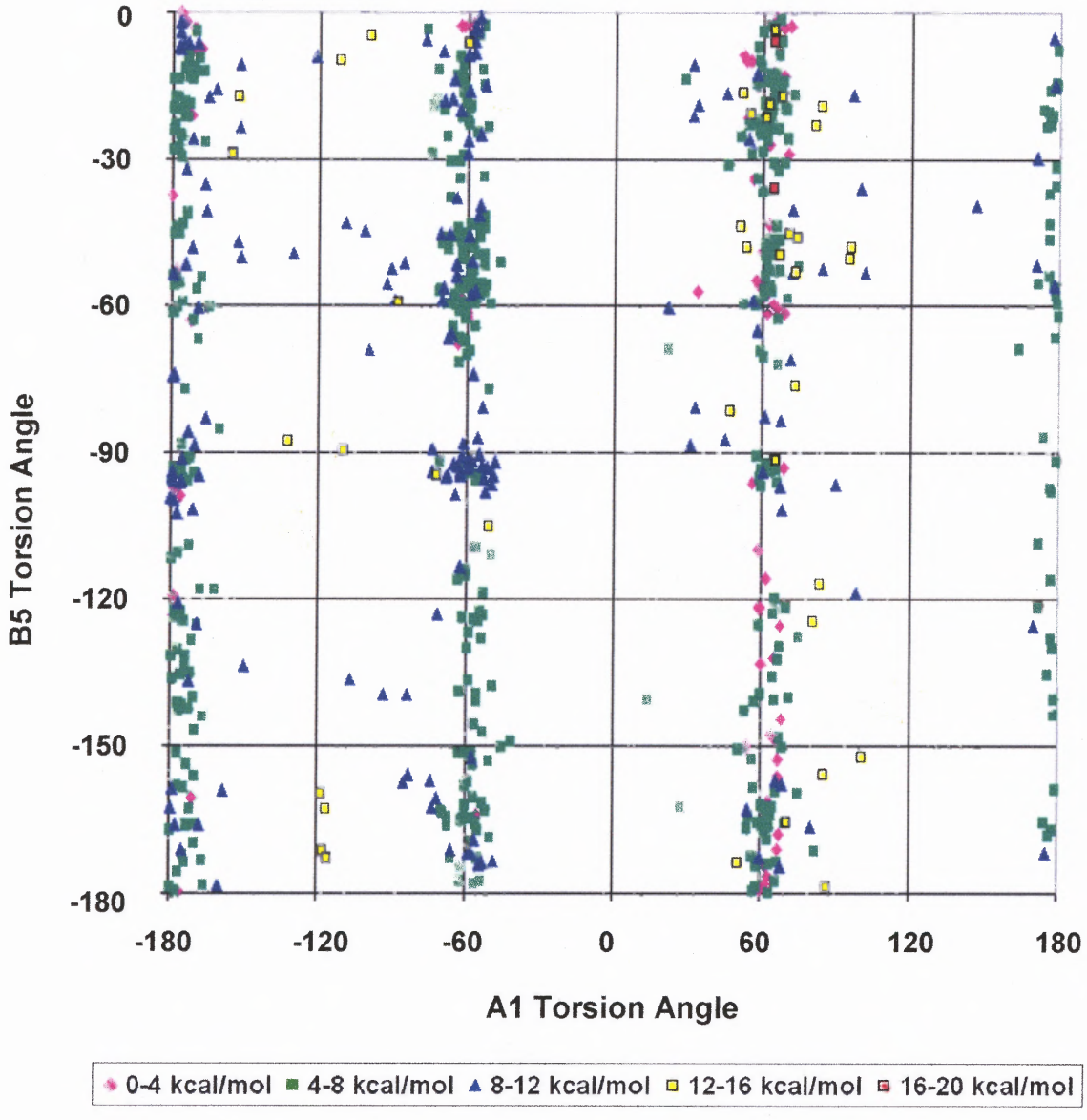

Figure D.17 Protonated DM324 (Tripos, solvent) B5 vs A1 torsion angles.

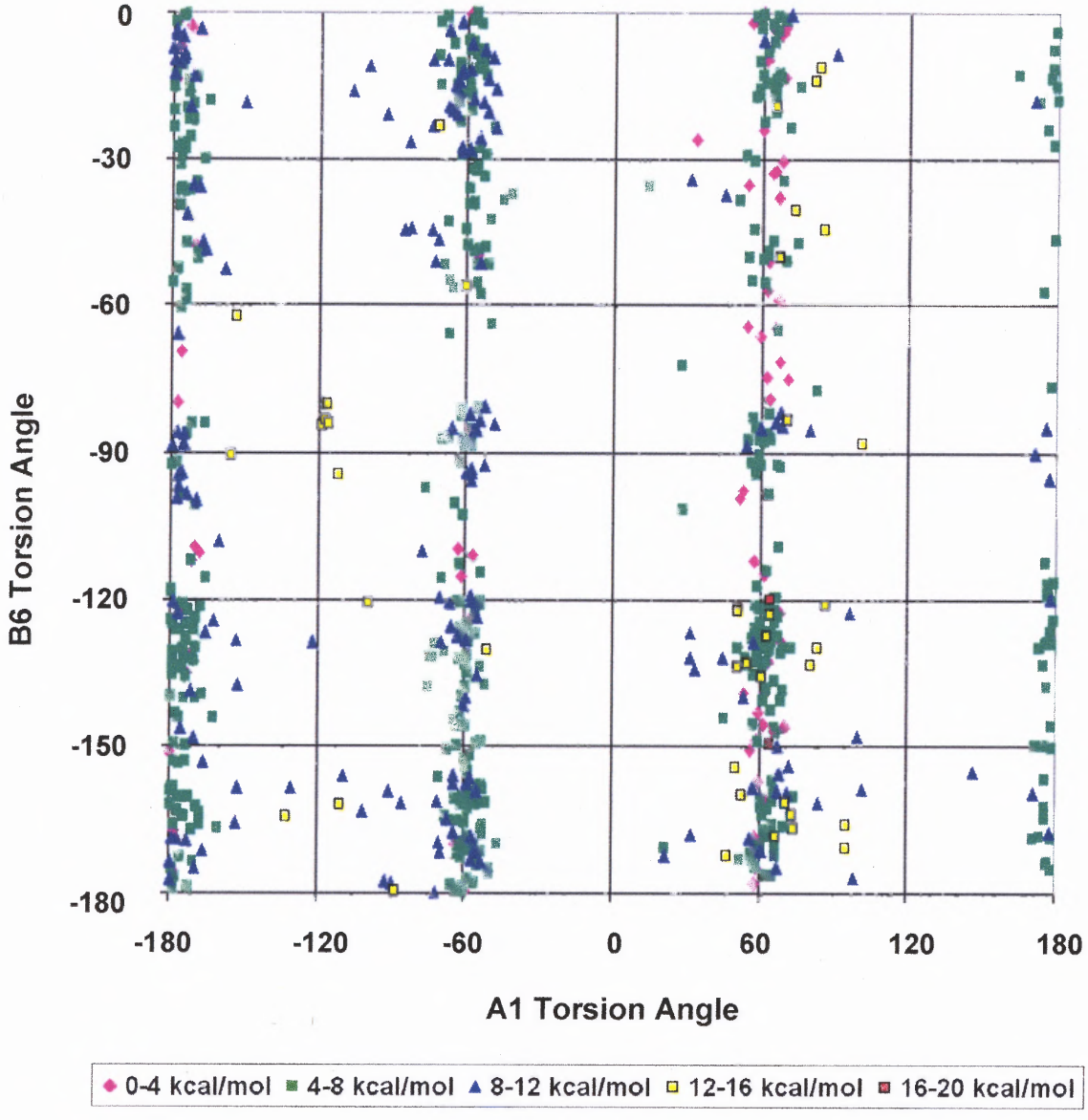

Figure D.18 Protonated DM324 (Tripos, solvent) B6 vs A1 torsion angles.

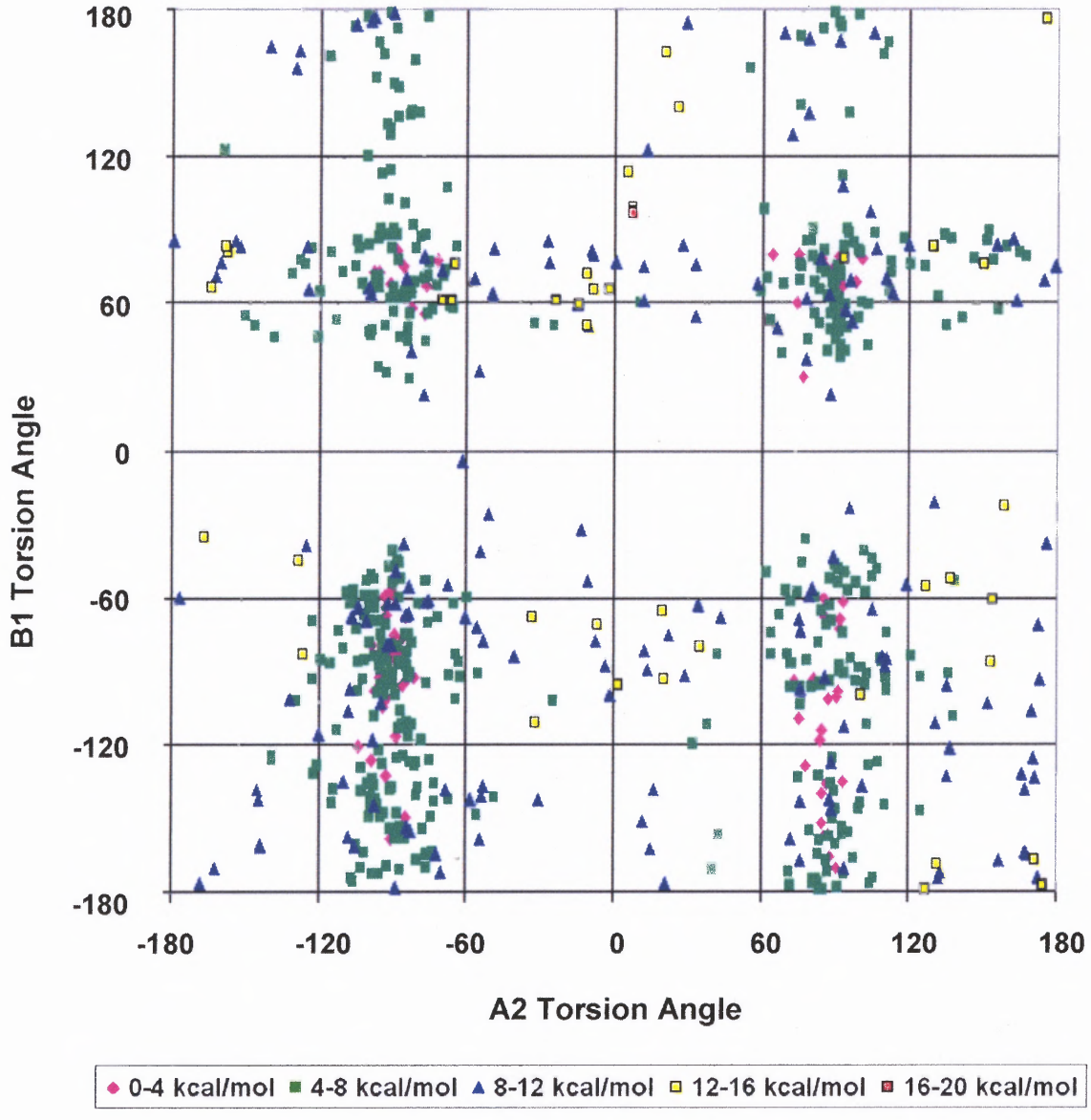

Figure D.19 Protonated DM324 (Tripos, solvent) B1 vs A2 torsion angles.

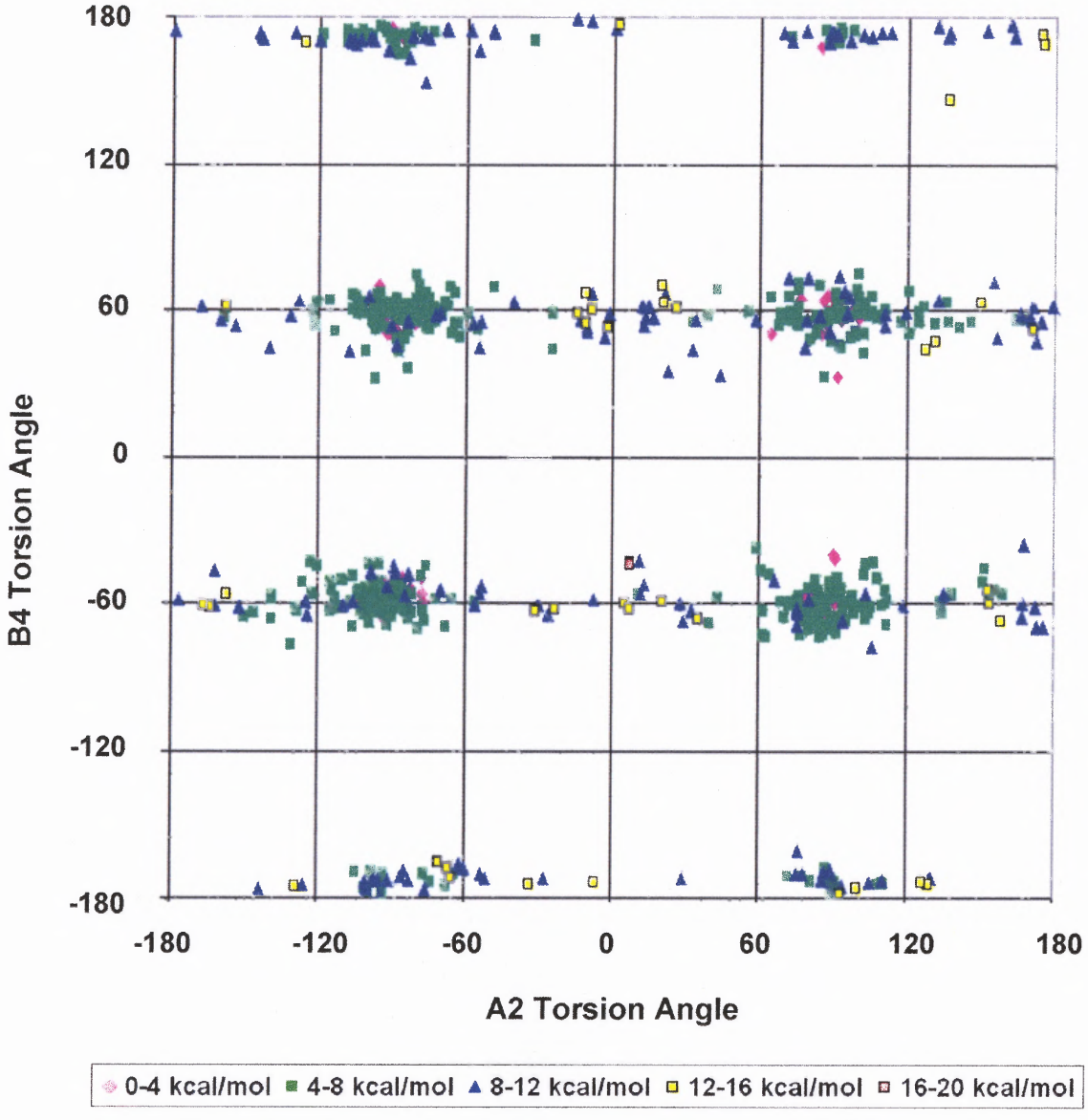

Figure D.20 Protonated DM324 (Tripos, solvent) B4 vs A2 torsion angles.

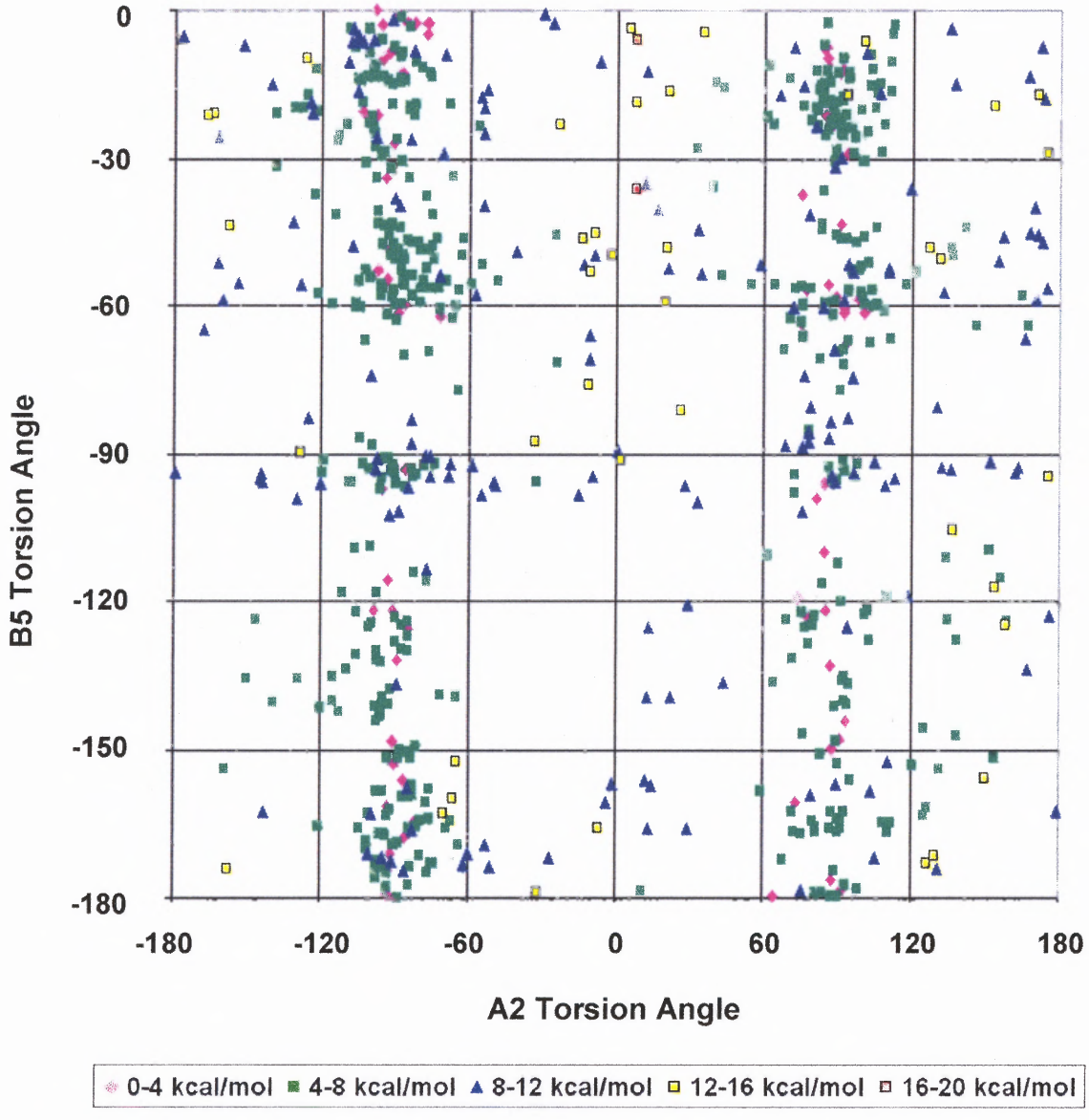

Figure D.21 Protonated DM324 (Tripos, solvent) B5 vs A2 torsion angles.

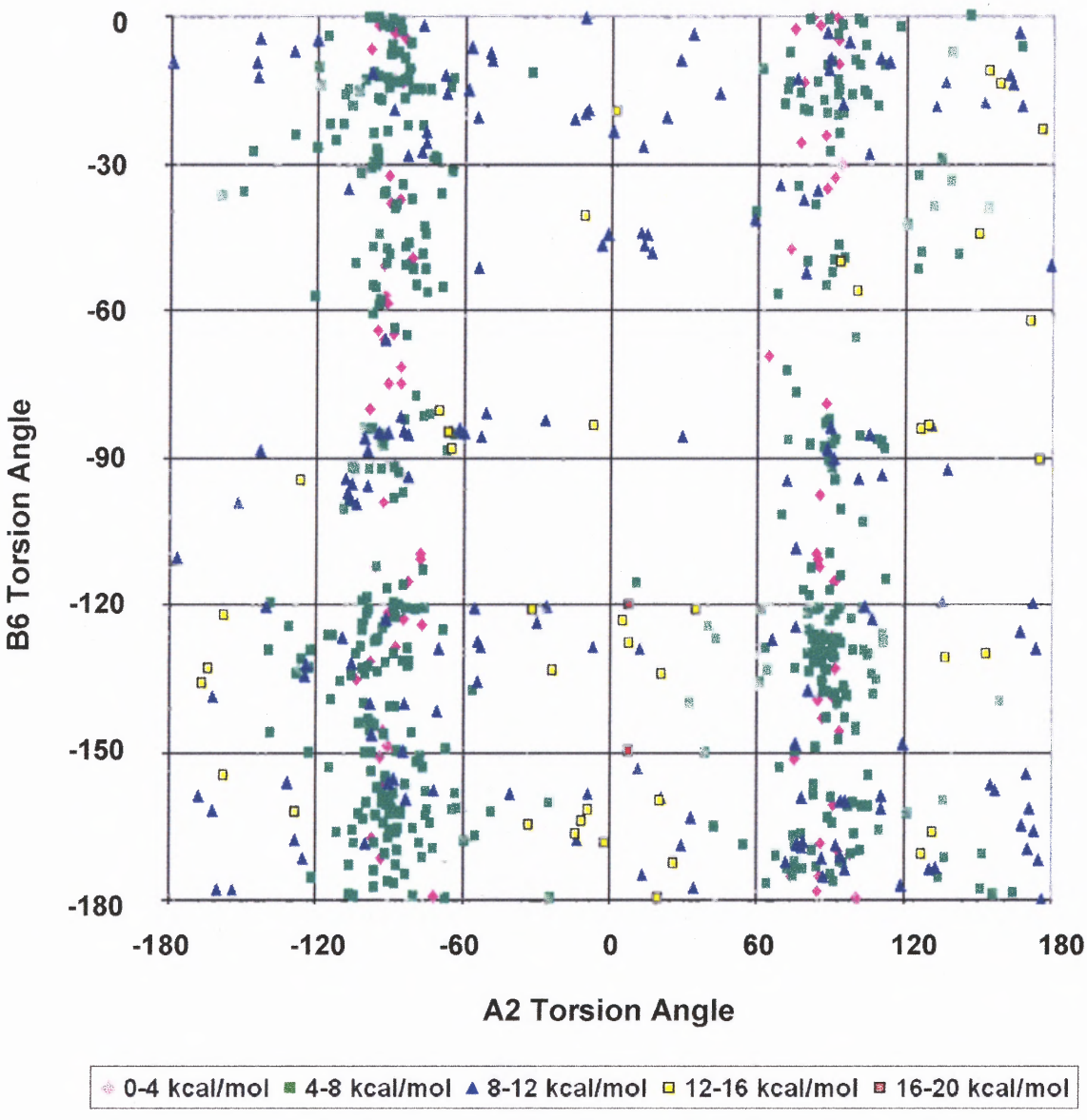

Figure D.22 Protonated DM324 (Tripos, solvent) B6 vs A2 torsion angles.

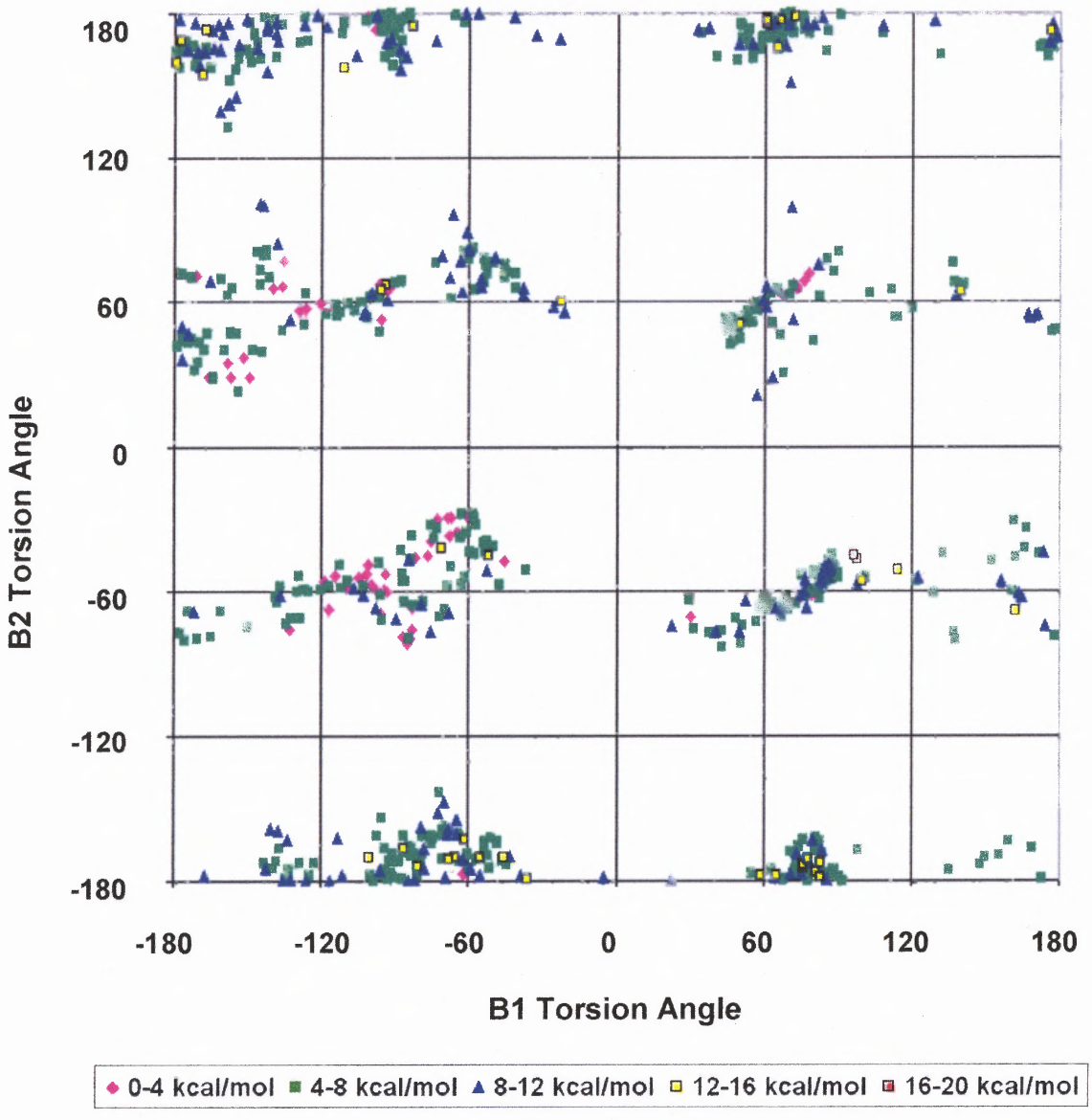

Figure D.23 Protonated DM324 (Tripos, solvent) B2 vs B1 torsion angles.

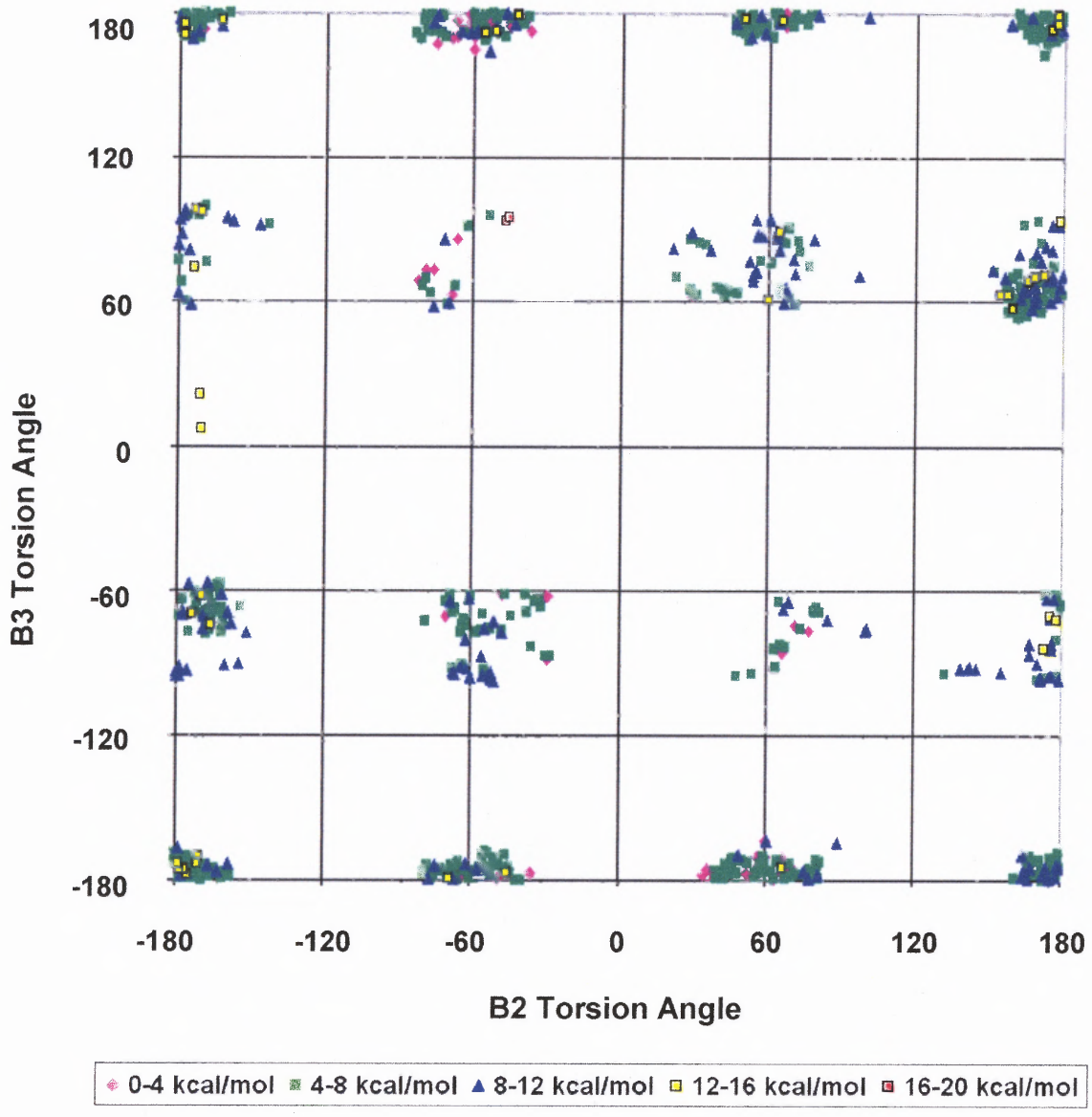

Figure D.24 Protonated DM324 (Tripos, solvent) B3 vs B2 torsion angles.

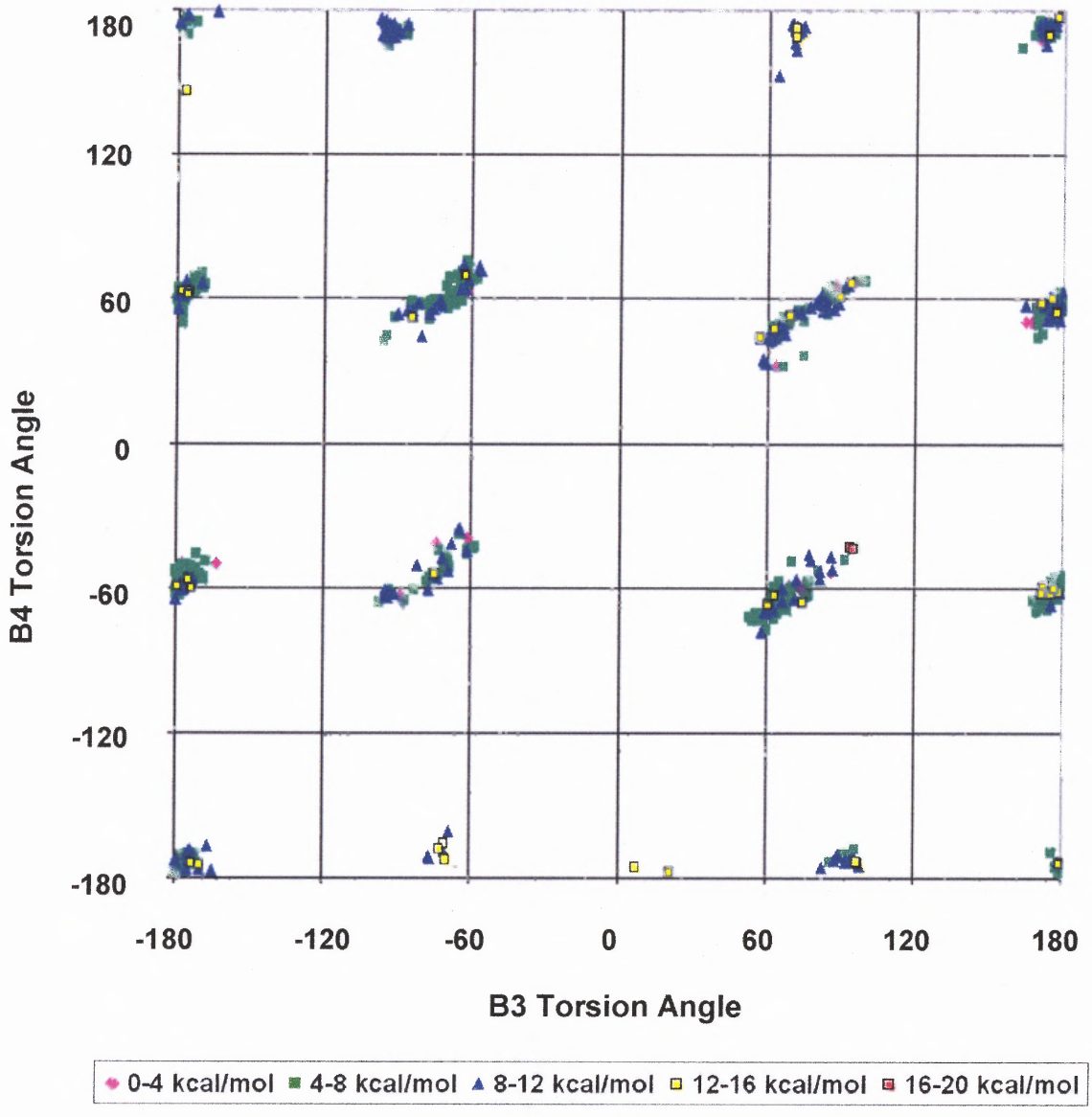

Figure D.25 Protonated DM324 (Tripos, solvent) B4 vs B3 torsion angles.

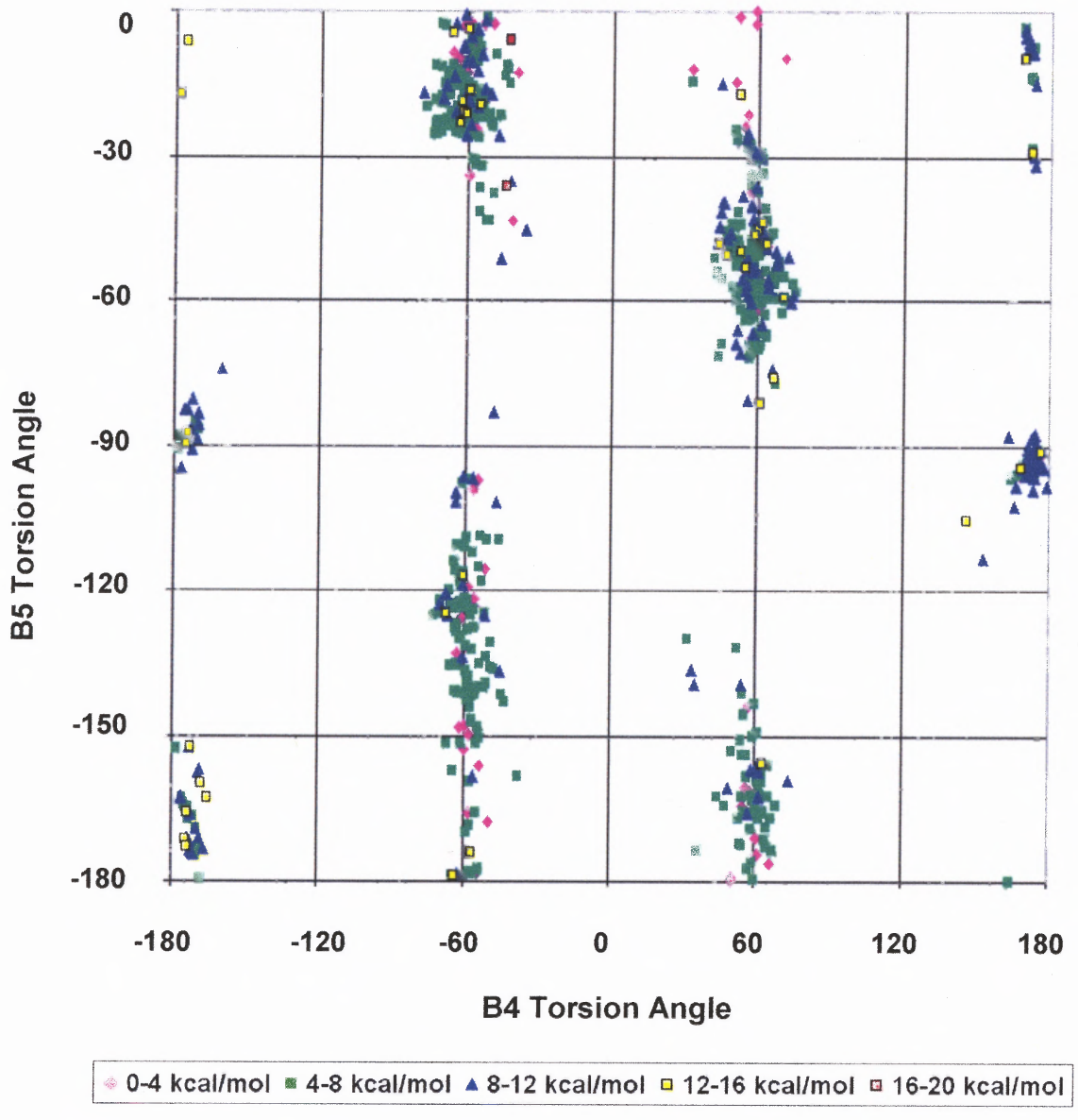

Figure D.26 Protonated DM324 (Tripos, solvent) B5 vs B4 torsion angles.

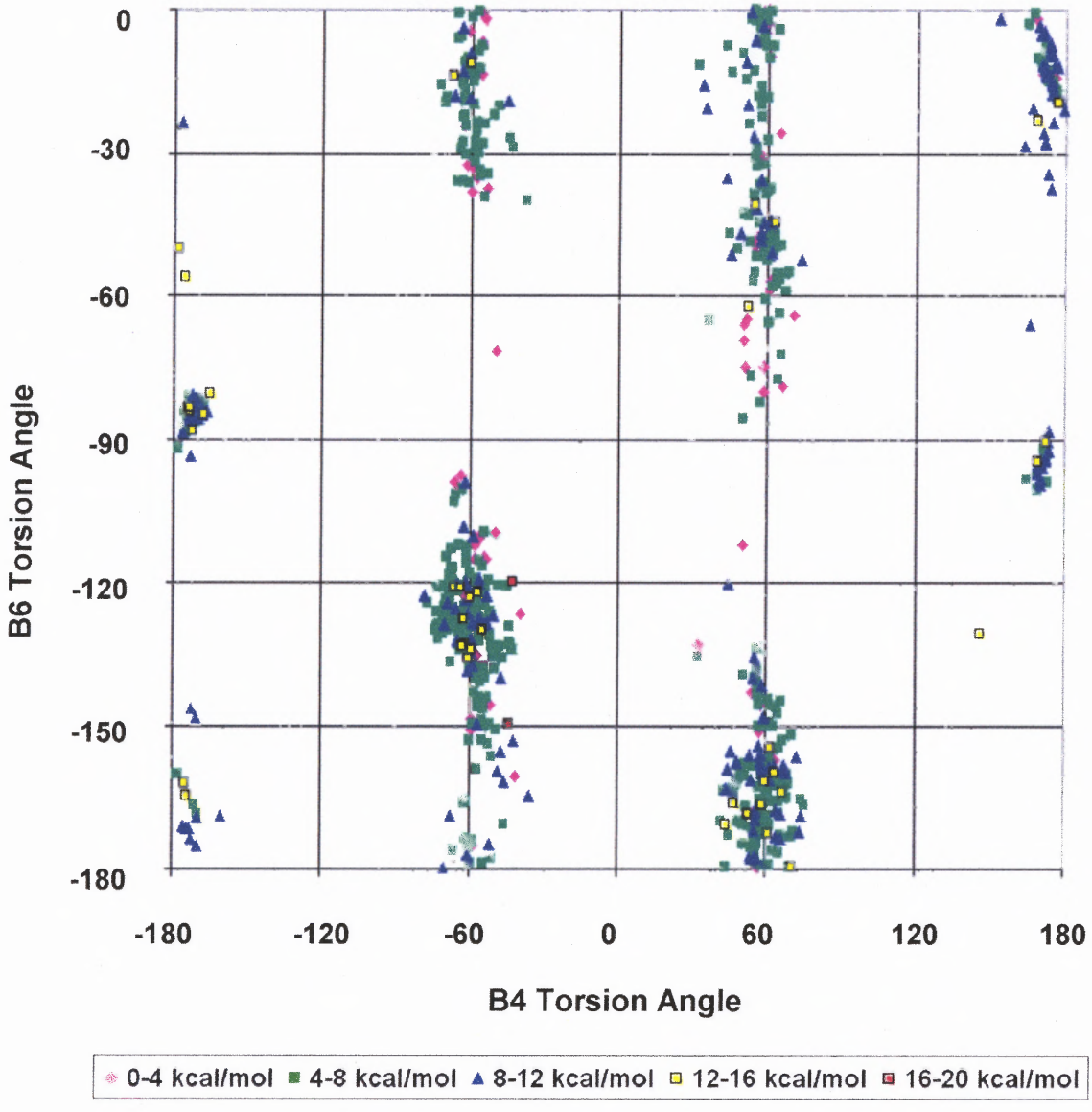

Figure D.27 Protonated DM324 (Tripos, solvent) B6 vs B4 torsion angles.

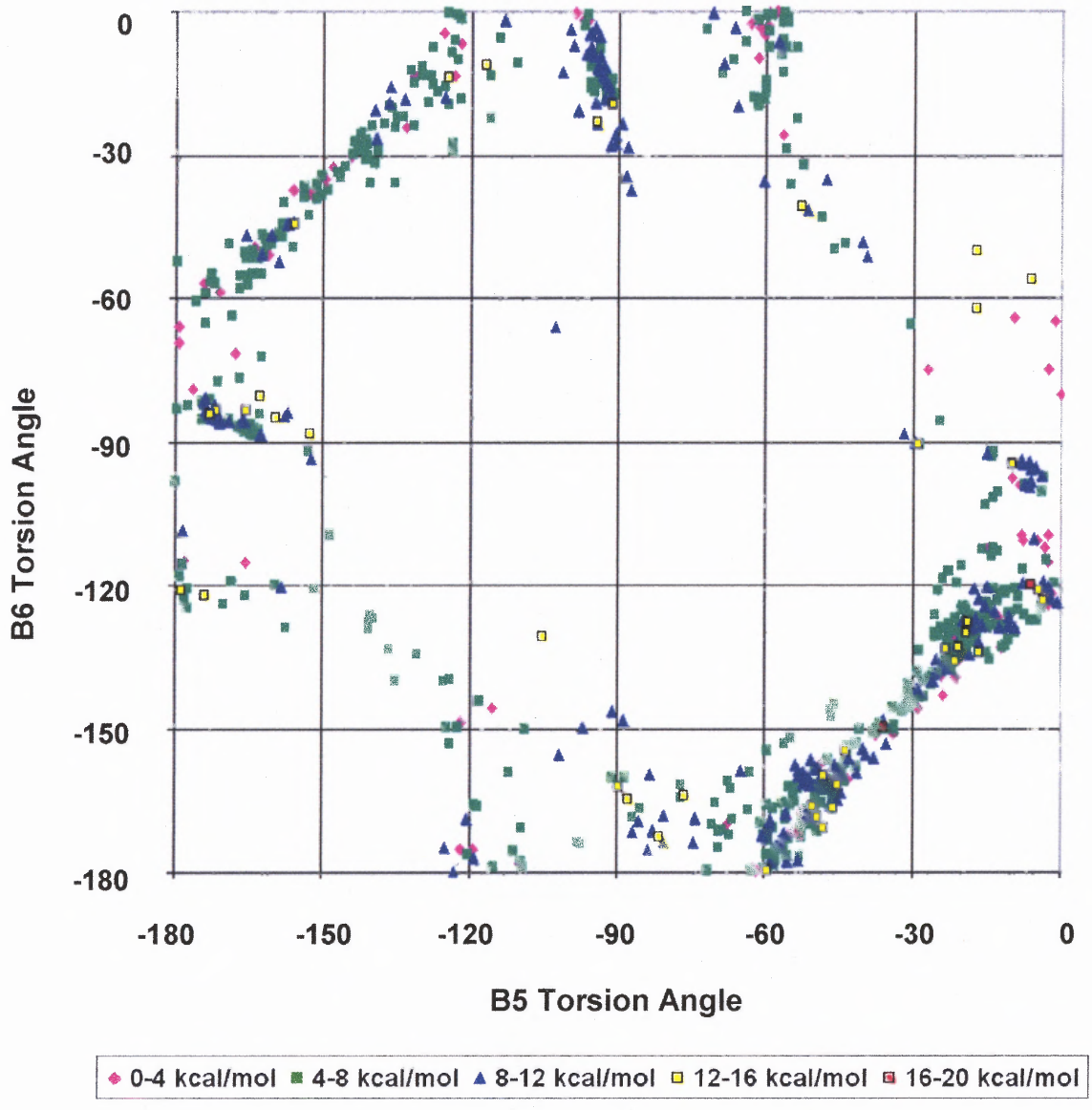

Figure D.28 Protonated DM324 (Tripos, solvent) B6 vs B5 torsion angles.

D.3 Tripos for DM324 and Vacuum – Second Set of Results

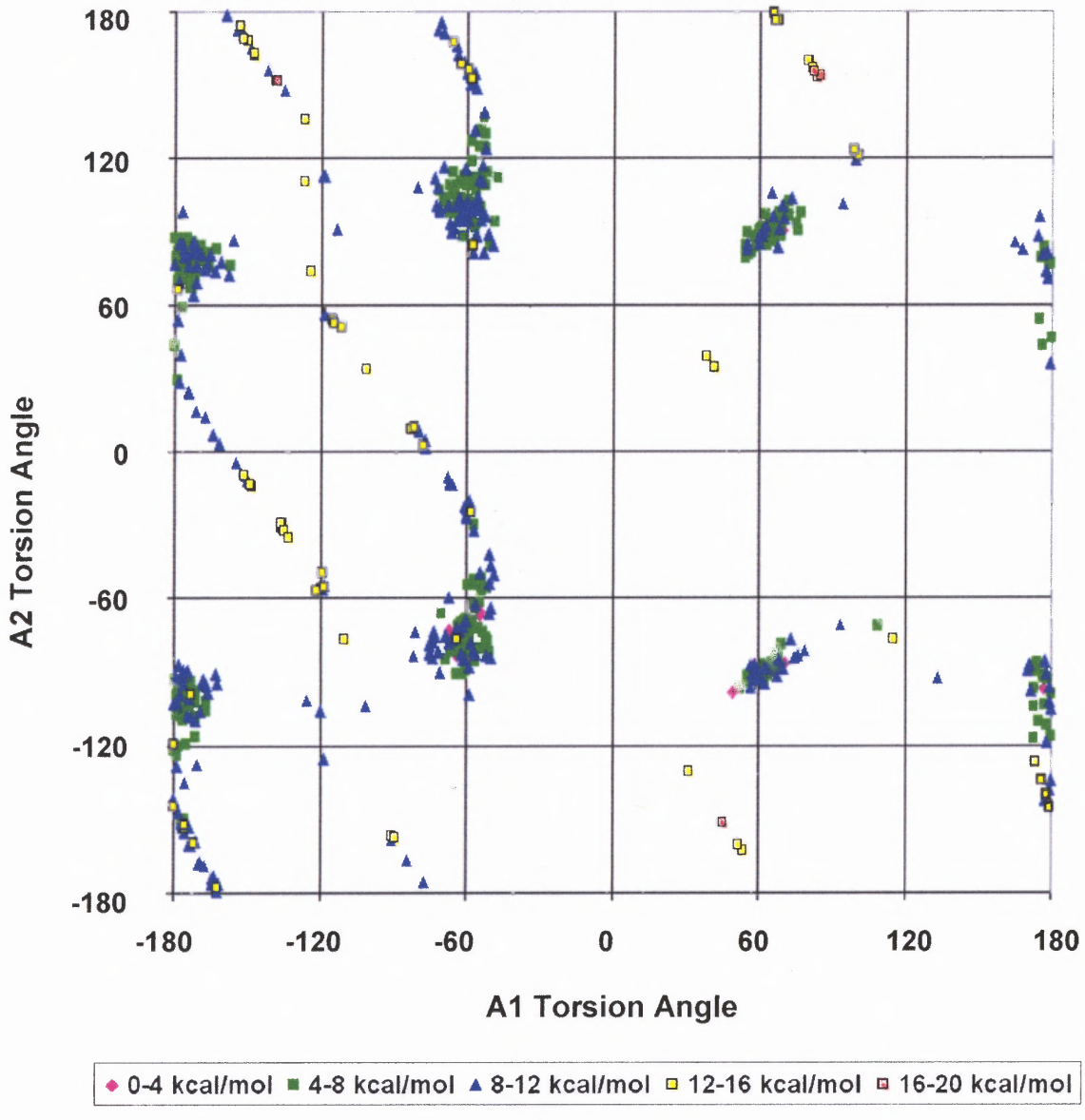

Figure D.29 Protonated DM324 (Tripos, 2nd vacuum) A2 vs A1 torsion angles.

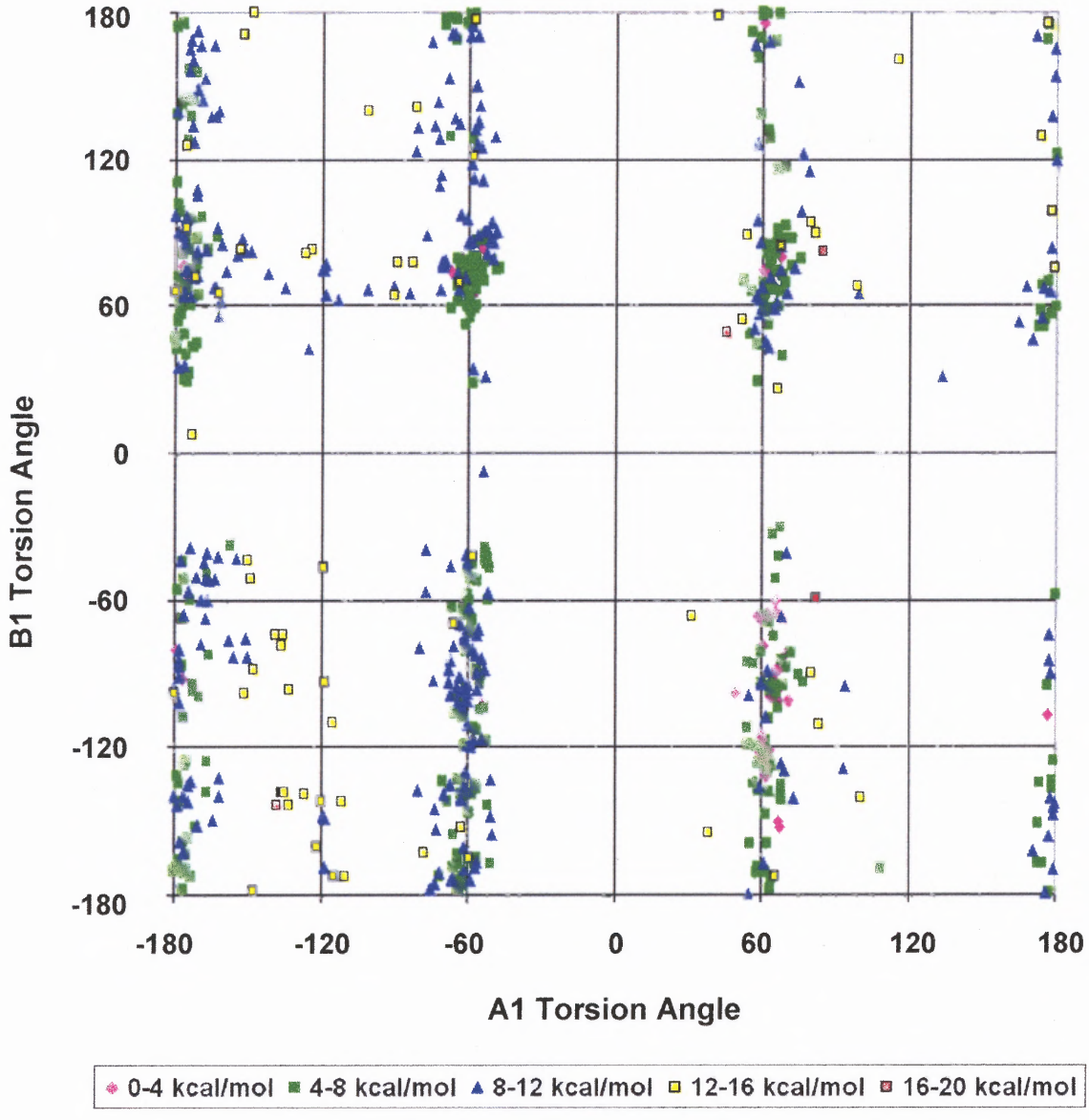

Figure D.30 Protonated DM324 (Tripos, 2nd vacuum) B1 vs A1 torsion angles.

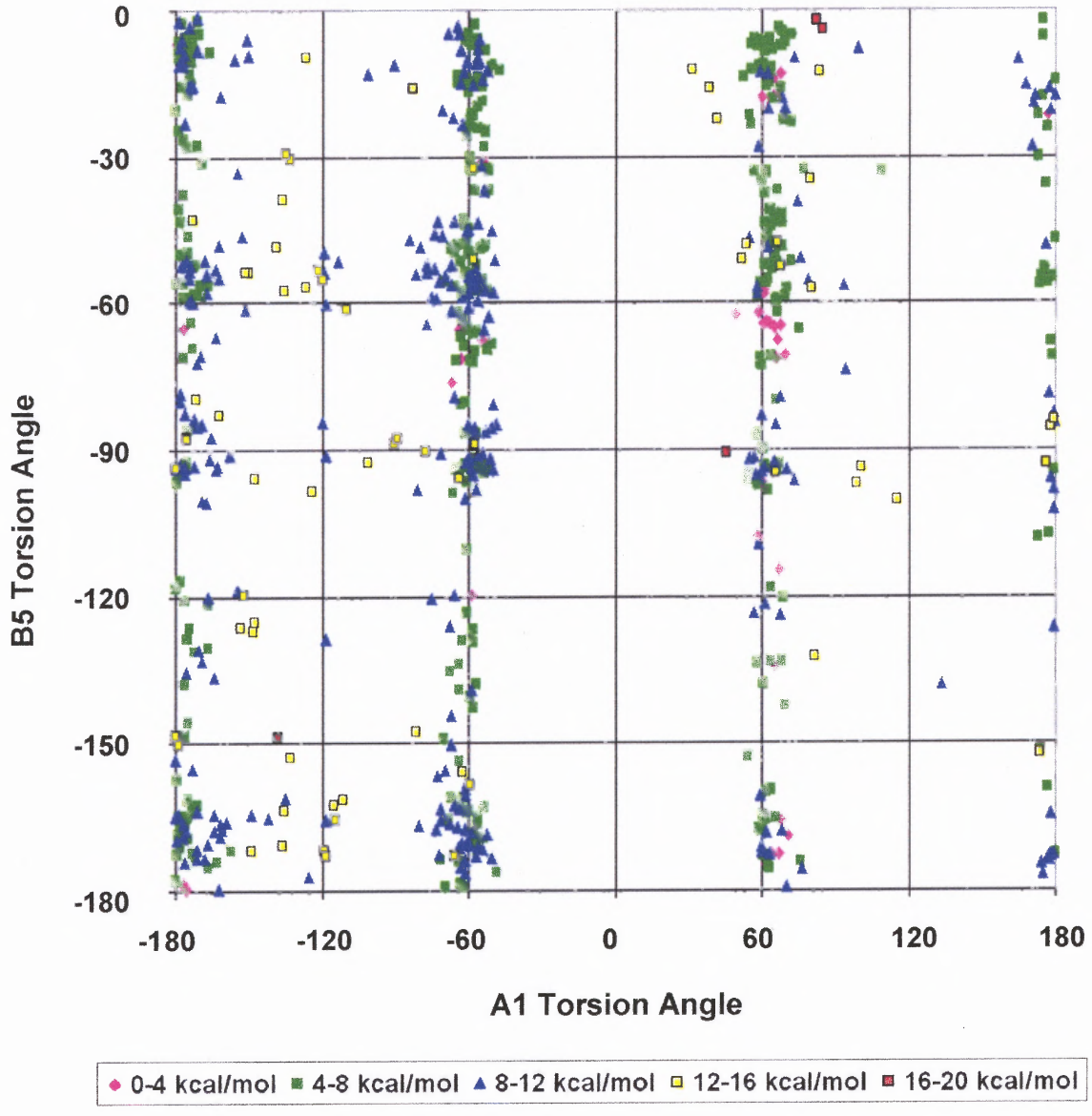

Figure D.31 Protonated DM324 (Tripos, 2nd vacuum) B5 vs A1 torsion angles.

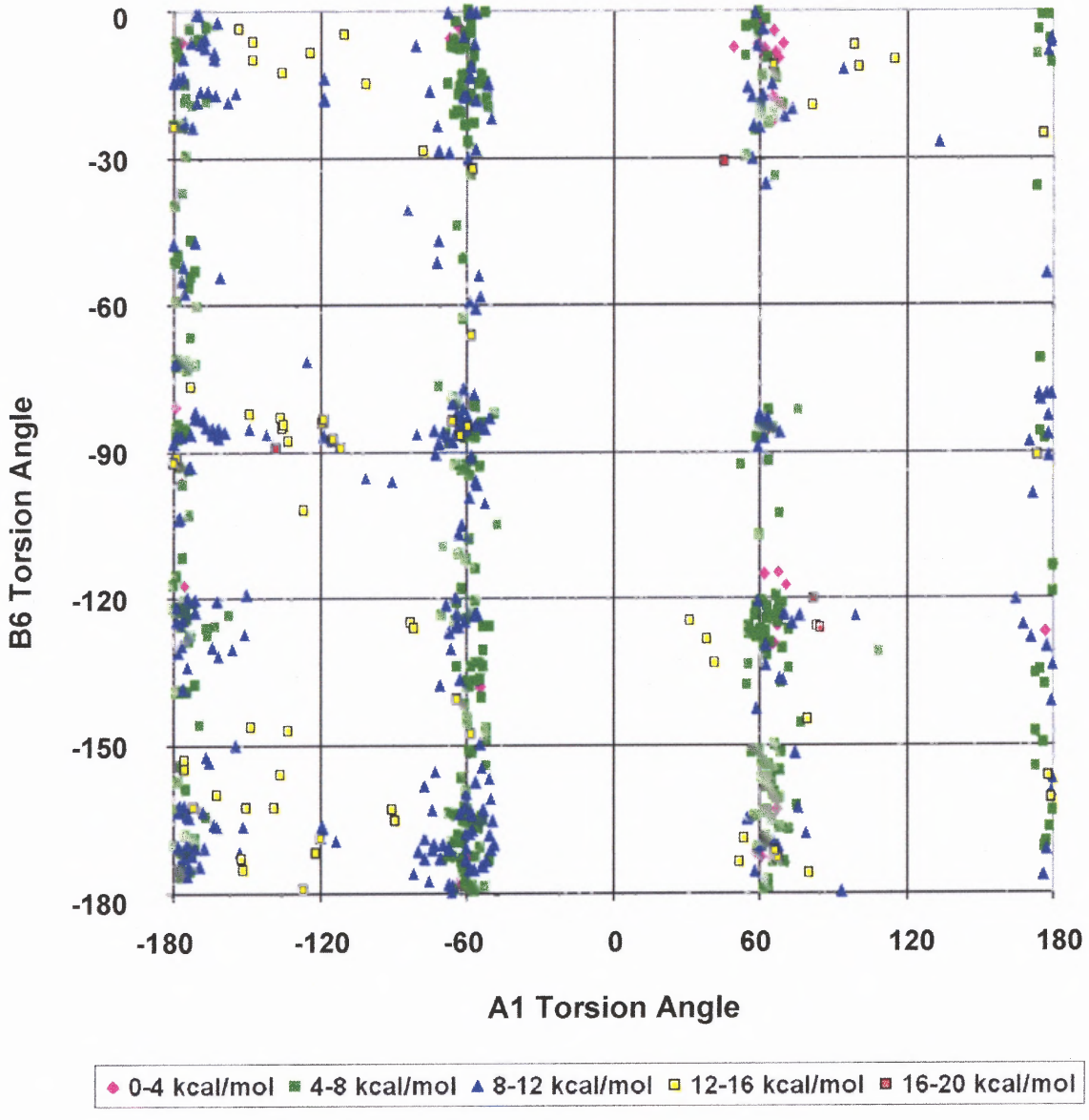

Figure D.32 Protonated DM324 (Tripos, 2nd vacuum) B6 vs A1 torsion angles.

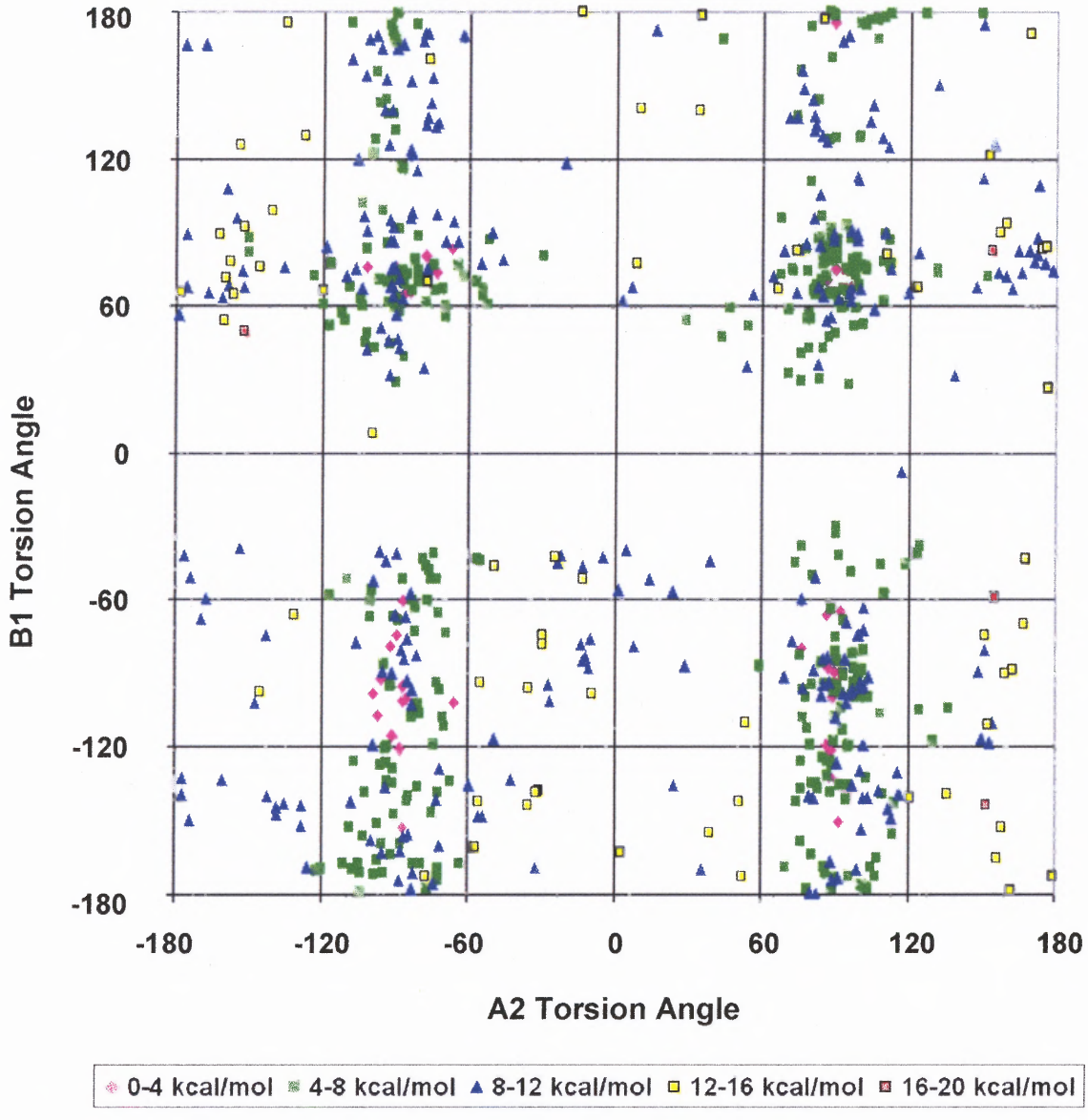

Figure D.33 Protonated DM324 (Tripos, 2nd vacuum) B1 vs A2 torsion angles.

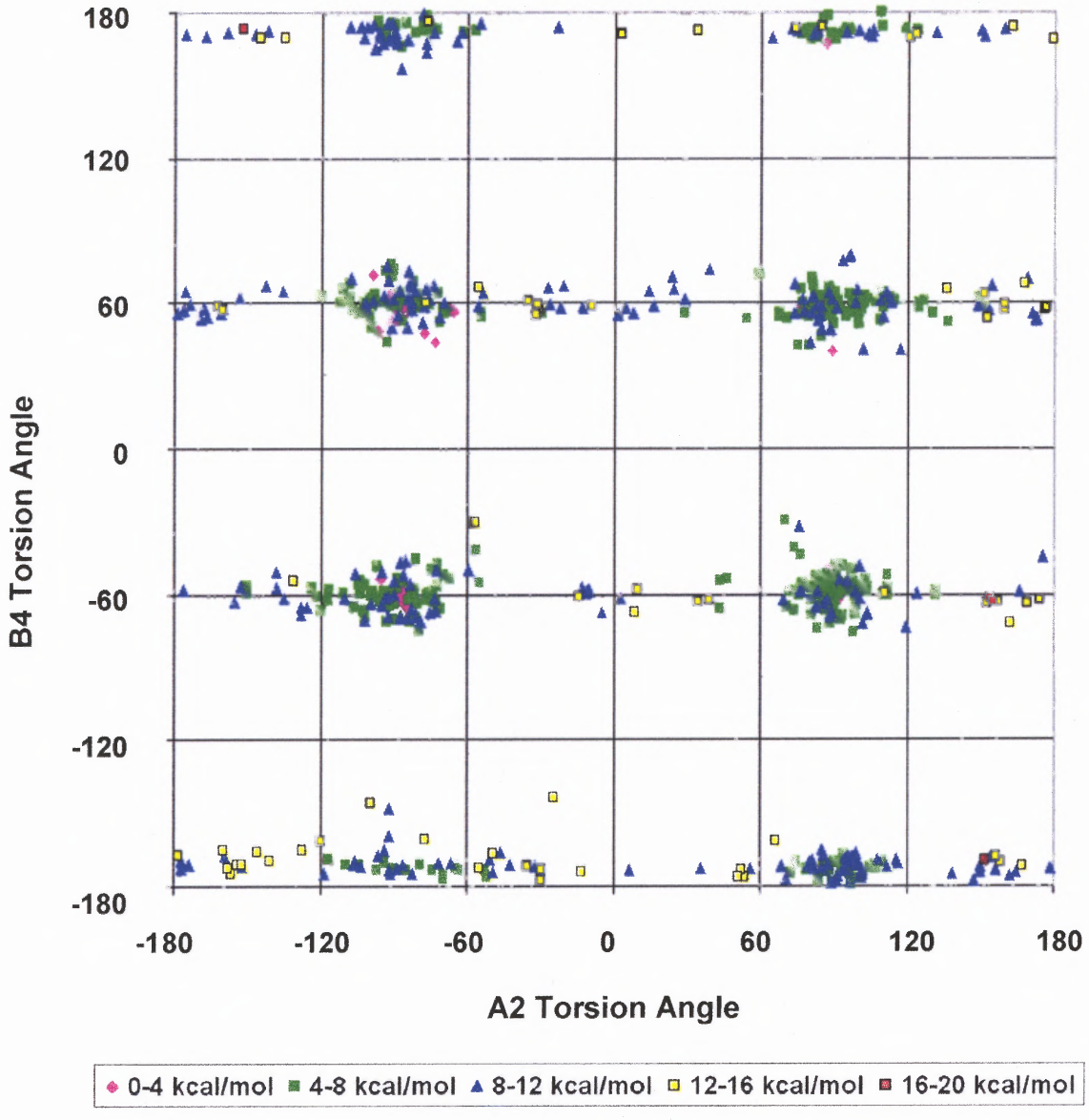

Figure D.34 Protonated DM324 (Tripos, 2nd vacuum) B4 vs A2 torsion angles.

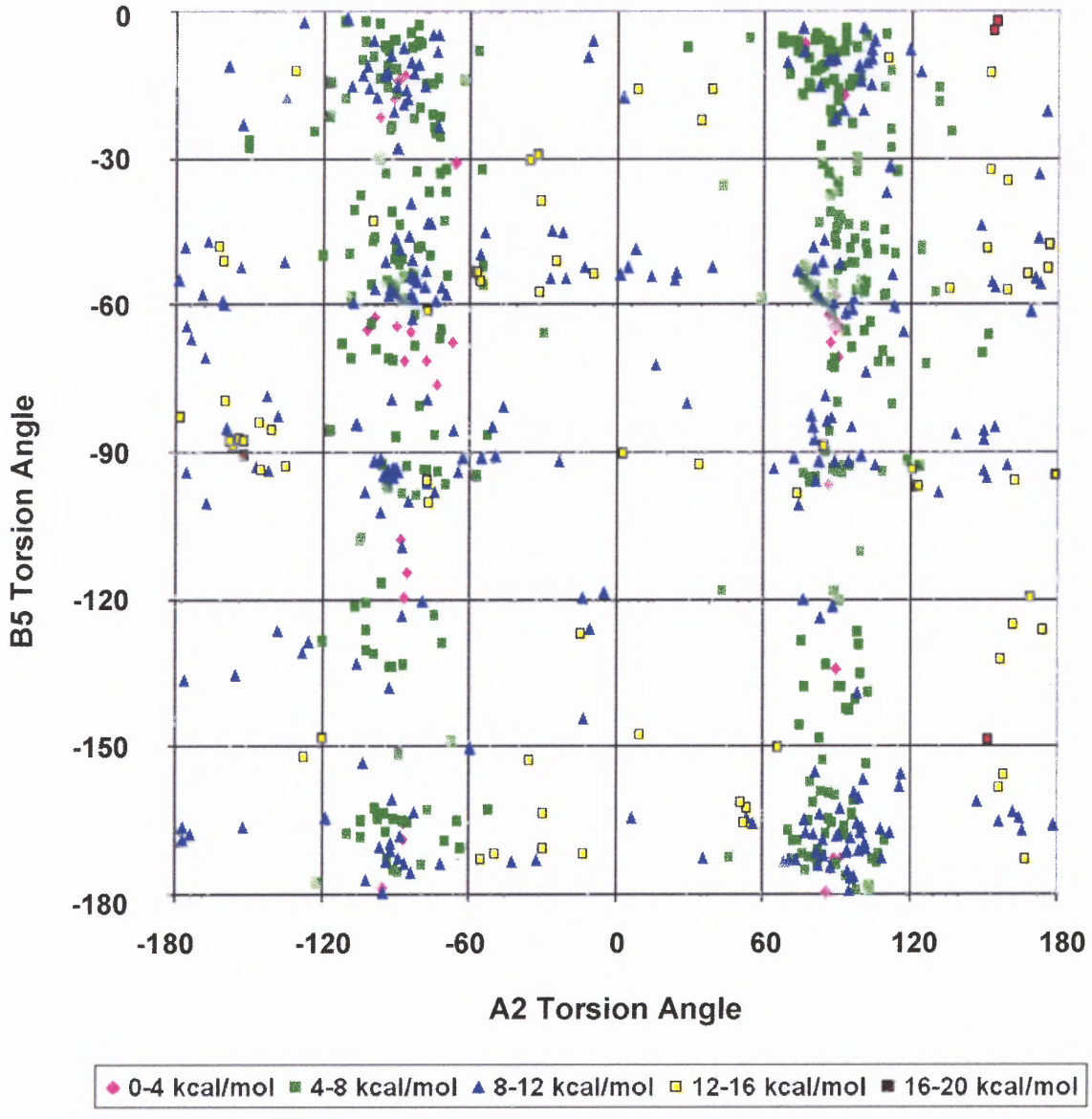

Figure D.35 Protonated DM324 (Tripos, 2nd vacuum) B5 vs A2 torsion angles.

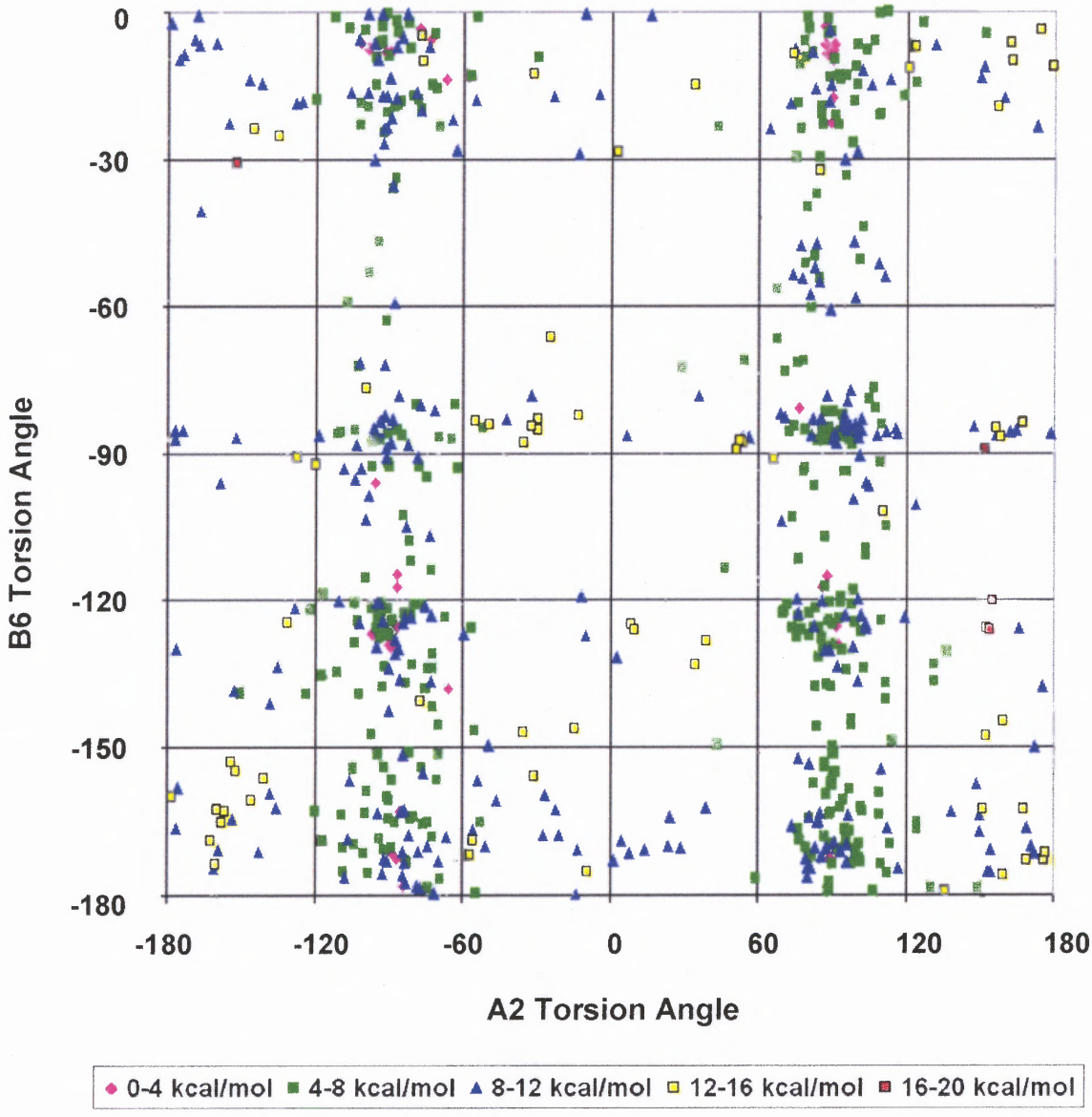

Figure D.36 Protonated DM324 (Tripos, 2nd vacuum) B6 vs A2 torsion angles.

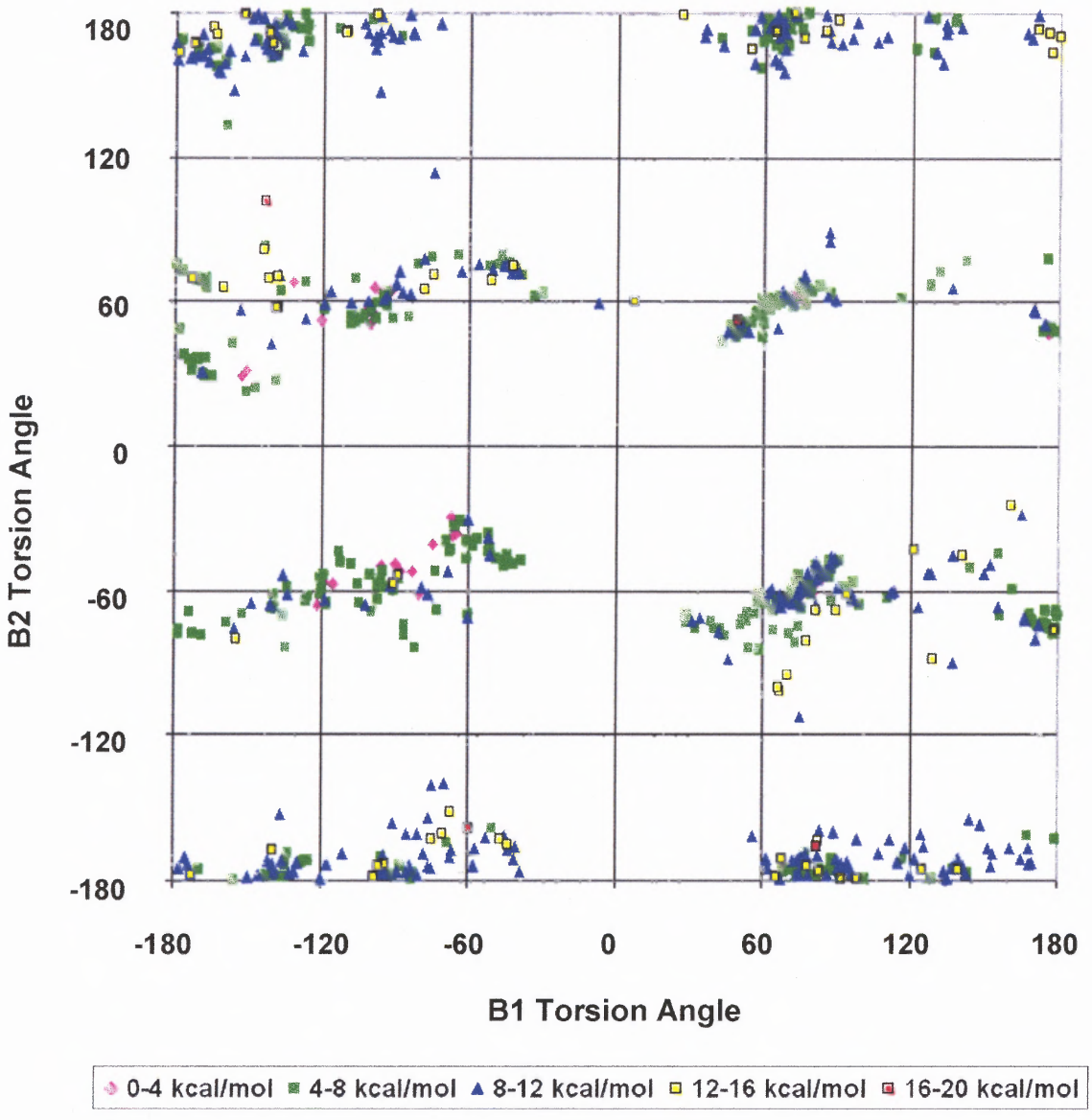

Figure D.37 Protonated DM324 (Tripos, 2nd vacuum) B2 vs B1 torsion angles.

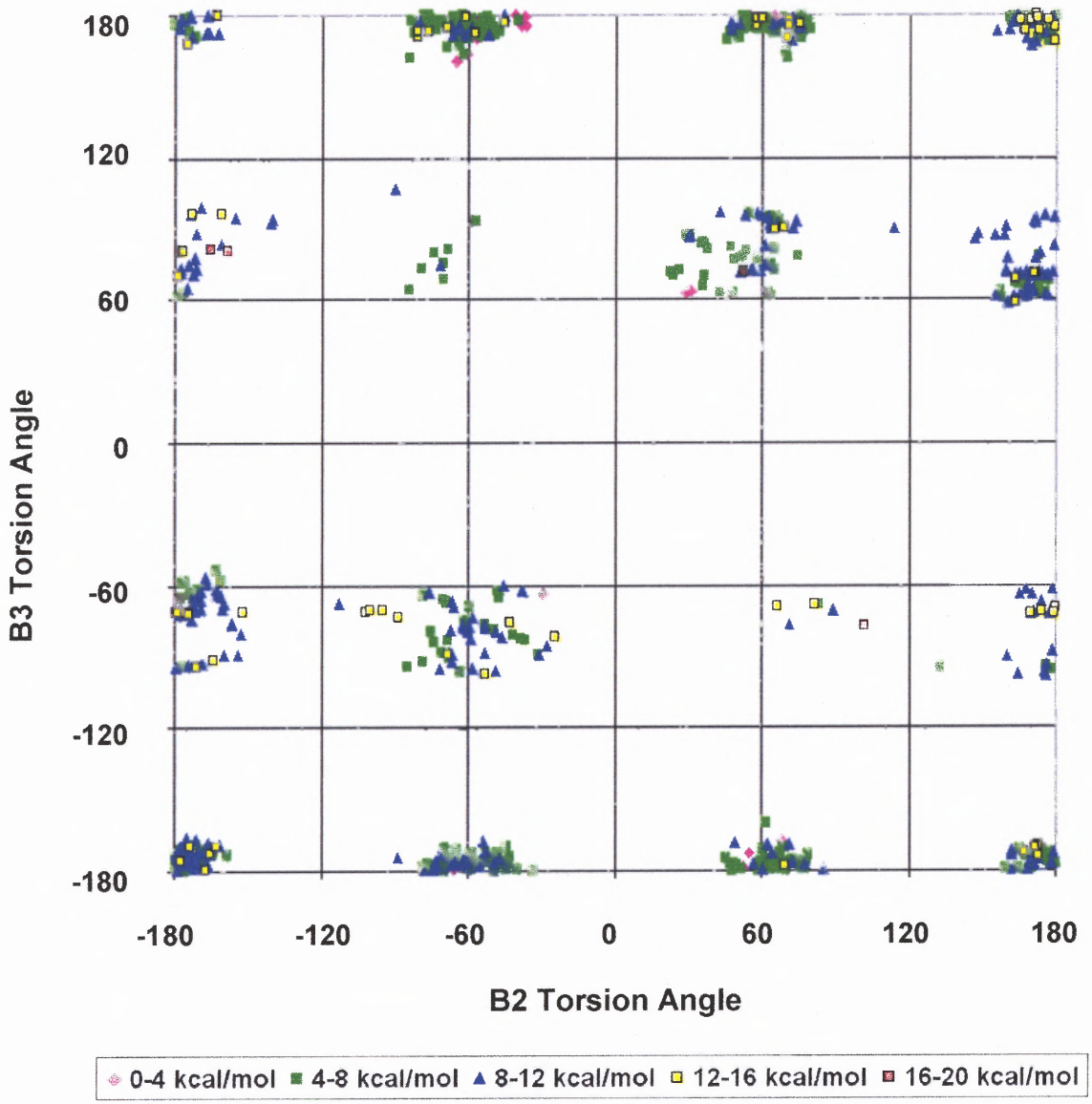

Figure D.38 Protonated DM324 (Tripos, 2nd vacuum) B3 vs B2 torsion angles.

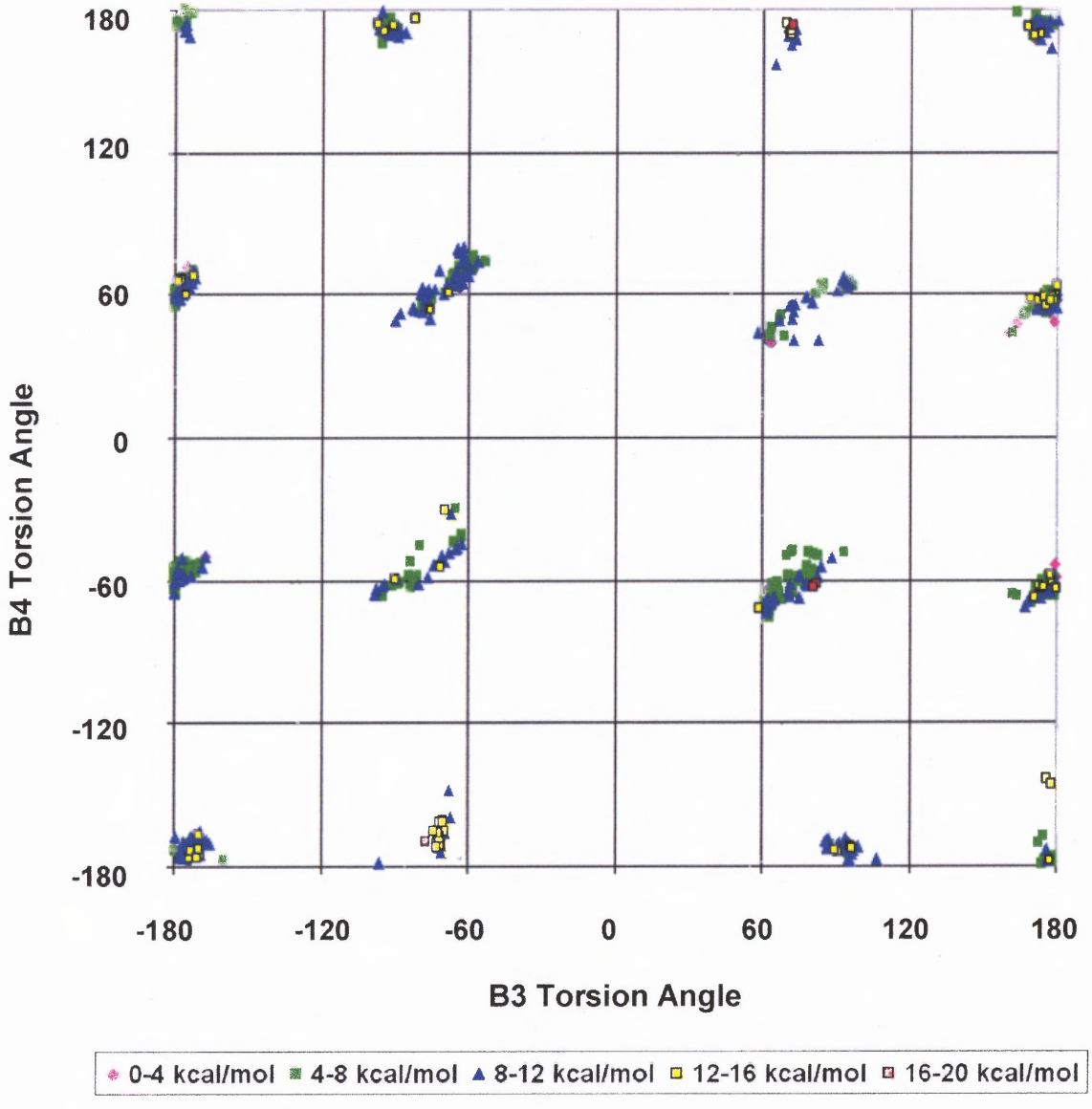

Figure D.39 Protonated DM324 (Tripos, 2nd vacuum) B4 vs B3 torsion angles.

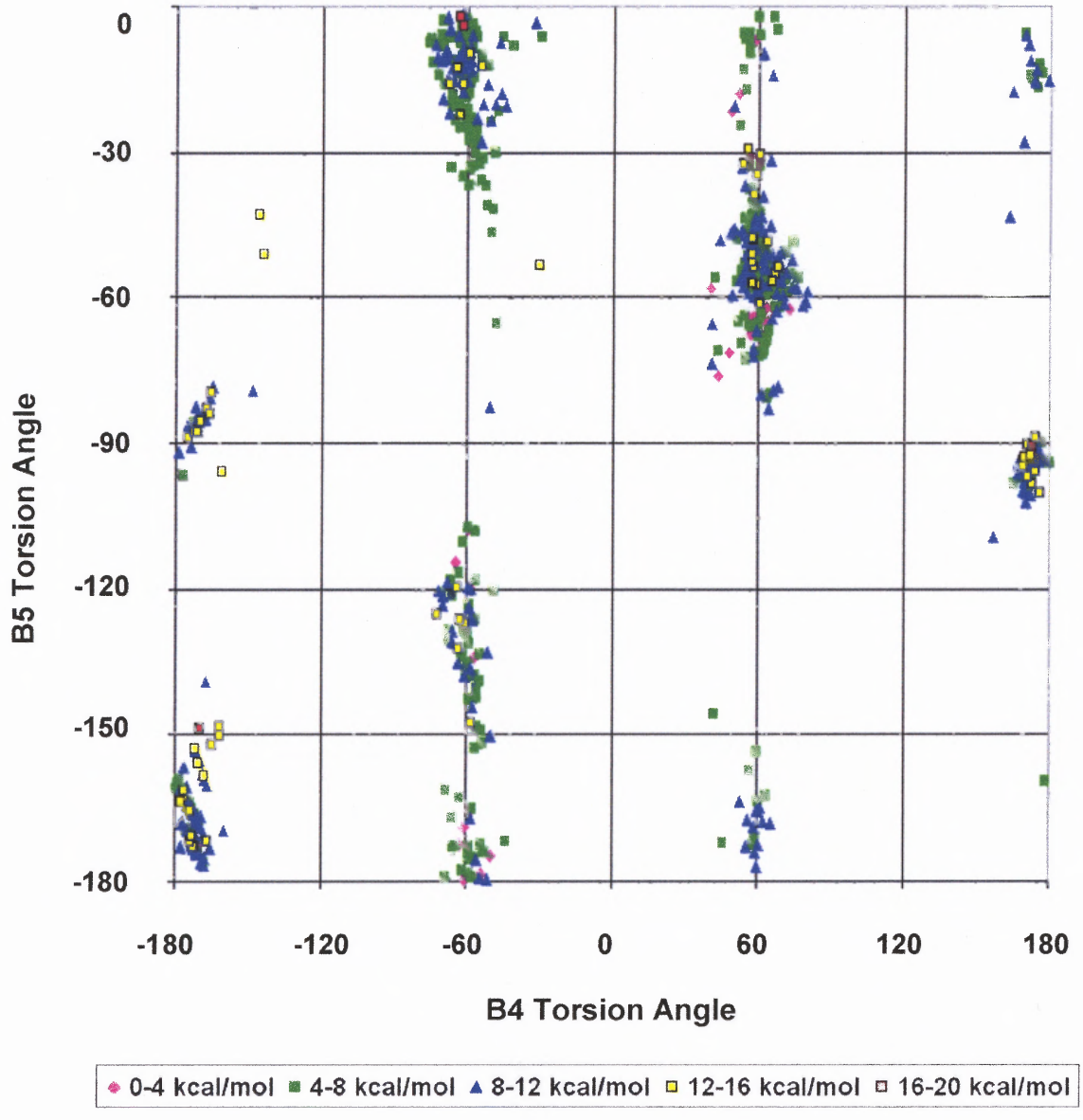

Figure D.40 Protonated DM324 (Tripos, 2nd vacuum) B5 vs B4 torsion angles.

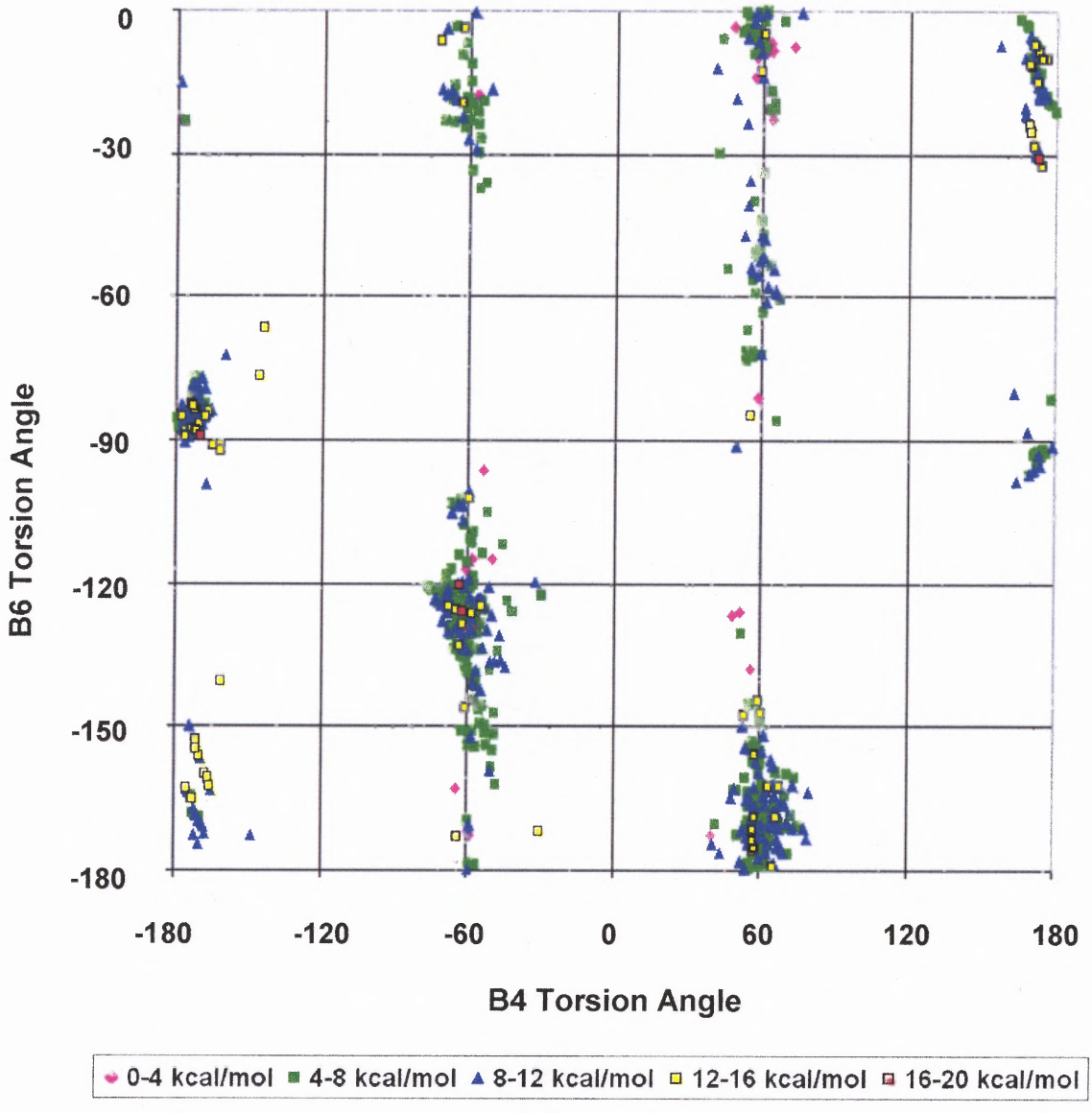

Figure D.41 Protonated DM324 (Tripos, 2nd vacuum) B6 vs B4 torsion angles.

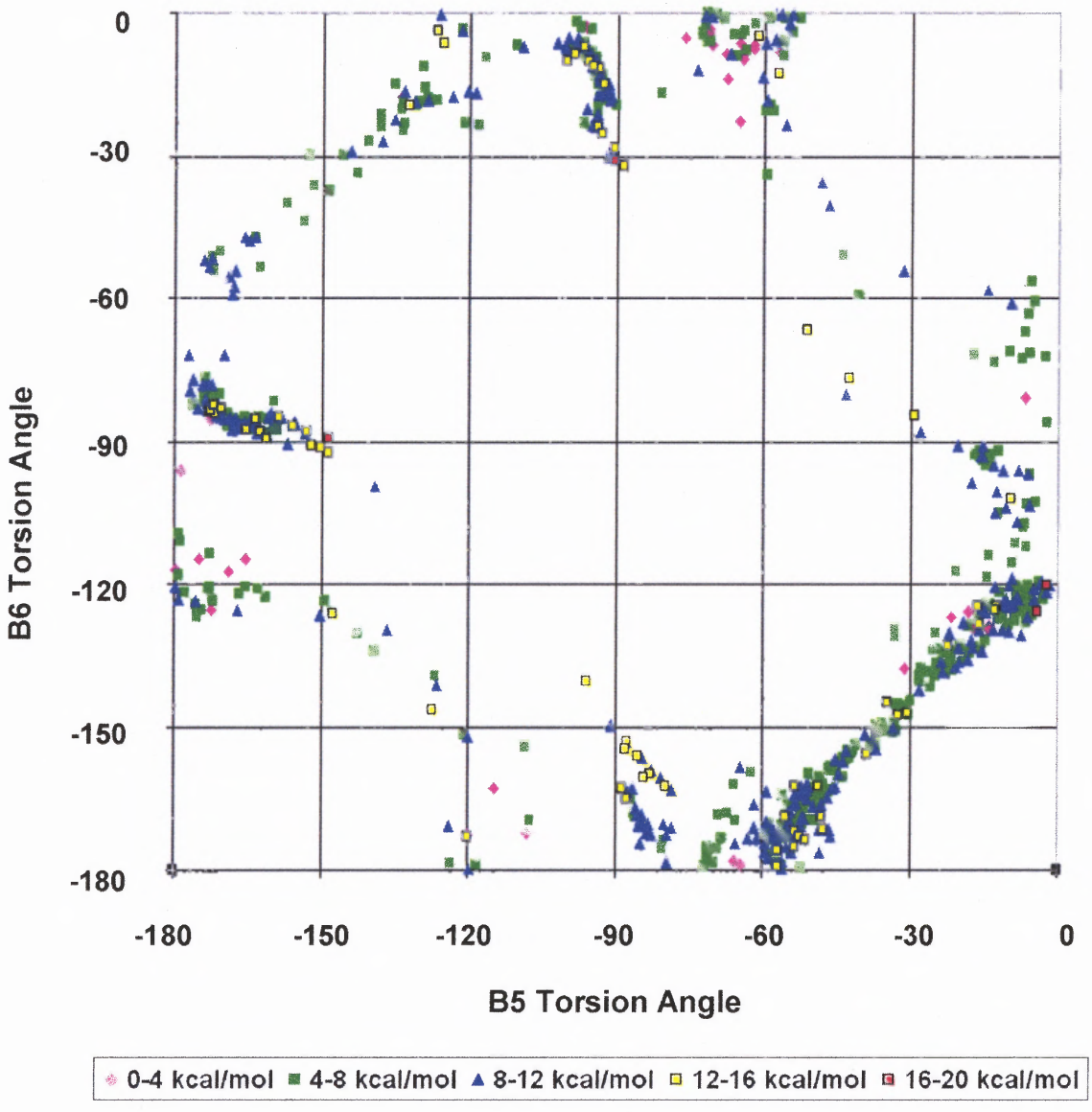

Figure D.42 Protonated DM324 (Tripos, 2nd vacuum) B6 vs B5 torsion angles.

D.4 Tripos for TP250 and Vacuum

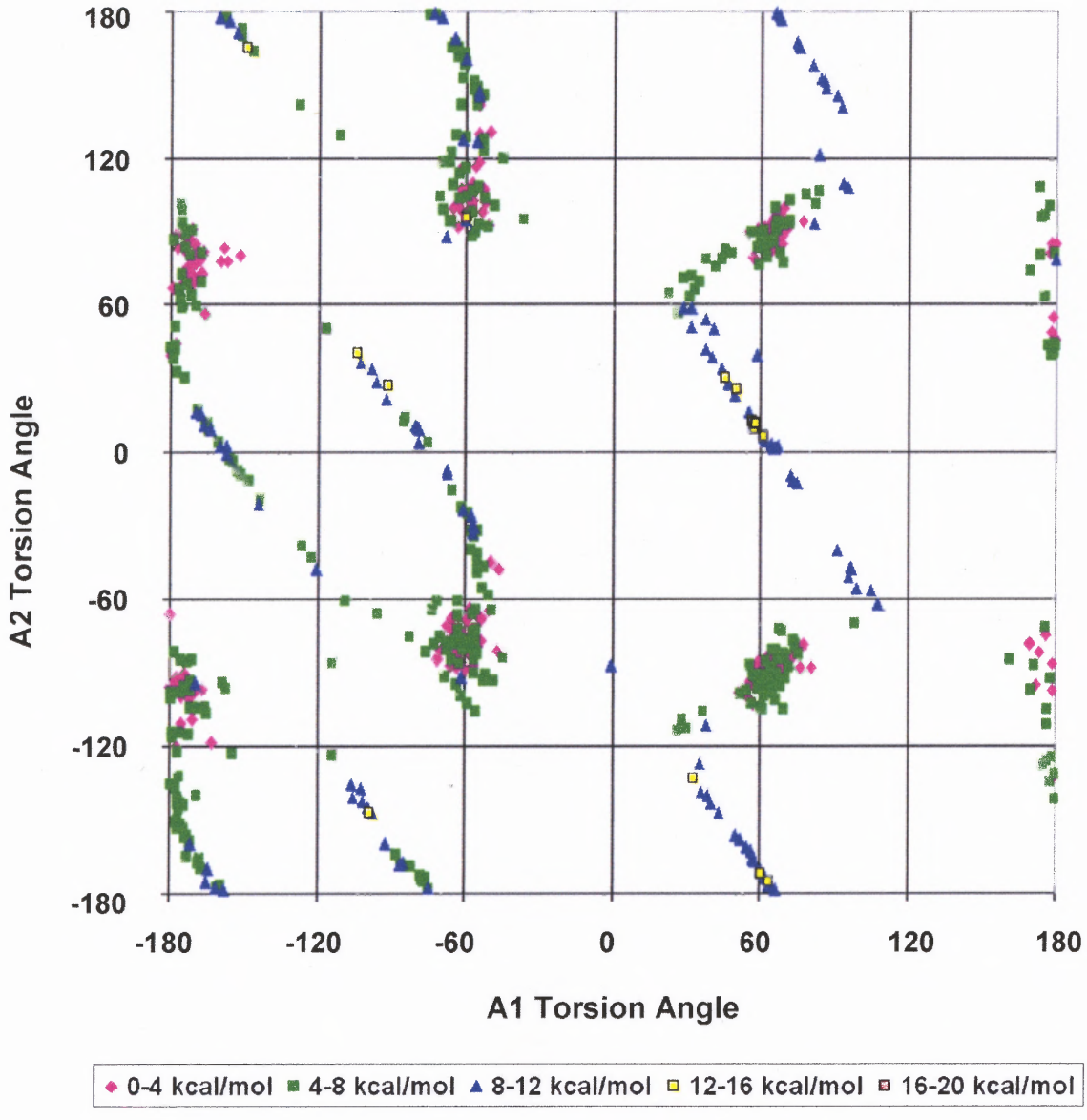

Figure D.43 Protonated TP250 (Tripos, vacuum) A2 vs A1 torsion angles.

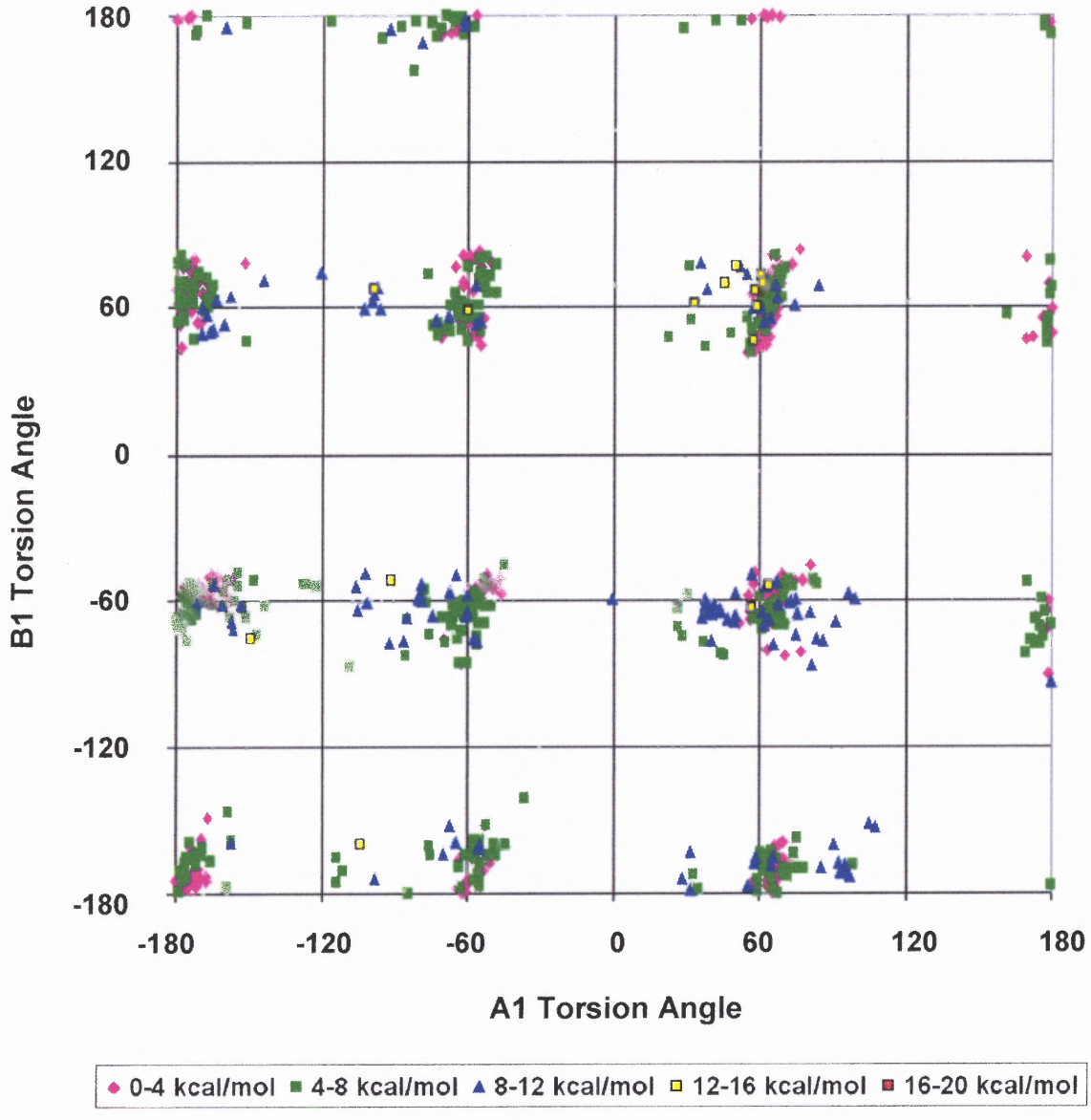

Figure D.44 Protonated TP250 (Tripos, vacuum) B1 vs A1 torsion angles.

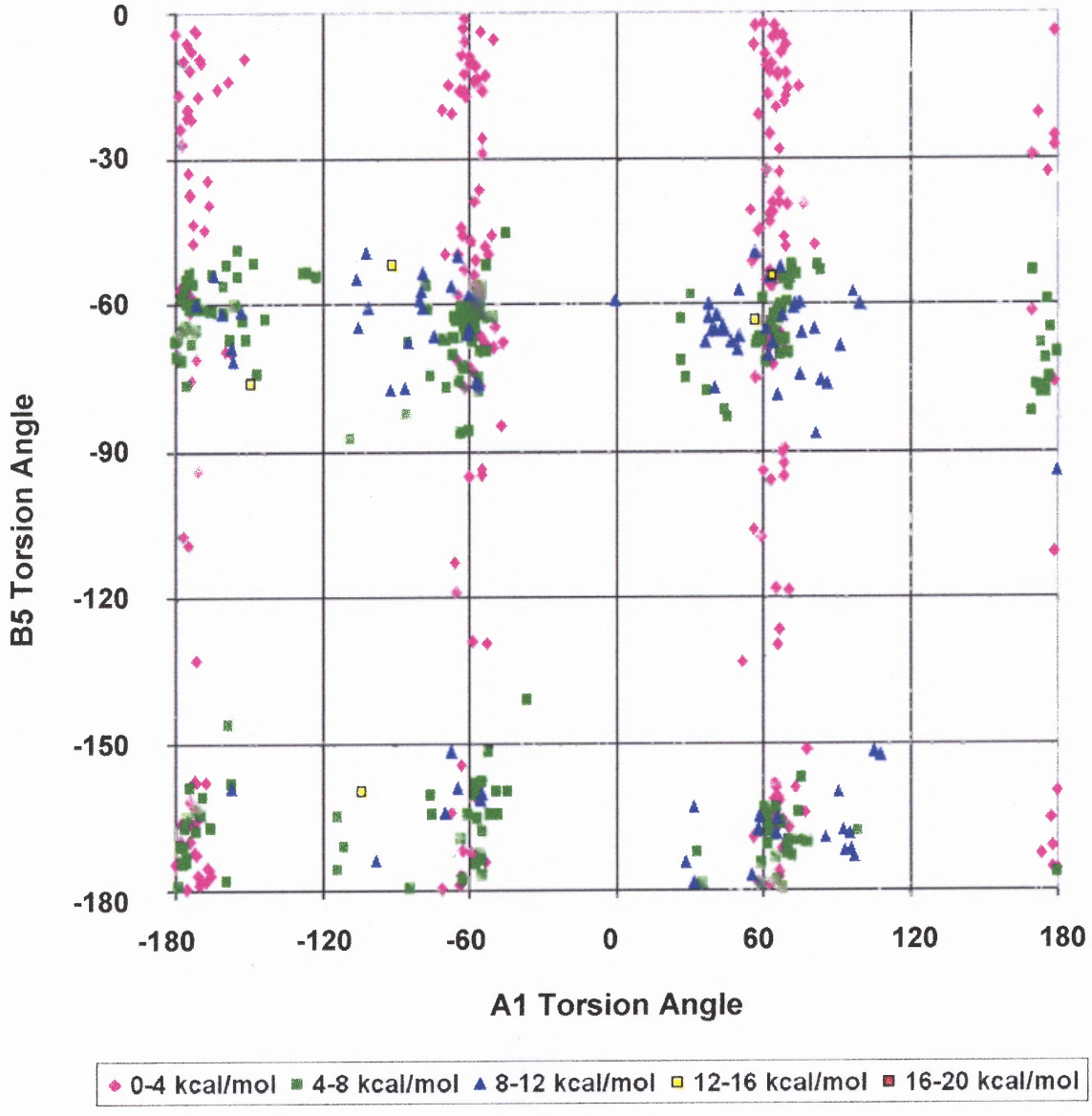

Figure D.45 Protonated TP250 (Tripos, vacuum) B5 vs A1 torsion angles.

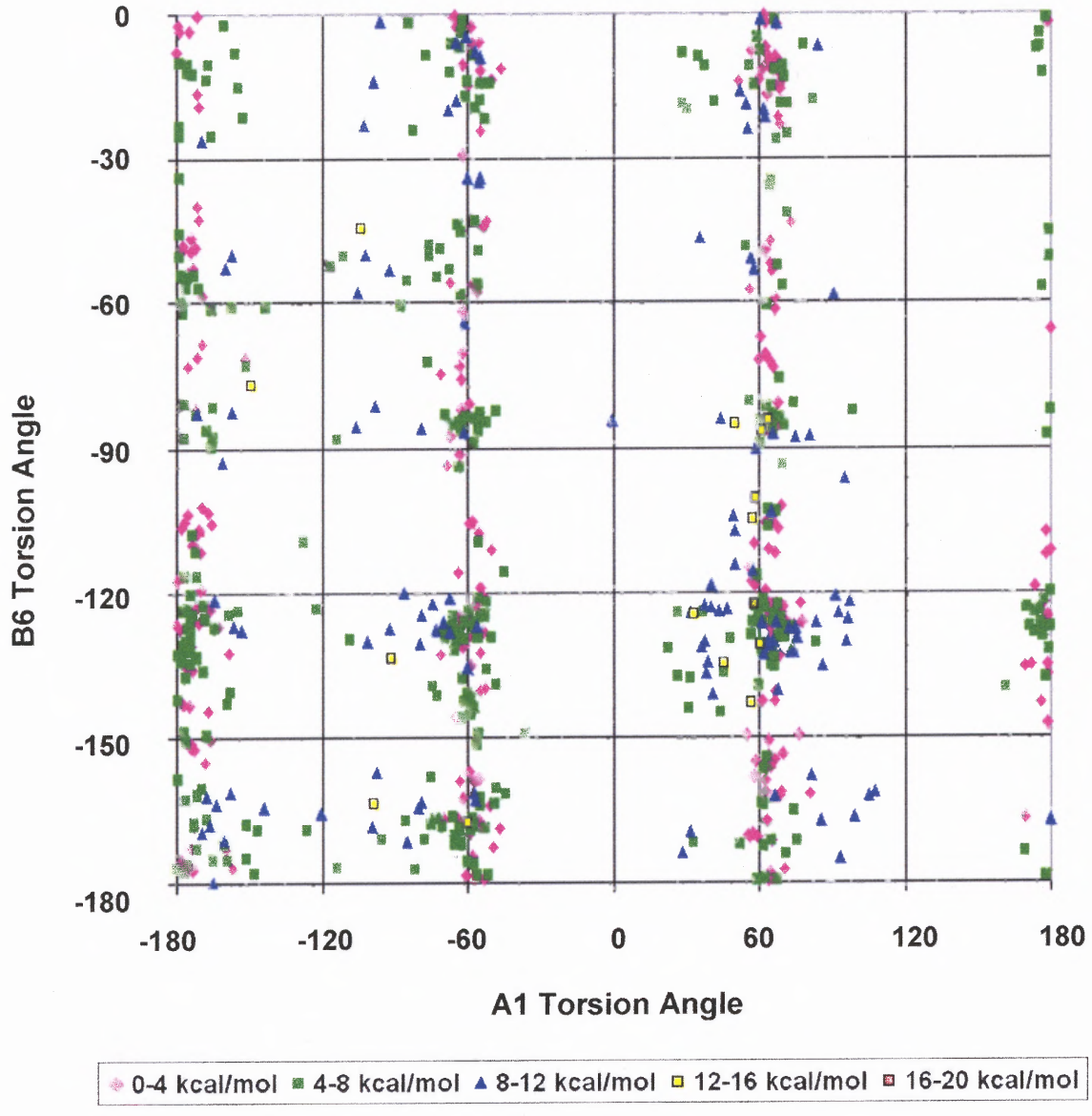

Figure D.46 Protonated TP250 (Tripos, vacuum) B6 vs A1 torsion angles.

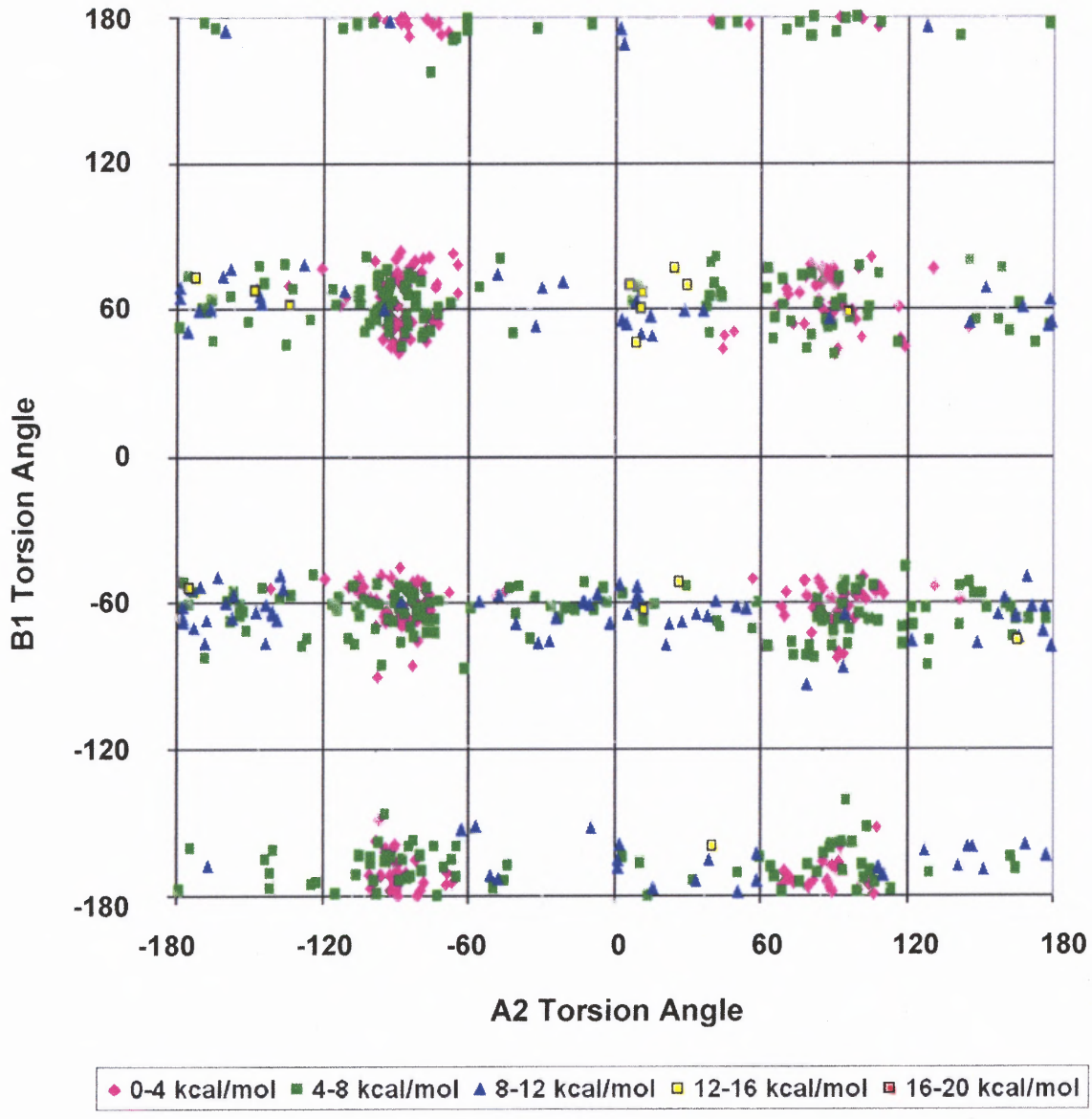

Figure D.47 Protonated TP250 (Tripos, vacuum) B1 vs A2 torsion angles.

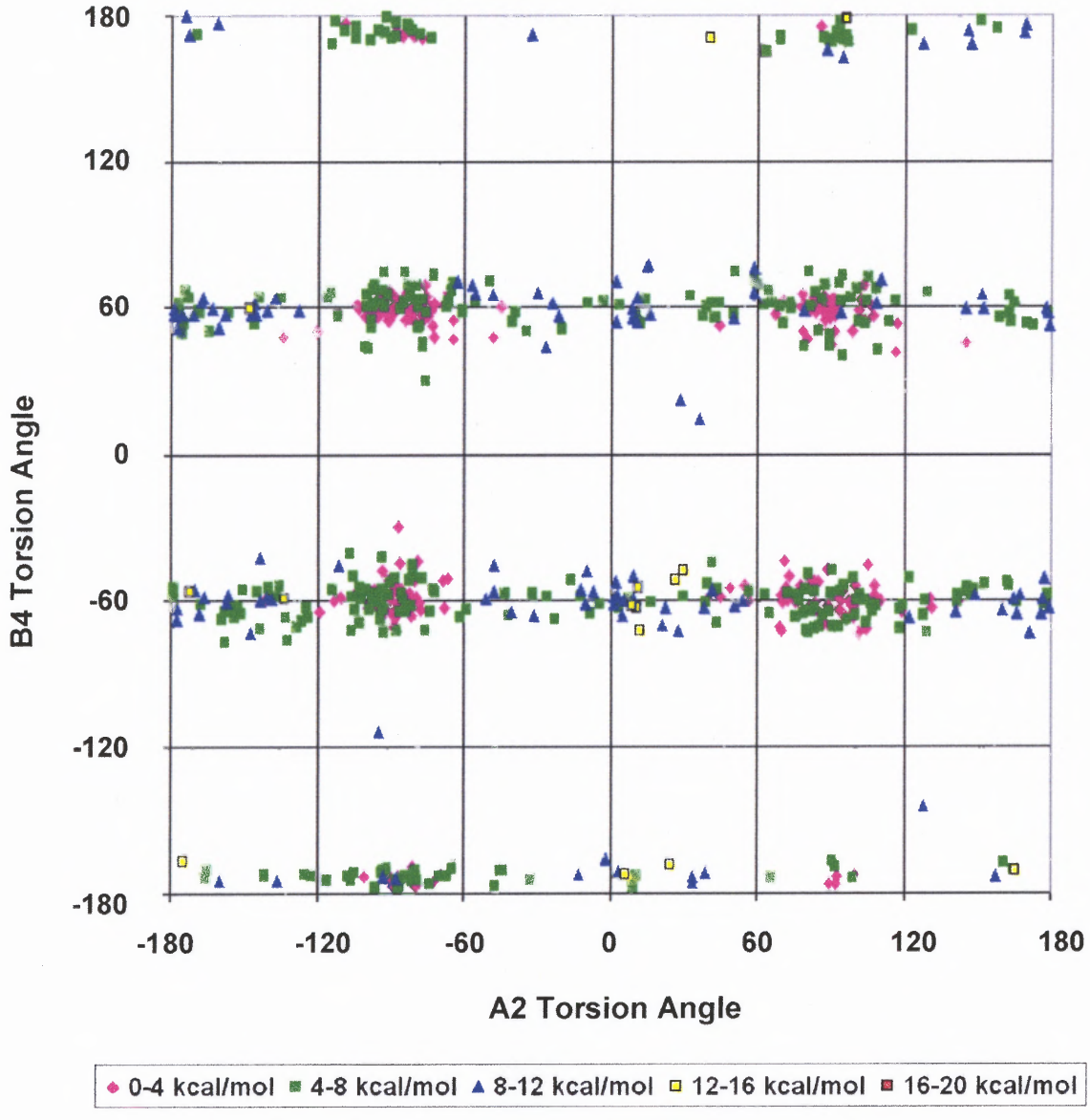

Figure D.48 Protonated TP250 (Tripos, vacuum) B4 vs A2 torsion angles.

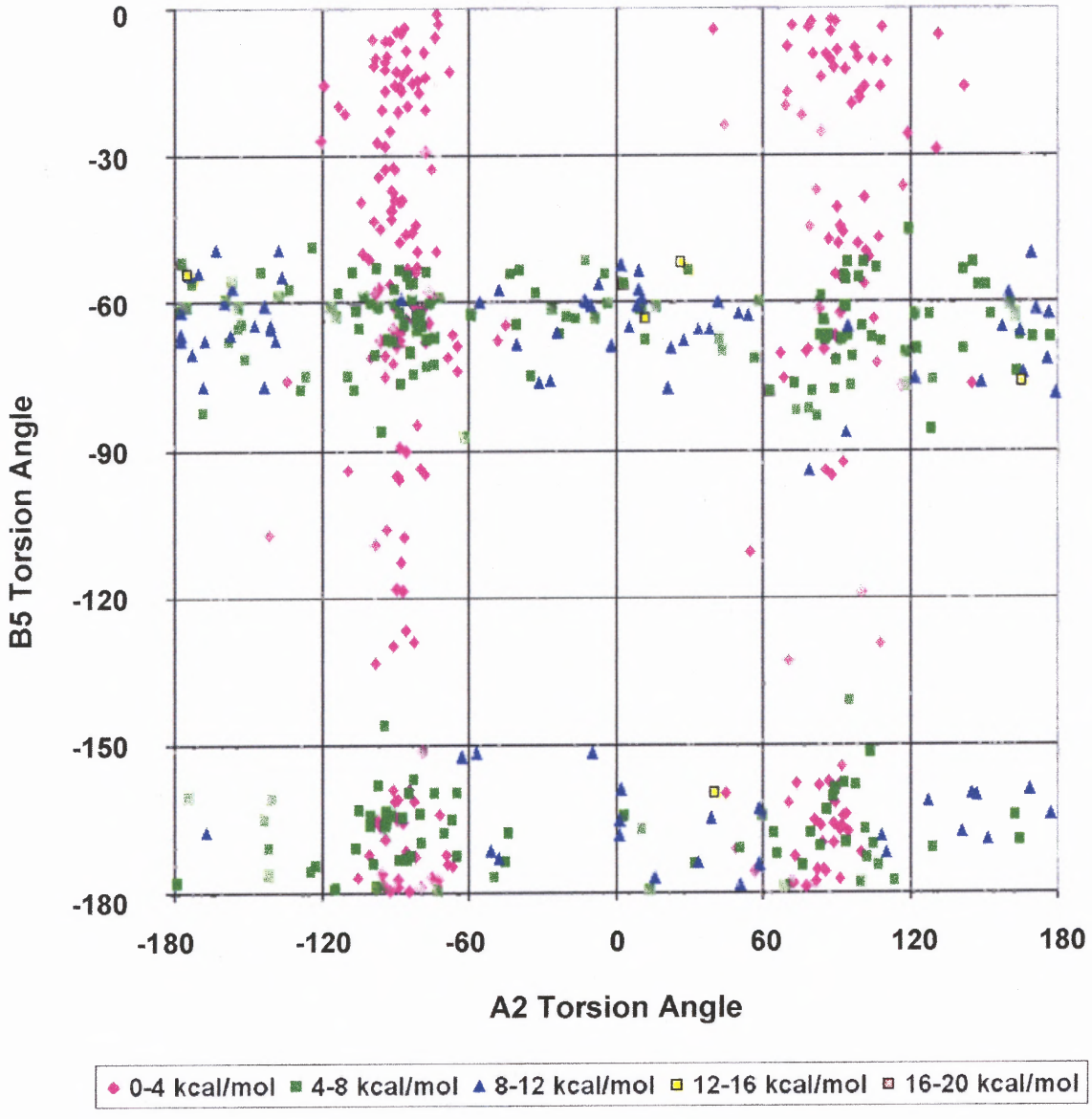

Figure D.49 Protonated TP250 (Tripos, vacuum) B5 vs A2 torsion angles.

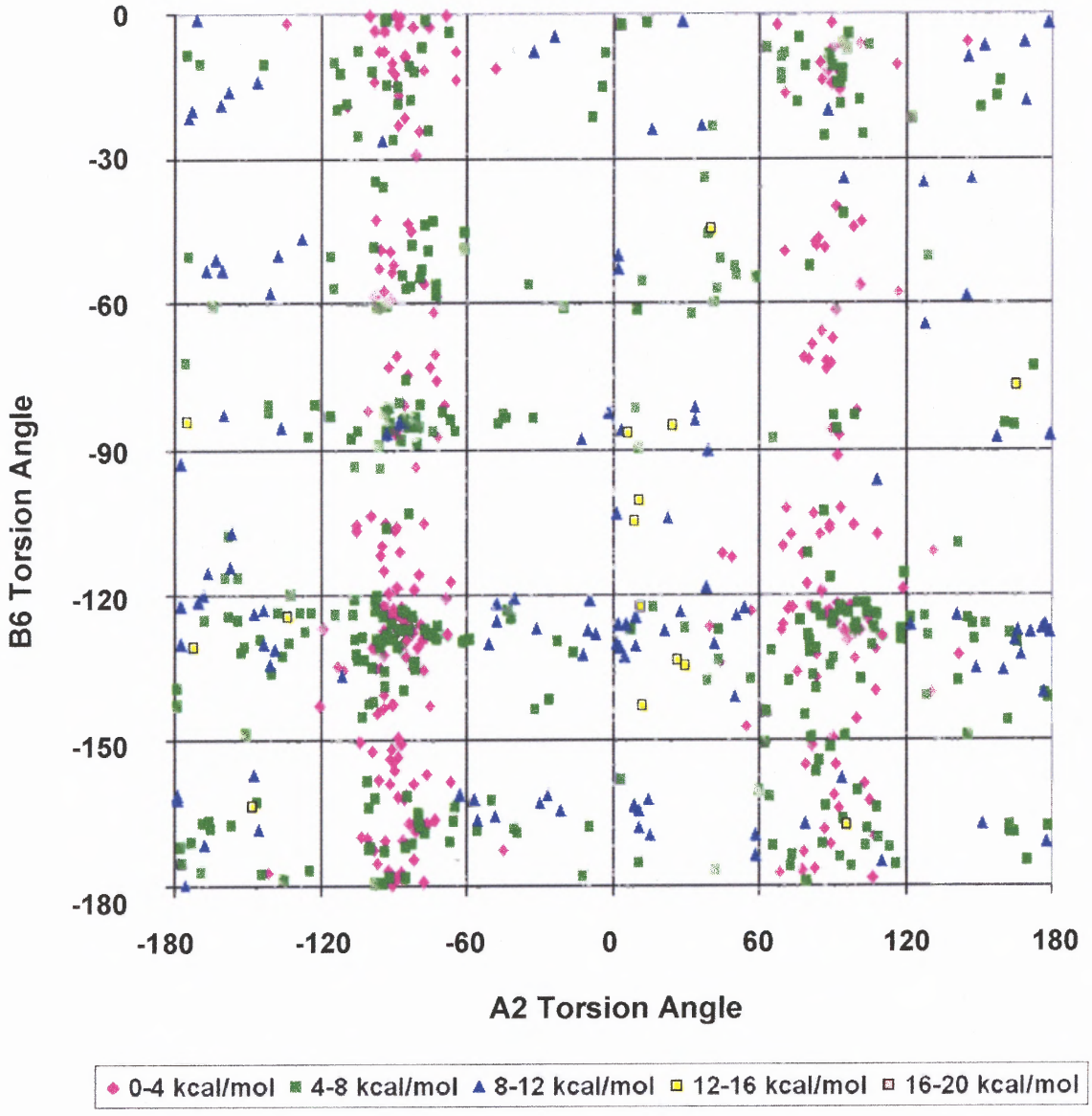

Figure D.50 Protonated TP250 (Tripos, vacuum) B6 vs A2 torsion angles.

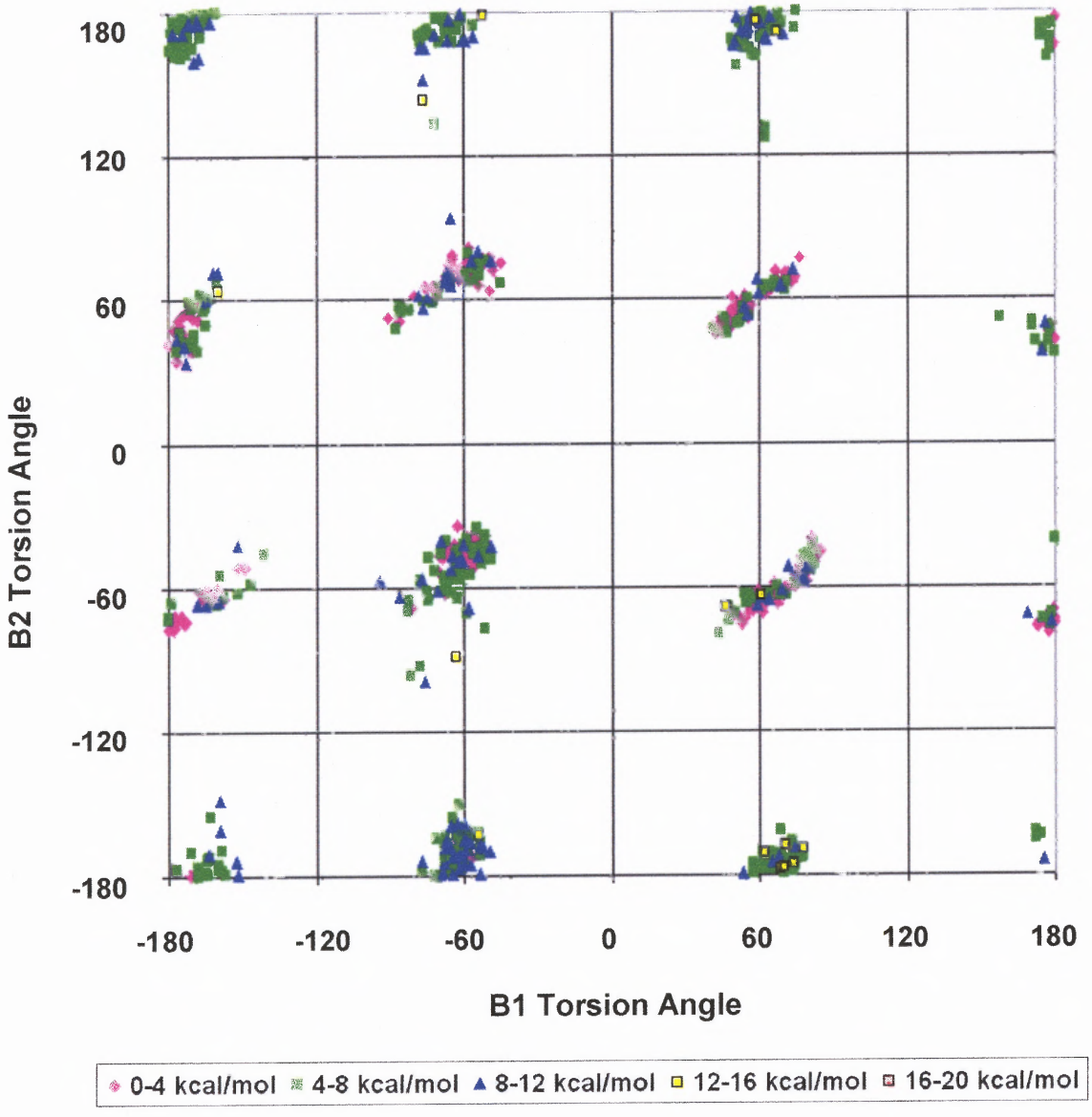

Figure D.51 Protonated TP250 (Tripos, vacuum) B2 vs B1 torsion angles.

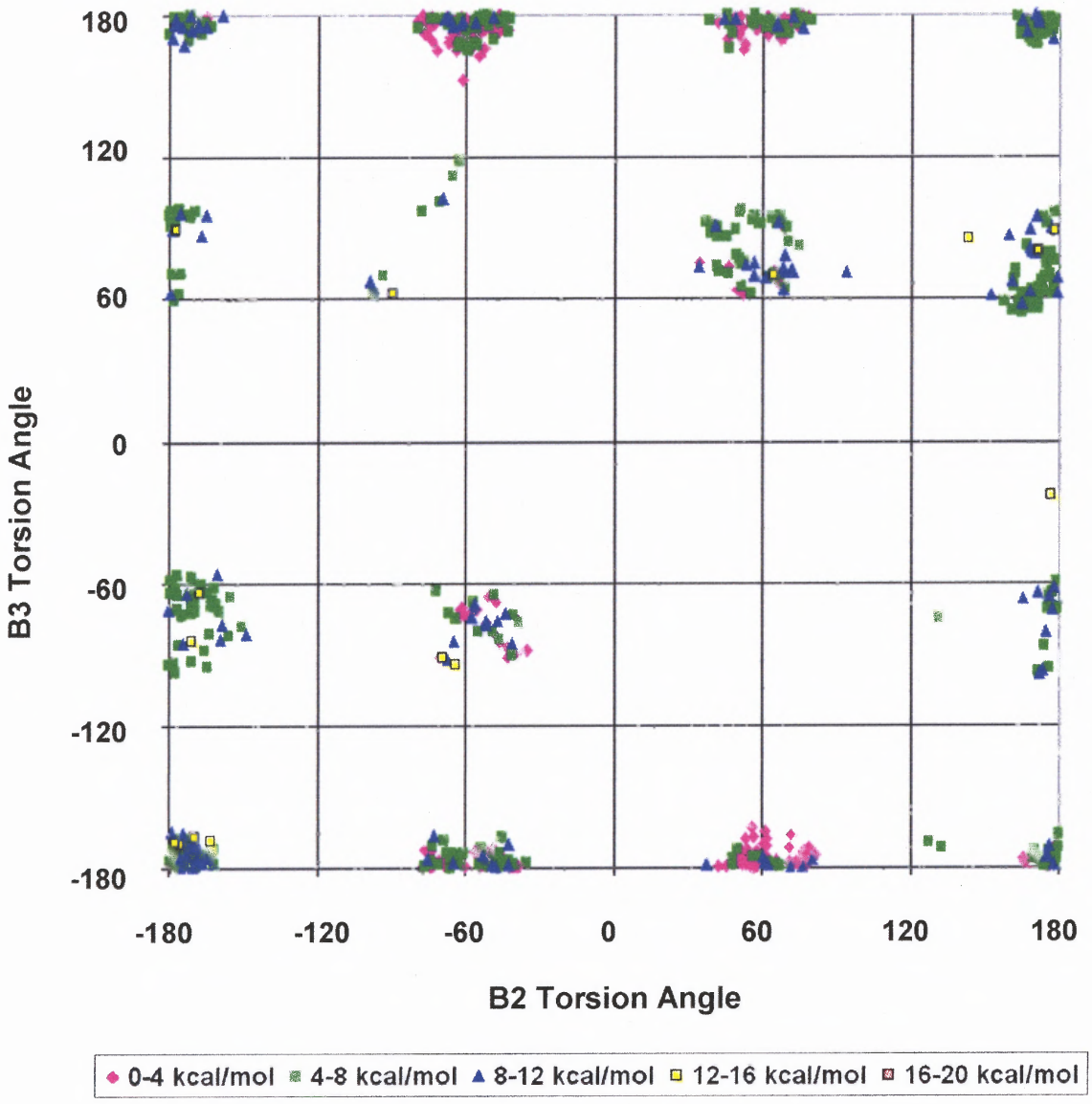

Figure D.52 Protonated TP250 (Tripos, vacuum) B3 vs B2 torsion angles.

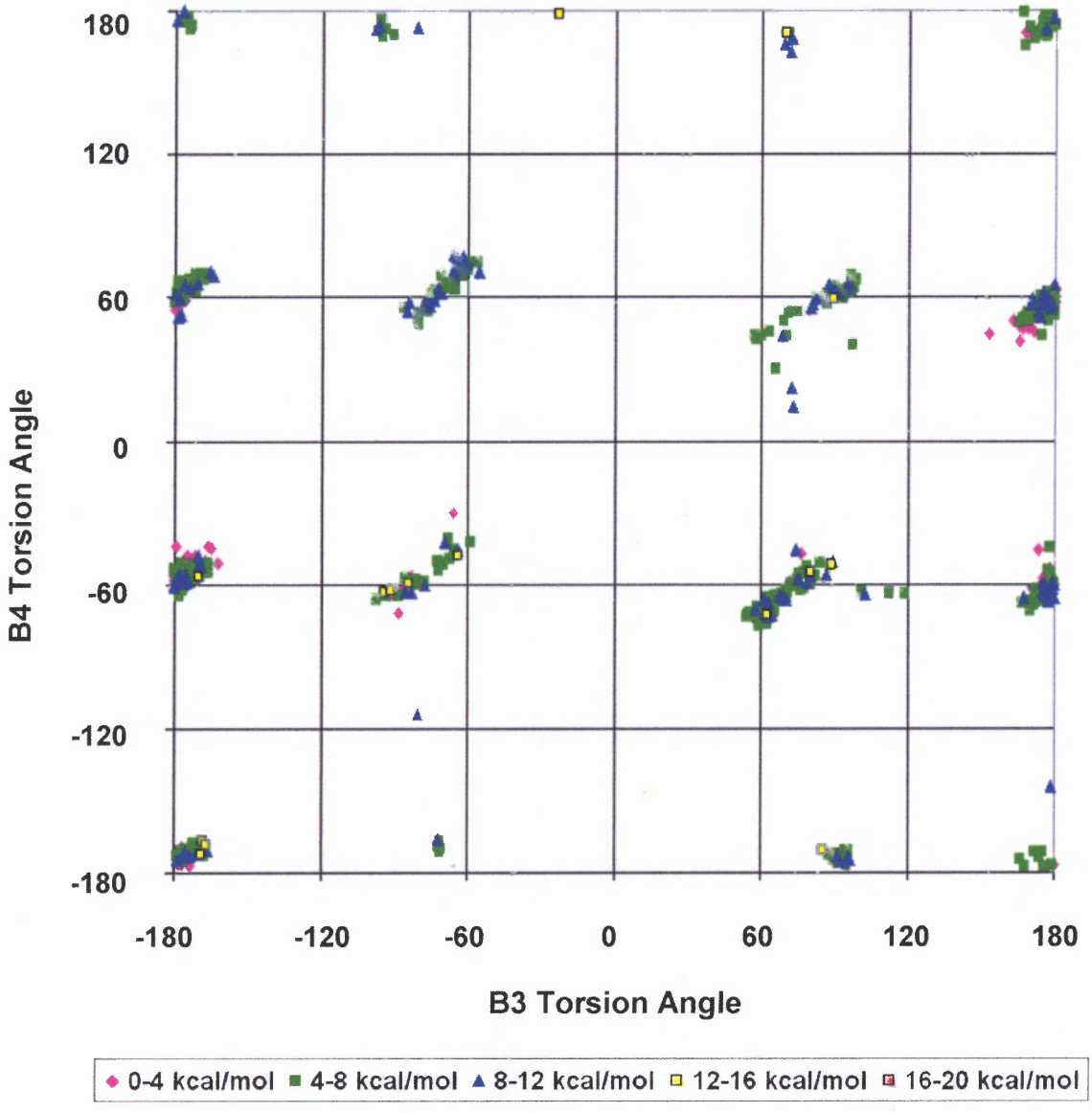

Figure D.53 Protonated TP250 (Tripos, vacuum) B4 vs B3 torsion angles.

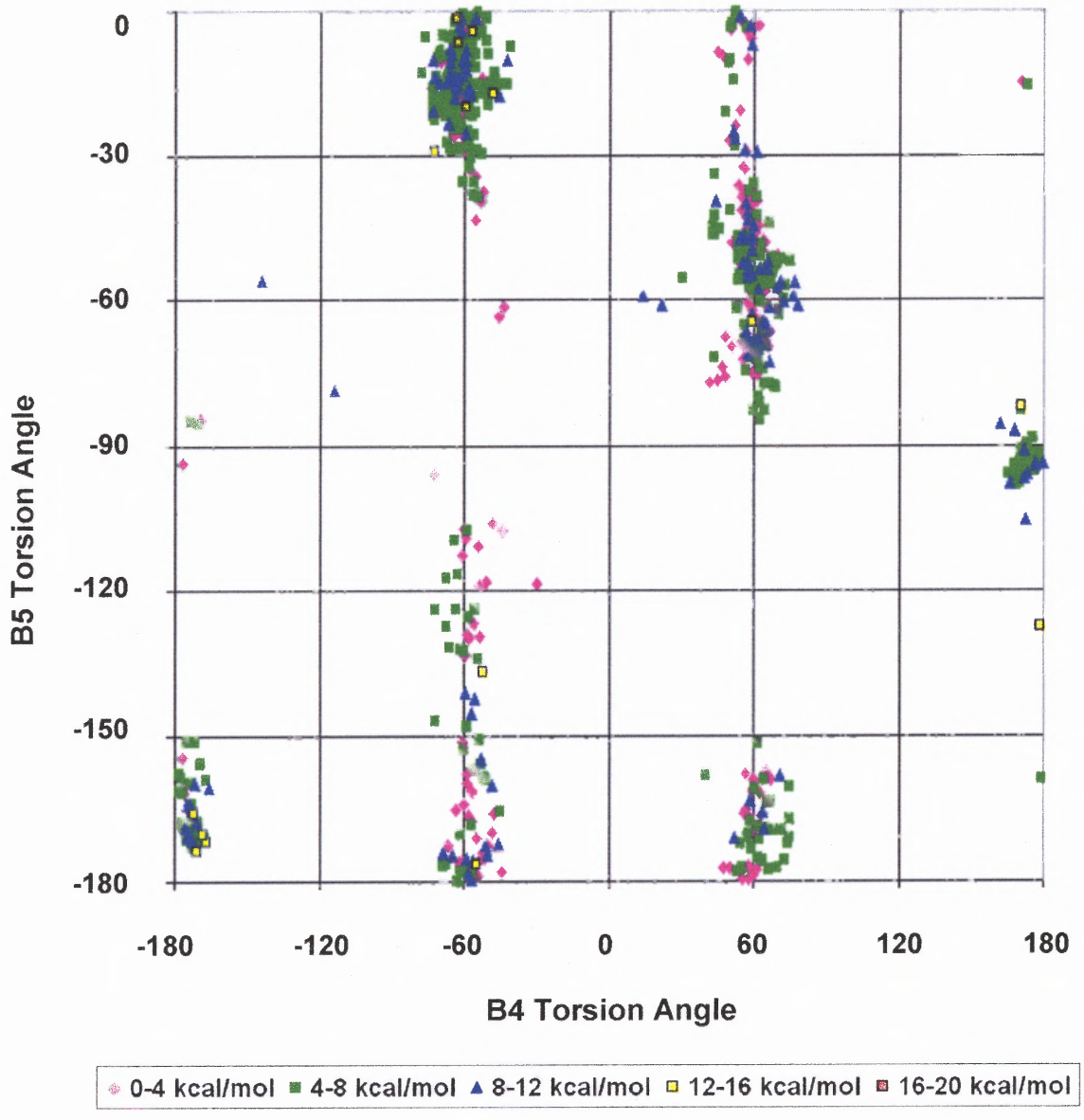

Figure D.54 Protonated TP250 (Tripos, vacuum) B5 vs B4 torsion angles.

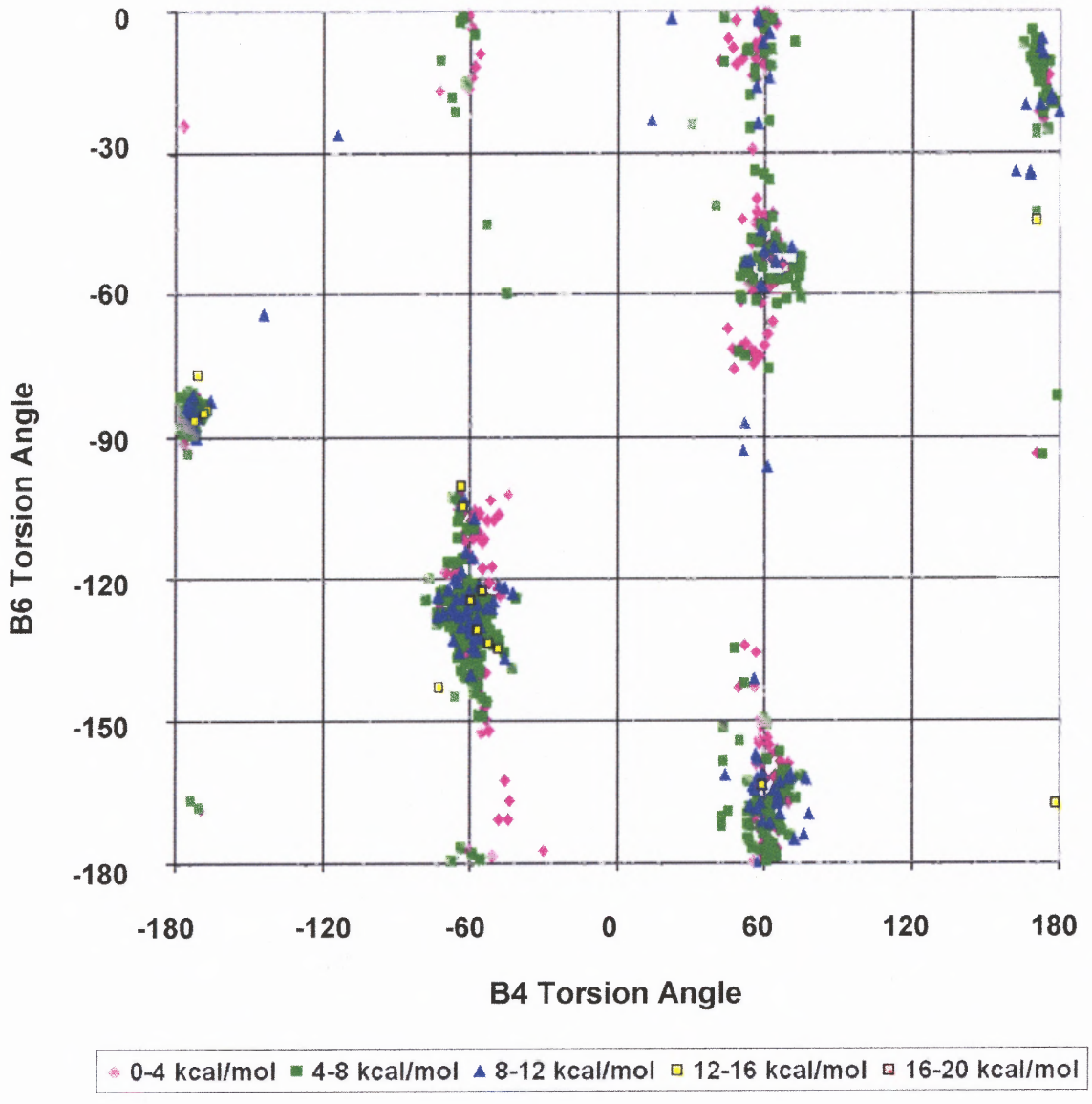

Figure D.55 Protonated TP250 (Tripos, vacuum) B6 vs B4 torsion angles.

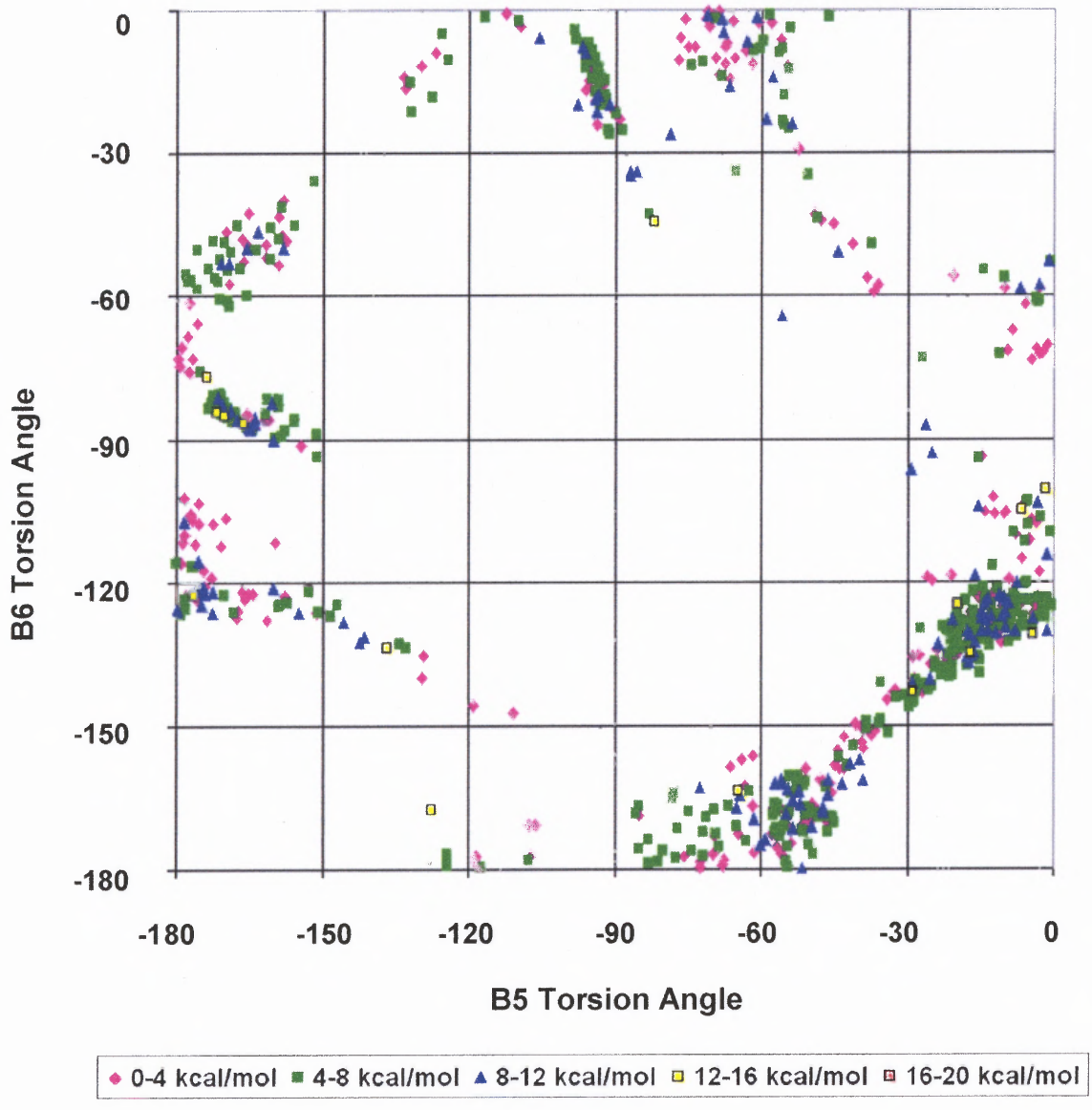

Figure D.56 Protonated TP250 (Tripos, vacuum) B6 vs B5 torsion angles.

D.5 Tripos for TP250 and Solvent

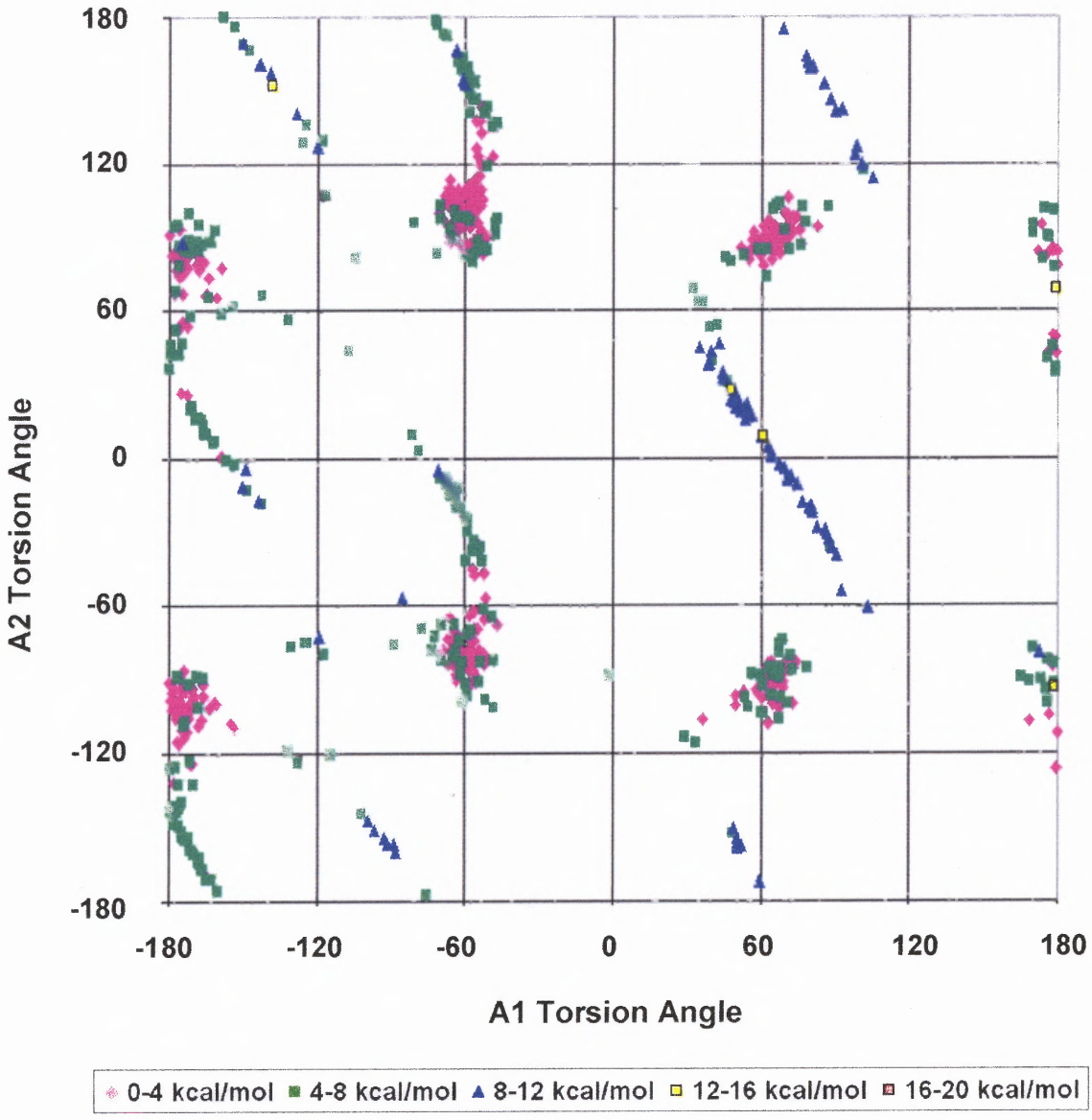

Figure D.57 Protonated TP250 (Tripos, solvent) A2 vs A1 torsion angles.

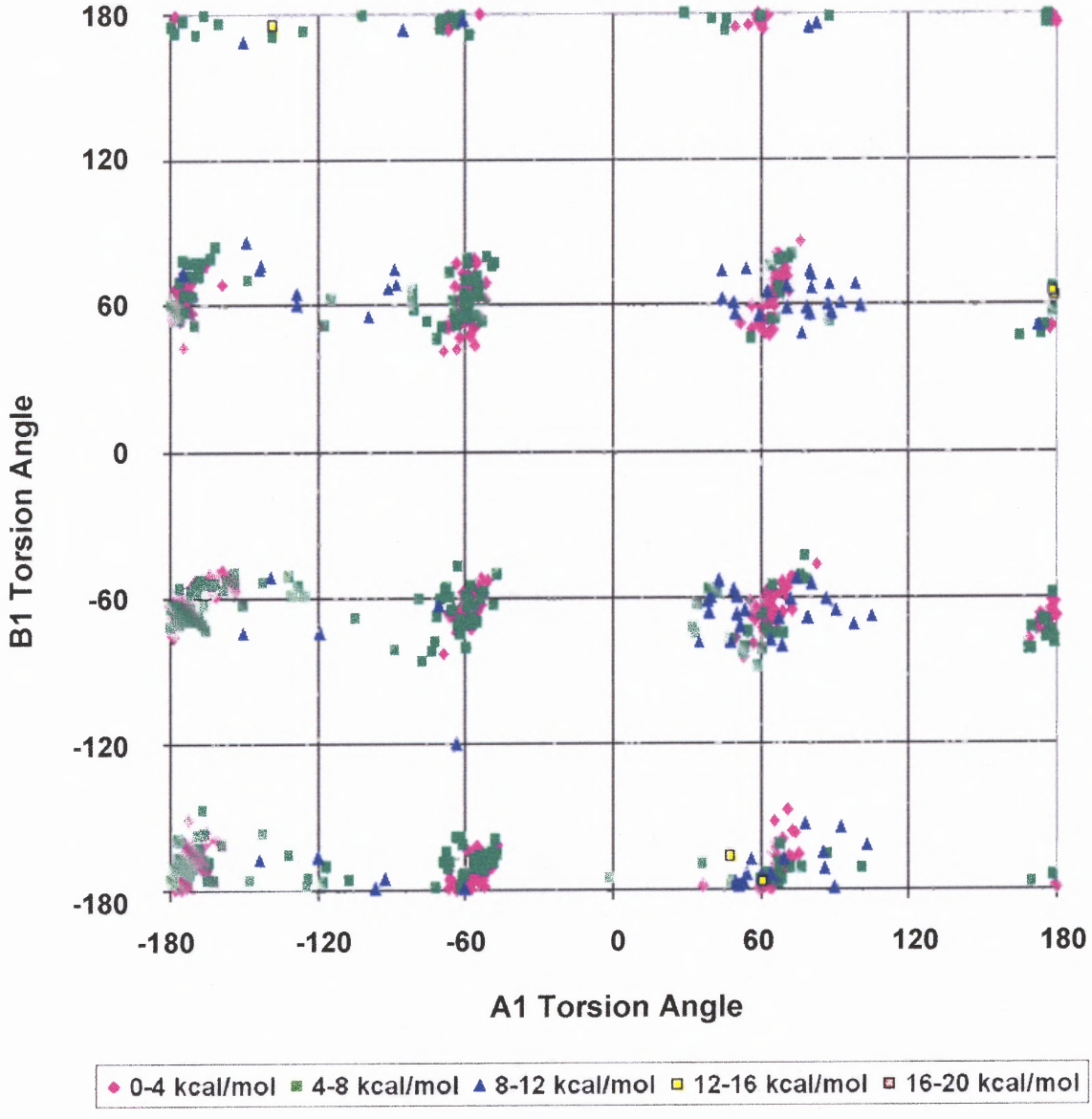

Figure D.58 Protonated TP250 (Tripos, solvent) B1 vs A1 torsion angles.

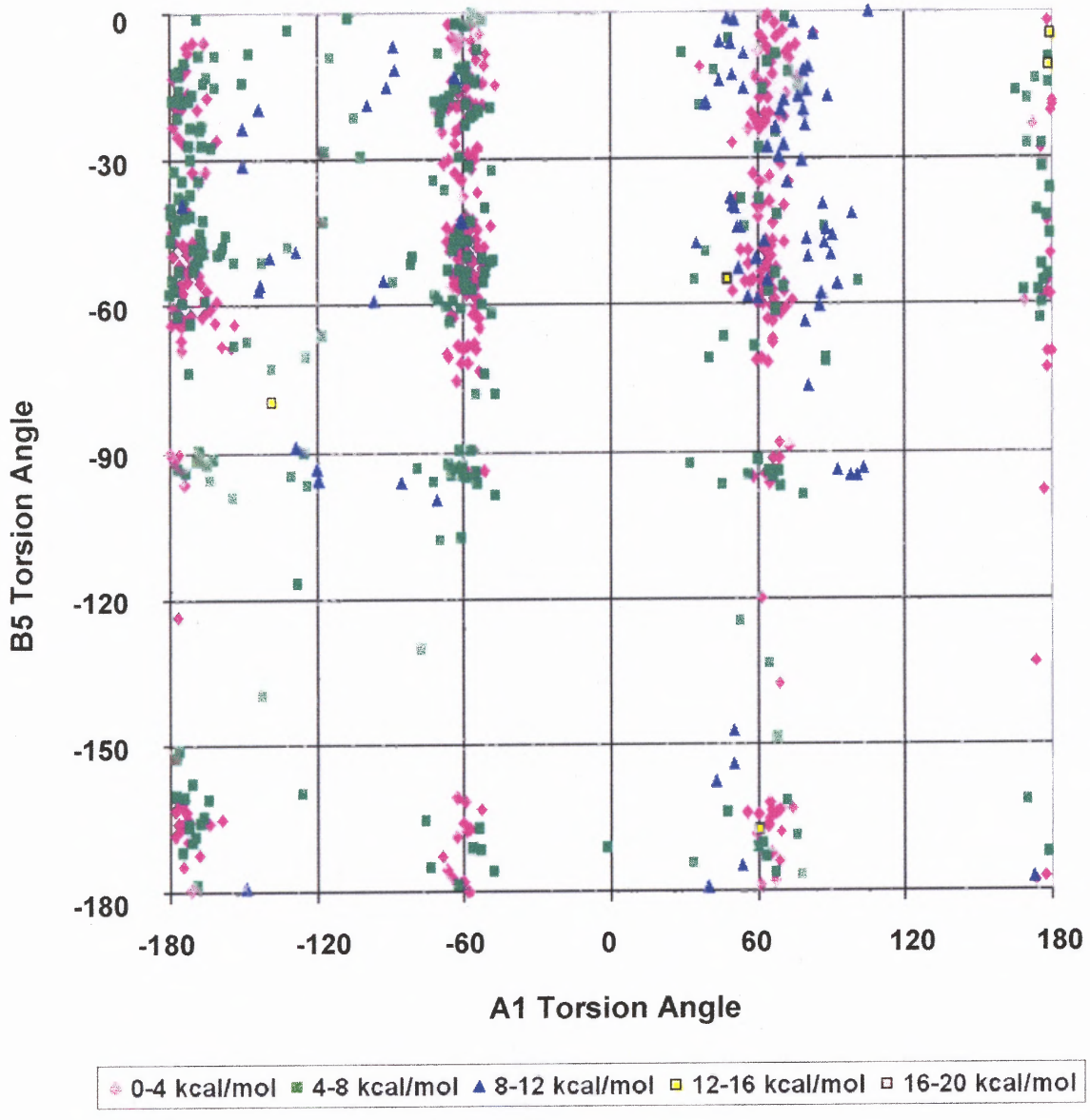

Figure D.59 Protonated TP250 (Tripos, solvent) B5 vs A1 torsion angles.

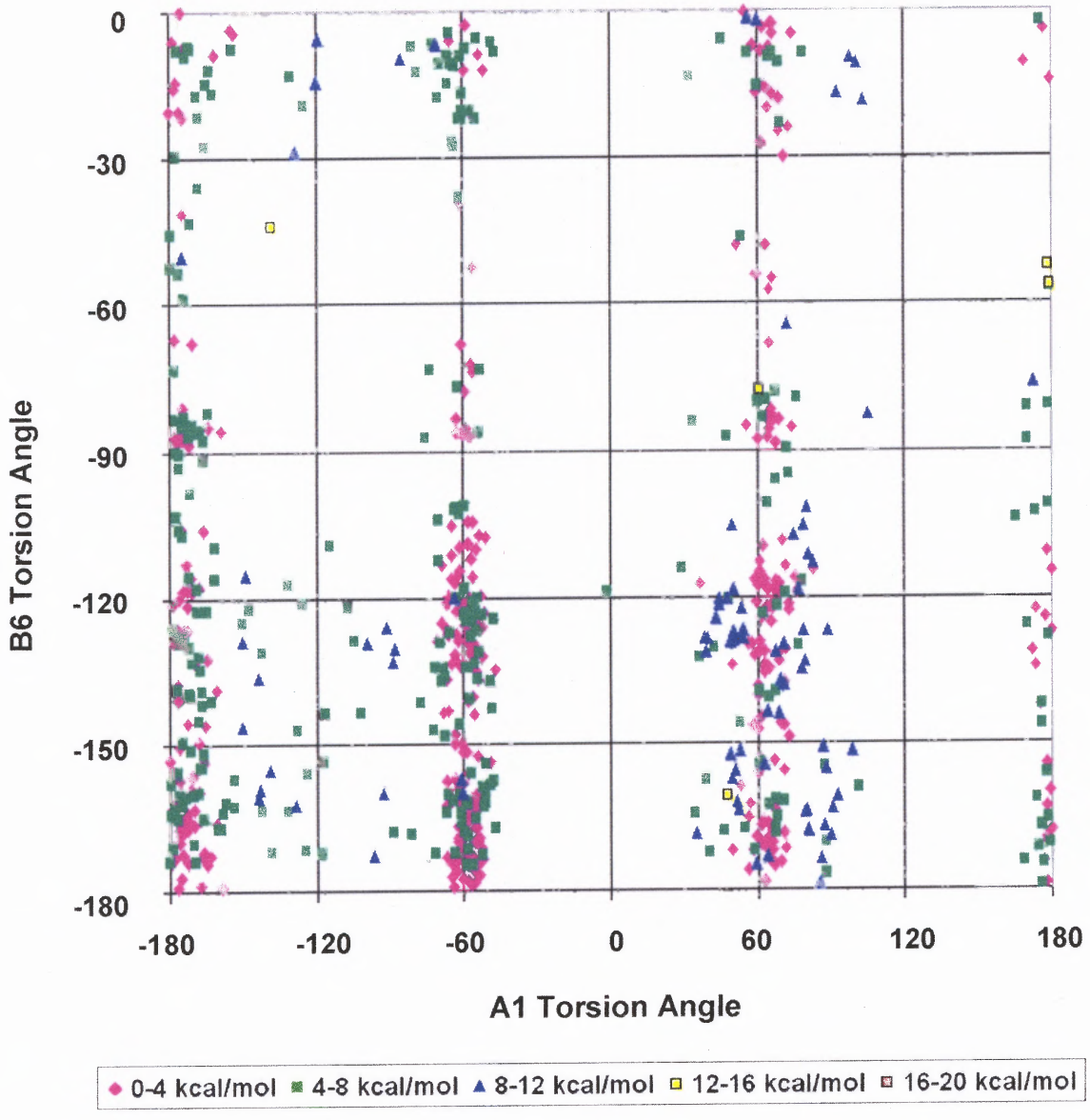

Figure D.60 Protonated TP250 (Tripos, solvent) B6 vs A1 torsion angles.

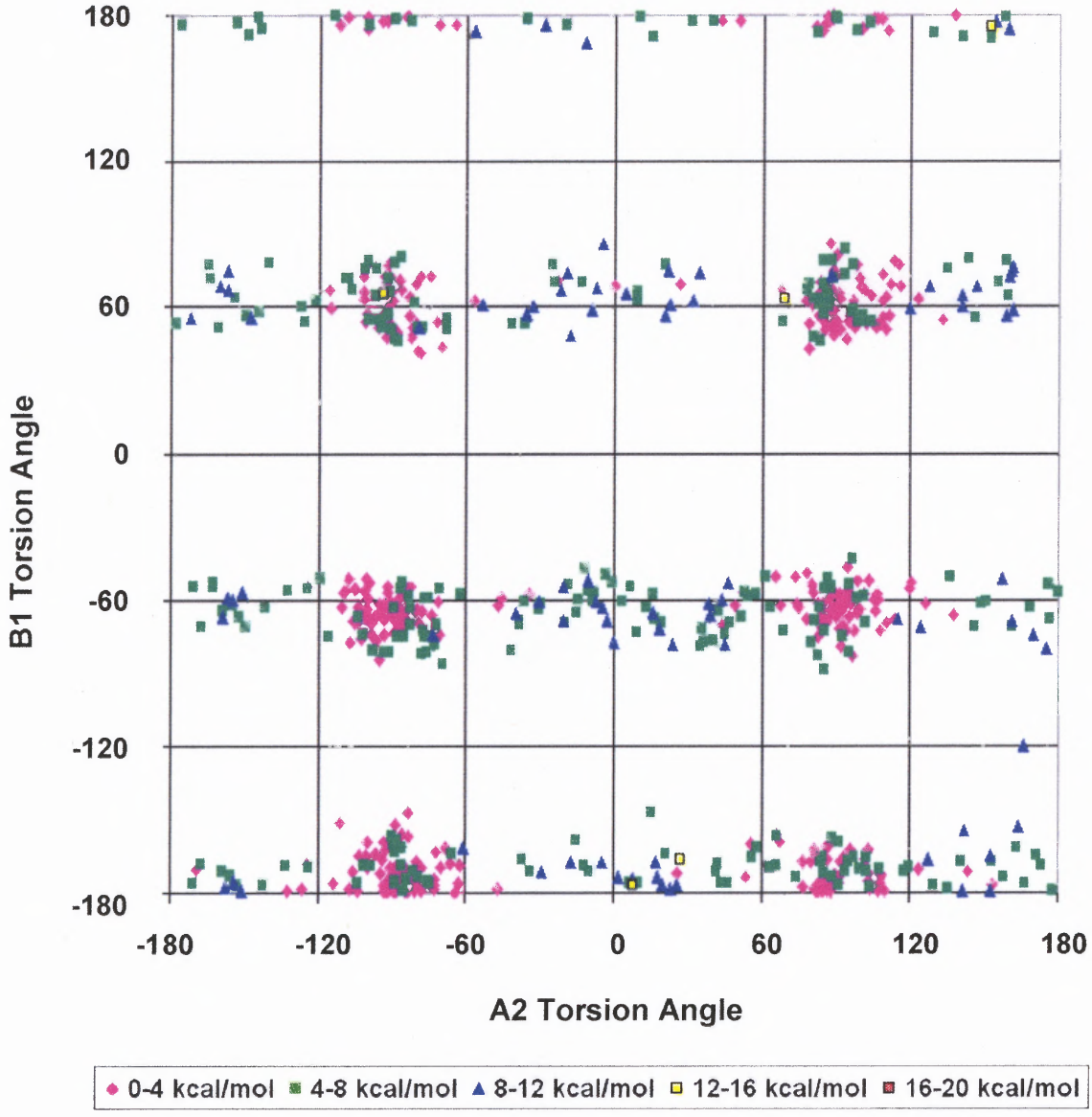

Figure D.61 Protonated TP250 (Tripos, solvent) B1 vs A2 torsion angles.

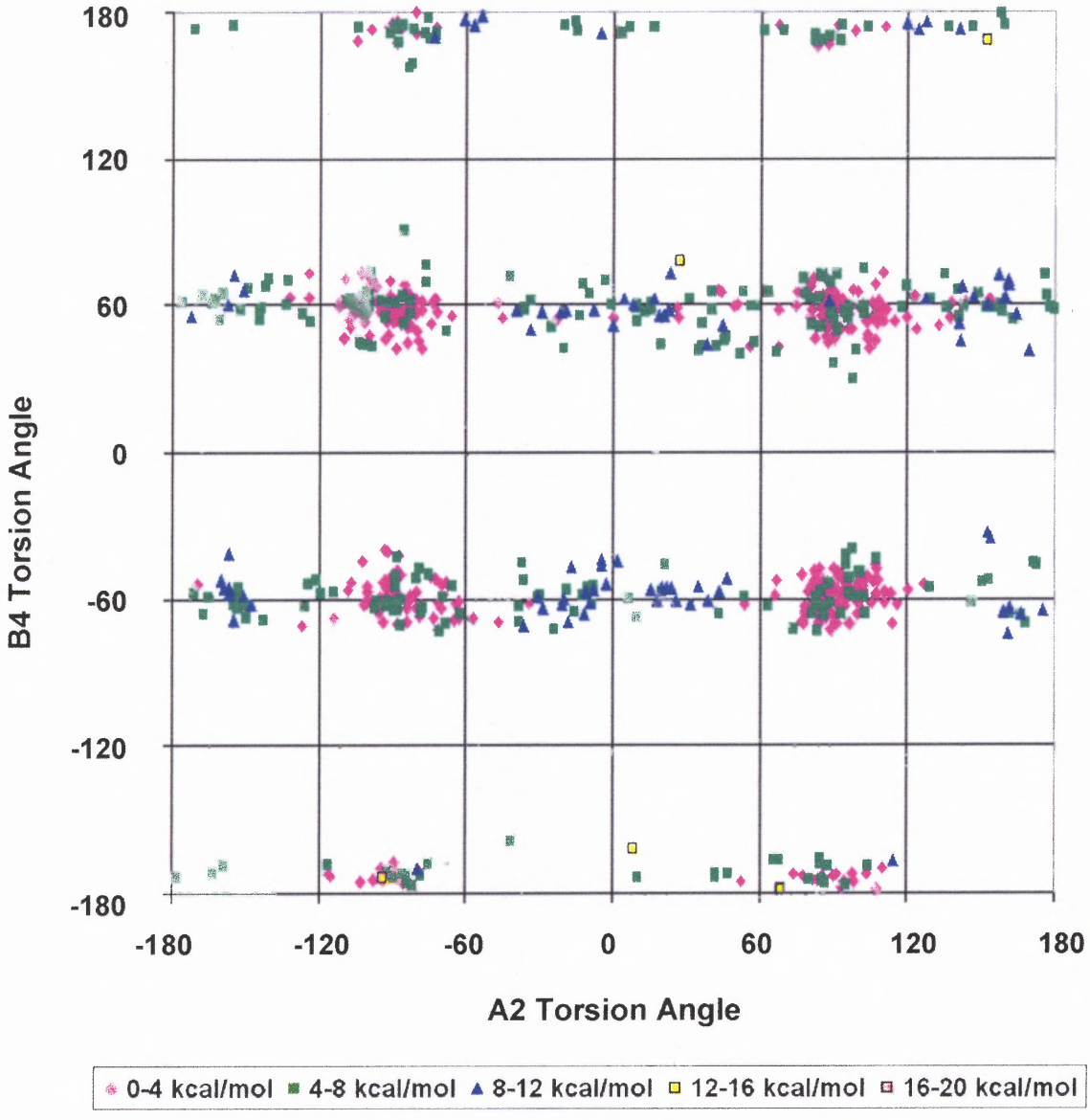

Figure D.62 Protonated TP250 (Tripos, solvent) B4 vs A2 torsion angles.

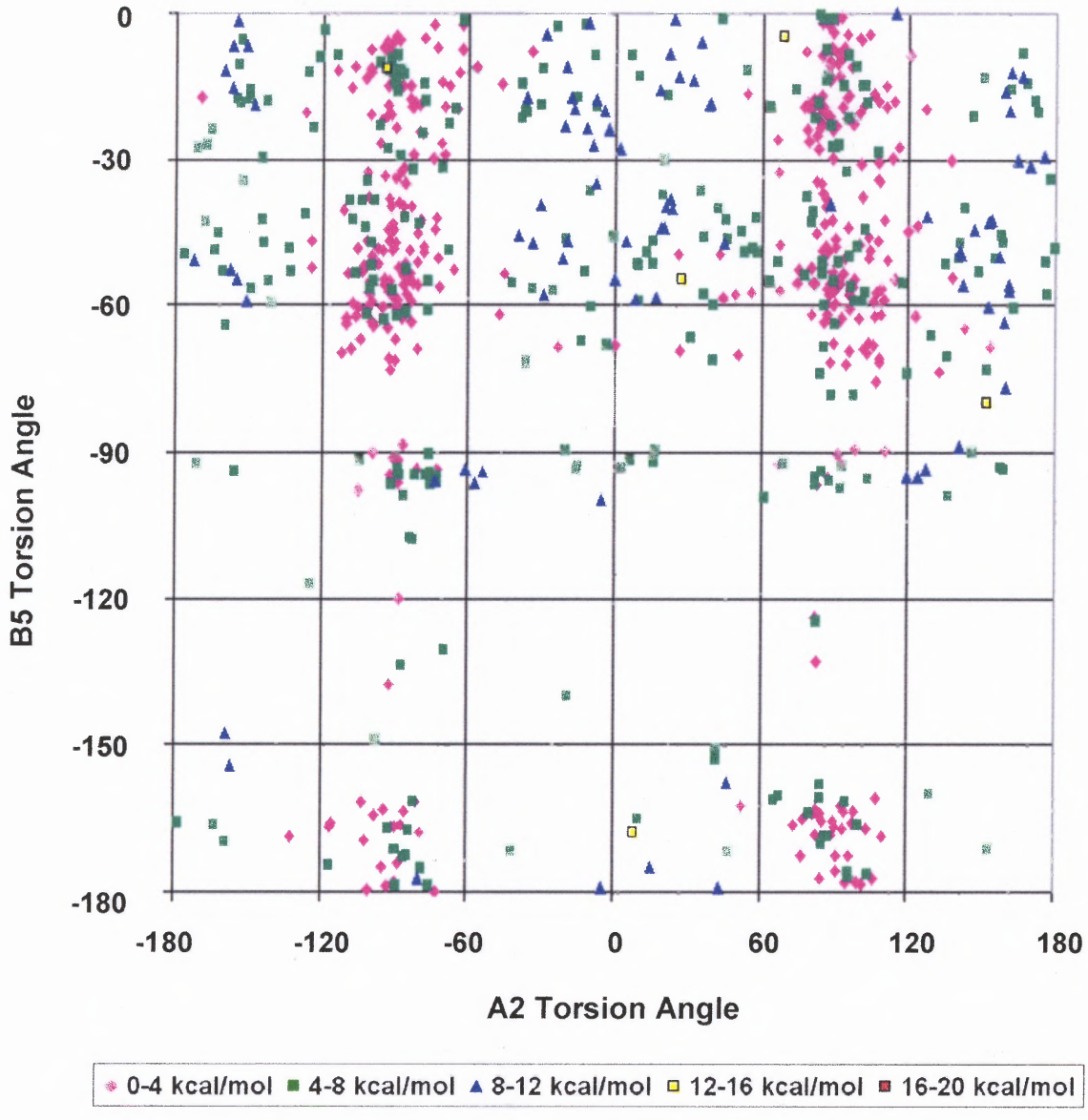

Figure D.63 Protonated TP250 (Tripos, solvent) B5 vs A2 torsion angles.

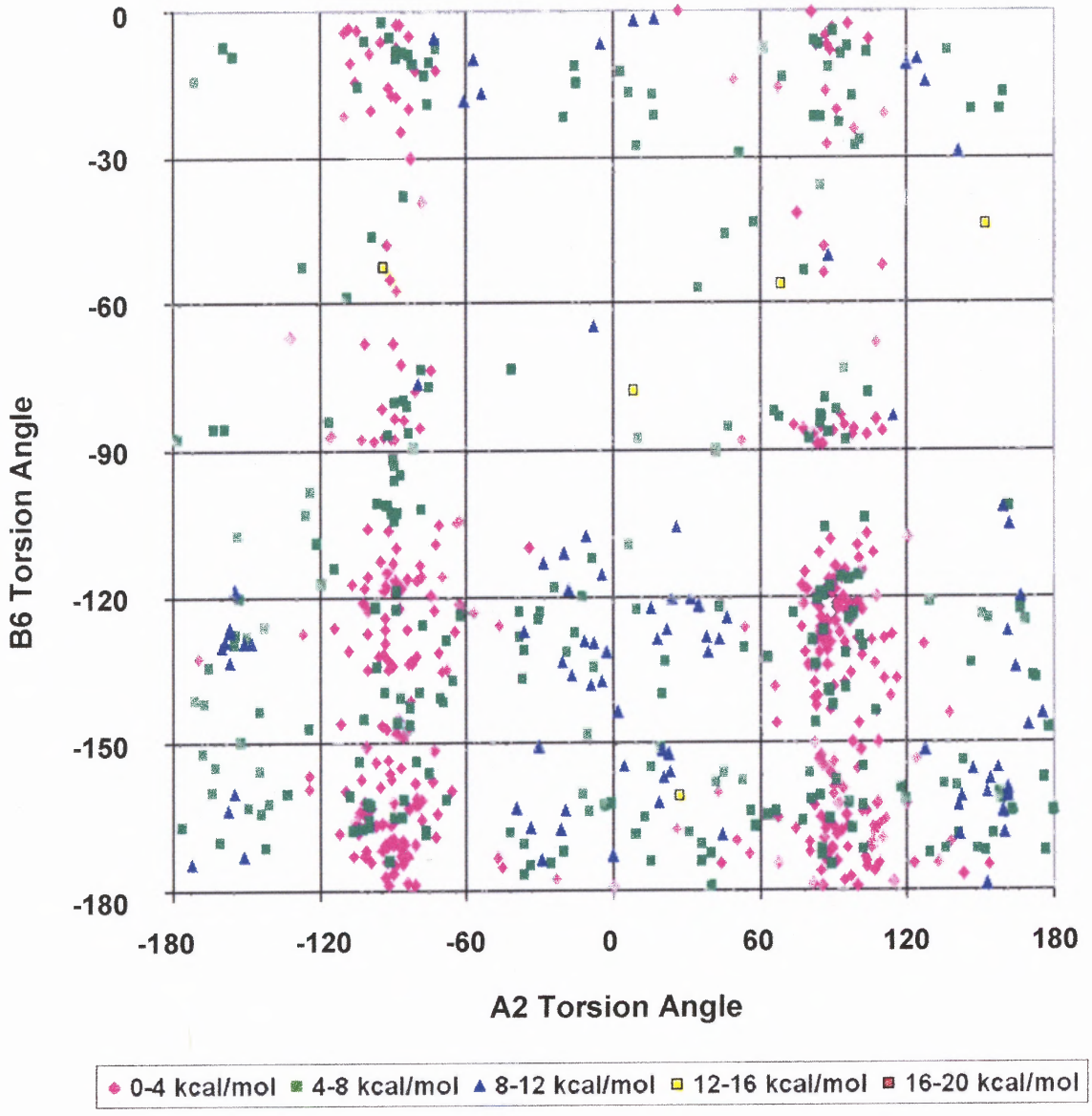

Figure D.64 Protonated TP250 (Tripos, solvent) B6 vs A2 torsion angles.

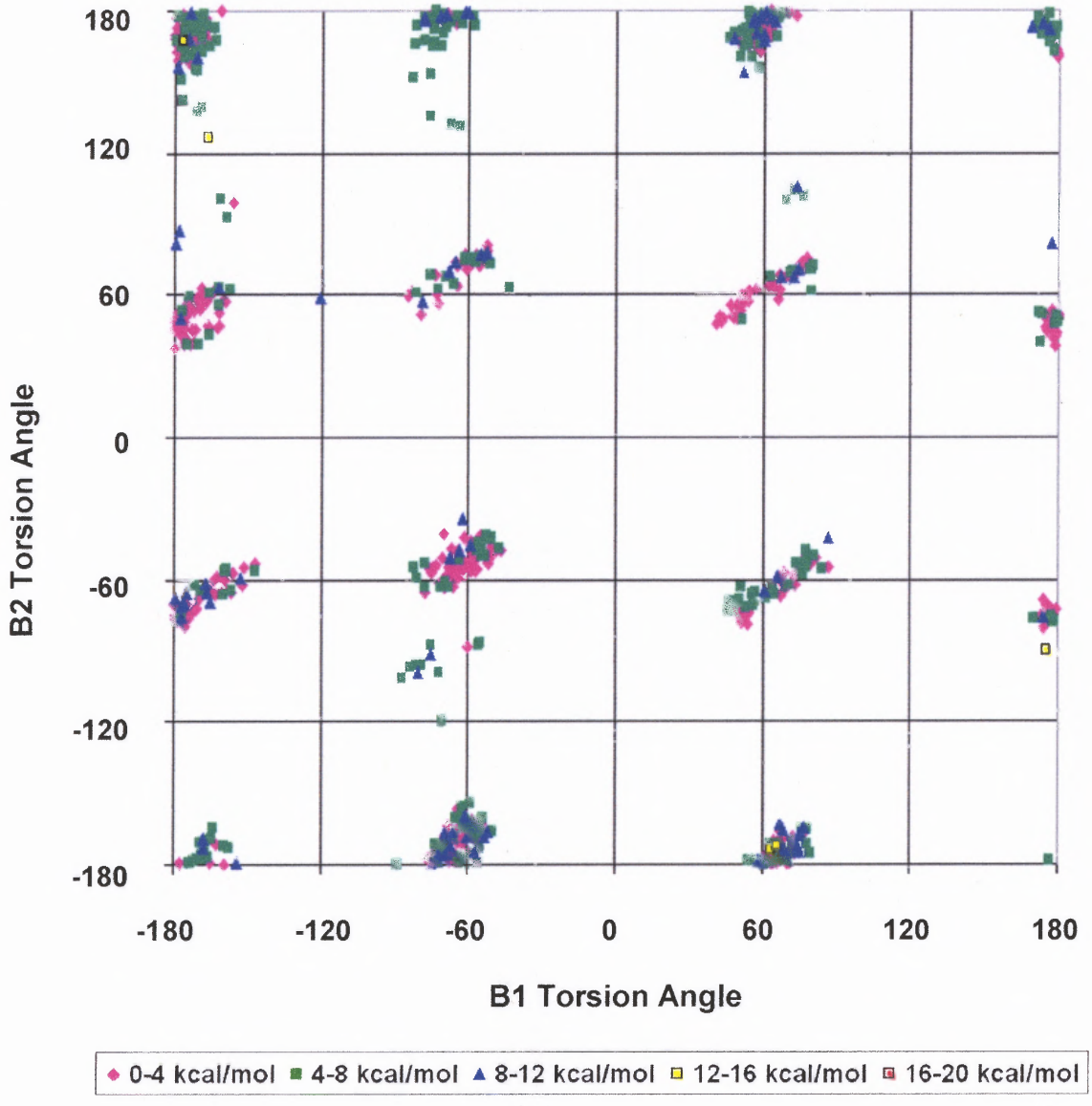

Figure D.65 Protonated TP250 (Tripos, solvent) B2 vs B1 torsion angles.

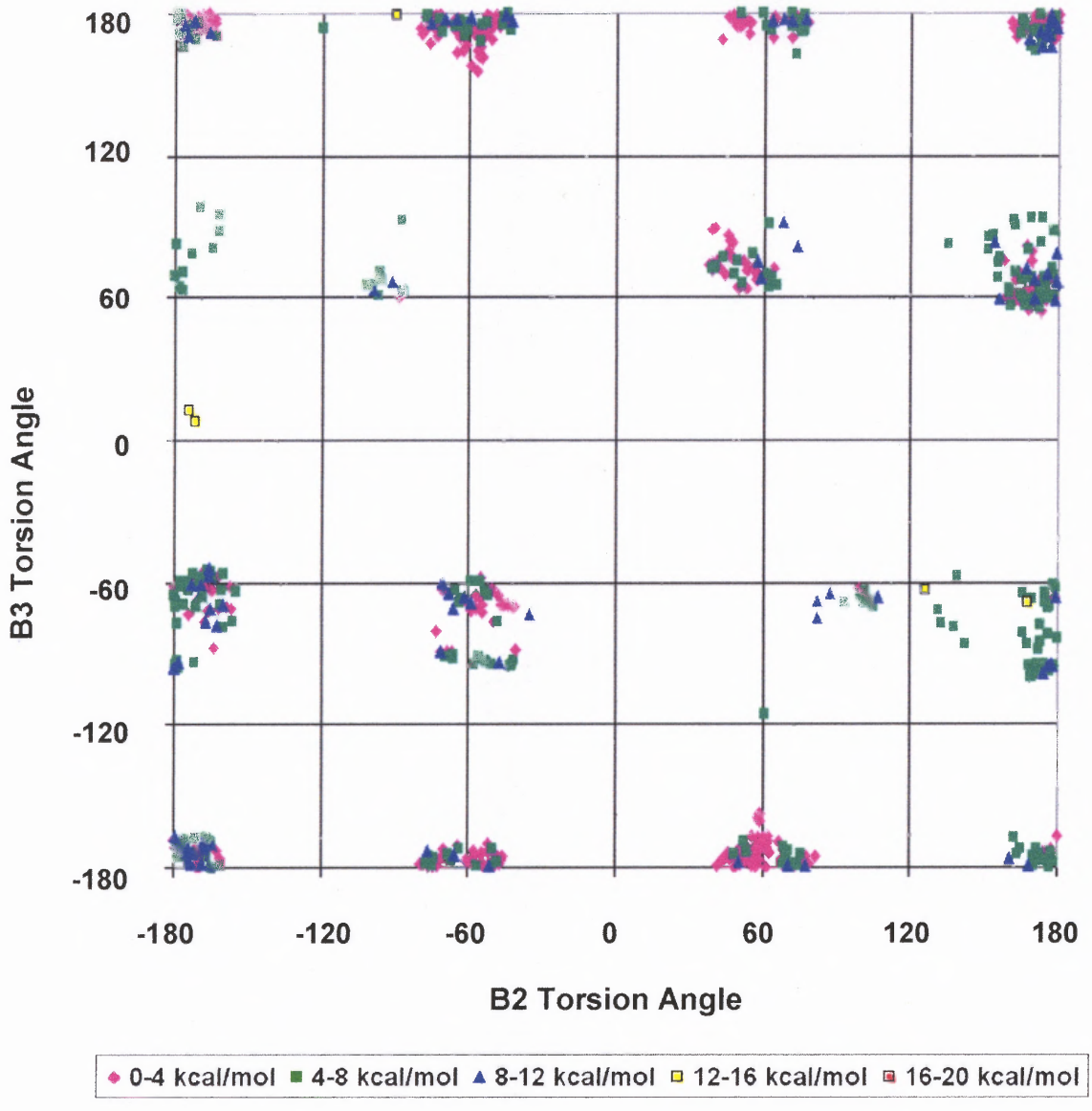

Figure D.66 Protonated TP250 (Tripos, solvent) B3 vs B2 torsion angles.

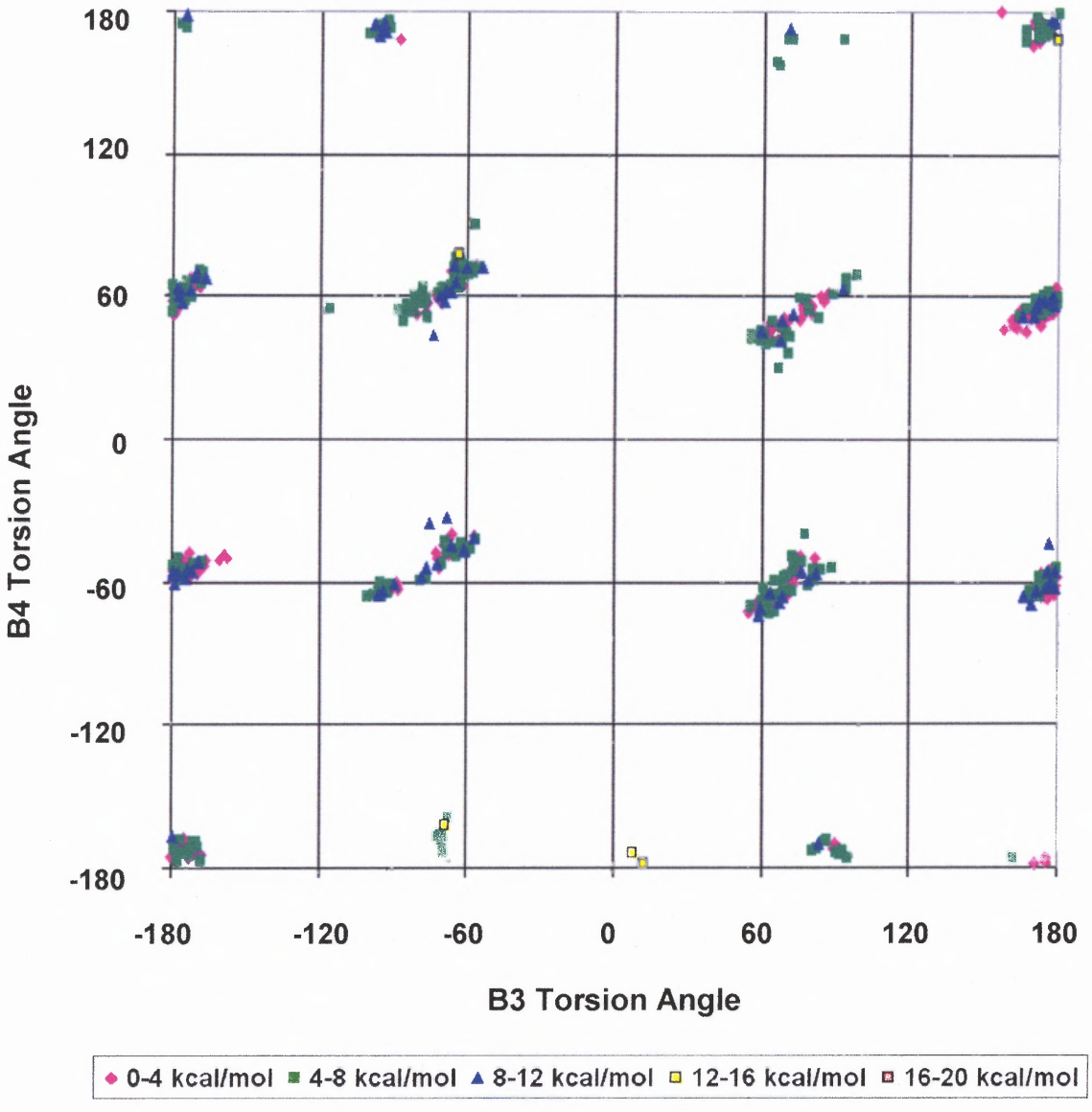

Figure D.67 Protonated TP250 (Tripos, solvent) B4 vs B3 torsion angles.

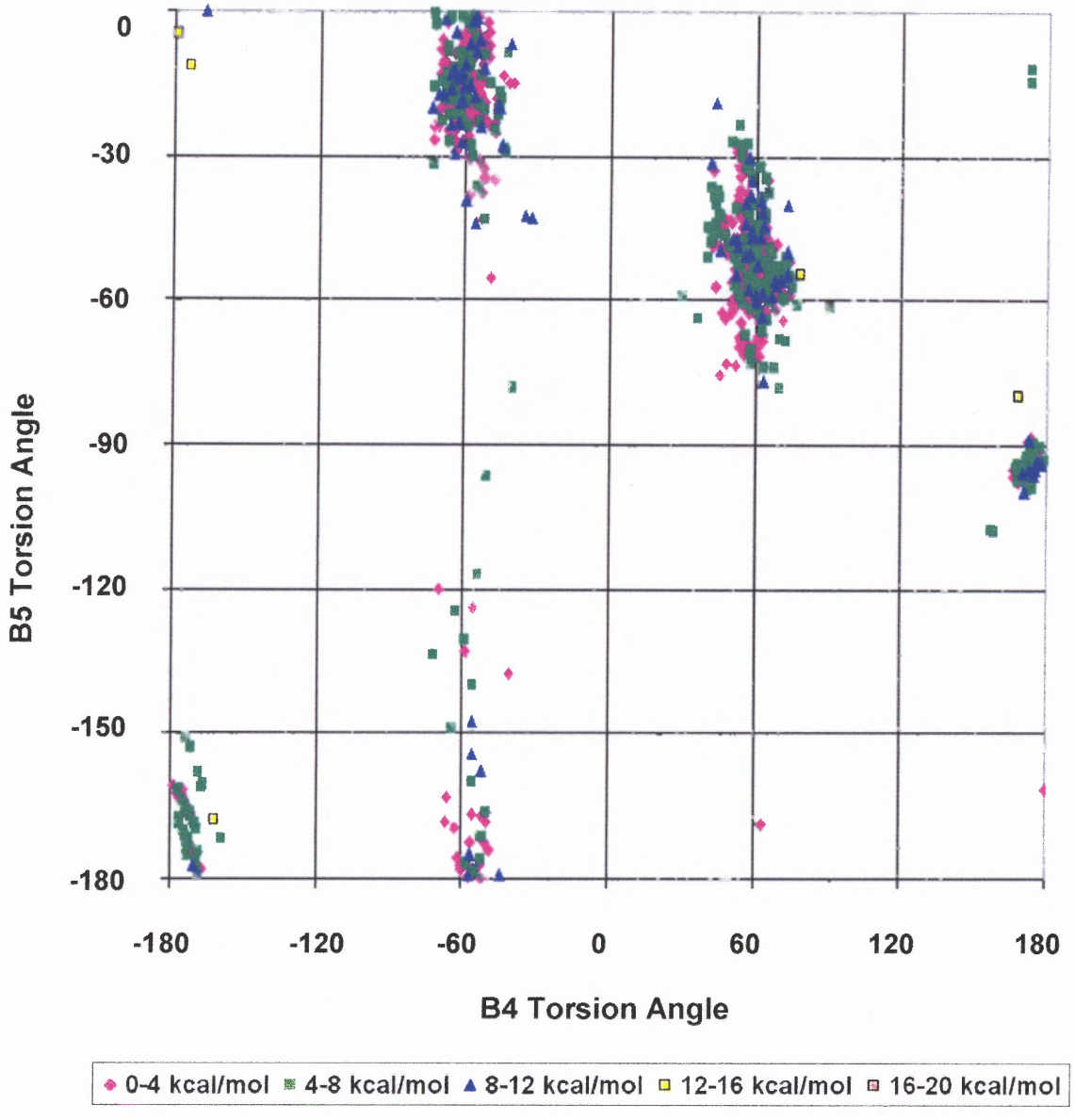

Figure D.68 Protonated TP250 (Tripos, solvent) B5 vs B4 torsion angles.

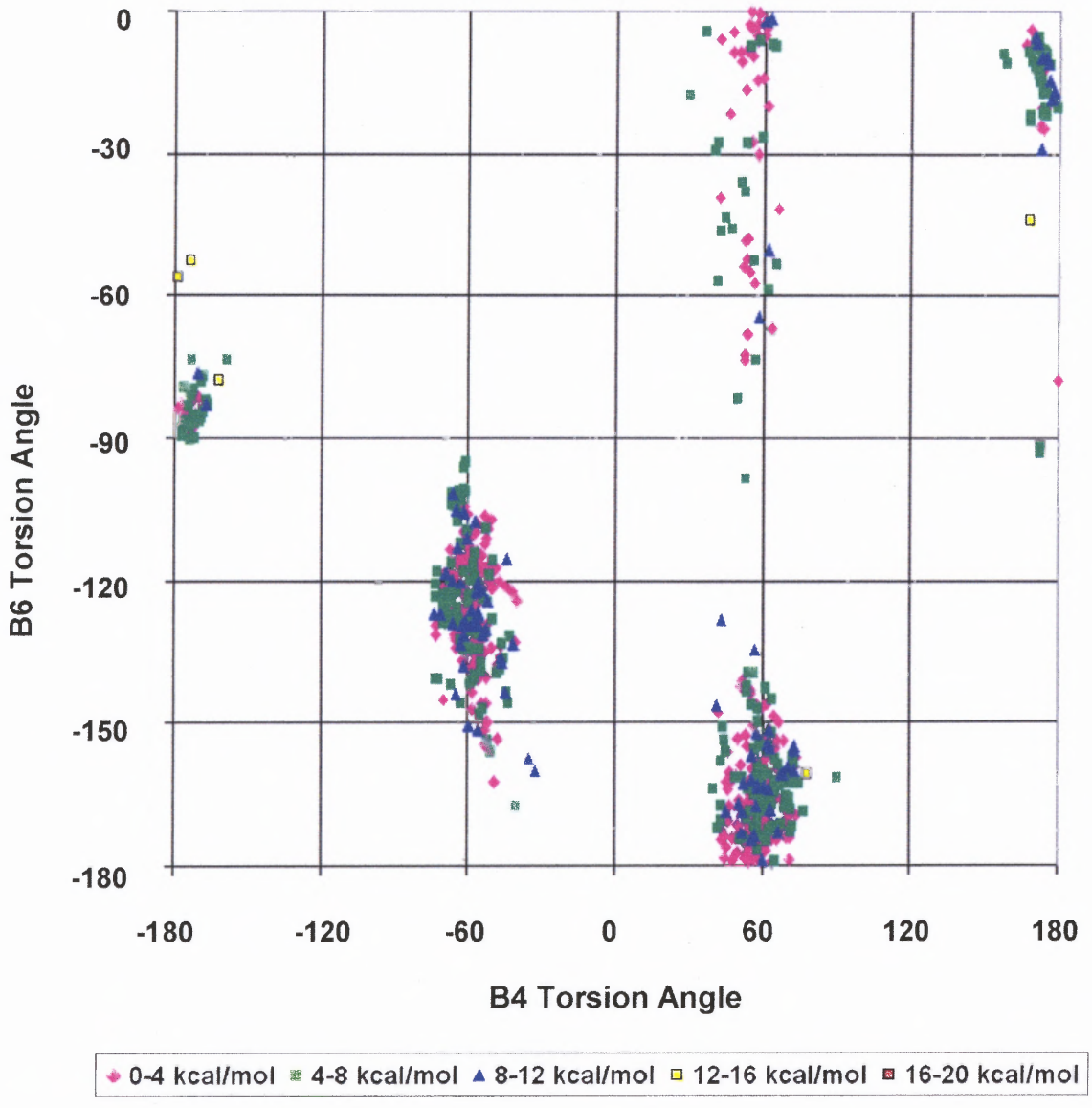

Figure D.69 Protonated TP250 (Tripos, solvent) B6 vs B4 torsion angles.

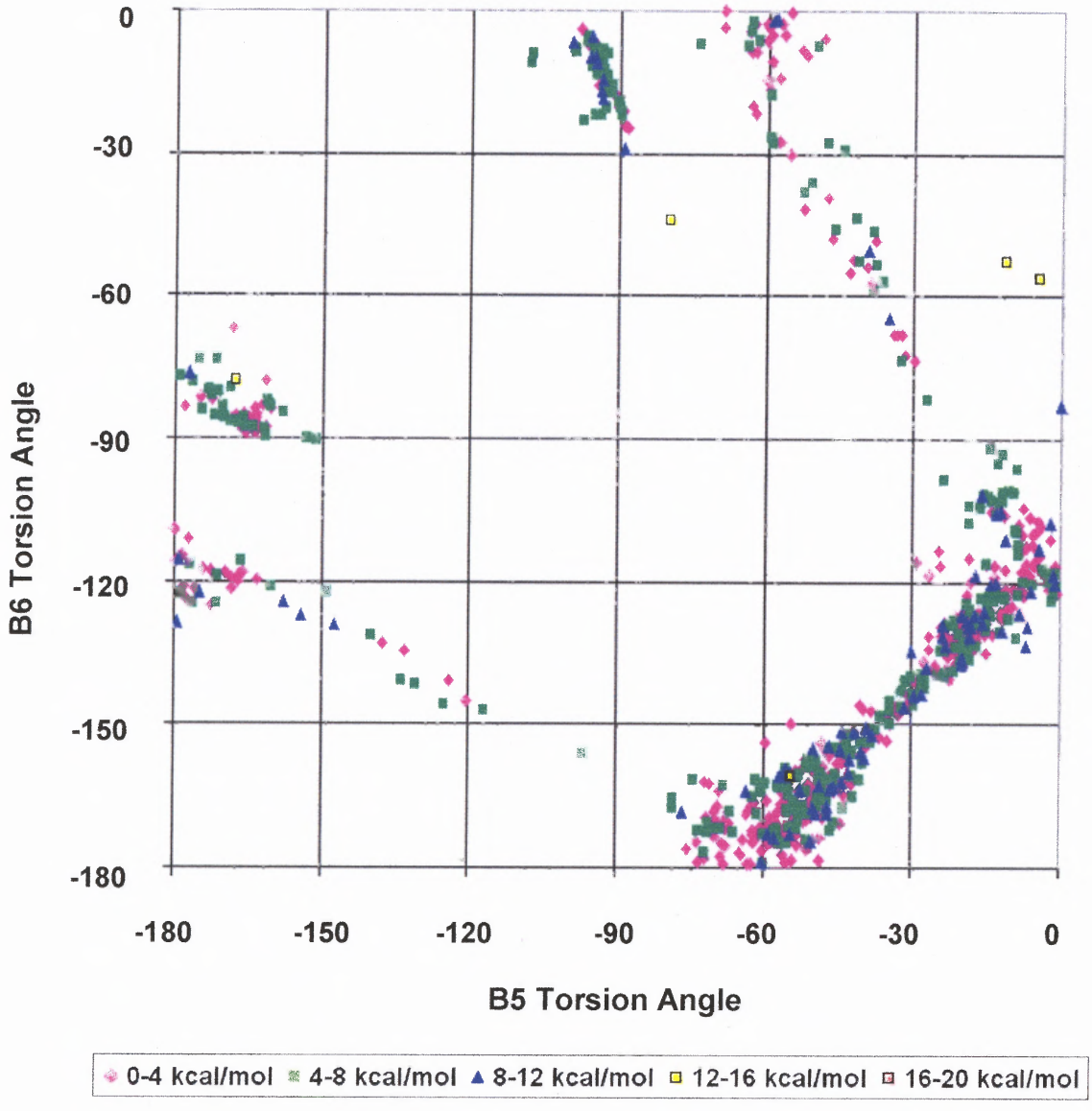

Figure D.70 Protonated TP250 (Tripos, solvent) B6 vs B5 torsion angles.

D.6 MMFF94 for DM324 and Vacuum

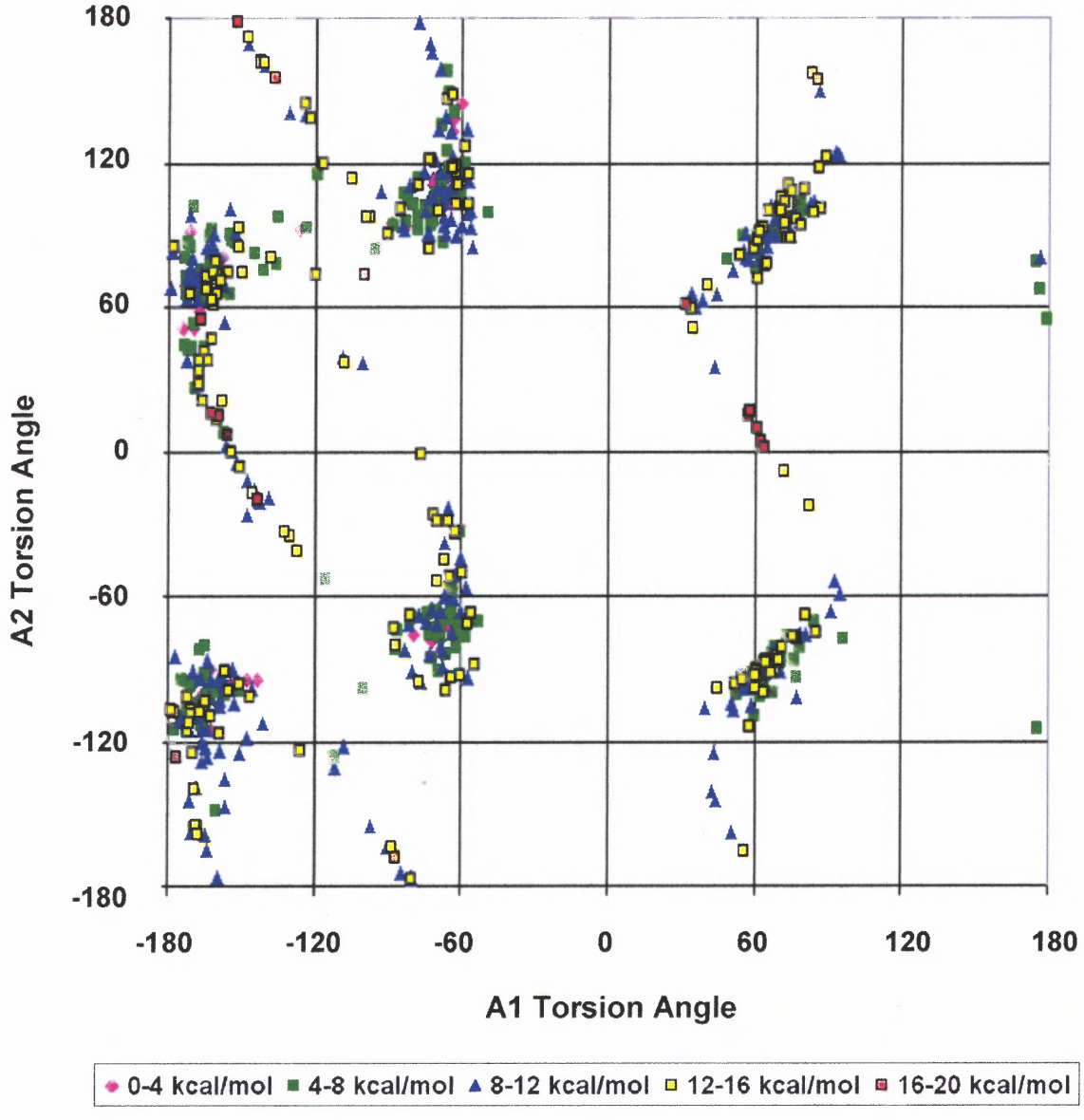

Figure D.71 Protonated DM324 (Tripos, vacuum) A2 vs A1 Torsion Angles.

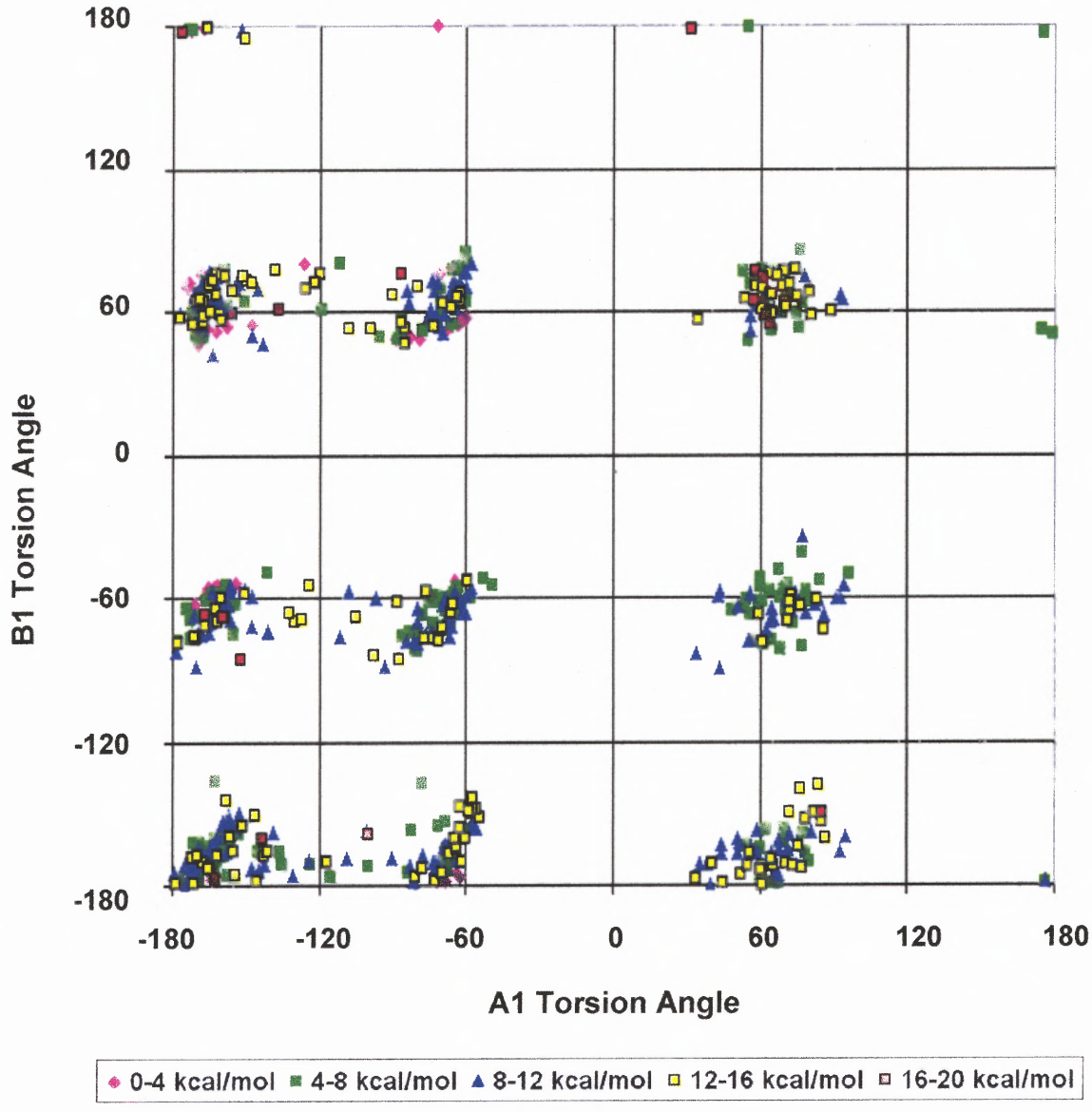

Figure D.72 Protonated DM324 (Tripos, vacuum) B1 vs A1 Torsion Angles.

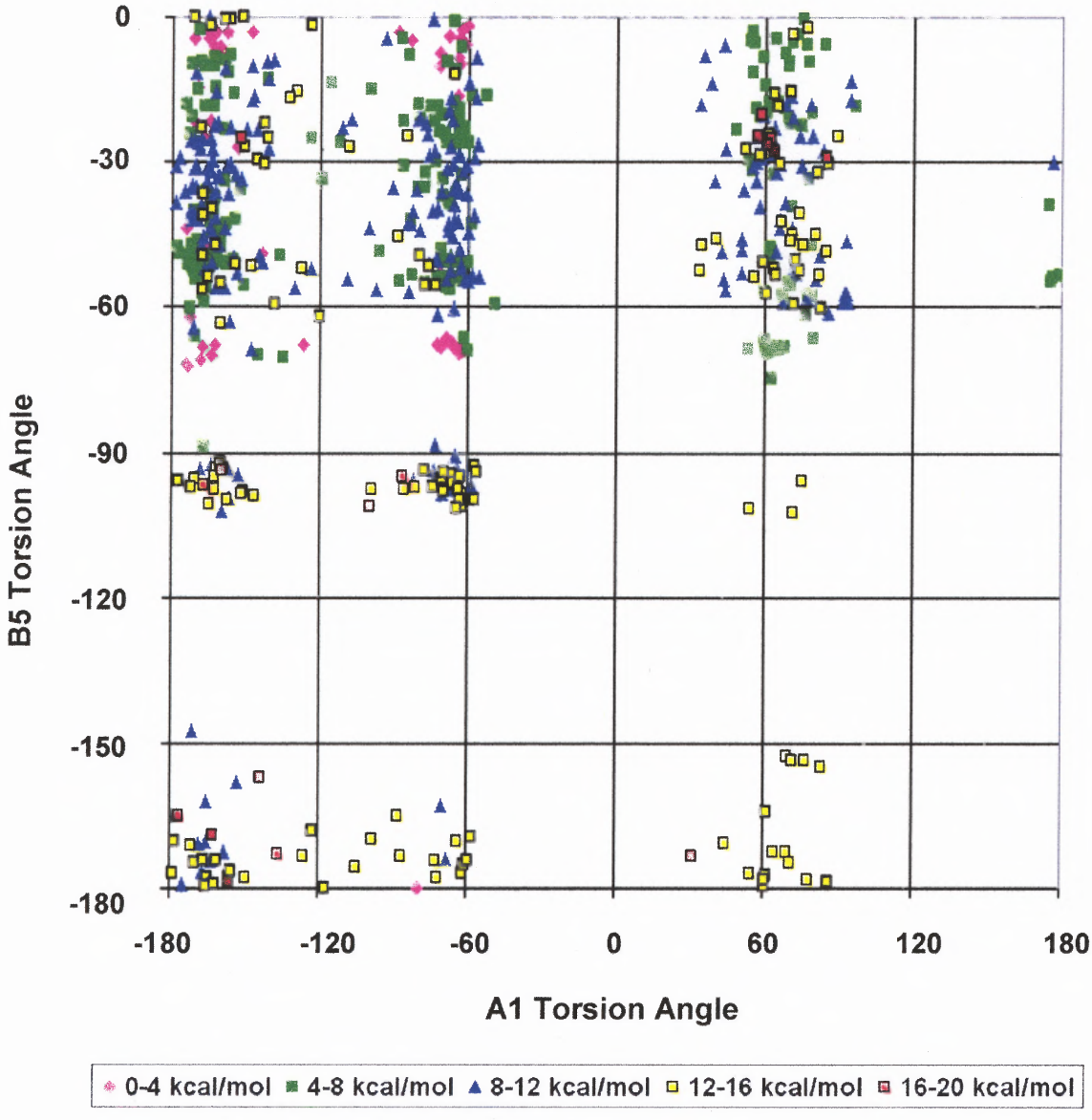

Figure D.73 Protonated DM324 (Tripos, vacuum) B5 vs A1 Torsion Angles.

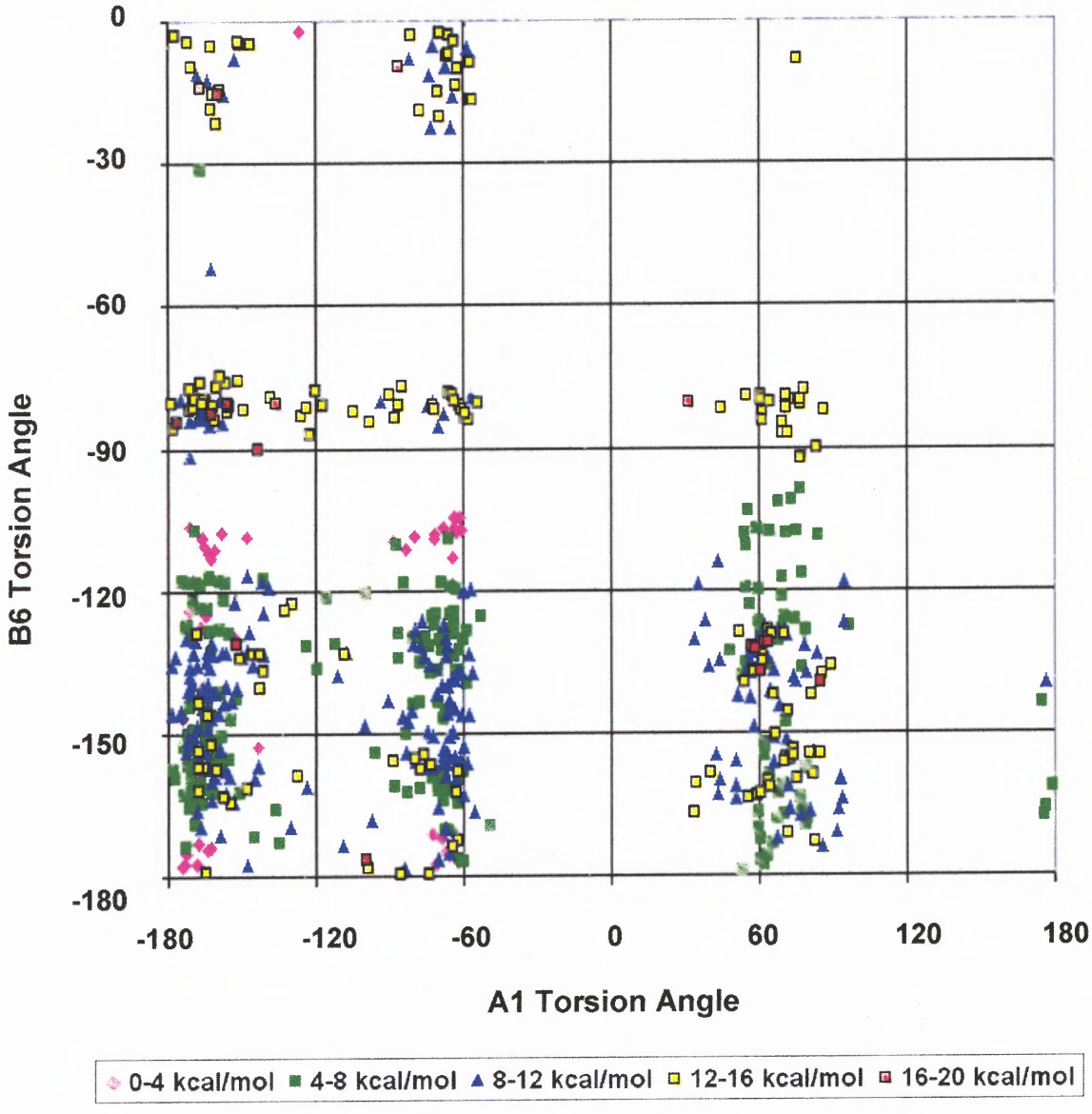

Figure D.74 Protonated DM324 (Tripos, vacuum) B6 vs A1 Torsion Angles.

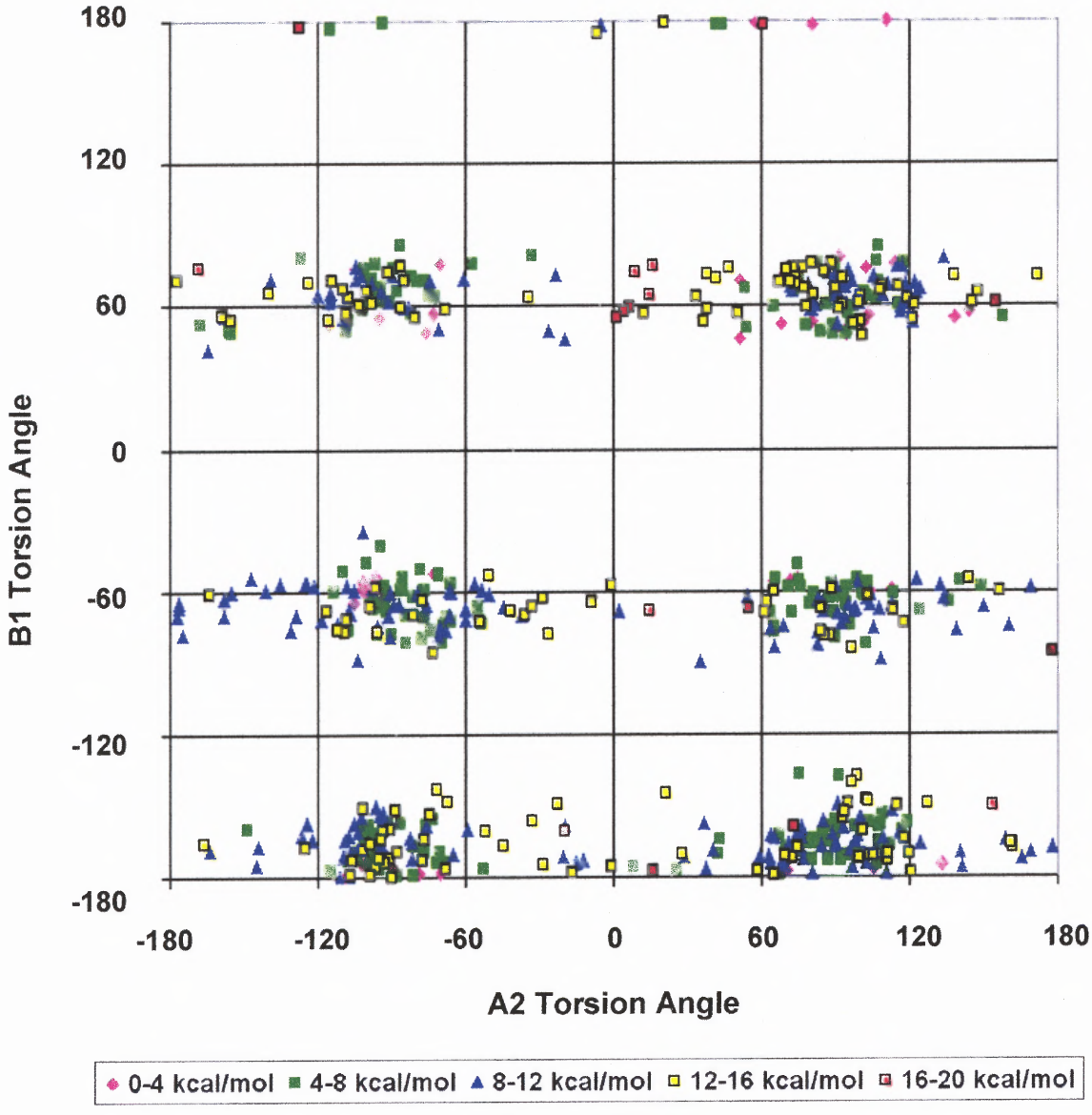

Figure D.75 Protonated DM324 (Tripos, vacuum) B1 vs A2 Torsion Angles.

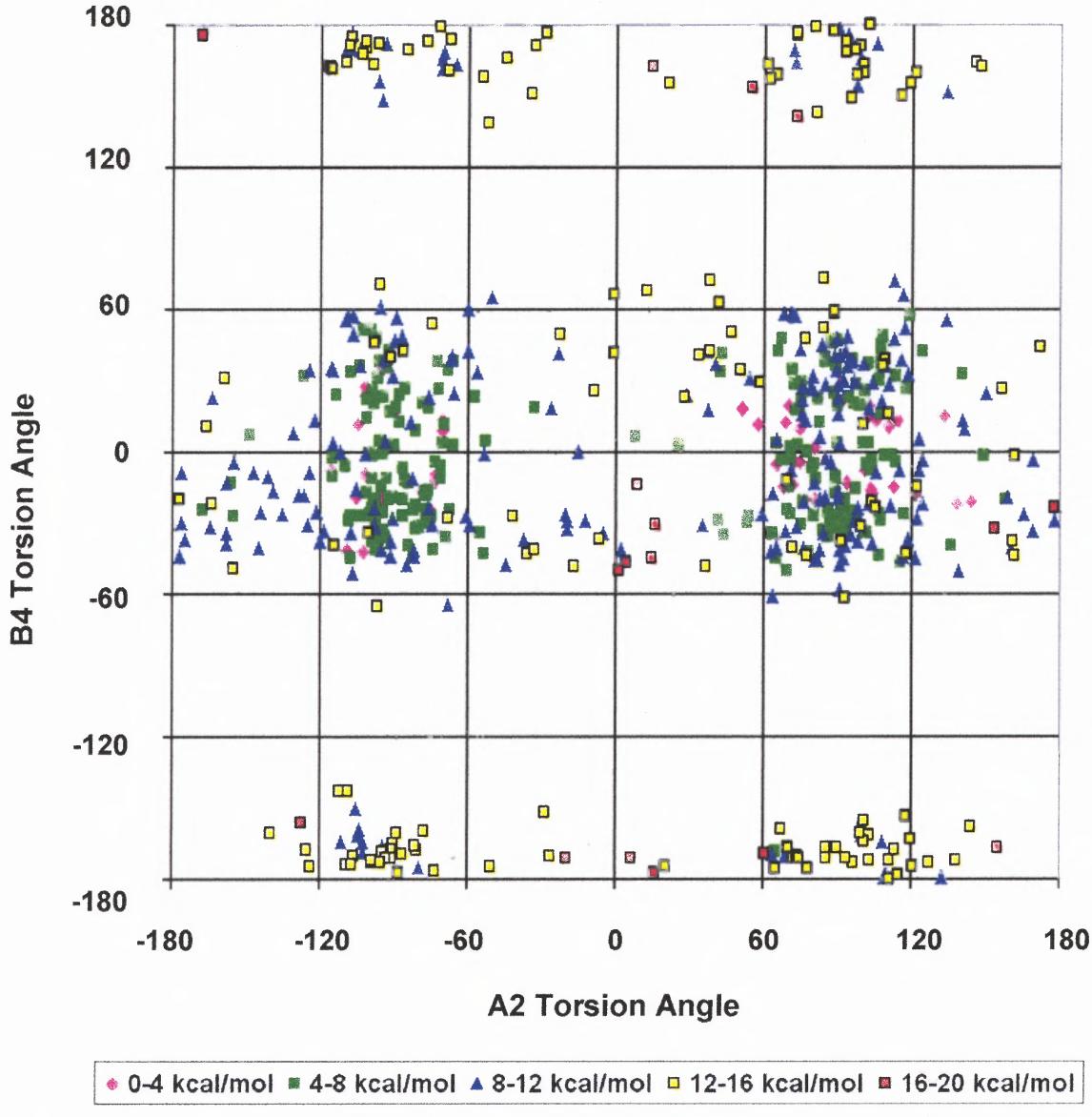

Figure D.76 Protonated DM324 (Tripos, vacuum) B4 vs A2 Torsion Angles.

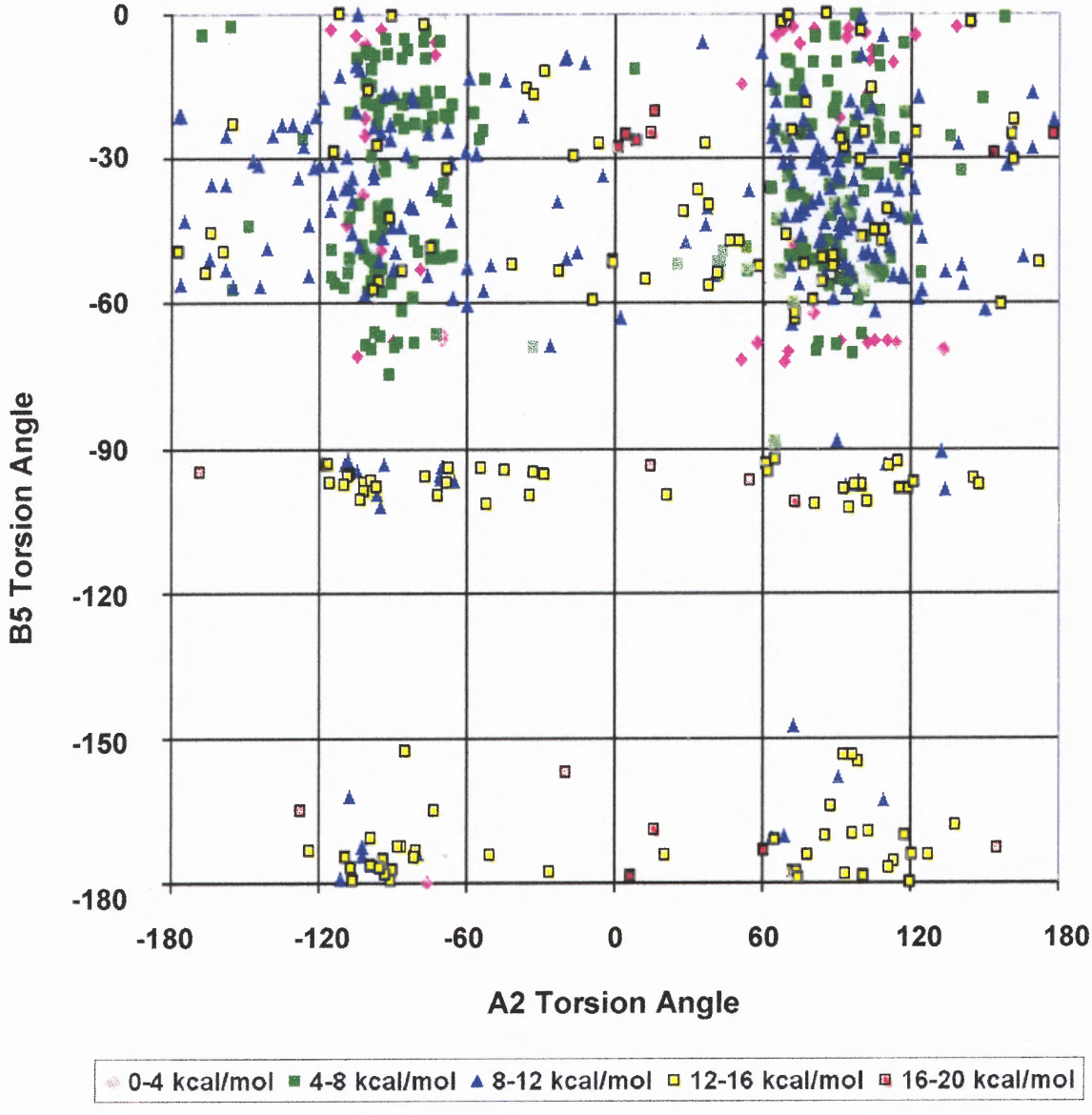

Figure D.77 Protonated DM324 (Tripos, vacuum) B5 vs A2 Torsion Angles.

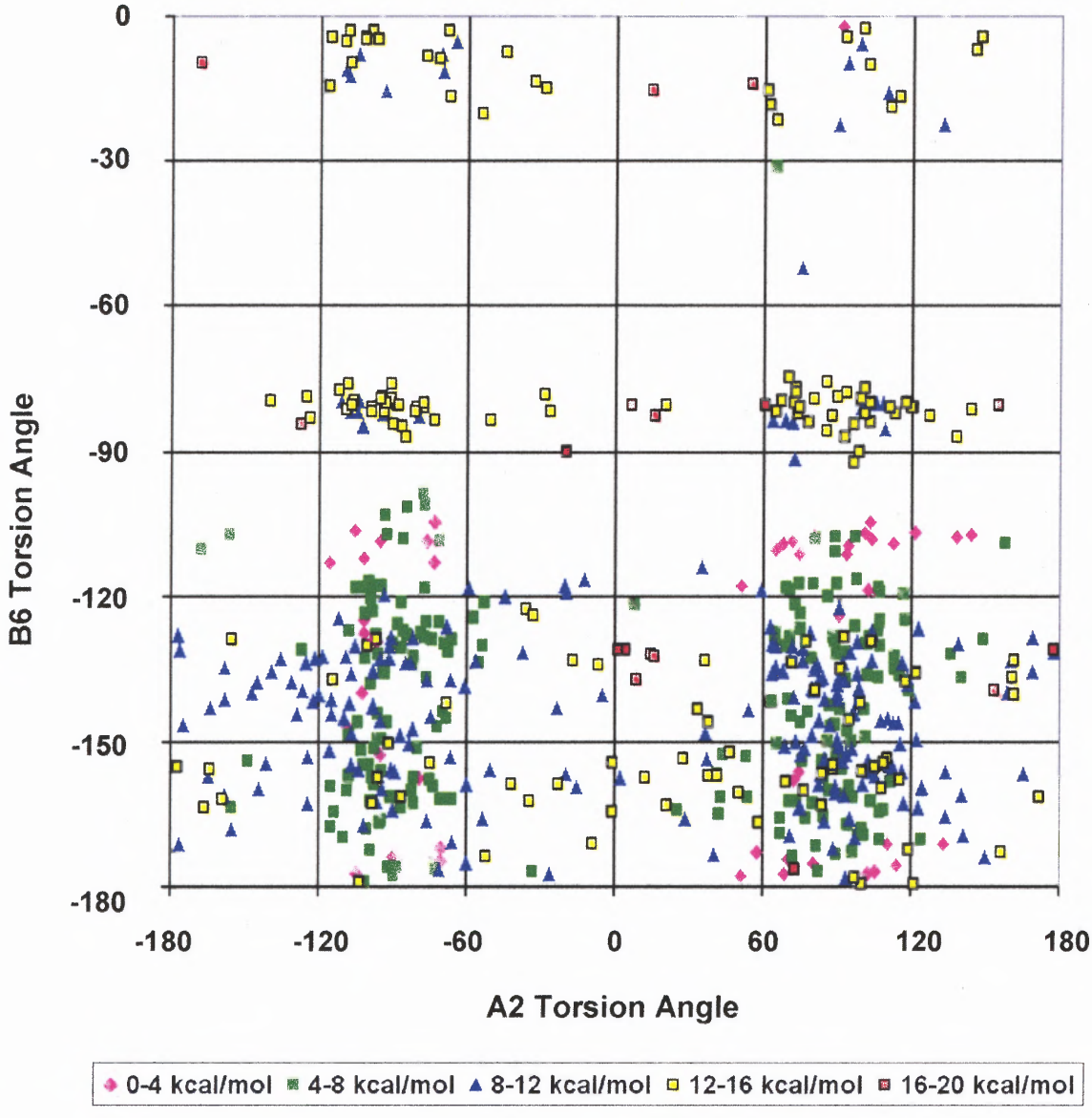

Figure D.78 Protonated DM324 (Tripos, vacuum) B6 vs A2 Torsion Angles.

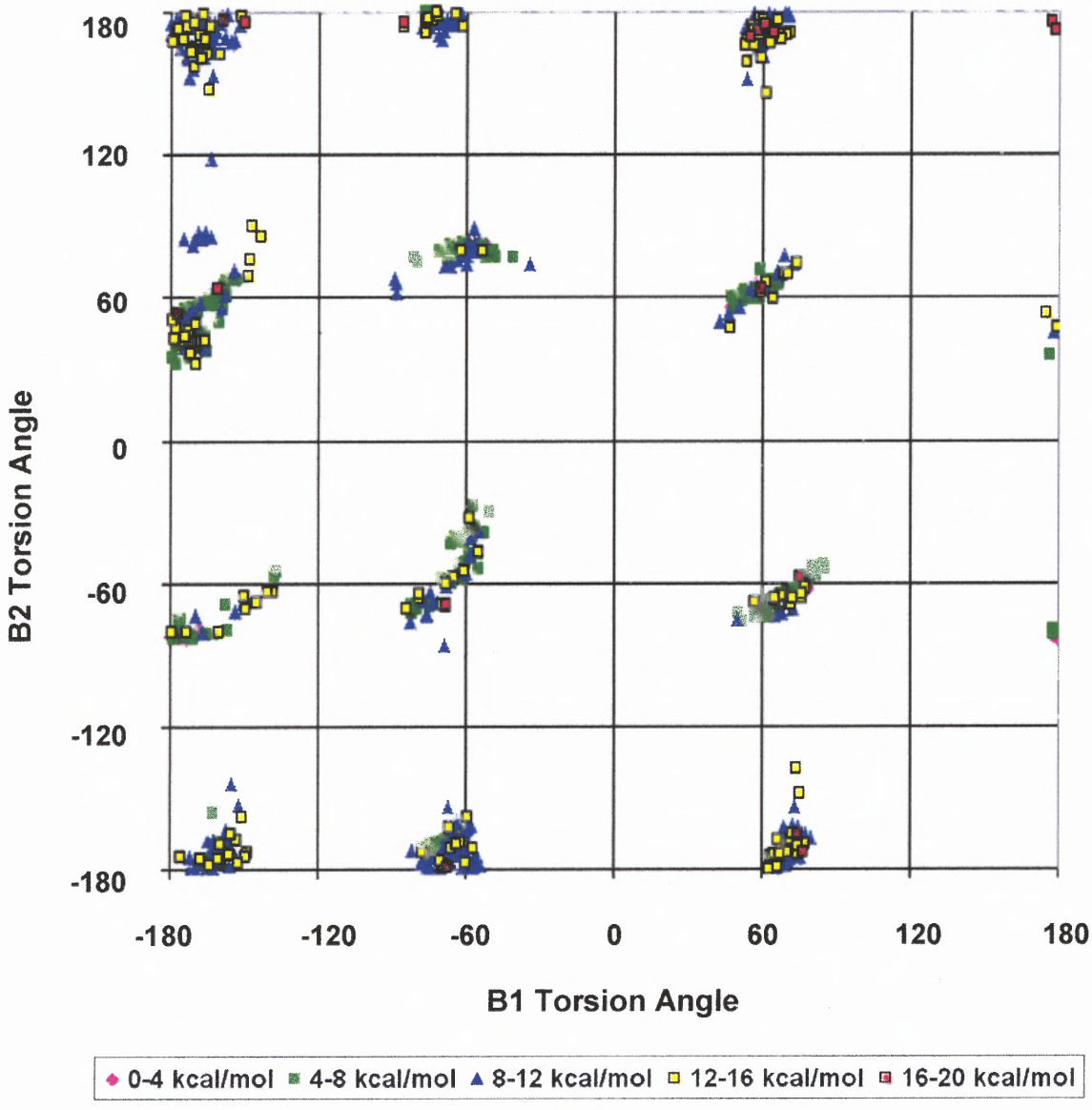

Figure D.79 Protonated DM324 (MMFF94, vacuum) B2 vs B1 Torsion Angles.

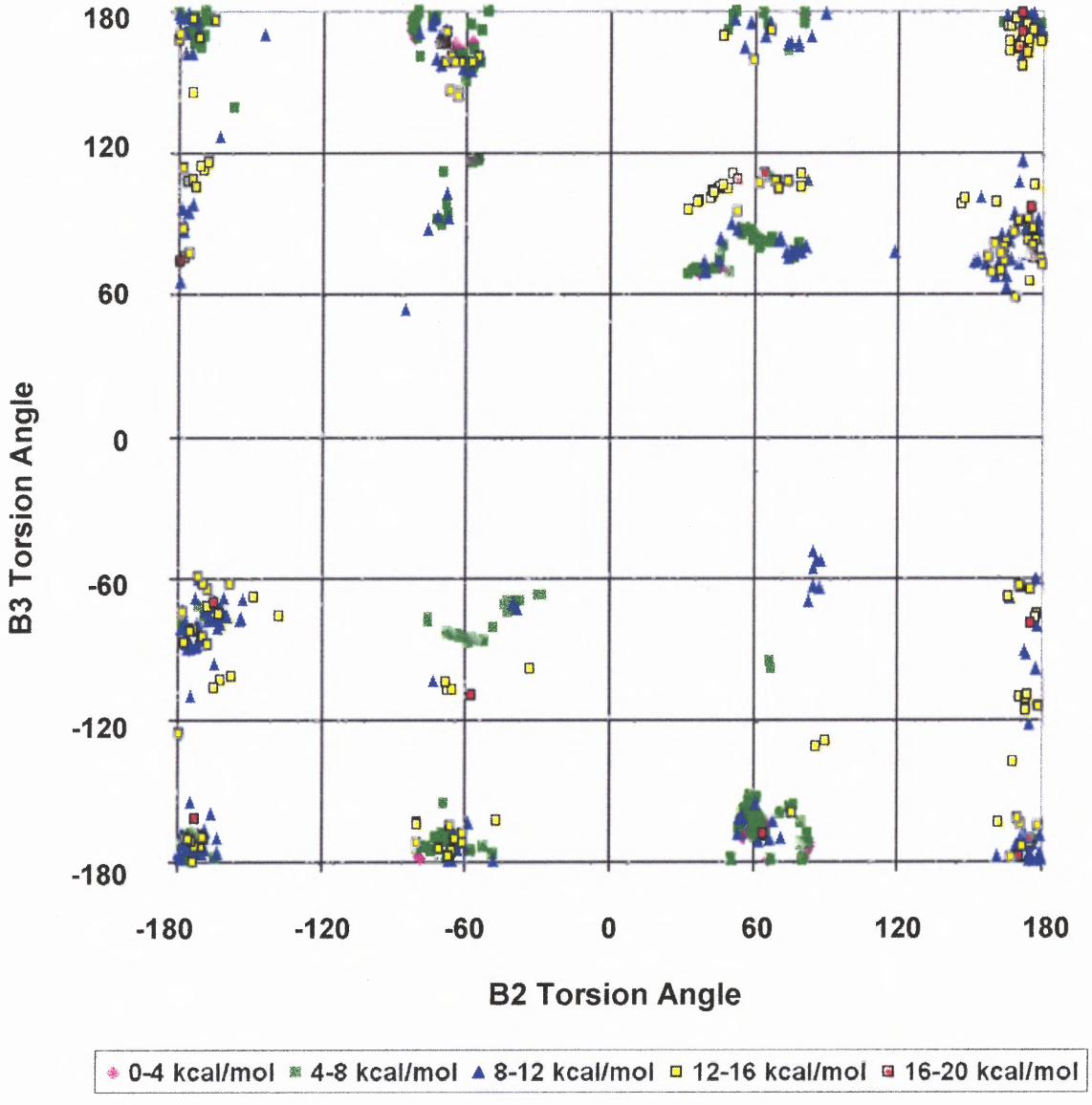

Figure D.80 Protonated DM324 (MMFF94, vacuum) B3 vs B2 Torsion Angles.

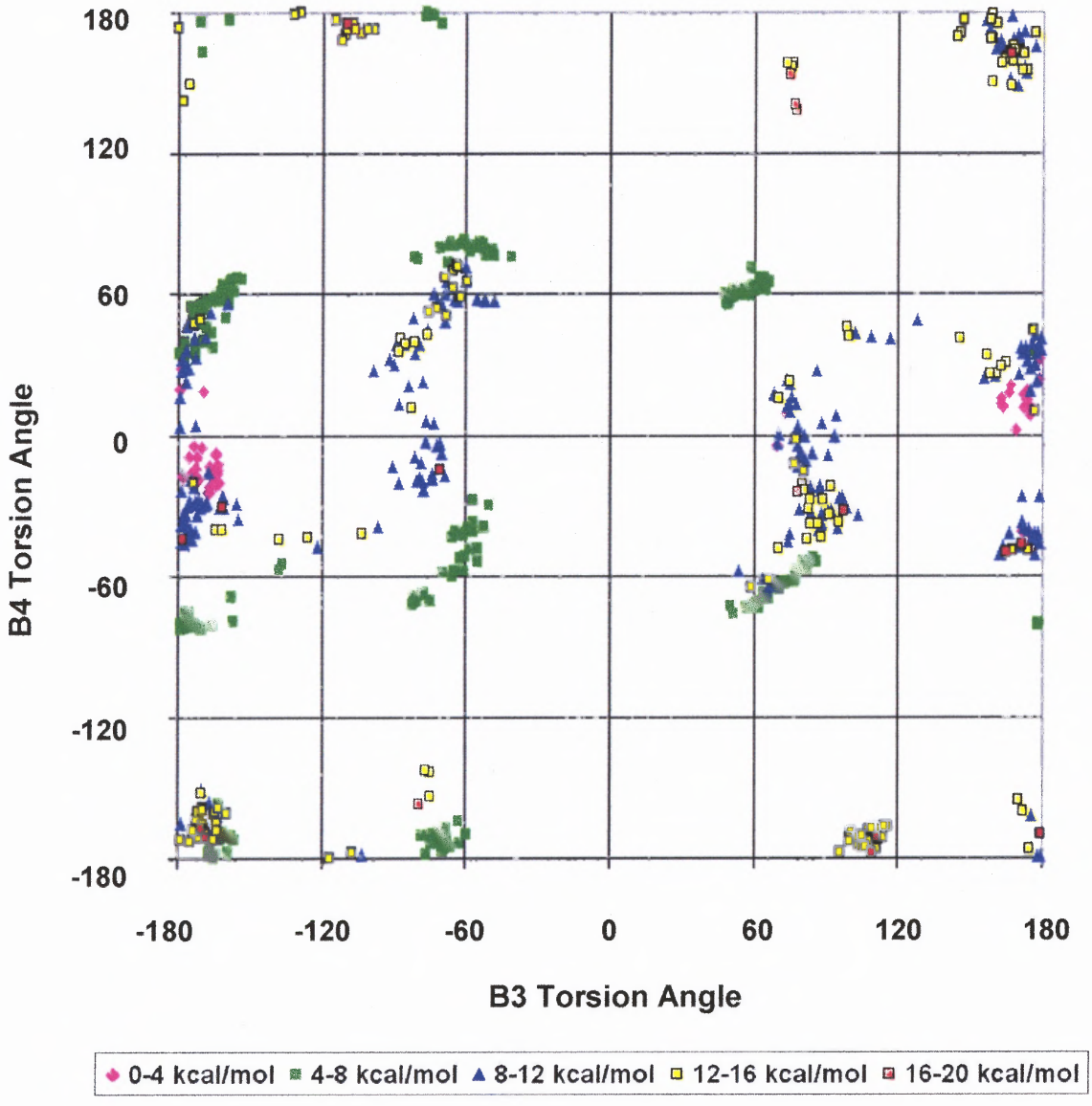

Figure D.81 Protonated DM324 (MMFF94, vacuum) B4 vs B3 Torsion Angles.

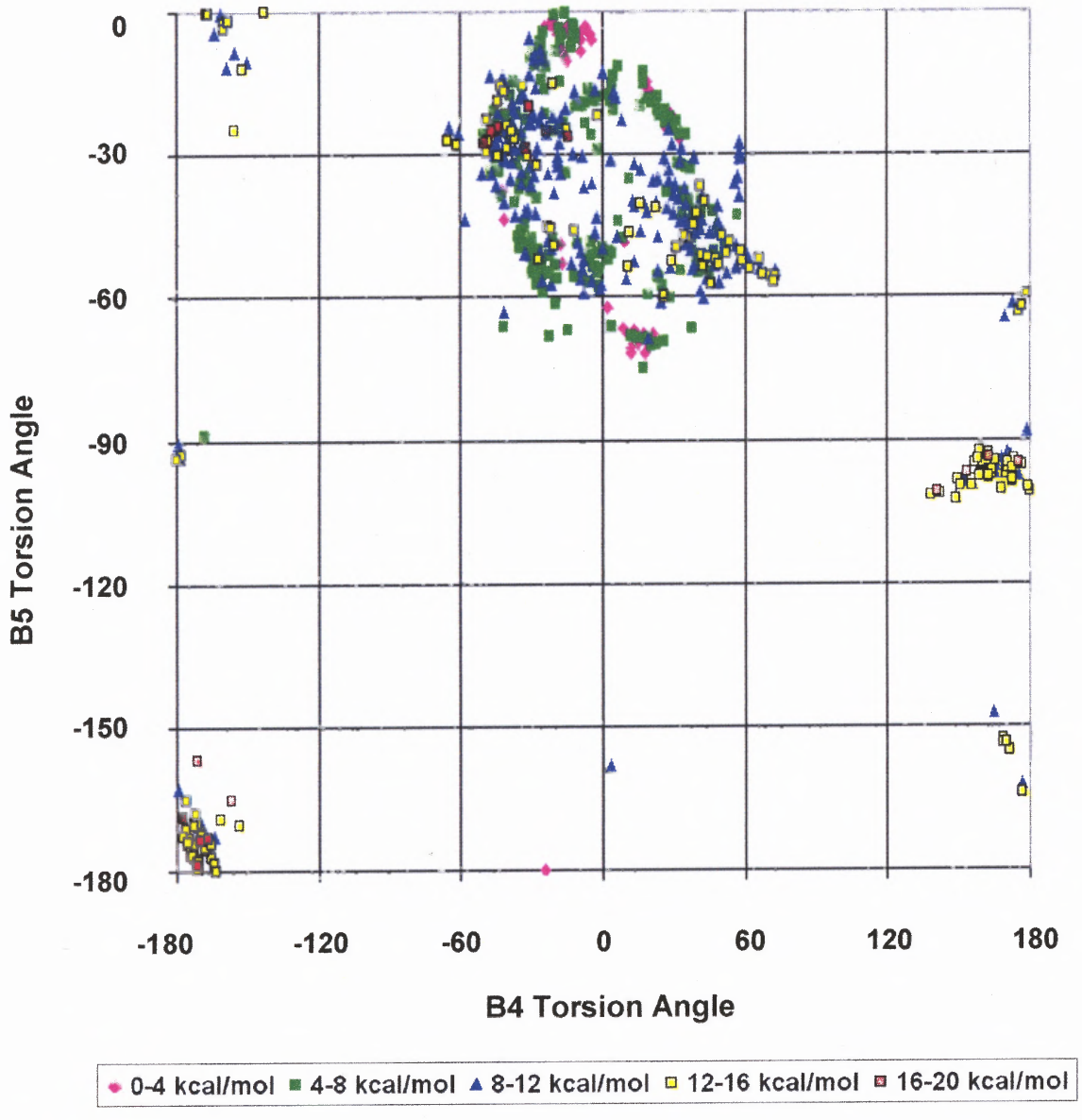

Figure D.82 Protonated DM324 (MMFF94, vacuum) B5 vs B4 Torsion Angles.

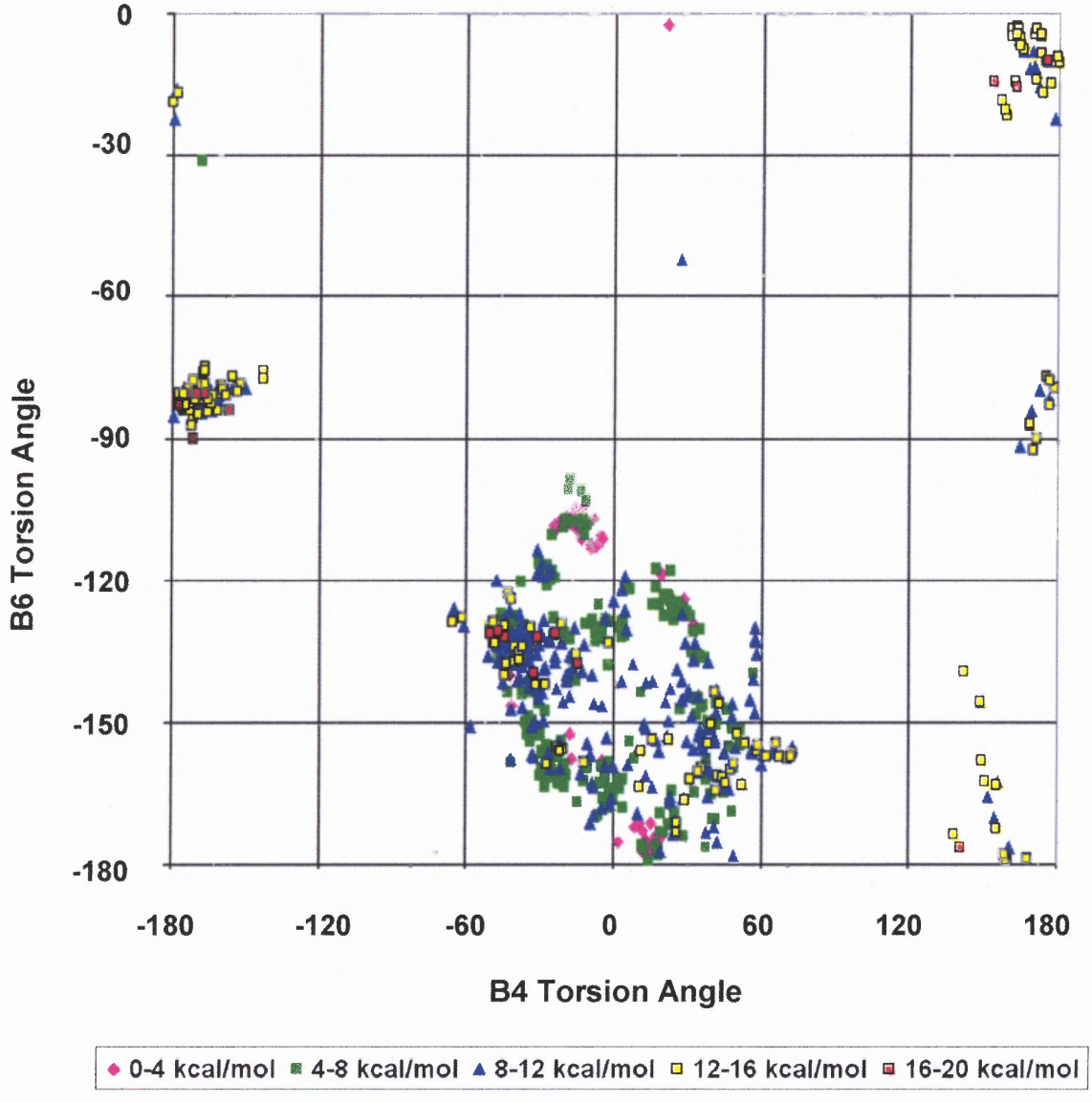

Figure D.83 Protonated DM324 (MMFF94, vacuum) B6 vs B4 Torsion Angles.

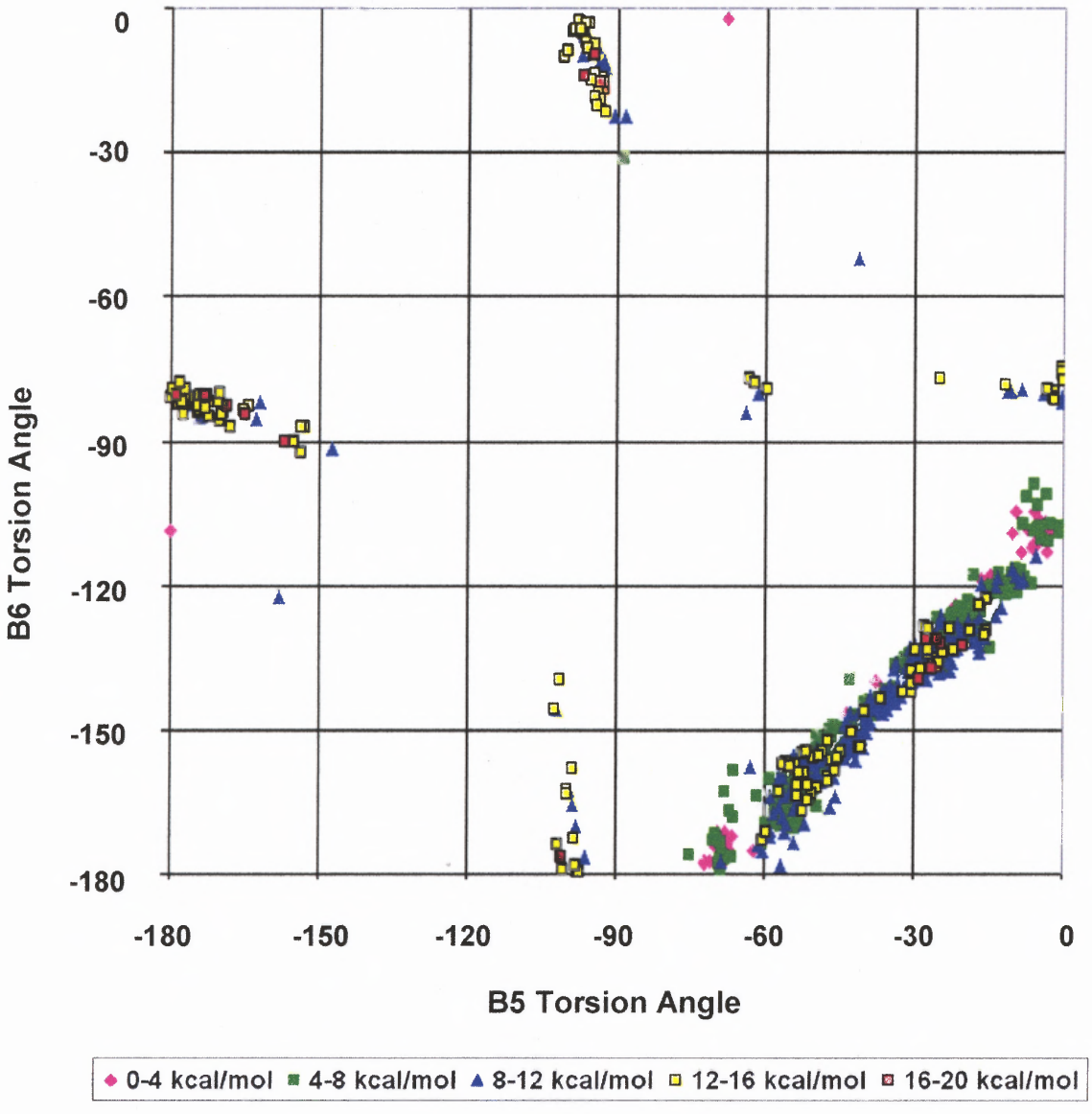

Figure D.84 Protonated DM324 (MMFF94, vacuum) B6 vs B5 Torsion Angles.

D.7 MMFF94 for DM324 and Solvent

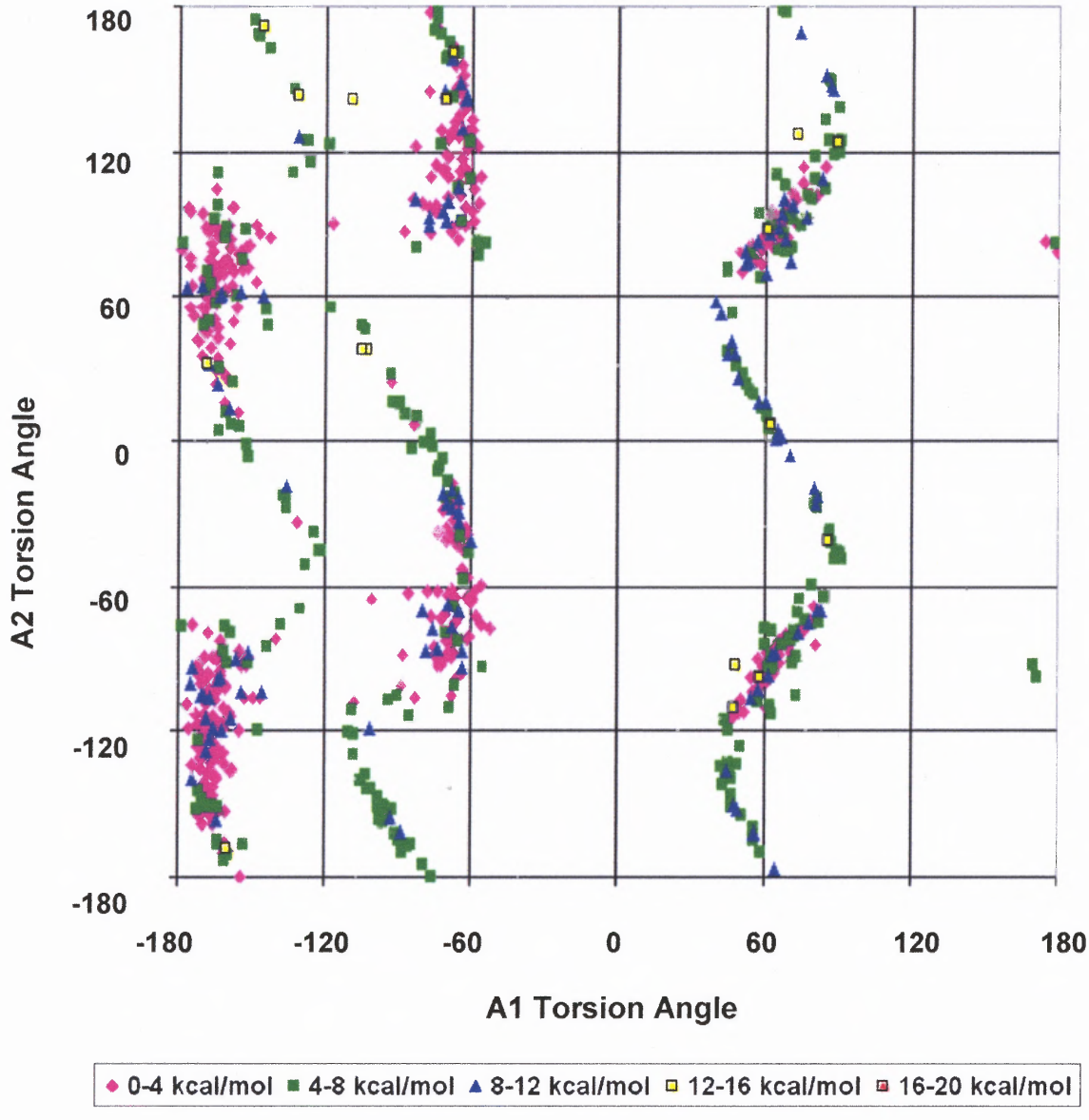

Figure D.85 Protonated DM324 (MMFF94, solvent) A2 vs A1 torsion angles.

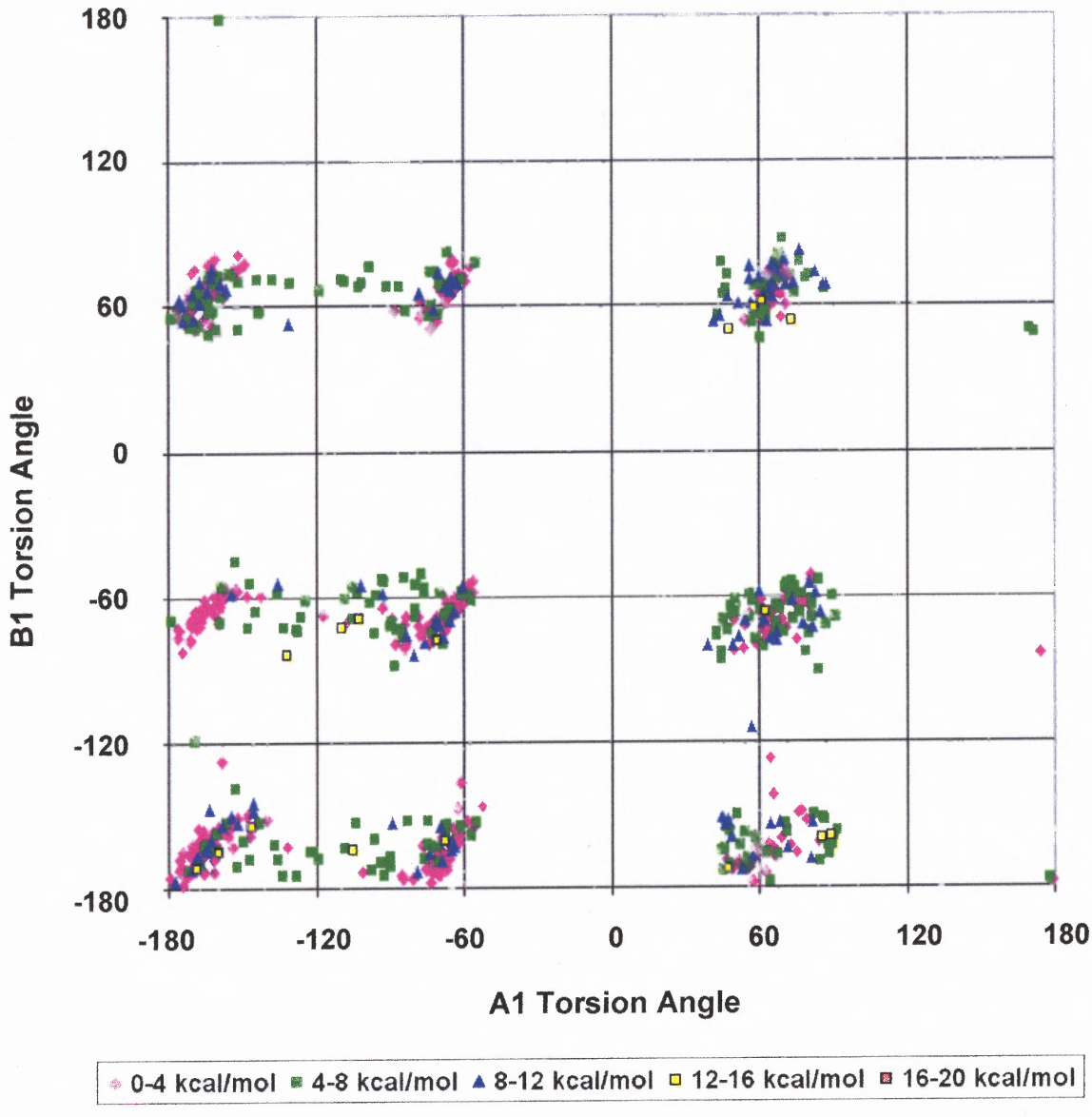

Figure D.86 Protonated DM324 (MMFF94, solvent) B1 vs A1 torsion angles.

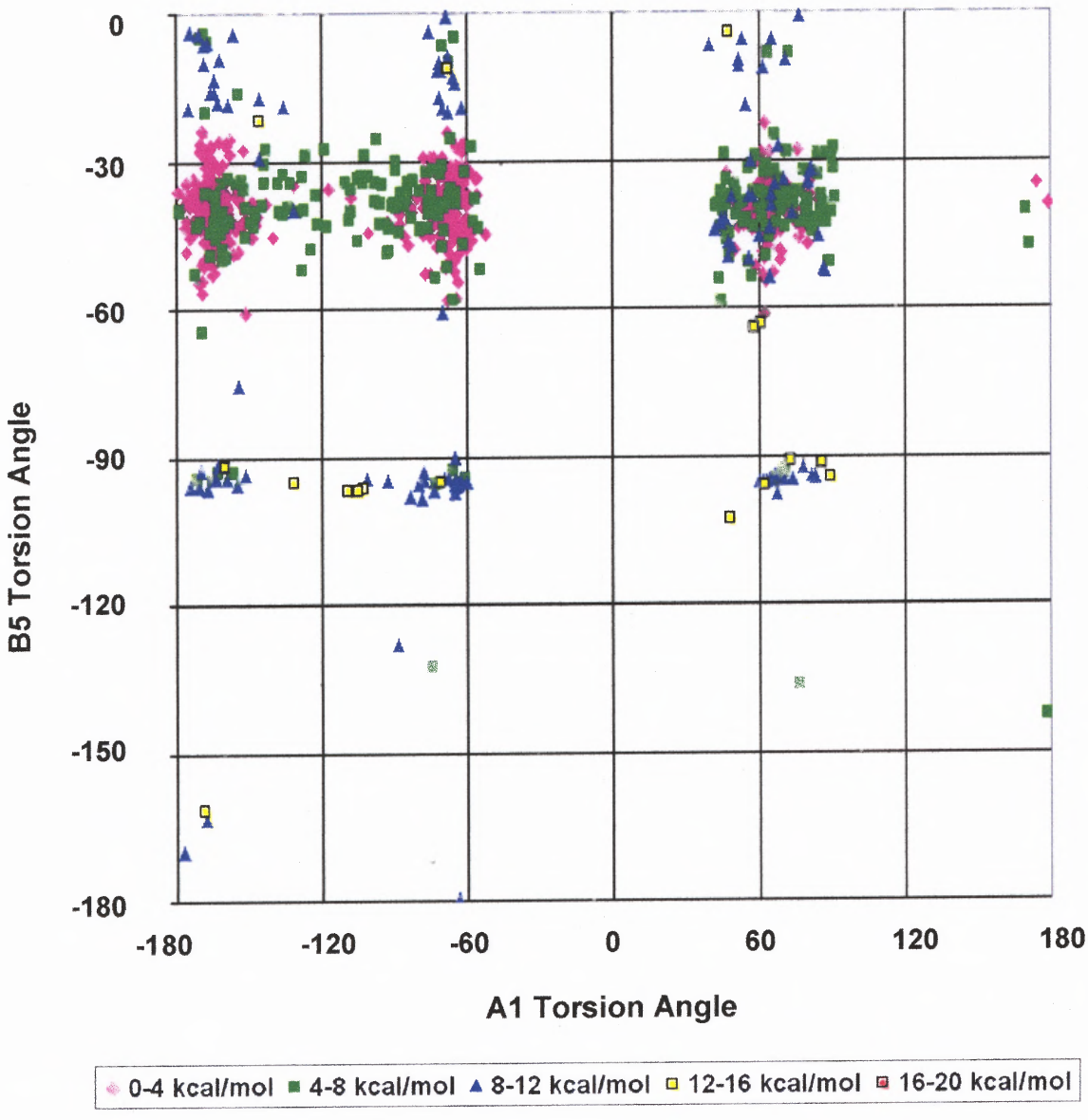

Figure D.87 Protonated DM324 (MMFF94, solvent) B5 vs A1 torsion angles.

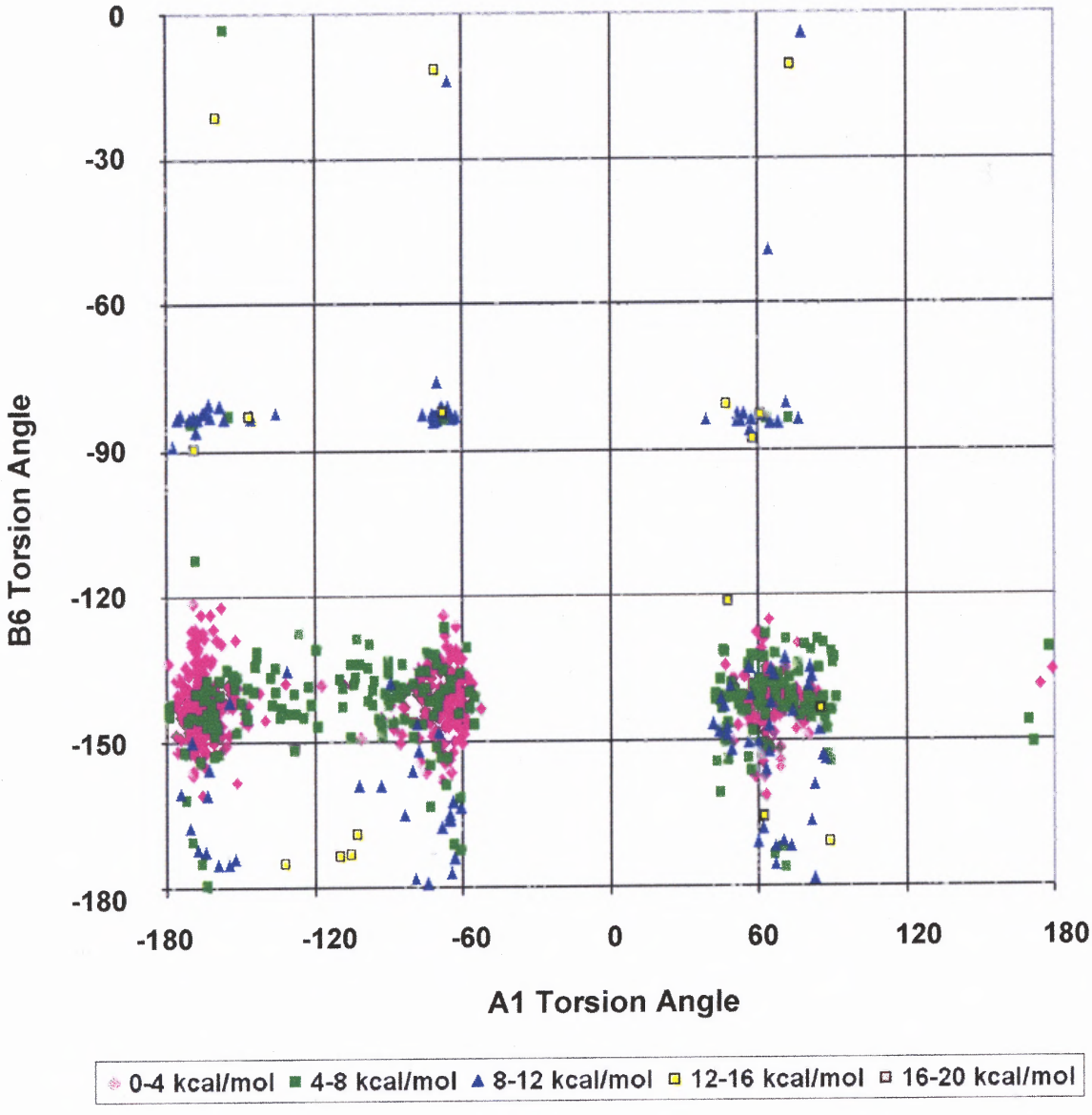

Figure D.88 Protonated DM324 (MMFF94, solvent) B6 vs A1 torsion angles.

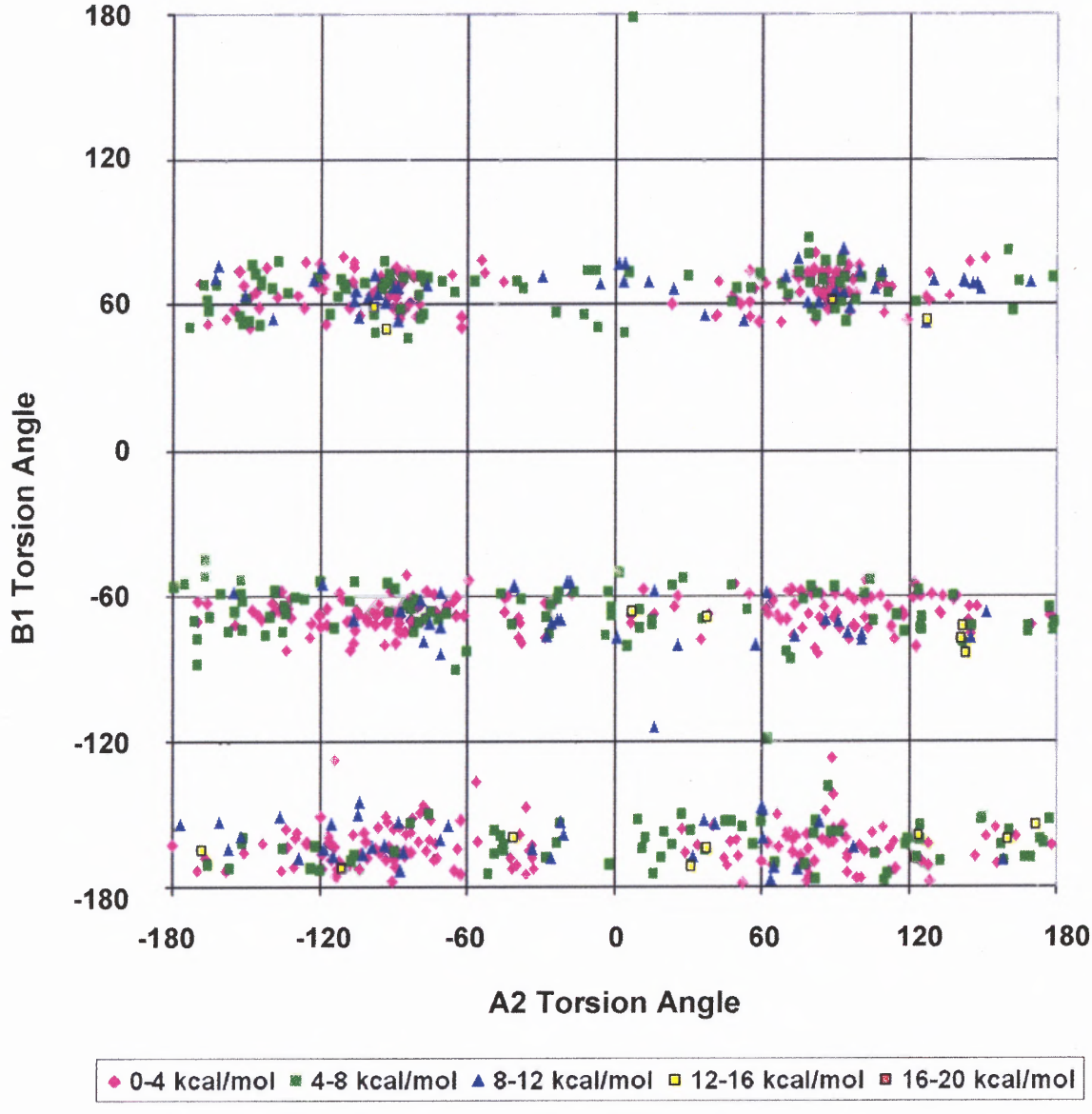

Figure D.89 Protonated DM324 (MMFF94, solvent) B1 vs A2 torsion angles.

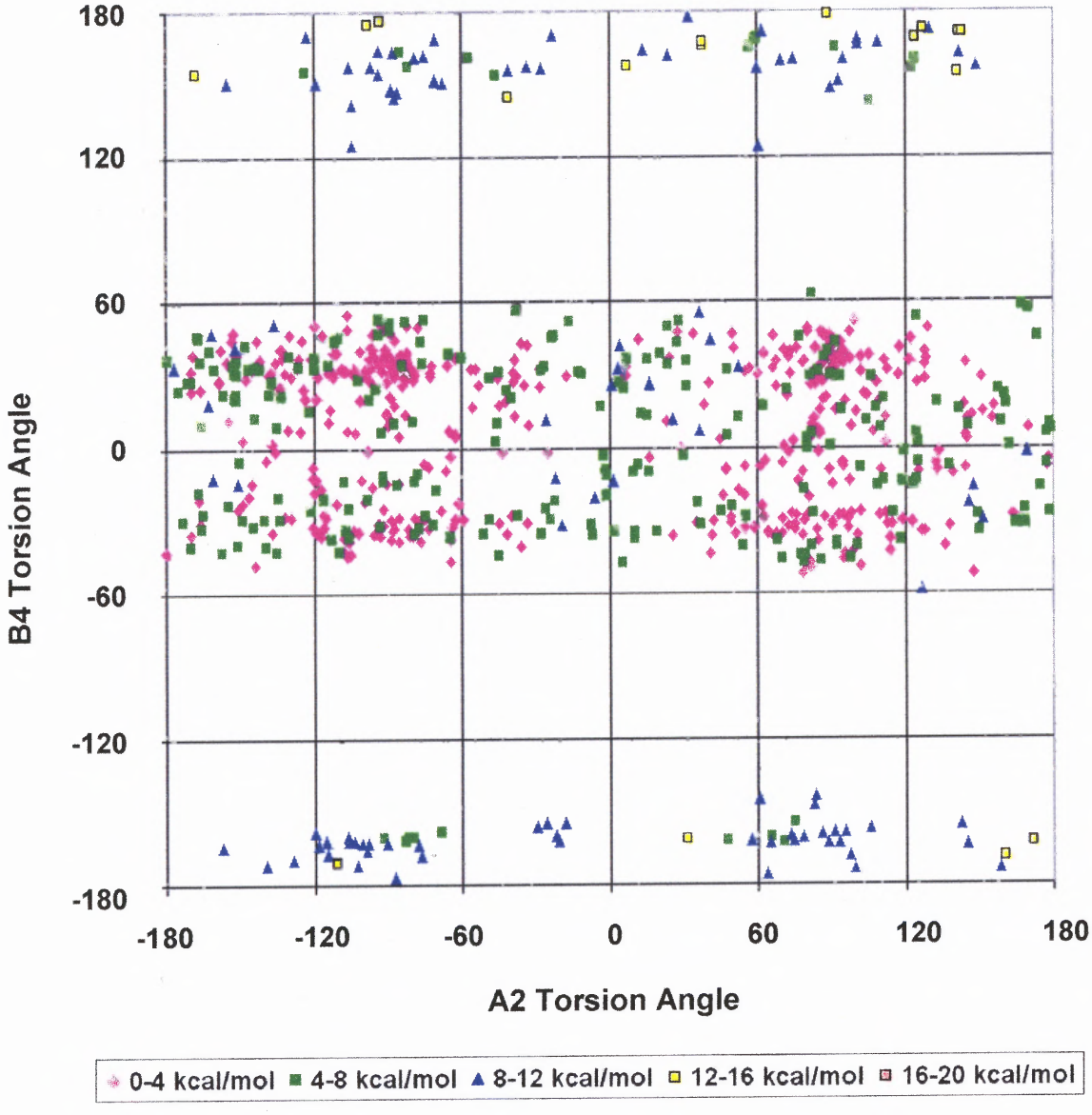

Figure D.90 Protonated DM324 (MMFF94, solvent) B4 vs A2 torsion angles.

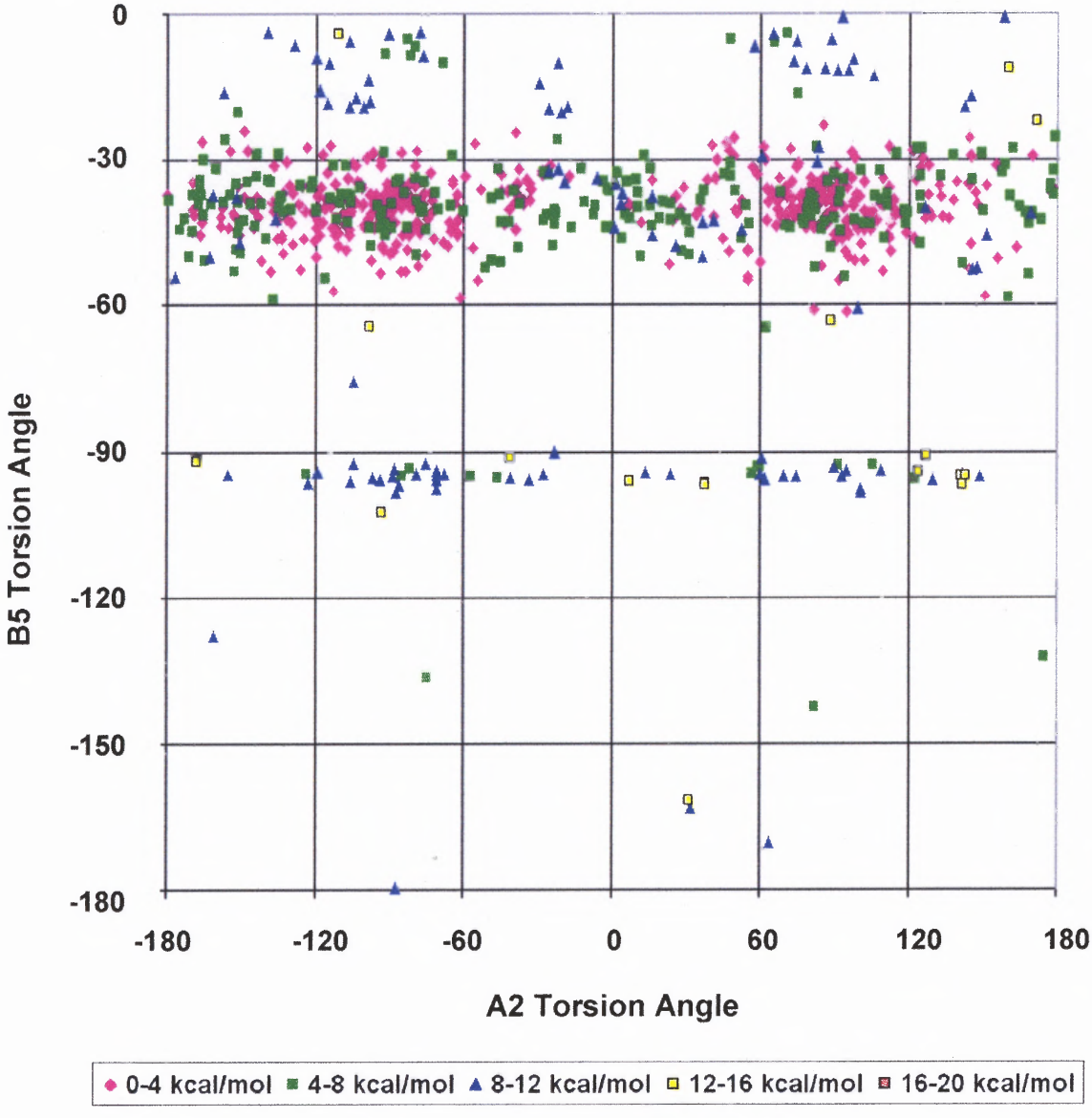

Figure D.91 Protonated DM324 (MMFF94, solvent) B5 vs A2 torsion angles.

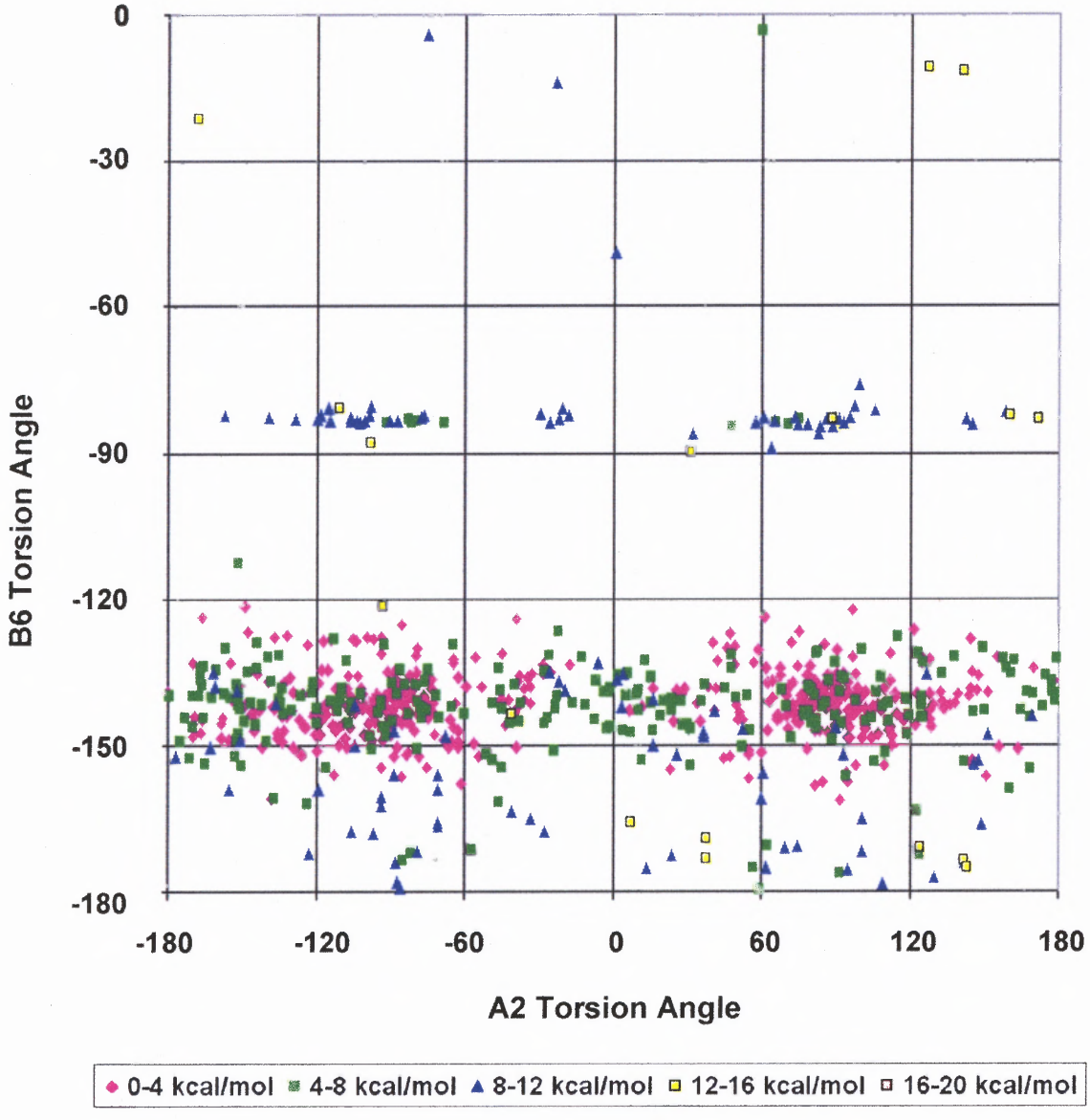

Figure D.92 Protonated DM324 (MMFF94, solvent) B6 vs A2 torsion angles.

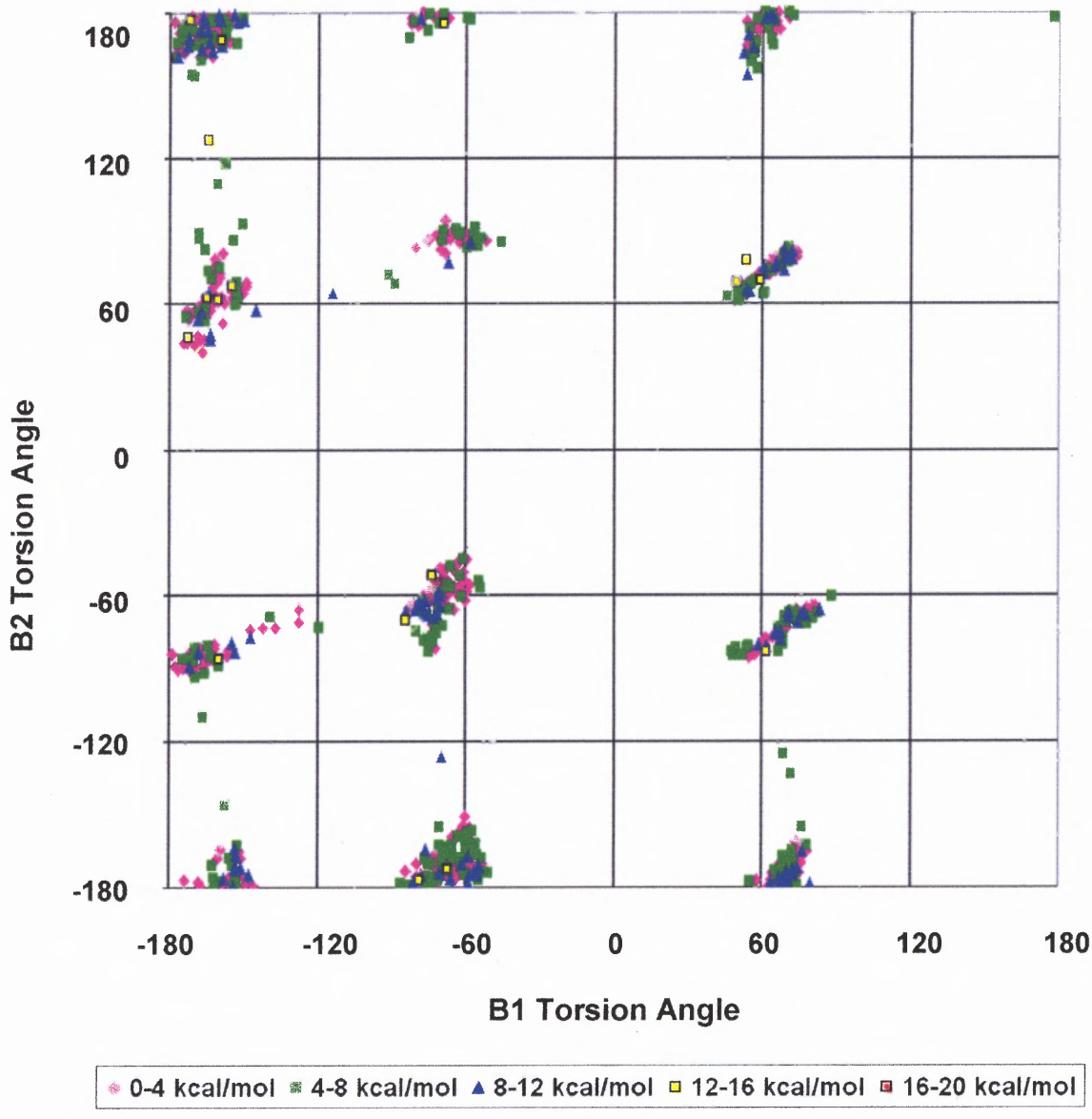

Figure D.93 Protonated DM324 (MMFF94, solvent) B2 vs B1 torsion angles.

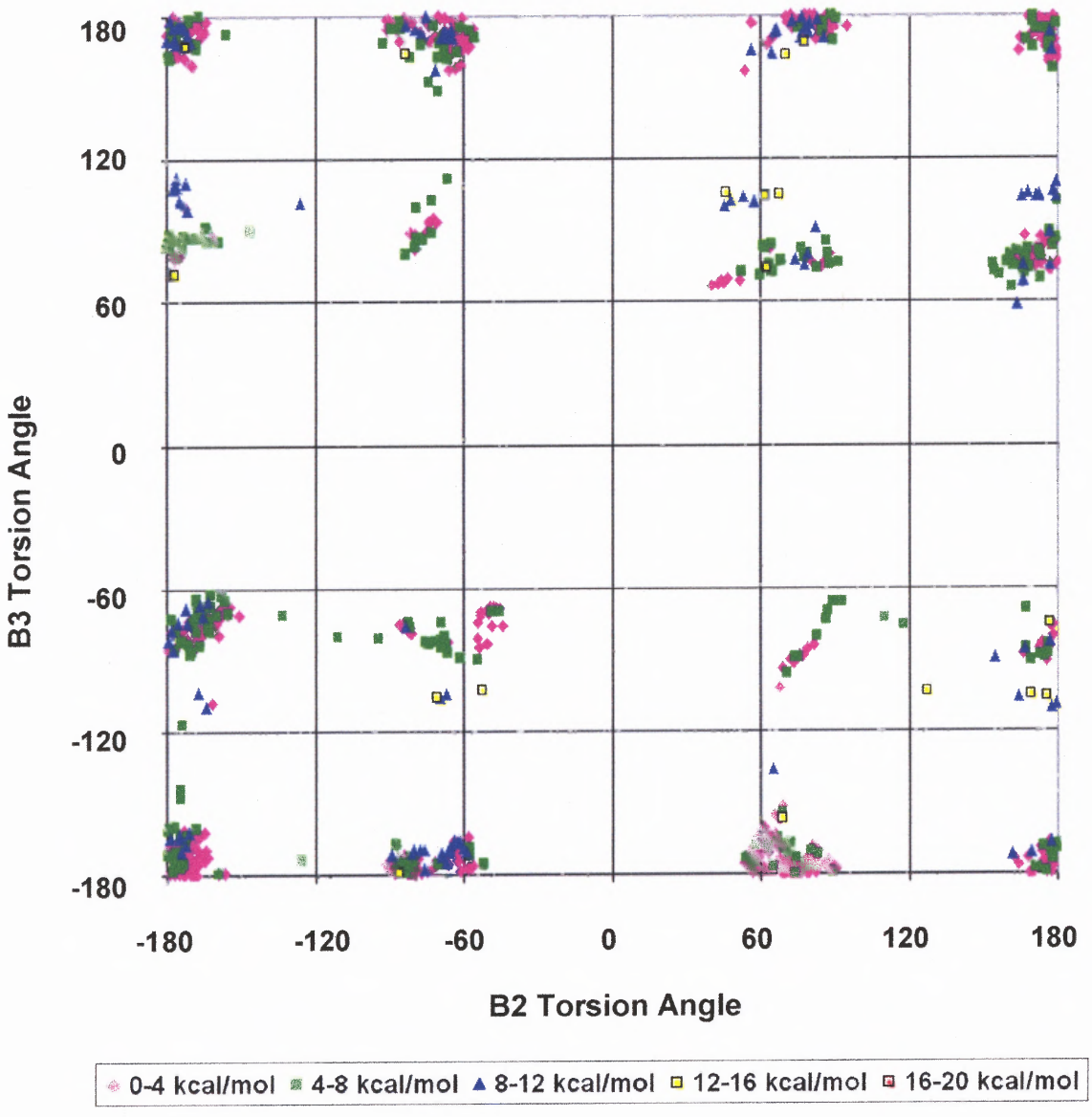

Figure D.94 Protonated DM324 (MMFF94, solvent) B3 vs B2 torsion angles.

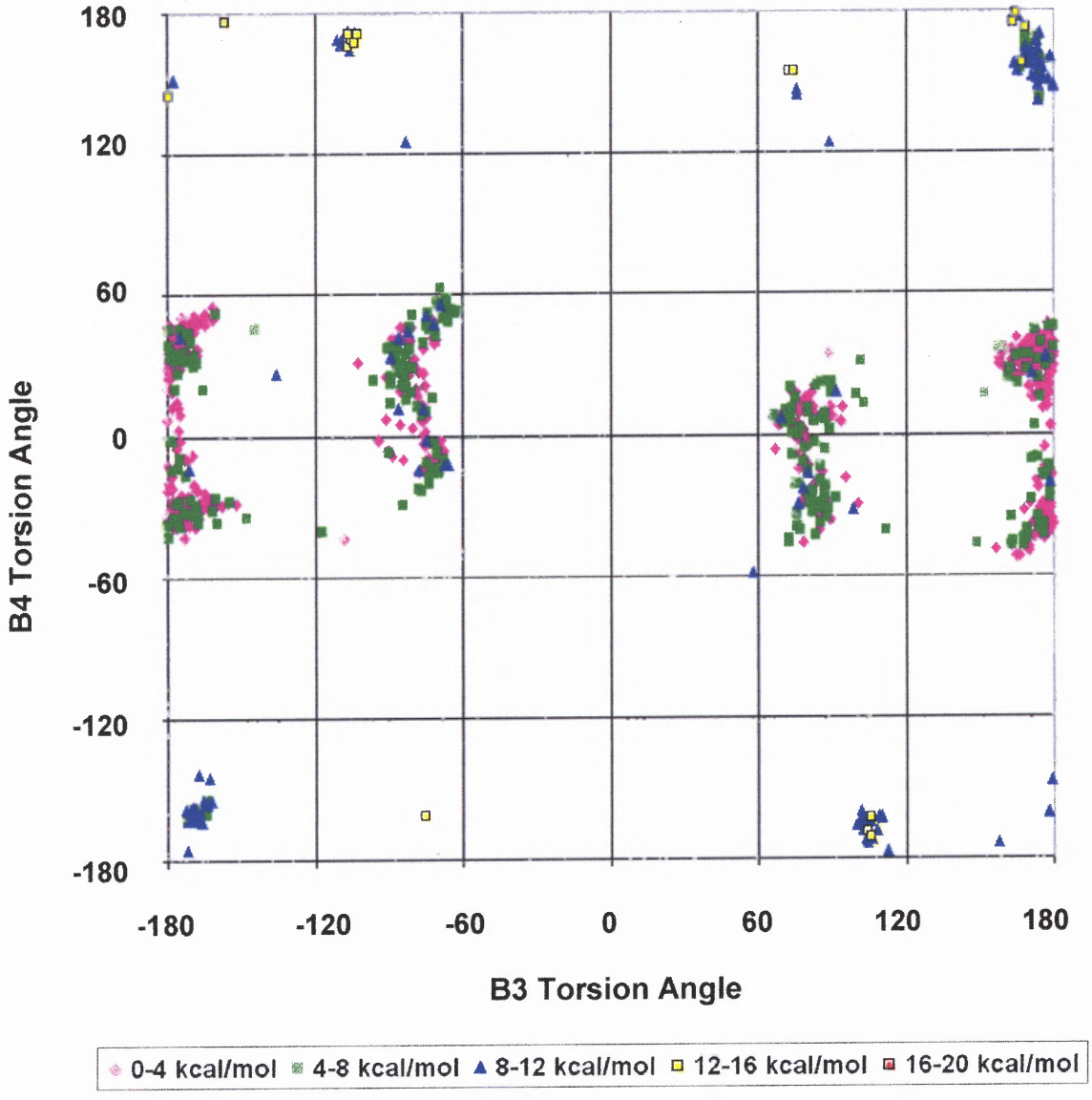

Figure D.95 Protonated DM324 (MMFF94, solvent) B4 vs B3 torsion angles.

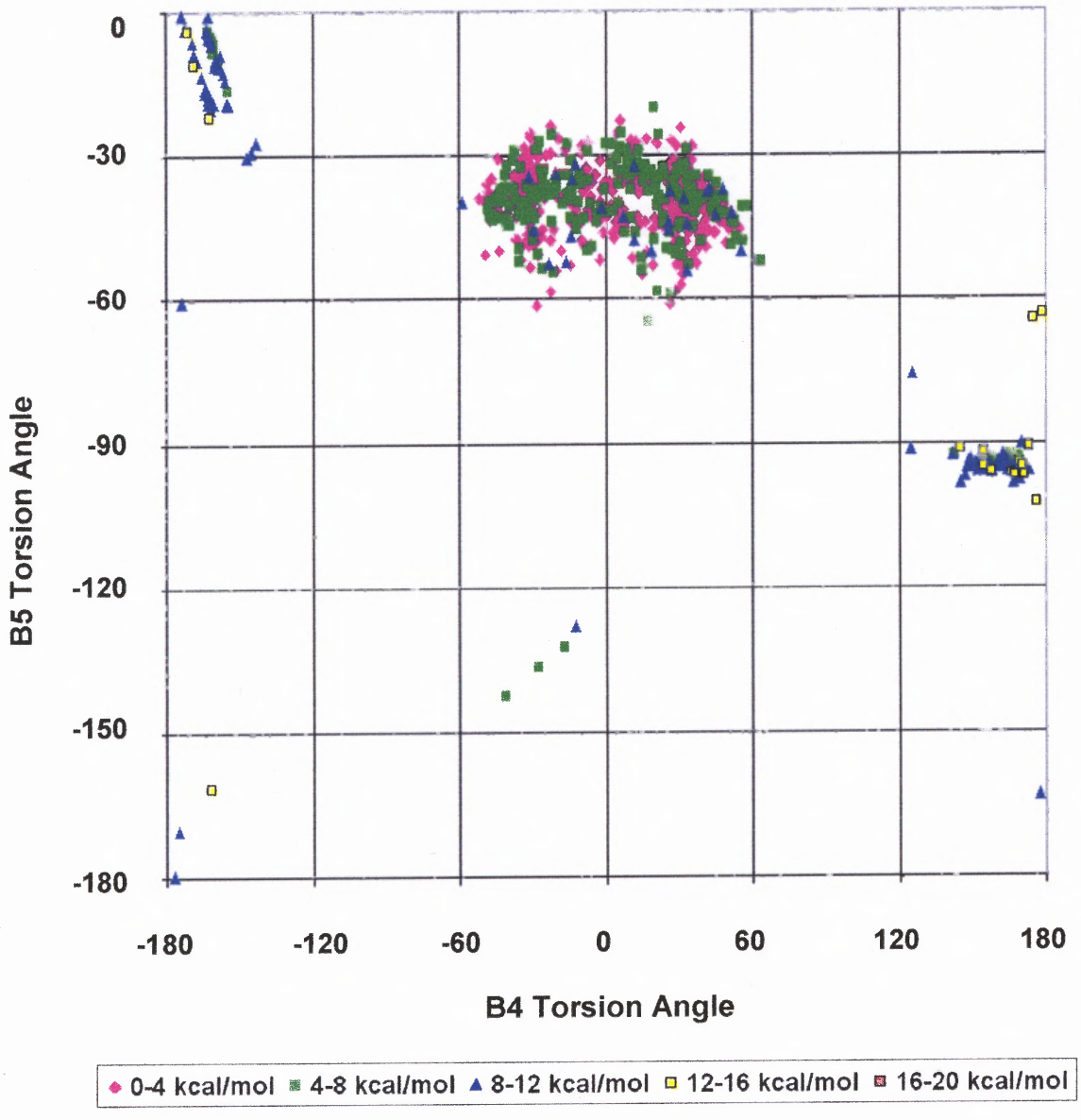

Figure D.96 Protonated DM324 (MMFF94, solvent) B5 vs B4 torsion angles.

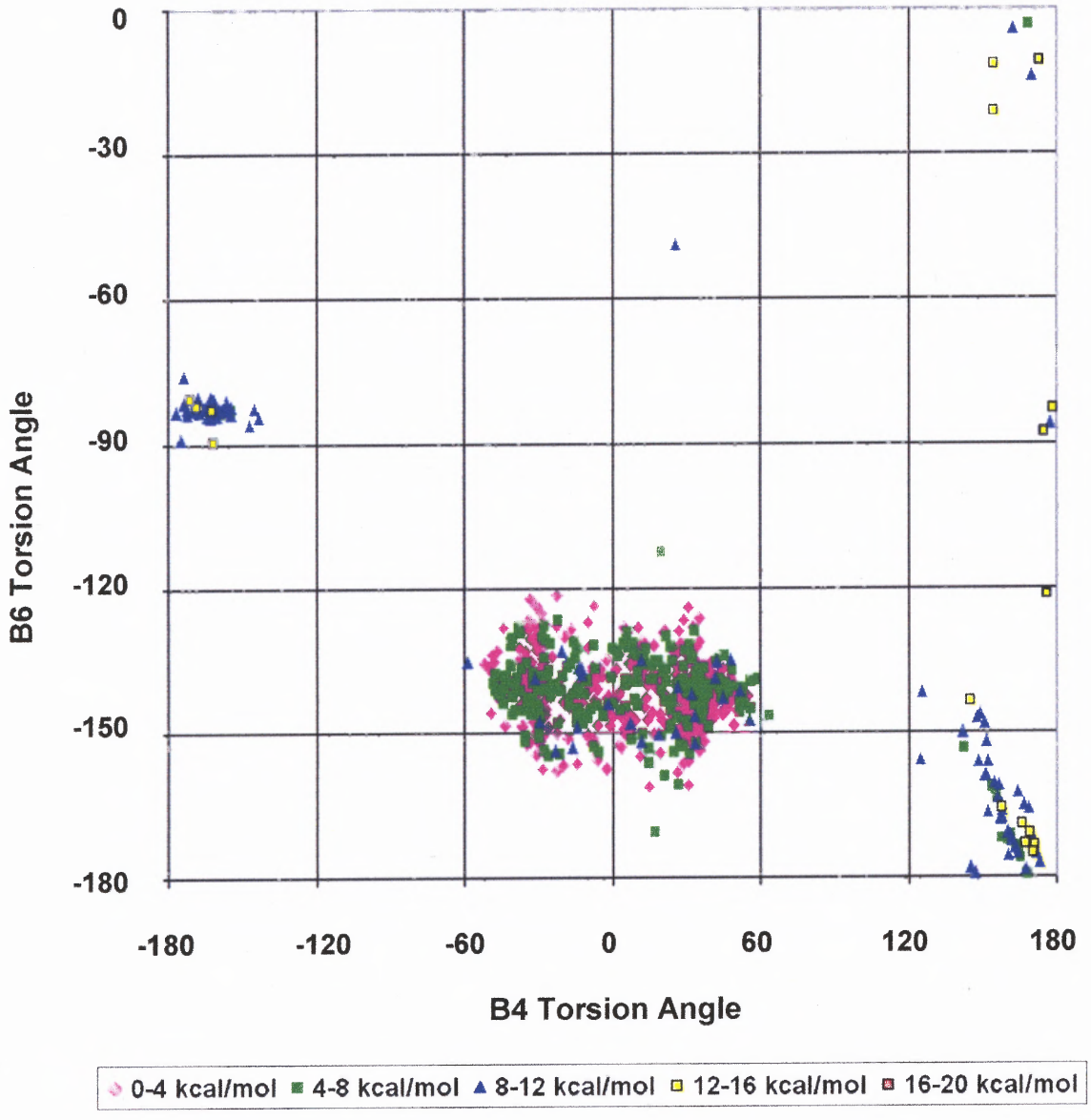

Figure D.97 Protonated DM324 (MMFF94, solvent) B6 vs B4 torsion angles.

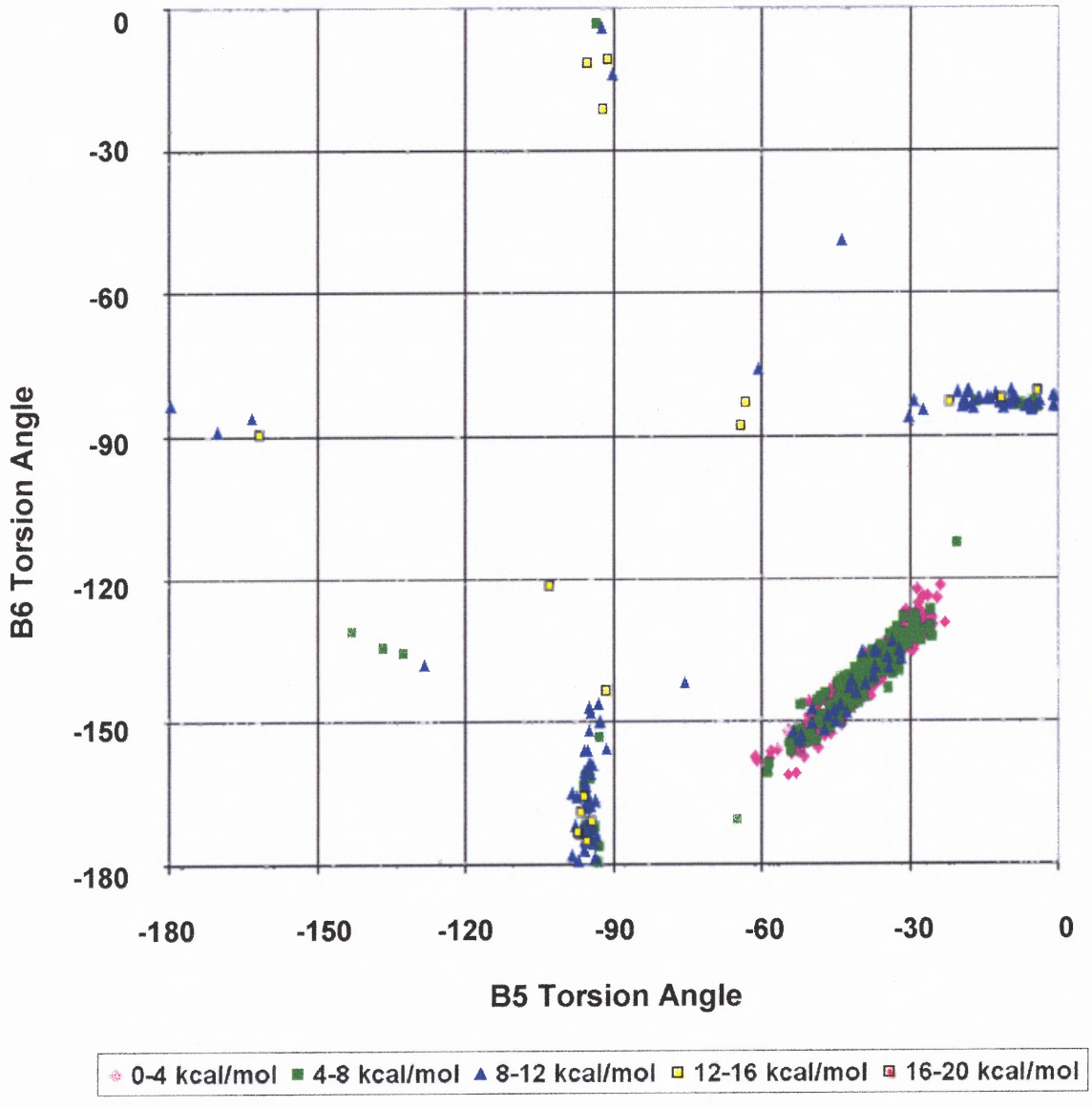

Figure D.98 Protonated DM324 (MMFF94, solvent) B6 vs B5 torsion angles.

D.8 MMFF94 for TP250 and Vacuum

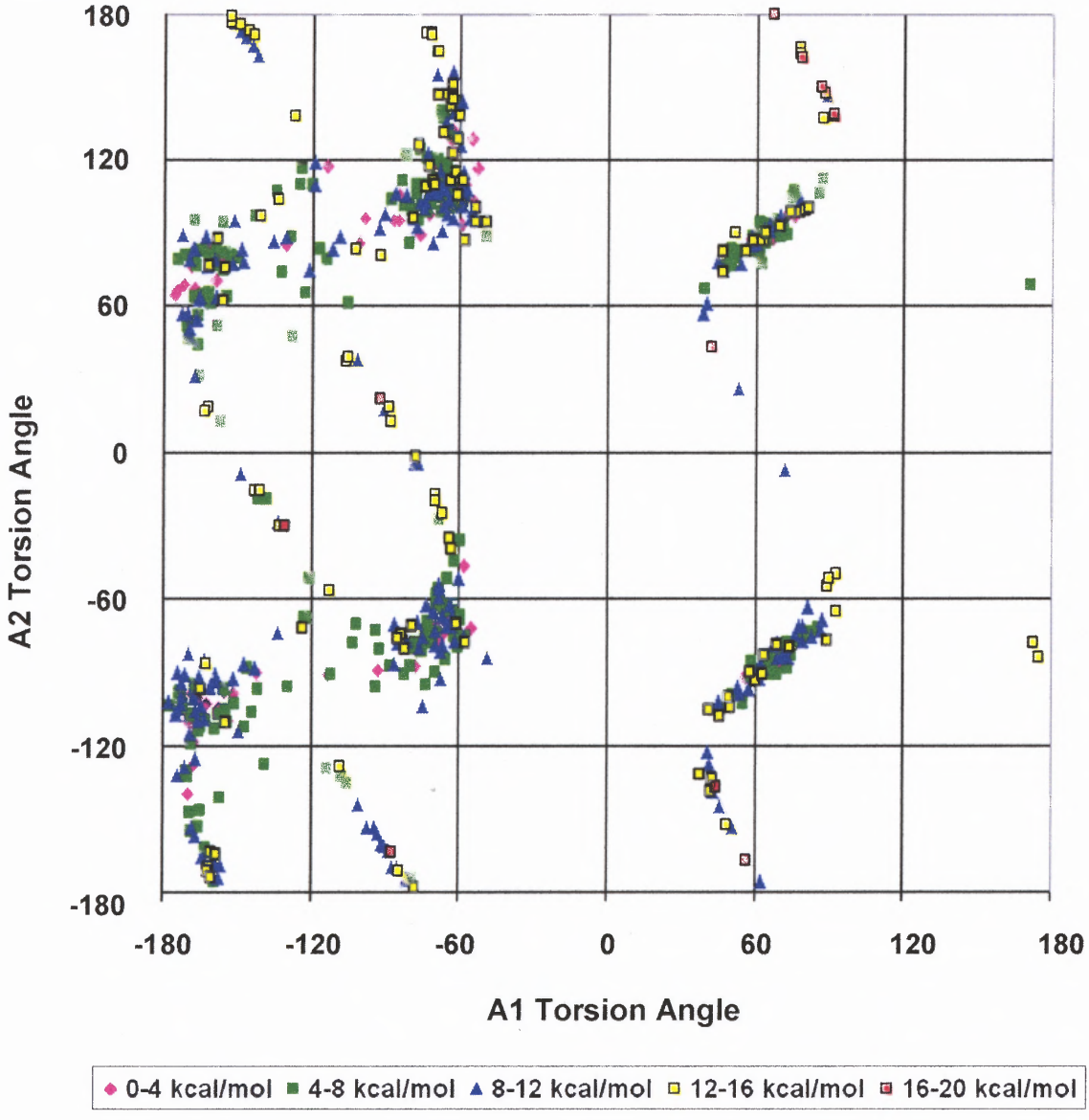

Figure D.99 Protonated TP250 (MMFF94, vacuum) A2 vs A1 torsion angles.

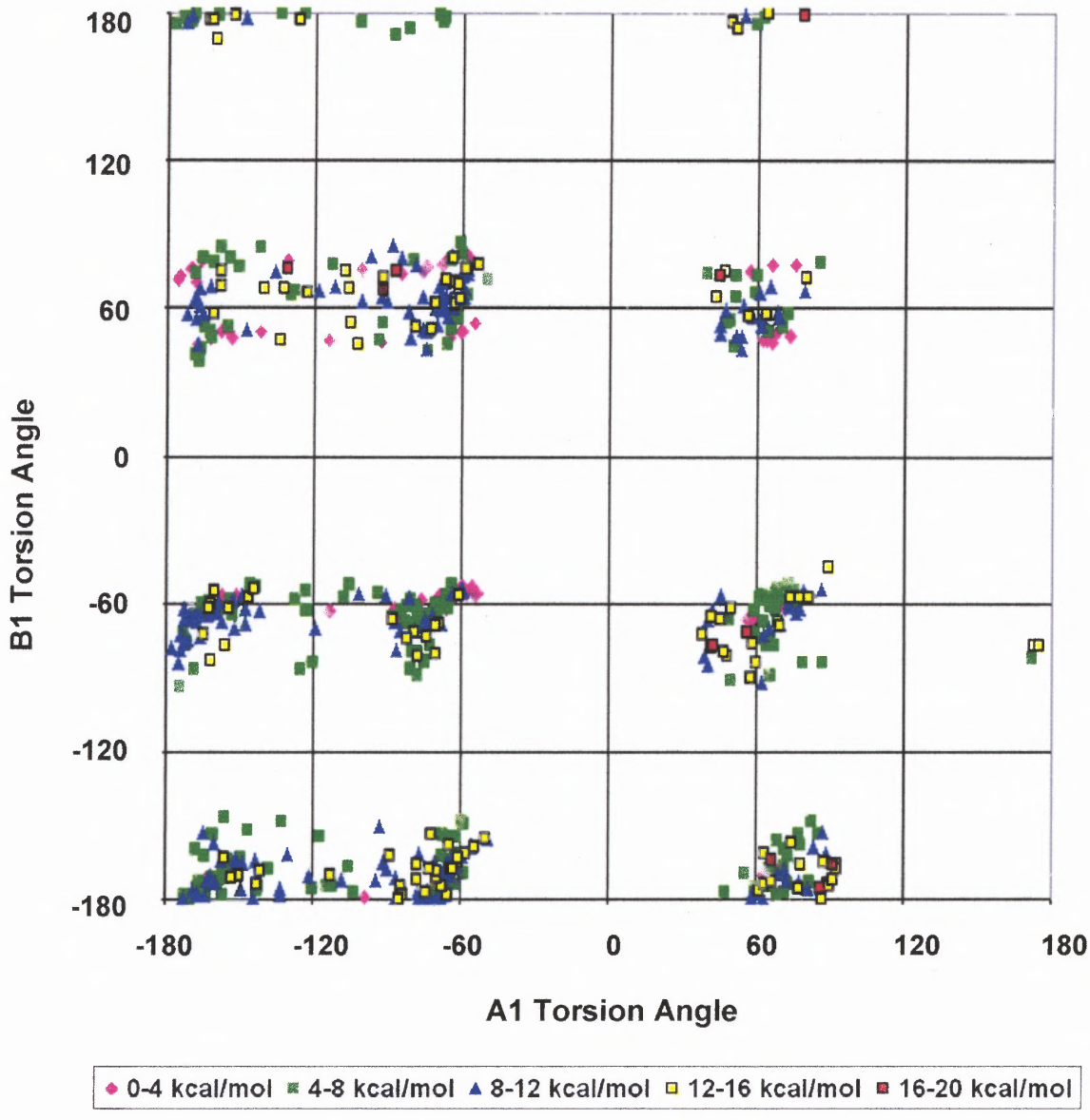

Figure D.100 Protonated TP250 (MMFF94, vacuum) B1 vs A1 torsion angles.

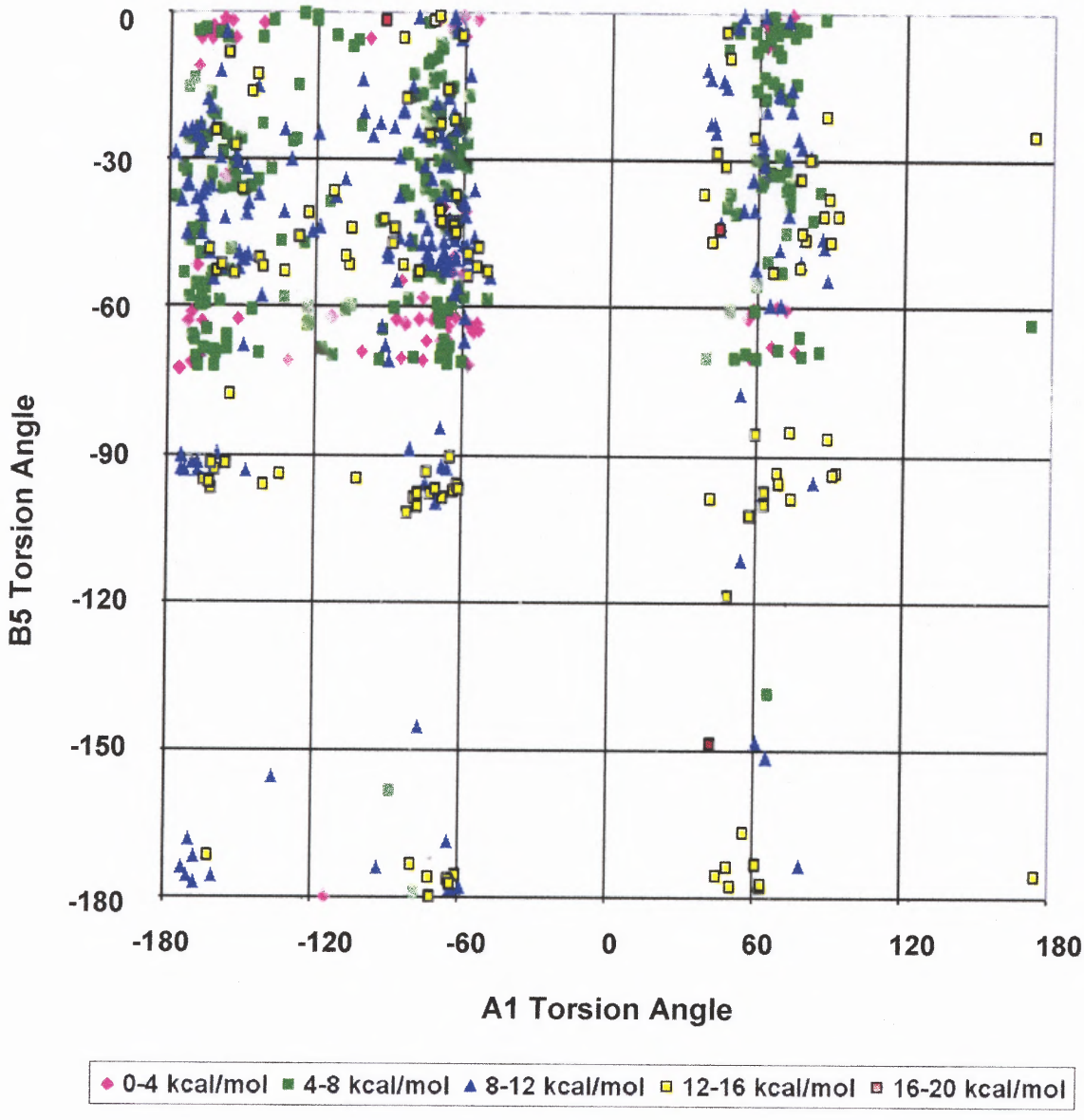

Figure D.101 Protonated TP250 (MMFF94, vacuum) B5 vs A1 torsion angles.

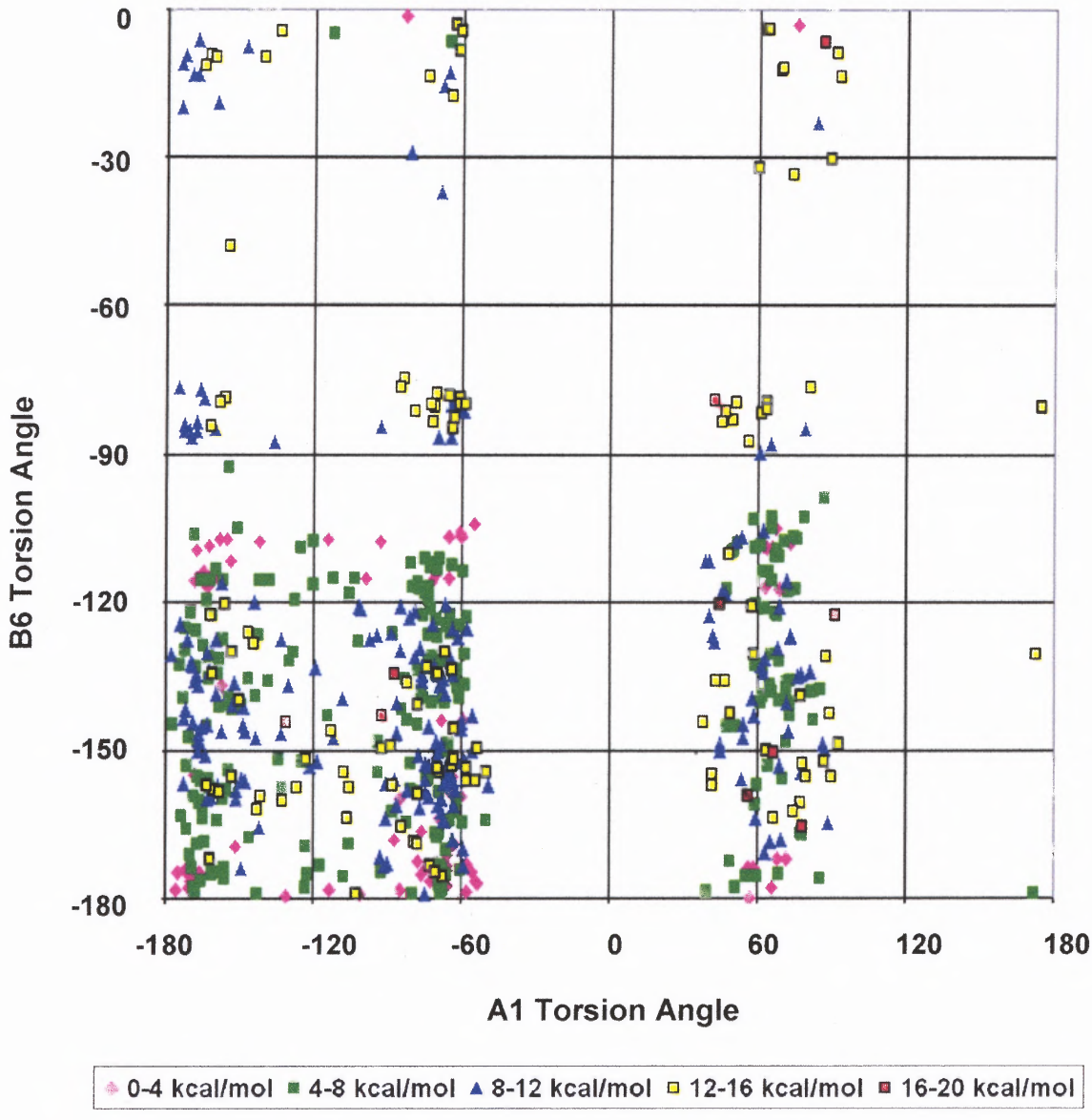

Figure D.102 Protonated TP250 (MMFF94, vacuum) B6 vs A1 torsion angles.

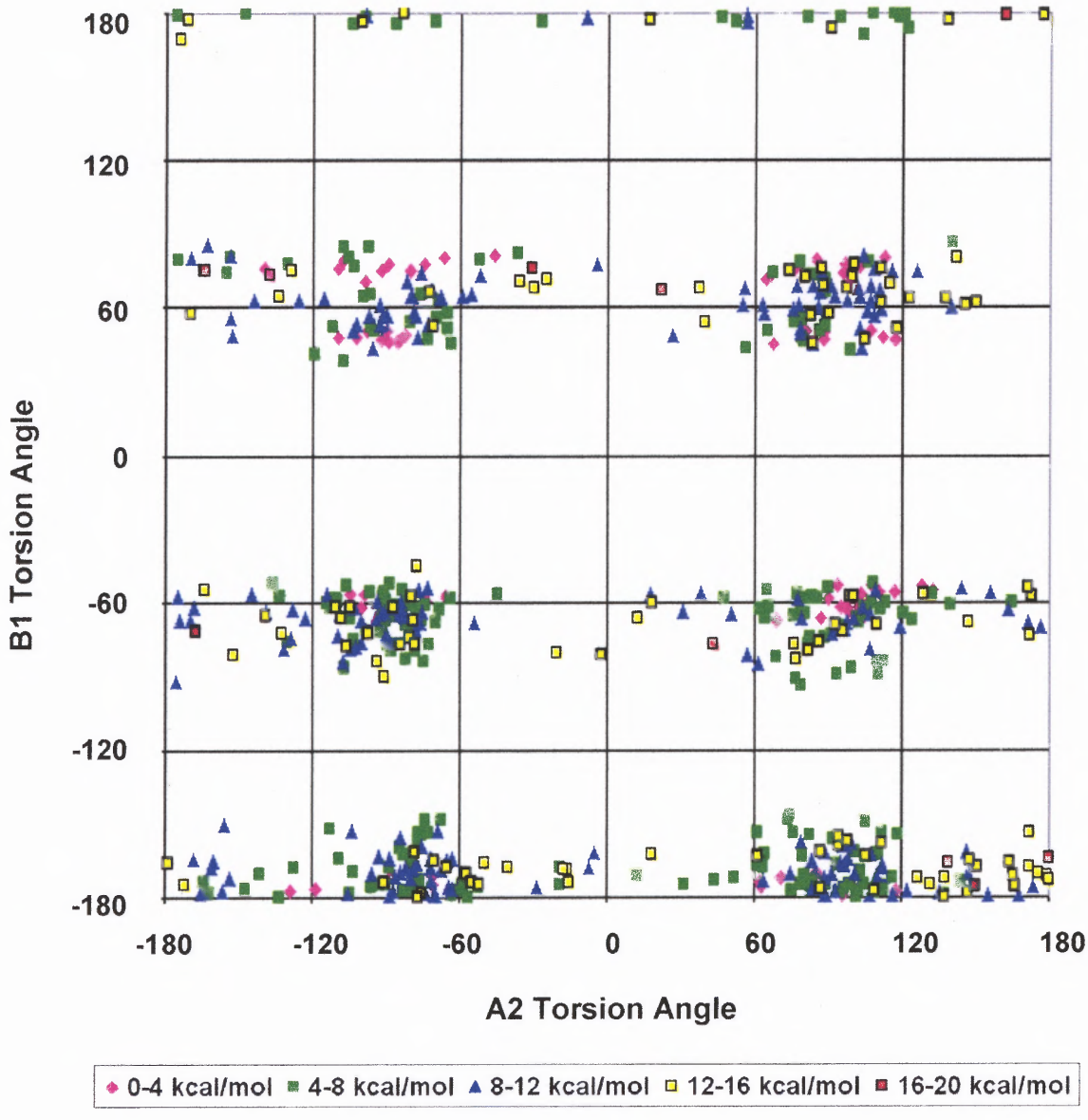

Figure D.103 Protonated TP250 (MMFF94, vacuum) B1 vs A2 torsion angles.

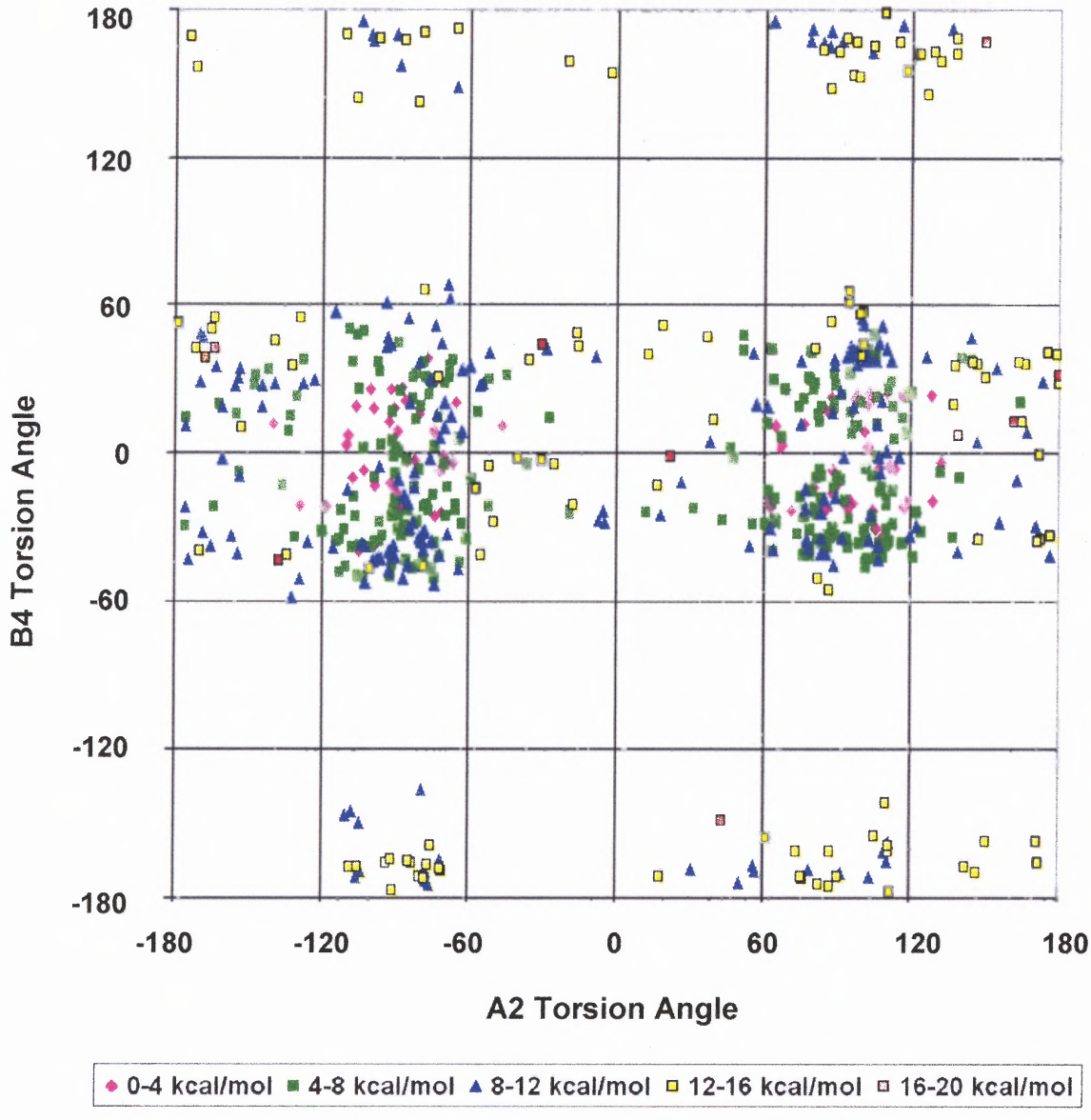

Figure D.104 Protonated TP250 (MMFF94, vacuum) B4 vs A2 torsion angles.

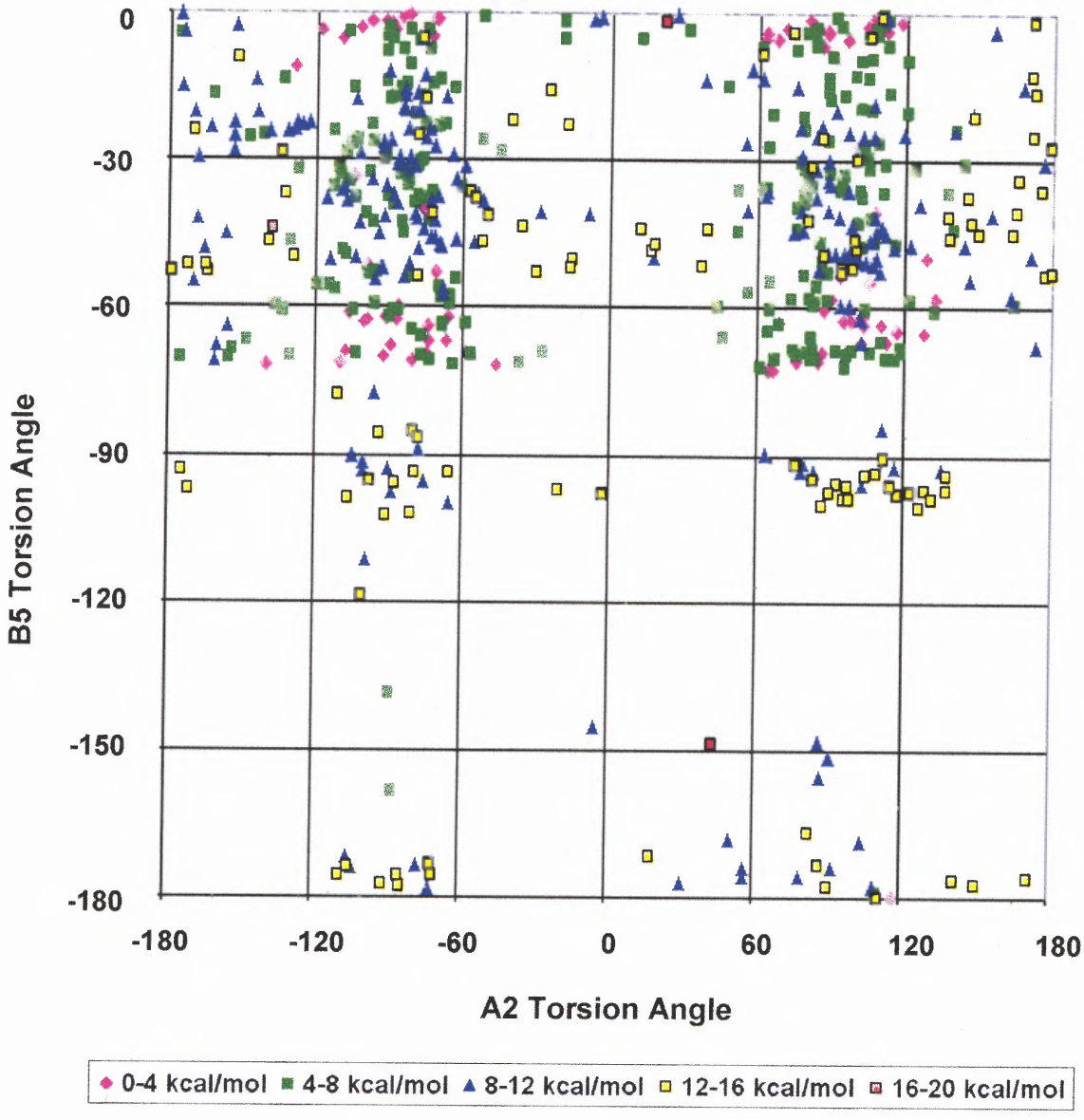

Figure D.105 Protonated TP250 (MMFF94, vacuum) B5 vs A2 torsion angles.

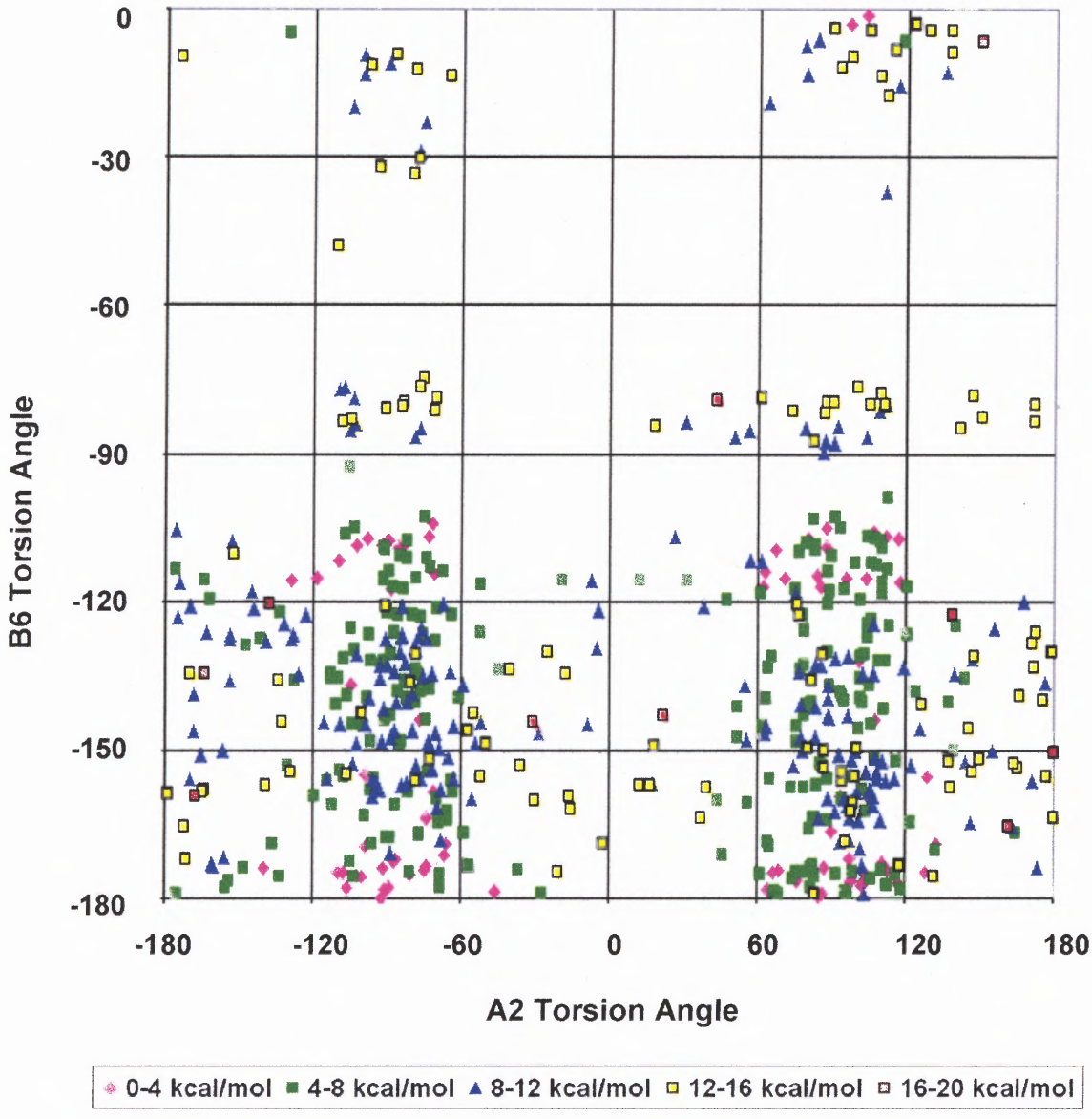

Figure D.106 Protonated TP250 (MMFF94, vacuum) B6 vs A2 torsion angles.

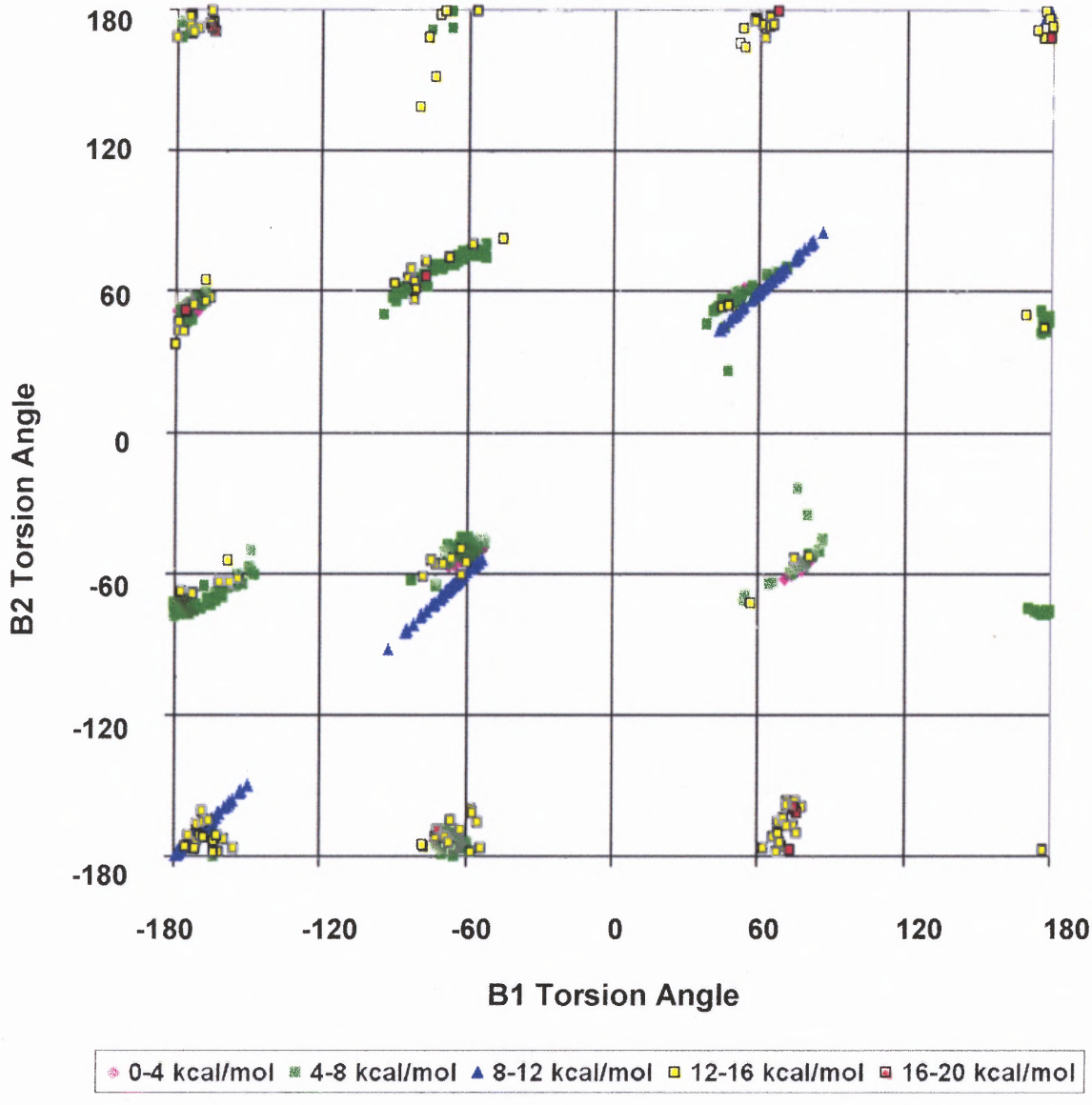

Figure D.107 Protonated TP250 (MMFF94, vacuum) B2 vs B1 torsion angles.

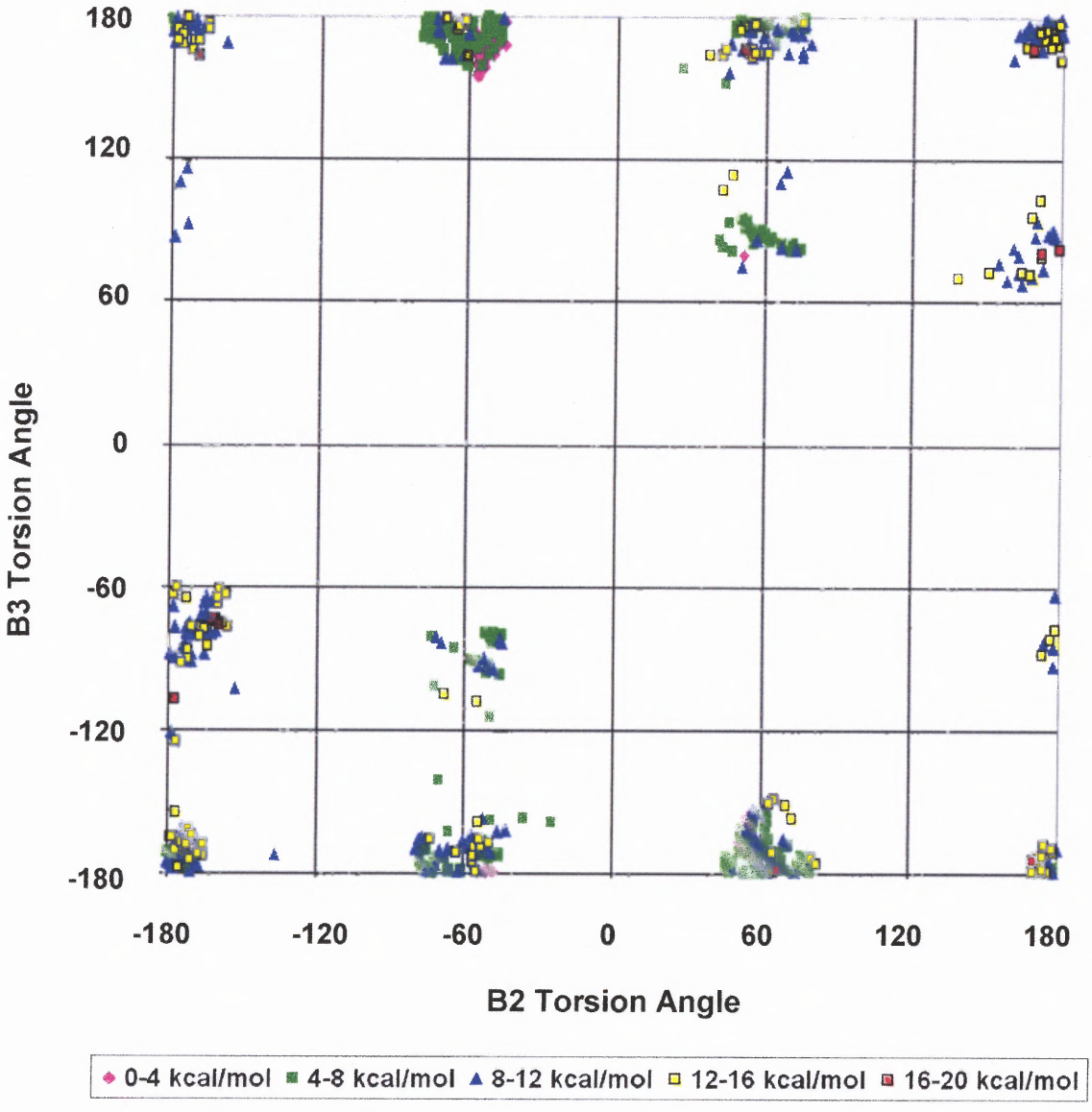

Figure D.108 Protonated TP250 (MMFF94, vacuum) B3 vs B2 torsion angles.

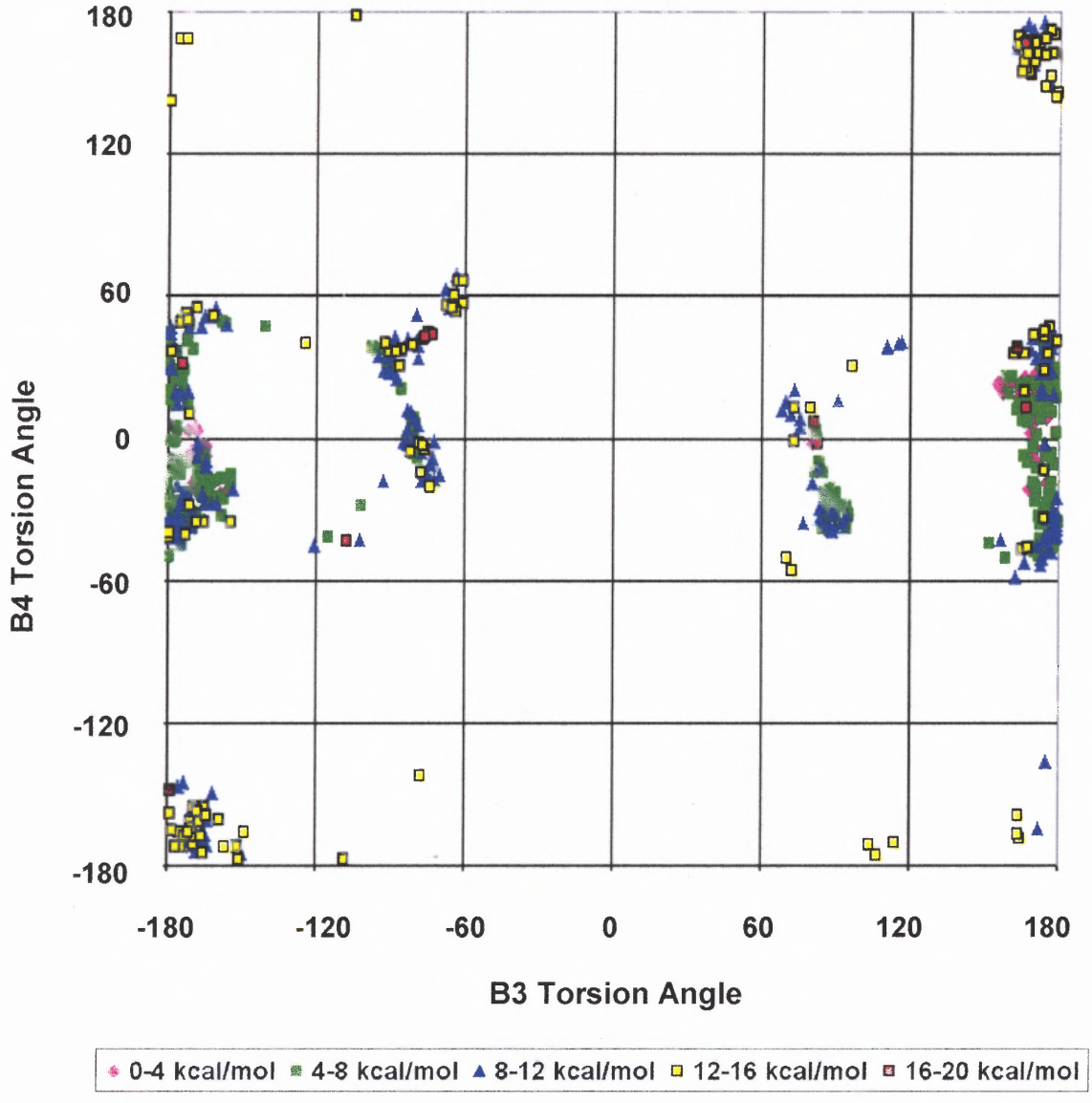

Figure D.109 Protonated TP250 (MMFF94, vacuum) B4 vs B3 torsion angles.

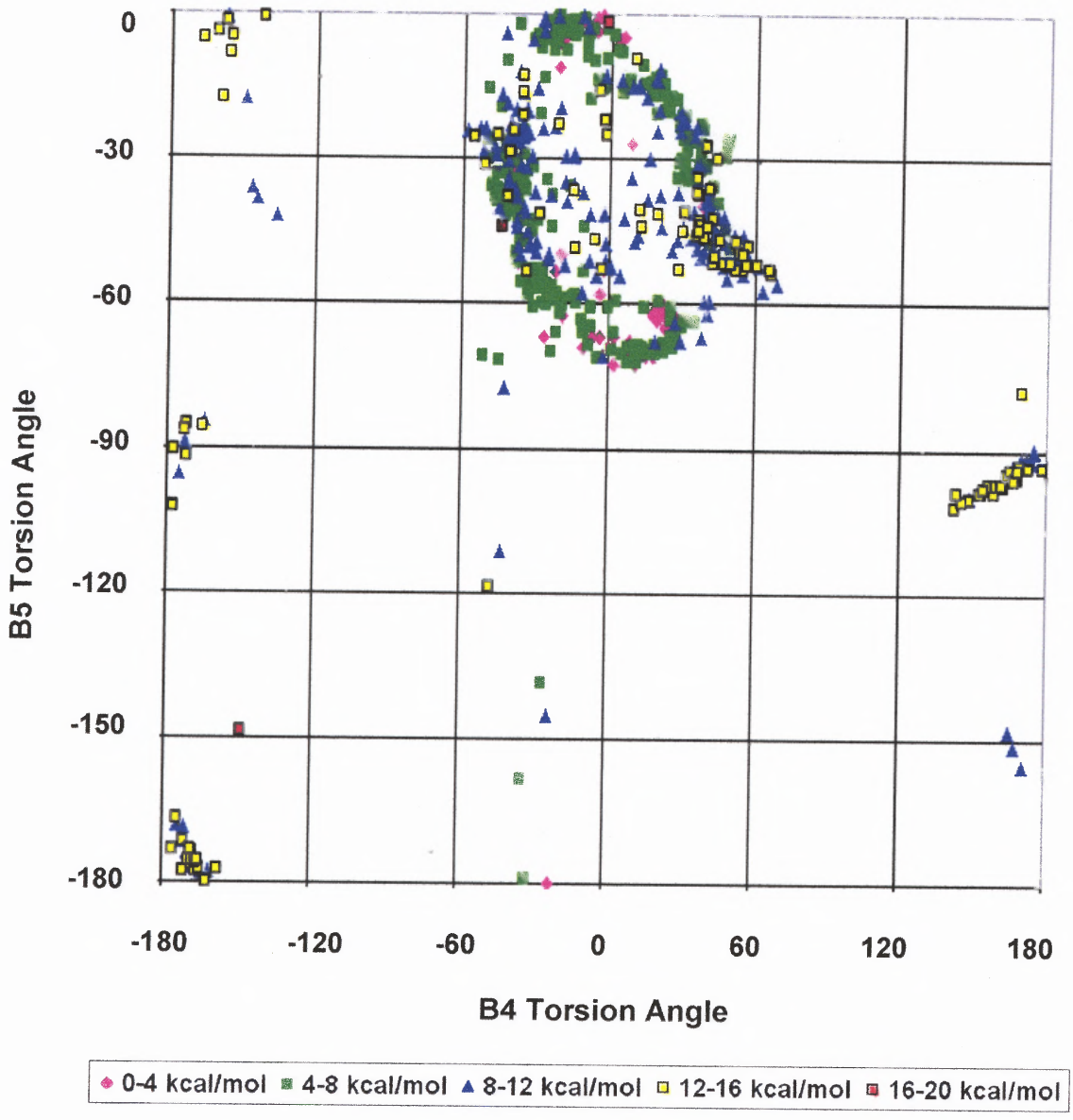

Figure D.110 Protonated TP250 (MMFF94, vacuum) B5 vs B4 torsion angles.

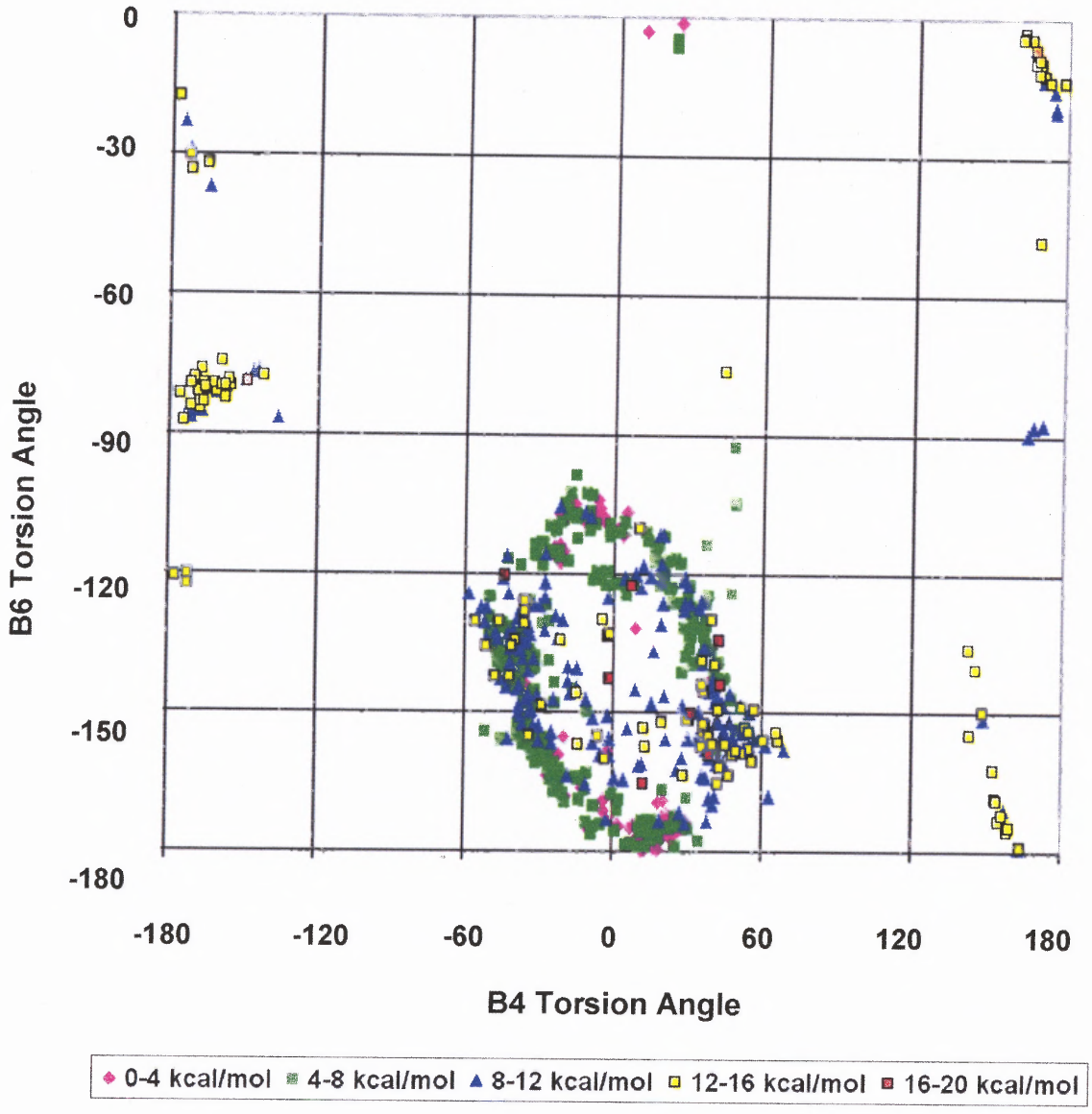

Figure D.111 Protonated TP250 (MMFF94, vacuum) B6 vs B4 torsion angles.

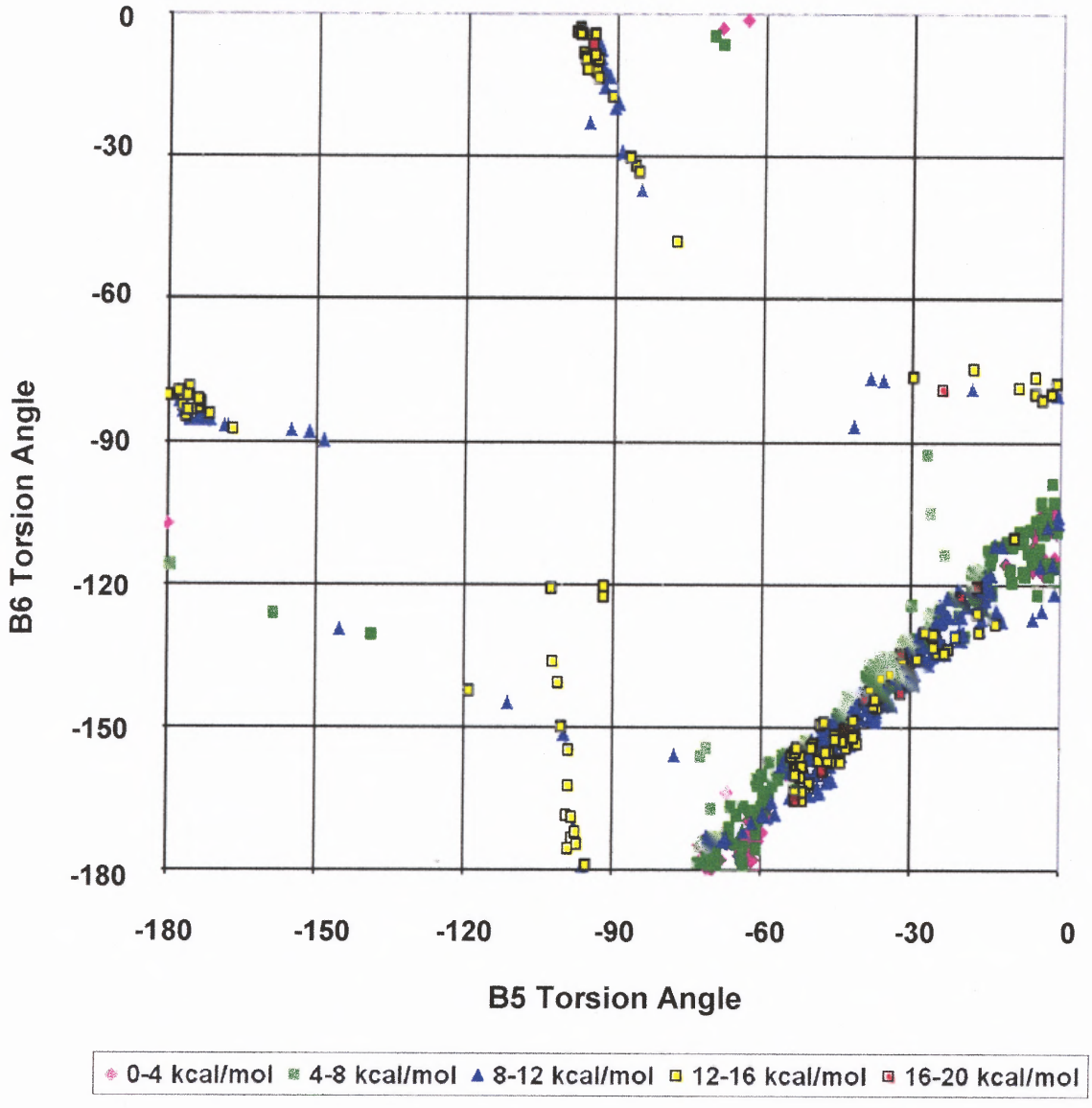

Figure D.112 Protonated TP250 (MMFF94, vacuum) B6 vs B5 torsion angles.

D.9 MMFF94 for TP250 and Solvent

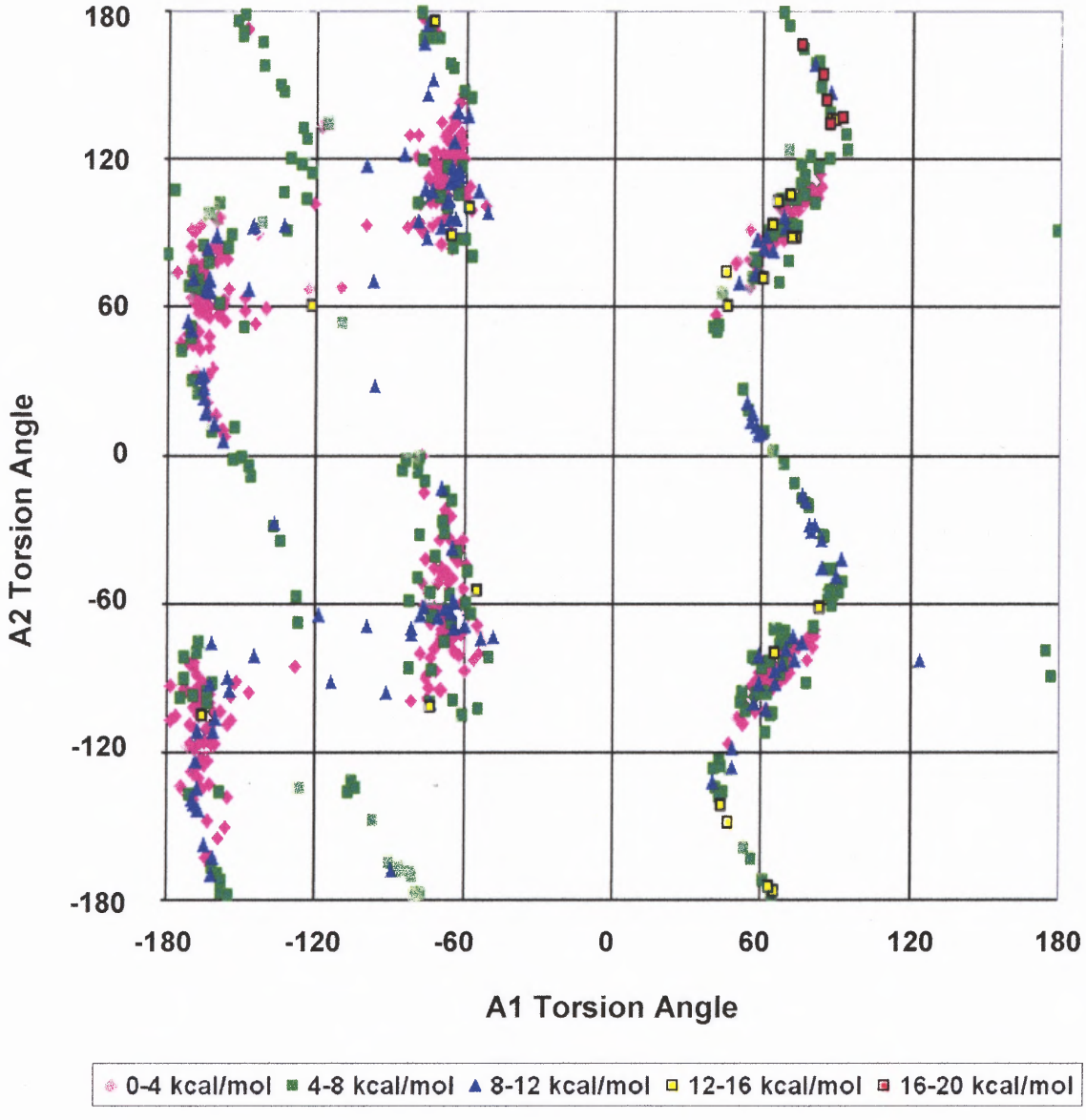

Figure D.113 Protonated TP250 (MMFF94, solvent) A2 vs A1 torsion angles.

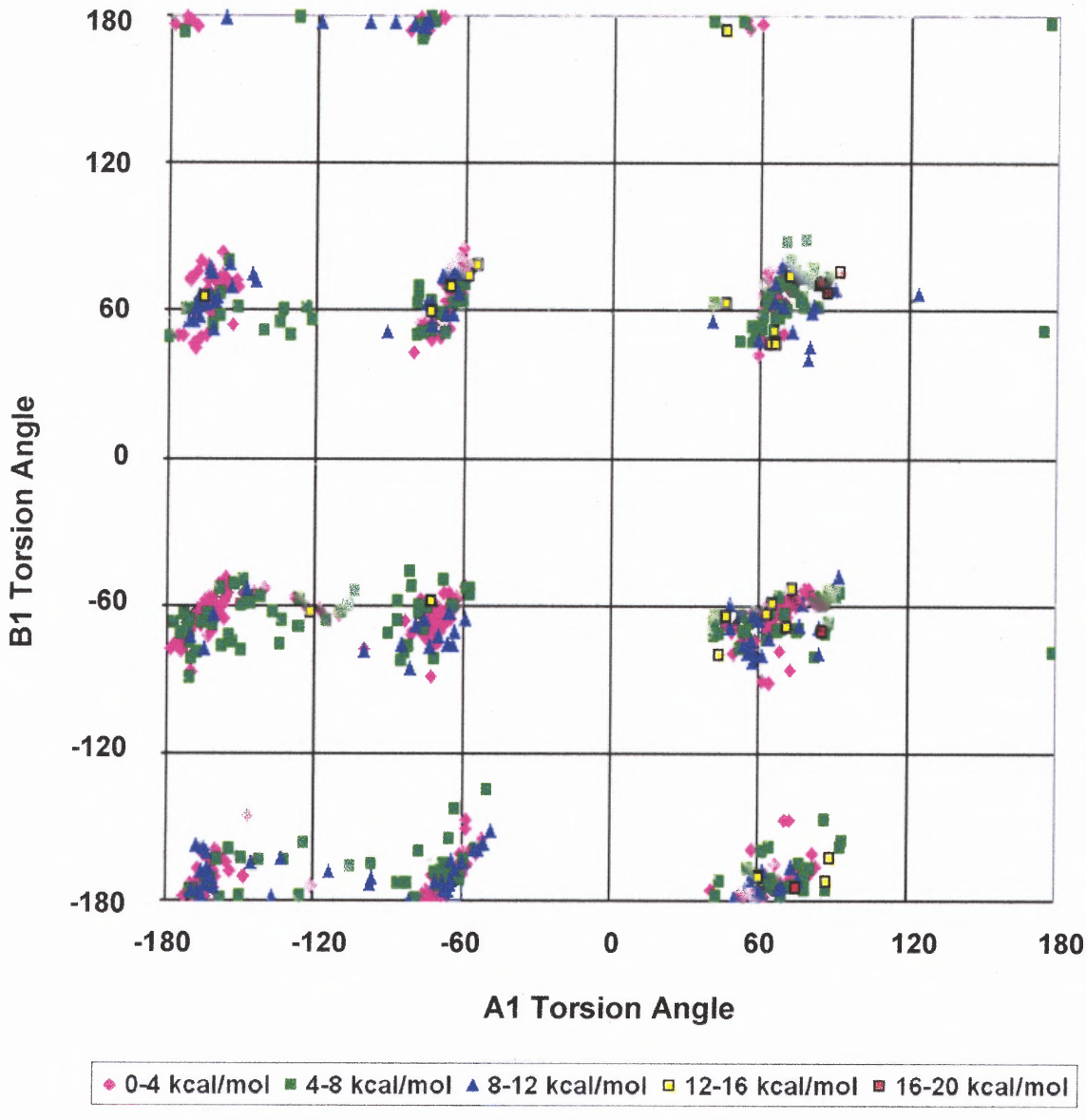

Figure D.114 Protonated TP250 (MMFF94, solvent) B1 vs A1 torsion angles.

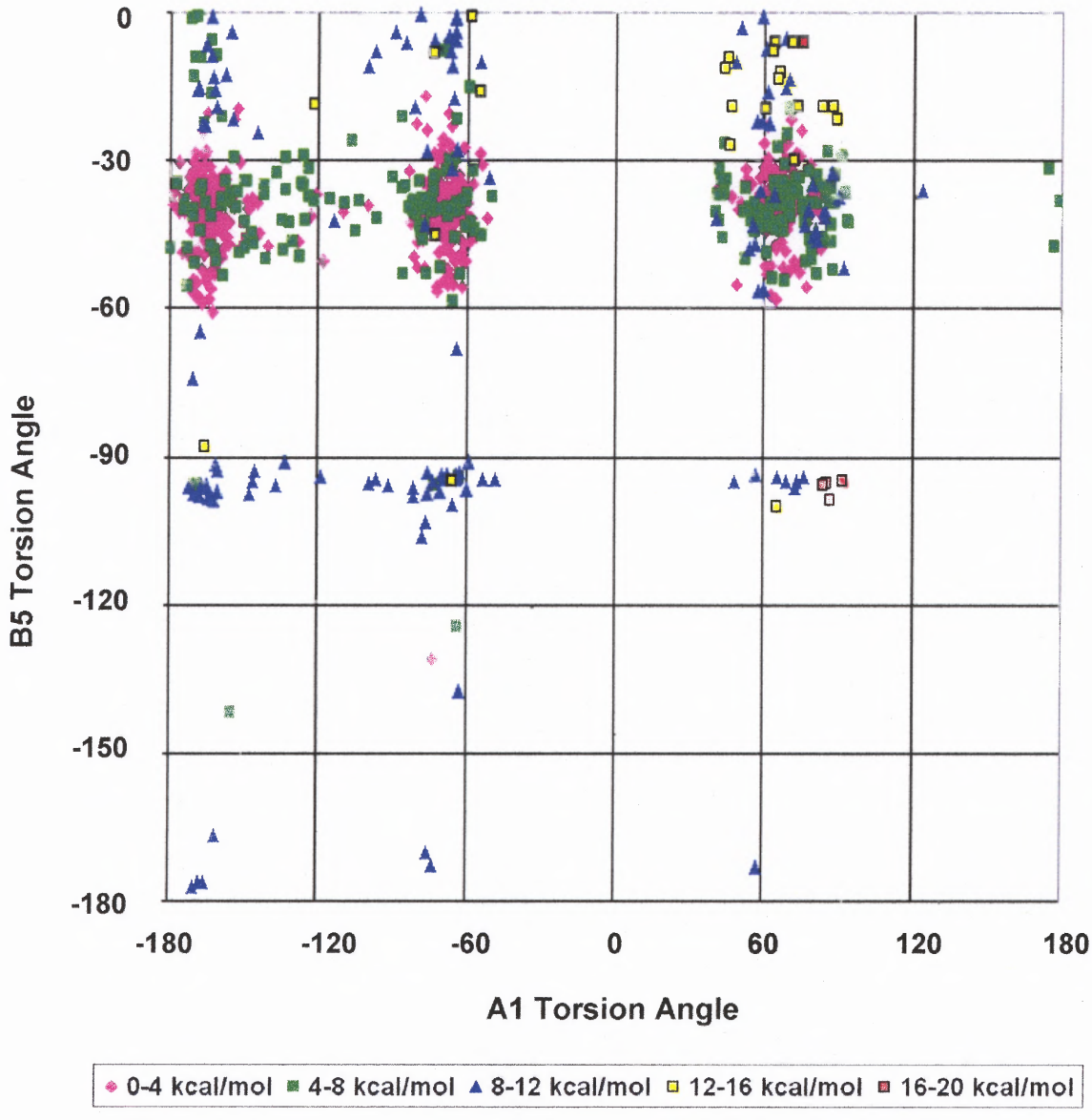

Figure D.115 Protonated TP250 (MMFF94, solvent) B5 vs A1 torsion angles.

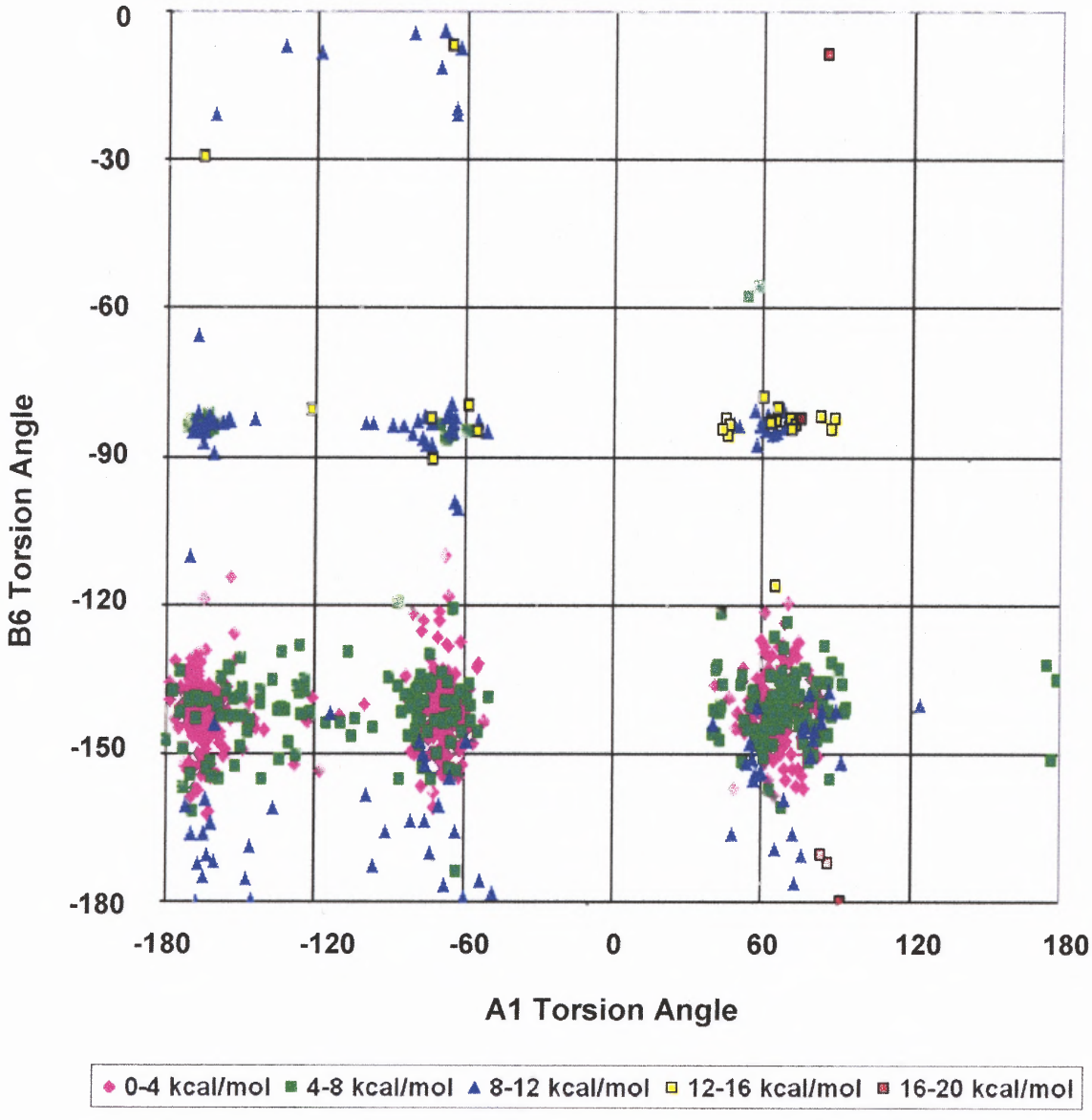

Figure D.116 Protonated TP250 (MMFF94, solvent) B6 vs A1 torsion angles.

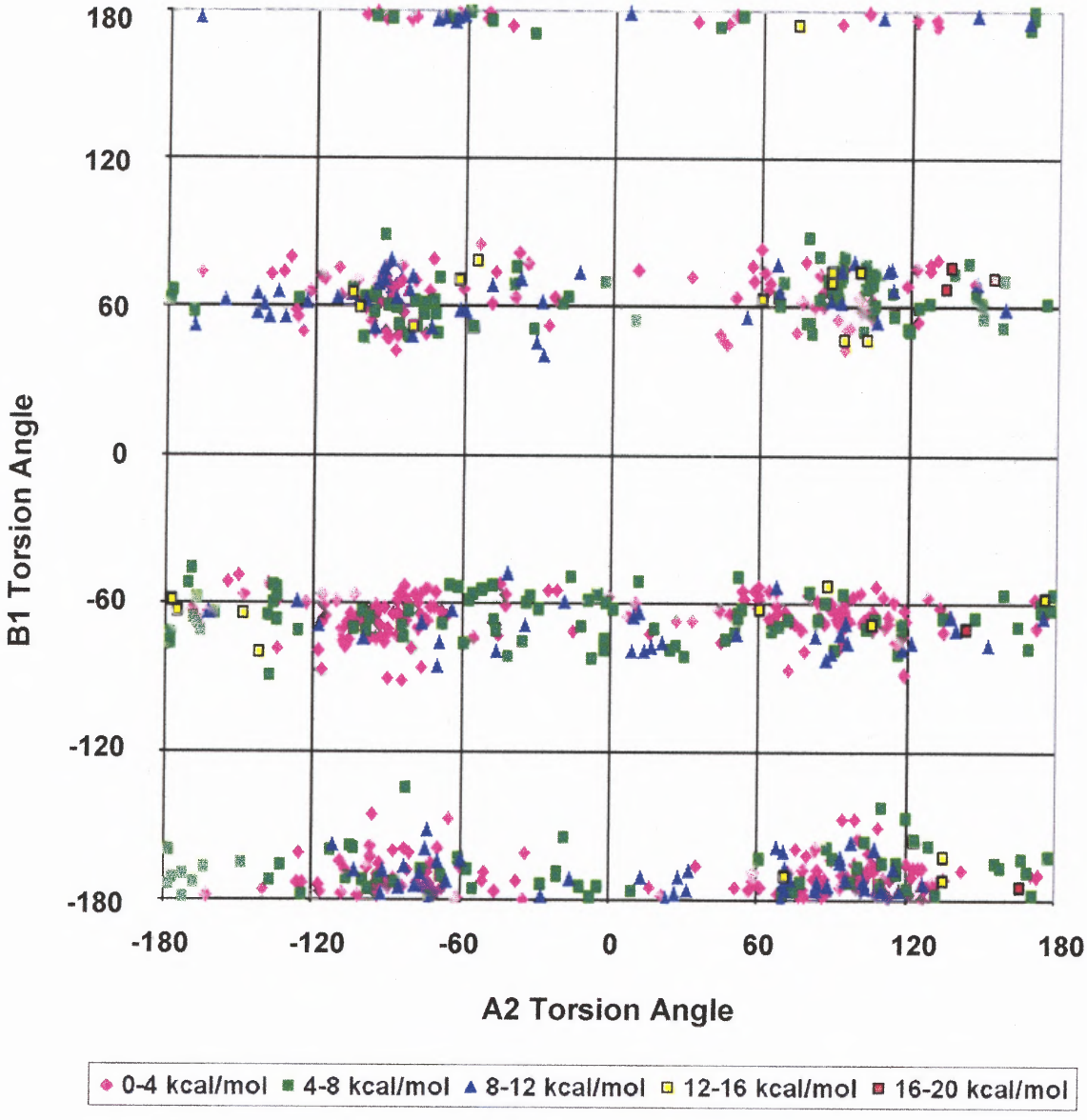

Figure D.117 Protonated TP250 (MMFF94, solvent) B1 vs A2 torsion angles.

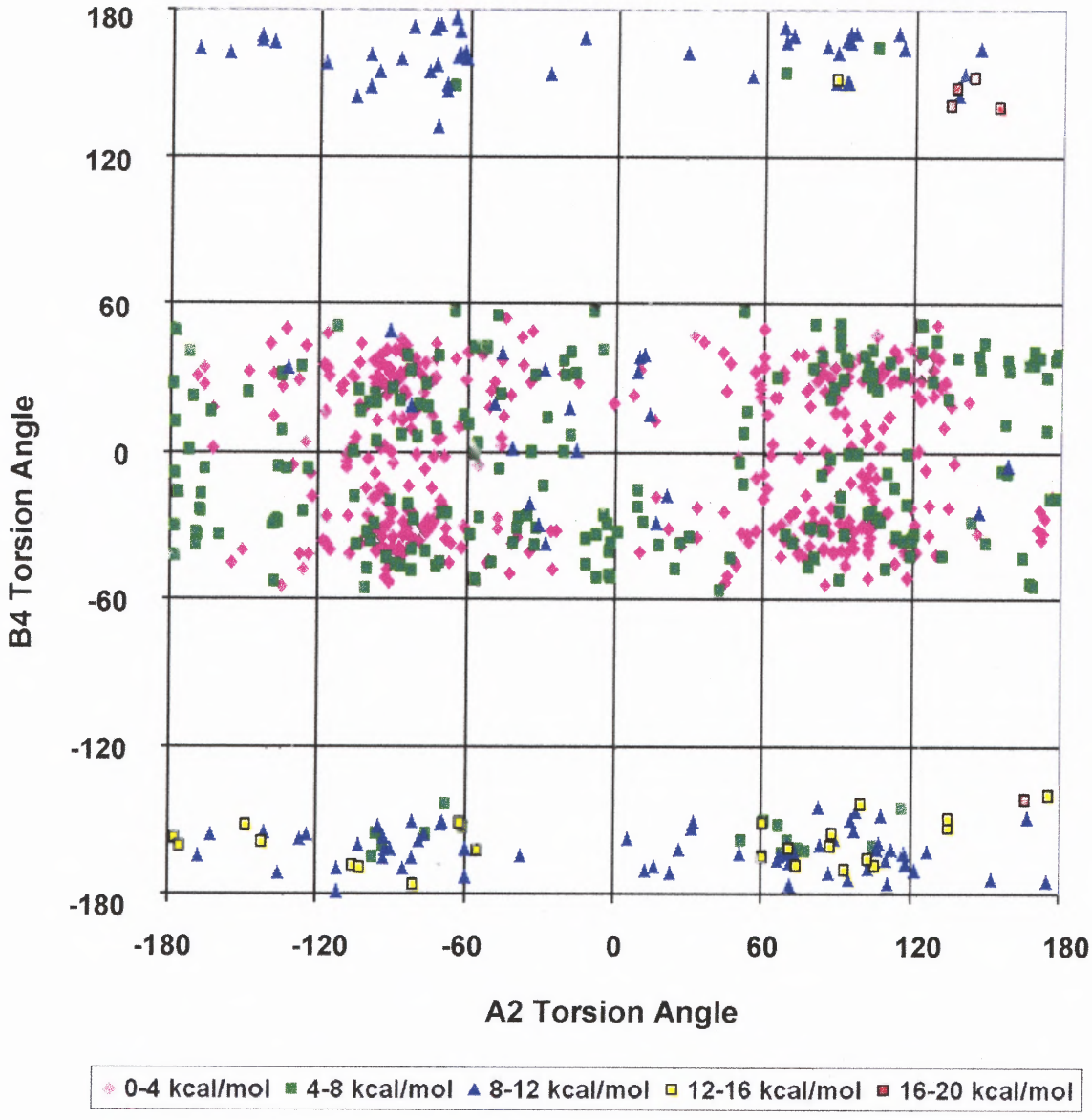

Figure D.118 Protonated TP250 (MMFF94, solvent) B4 vs A2 torsion angles.

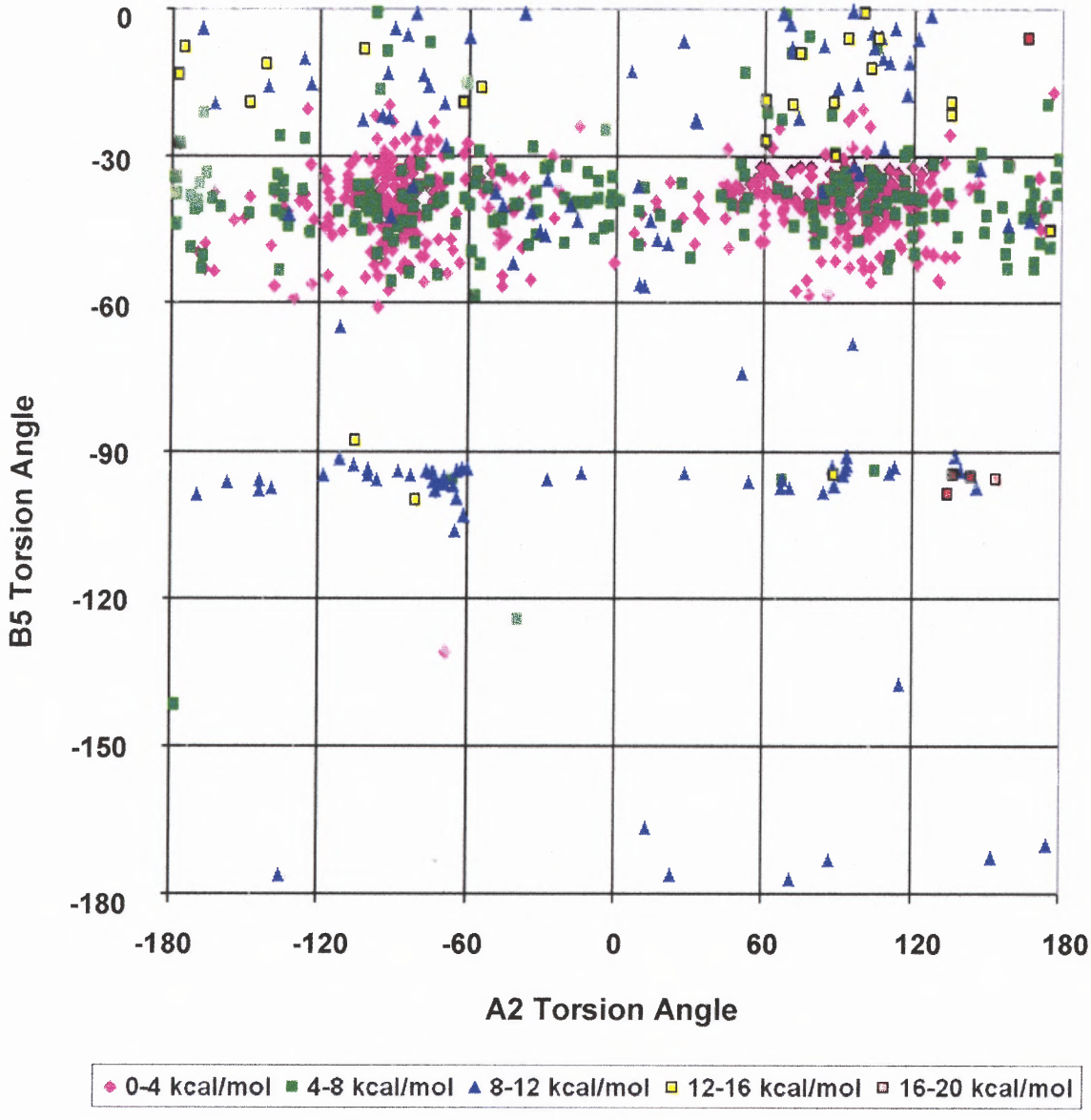

Figure D.119 Protonated TP250 (MMFF94, solvent) B5 vs A2 torsion angles.

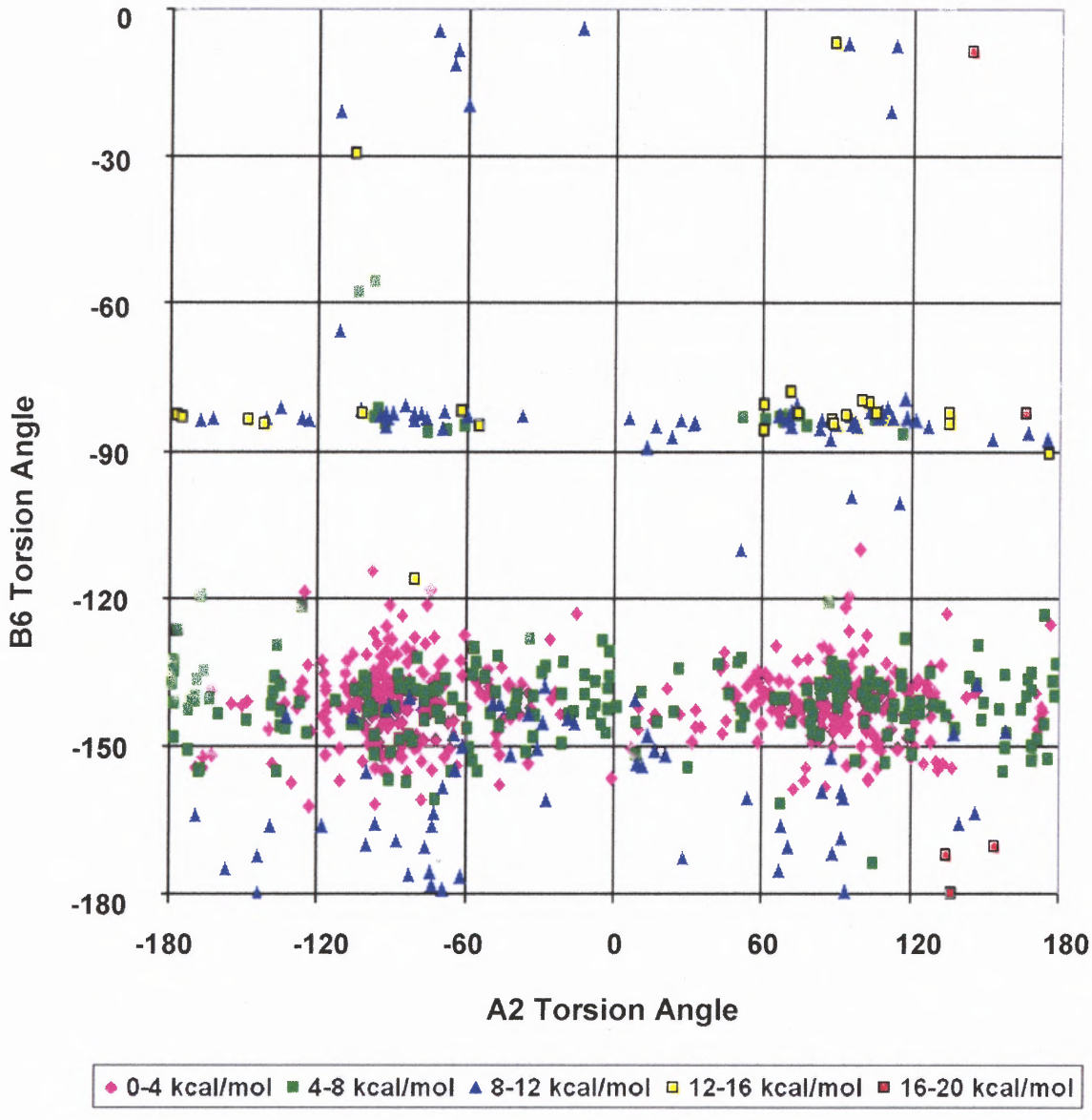

Figure D.120 Protonated TP250 (MMFF94, solvent) B6 vs A2 torsion angles.

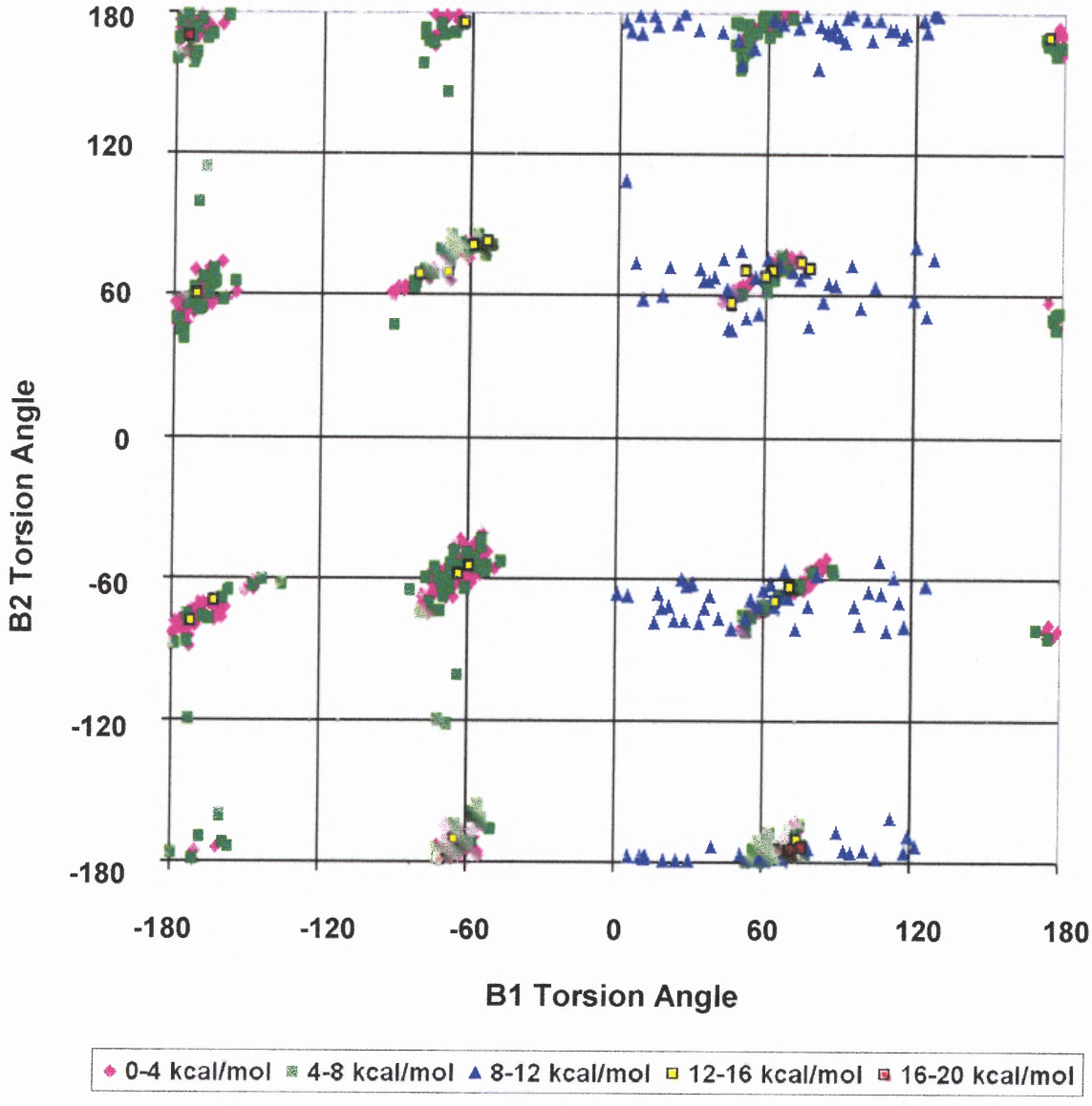

Figure D.121 Protonated TP250 (MMFF94, solvent) B2 vs B1 torsion angles.

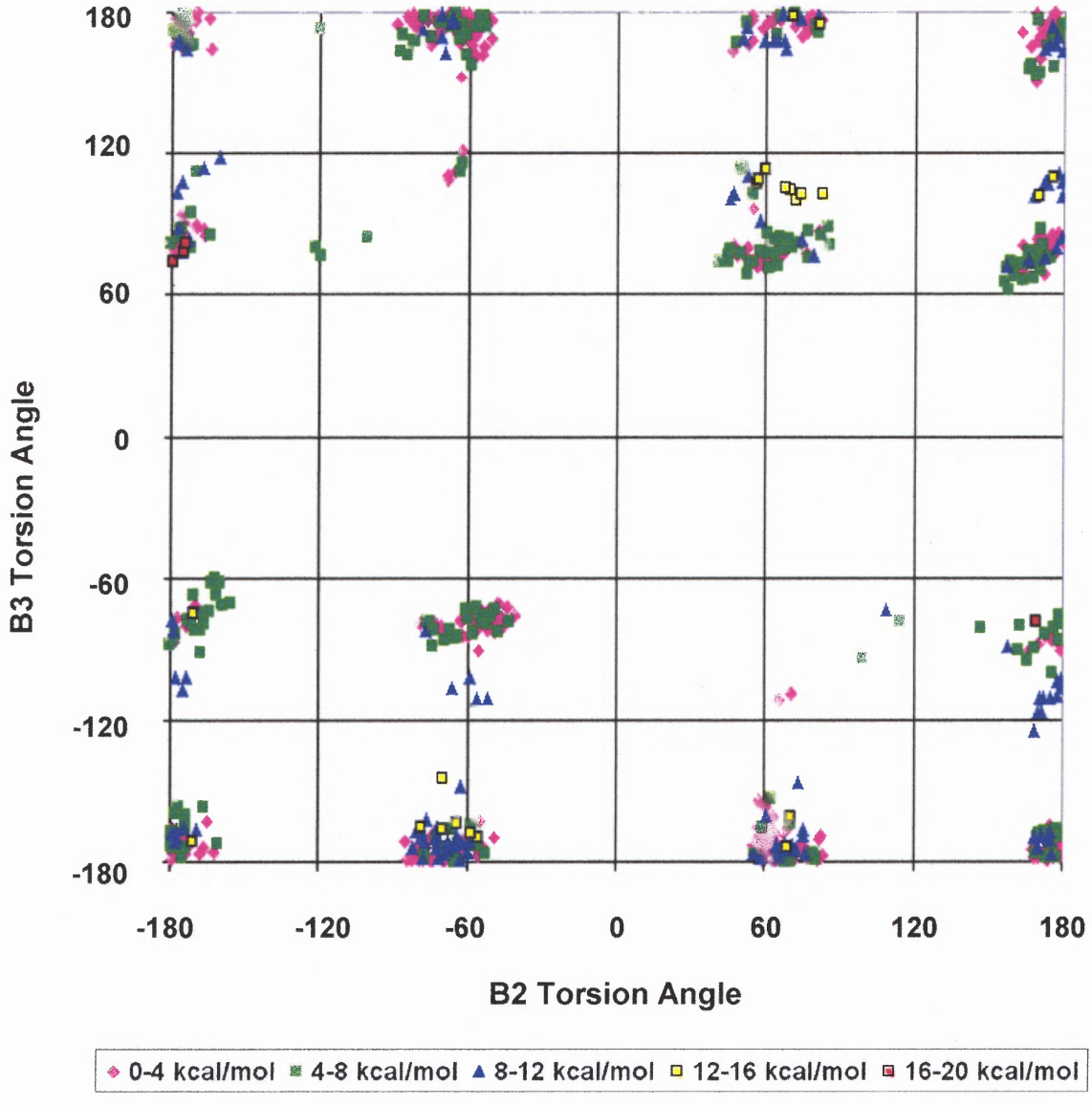

Figure D.122 Protonated TP250 (MMFF94, solvent) B3 vs B2 torsion angles.

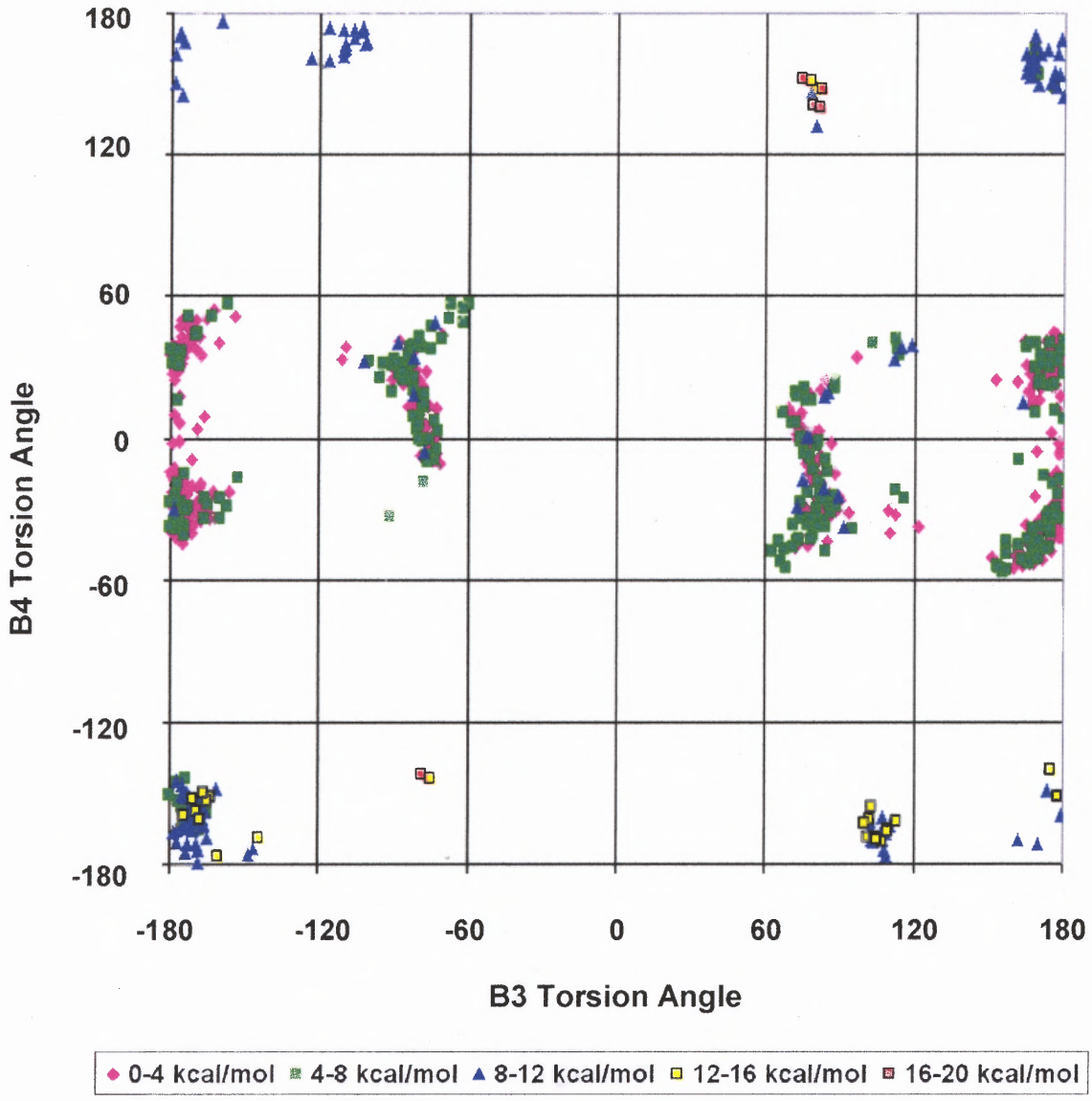

Figure D.123 Protonated TP250 (MMFF94, solvent) B4 vs B3 torsion angles.

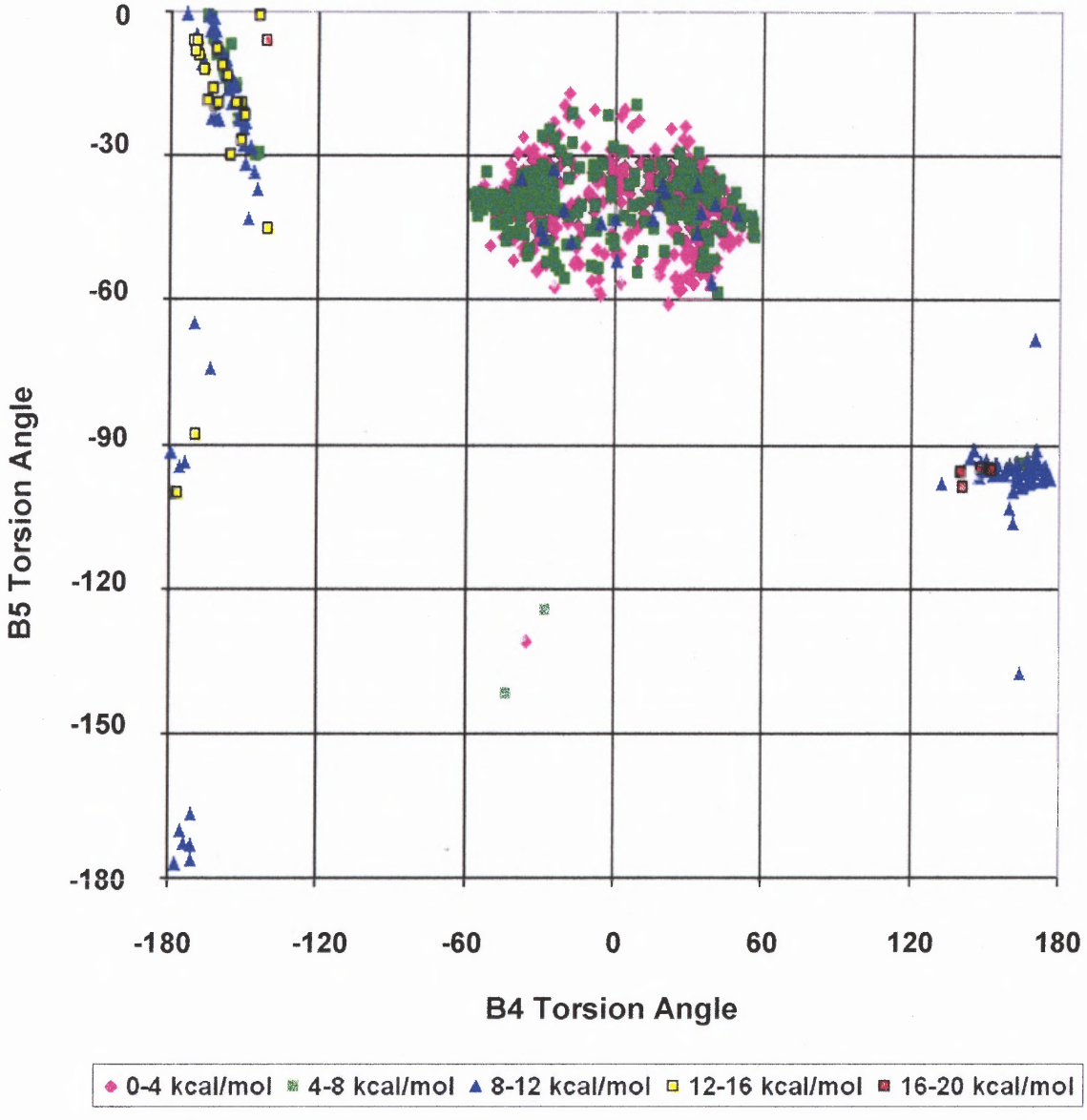

Figure D.124 Protonated TP250 (MMFF94, solvent) B5 vs B4 torsion angles.

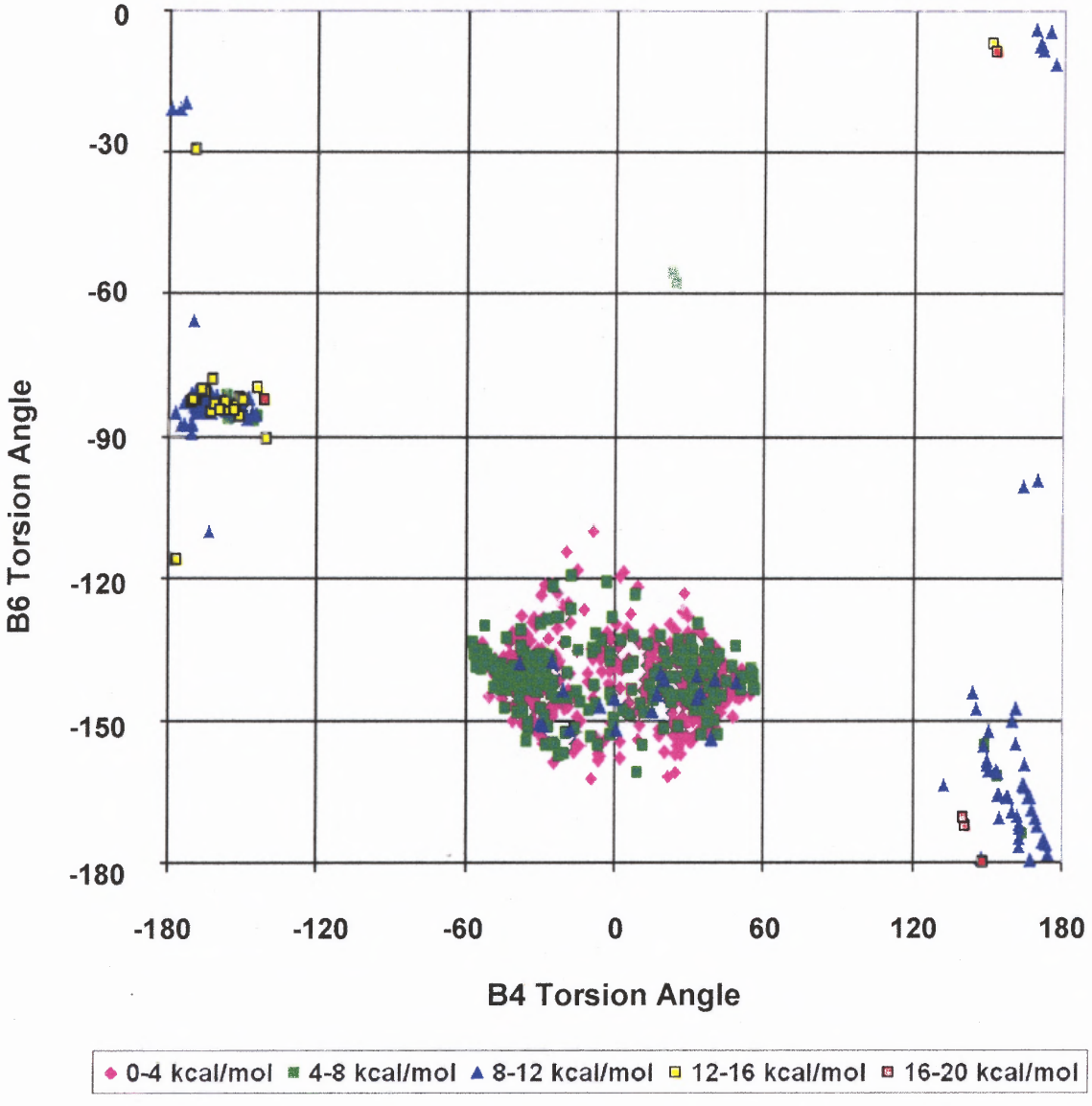

Figure D.125 Protonated TP250 (MMFF94, solvent) B6 vs B4 torsion angles.

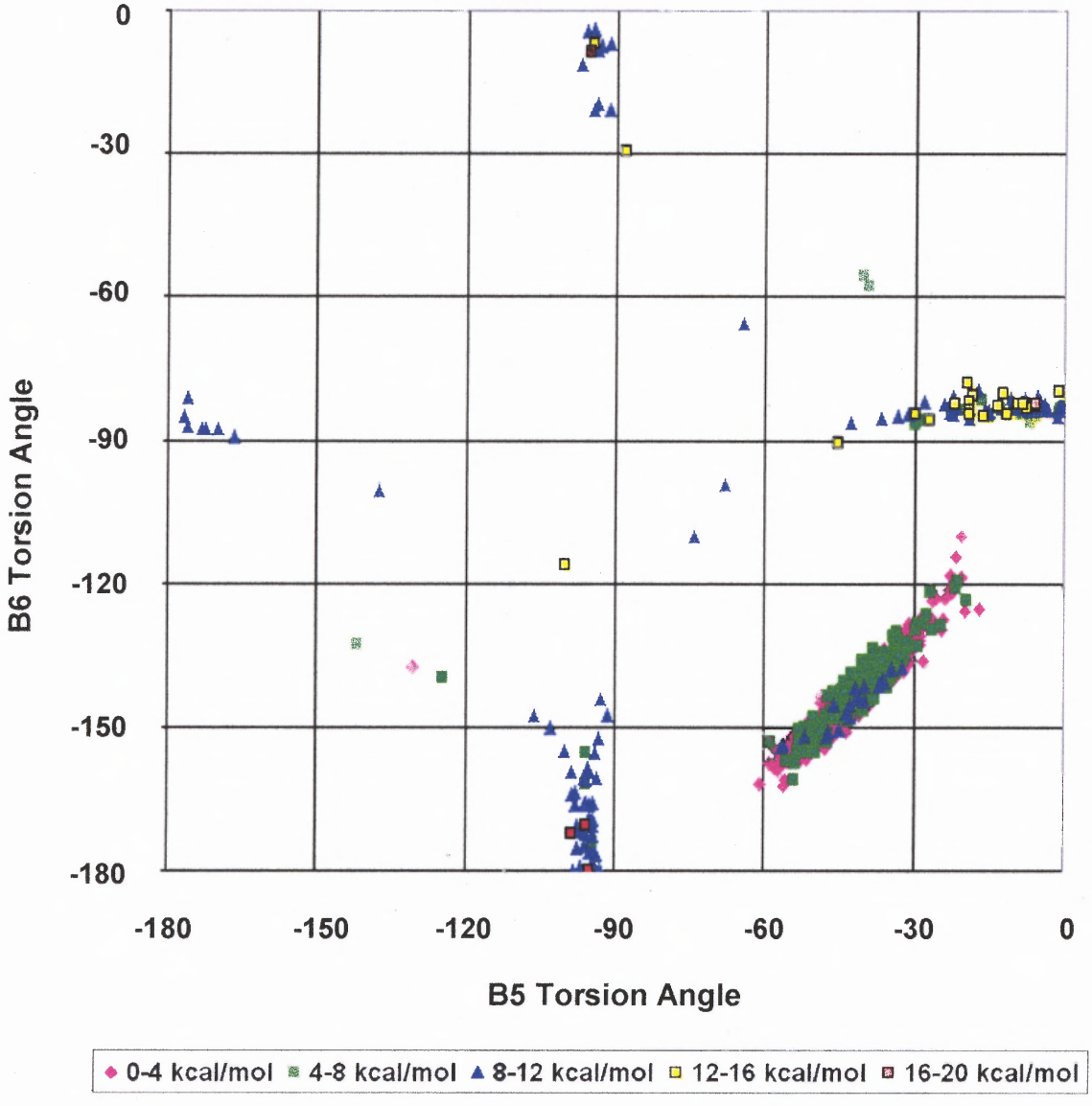

Figure D.126 Protonated TP250 (MMFF94, solvent) B6 vs B torsion angles.

REFERENCES

1. NIDA (National Institute for Drug Abuse) (1999). Cocaine Abuse and Addiction. In NIDA Research Report Series; U.S. Department of Health and Human Services - National Institutes of Health, 4-6.

2. Singh, S. C. (2000). Chemistry, Design, and Structure-Activity Relationship of Cocaine Antagonists, Chem. Rev., 100, 925-1024.

3. Dutta, A. K., Zhang, S., Kolhatkar, R., Reith, M.E.A. (2003). Dopamine Transporter as Target for Drug Development of Cocaine Dependence Medications, Eur. J. Pharmacol., 479, 93-106.

4. Carroll, F. I., Howell, L.L., Kuhar, M.J. (1999). Pharmacotherapies for Treatment of Cocaine Abuse: Preclinical Aspects, J. Med. Chem., 42, 2721-2736.

5. Kuhar, M. J., Ritz, M.C., Boja, J.W. (1991). The Dopamine Hypothesis of the Reinforcing Properties of Cocaine, Trends Neurosci., 14, 299-302.

6. Koob, G. F., Bloom, F.E. (1988). Cellular and Molecular Mechanisms of Drug Dependence, Science, 242, 715-723.

7. Witkin, J. M., Nichols, D.E., Terry, P., Katz, J.L. (1991). Behavioral Effects of Selective Dopaminergic Compounds in Rats Discriminating Cocaine, J. Pharmacol. Exp. Ther., 357, 706-713.

8. Giros, B., Jaber, M., Jones, S.R., Wightman, R.M., Caron, M.G. (1996). Hyperlocomotion and Indifference to Cocaine and Amphetamine in Mice Lacking the Dopamine Transporter, Nature, 379, 606-612.

9. Chen, N., Vaughan, R.A., Reith, M.E.A. (2001). The Role of Conserved Tryptophan and Acidic Residues in the Human Dopamine Transporter as Characterized by Site-Directed Mutagenesis, J. Neurochem., 77, 1116-1127.

10. Glowa, J. R. (1996). Dose-Response Analysis in Risk Assessment: Evaluation of Behavioral Specificity, Environ. Health Perspect., 104, 391-396.

11. Prisinzano, T., Rice, K.C., Baumann, M.H., Rothman R.B. (2004). Development of Neurochemical Normalization ("Agonist Substitution") Therapeutics for Stimulant Abuse: Focus on the Dopamine Uptake Inhibitor, GBR12909, Curr. Med. Chem. – Central Nervous System Agents, 4, 47-59.

12. Matecka, D., Lewis, D., Rothman, R.B., Dersch, C.M., Wojnicki, F.H.E., Glowa, J.R., De Vries, A.C., Pert, A., Rice, K.C. (1997). Heteroaromatic Analogs of 1-[2-(Diphenylmethoxy)ethyl]- and 1-[2-[Bis(4-fluorophenyl)methoxy]ethyl]-4-3-phenylpropyl)piperazines (GBR 12935 and GBR 12909) as High-Affinity Dopamine Reuptake Inhibitors, J. Med. Chem., 40, 705-716.

13. Glowa, J. R.; Rice, K. C., Matecka, D., Rothman, R. B. (1997). Phenteramine/Fenfluramine Decreases Cocaine Self-Administration in Rhesus Monkeys, NeuroReport, 8, 1347-1351.

14. Prisinzano, T., Greiner, E., Johnson, II, E.M., Dersch, C.M., Marcus, J., Partilla, J.S., Rothman, R.B., Jacobson, A.E., Rice, K.C. (2002). Piperadine Analogues of GBR 12909: High Affinity Ligands for the Dopamine Transporter, J. Med. Chem., 45, 4371-4374.

15. Dutta, A.K., Meltzer, P.C., Madras, B.K. (1993). Positional Importance of the Nitrogen Atom in Novel Piperidine Analogs of GBR 12909: Affinity and Selectivity for the Dopamine Transporter, Med. Chem. Res., 3, 209-222.

16. Rappe, A.K., Casewit, C.J. *Molecular Mechanics across Chemistry.* University Science Books, Sausalito, CA, 1997; p. 197.

17. Leach, A.R. *Molecular Modeling Principles and Applications.* Addison-Wesley Longman Ltd., Harlow, Essex, England, 1996; p. 169.

18. http://scienceworld.wolfram.com/physics/ElectricPermittivity.html retrieved 4-19-04

19. http://www.pa.msu.edu/courses/1997spring/PHY232/lectures/coulombslaw/electric.htm retrieved 4-1-04

20. Leach, op.cit., p. 170.

21. Tripos Inc. (2002). Conformational Analysis. *Tripos Bookshelf* (Version 6.9). St Louis, MO: Tripos, Inc.; p. 57.

22. Leach, op.cit., p. 132.

23. ibid. p. 174.

24. ibid. p. 135.

25. Tripos, Inc. (2002). Force Field. *Tripos Bookshelf* (Version 6.9). St Louis, MO: Tripos, Inc.; p. 46.

26. ibid. pp. 16-18.

27. Halgren, T.A. (1996). Merck Molecular Force Field. I. Basis, Form, Scope, Parameterization, and Performance of MMFF94, J. Comput. Chem., 17, 490-519.

28. Halgren, T.A. (1996). Merck Molecular Force Field. II. MMFF94 van der Waals and Electrostatic Parameters for Intermolecular Interactions, J. Comput. Chem., 17, 520-552.

29. Cramer, C.J. *Essentials of Computational Chemistry Theories and Models.* John Wiley & Sons, Ltd, Chichester, West Sussex, England, 2002; p. 6.

30. Leach, op.cit., pp. 422-424.

31. Tripos Inc. Conformational Analysis, op.cit., pp. 57,62.

32. Saunders, M. (1987). Stochastic exploration of molecular mechanics energy surfaces. Hunting for the global minimum, J. Am. Chem. Soc., 109, 3150-3152.

33. Berfield, J.L., Wang, L.C., Reith, M.E.A. (1999). Which Form of Dopamine is the Substrate for the Human Dopamine Transporter: the Cationic or the Uncharged Species?, J. Biol. Chem., 274, 4876-4882.

34. Xu, C., Reith, M.E.A. (1996). Modeling the pH Dependence of the Binding of WIN 35,428 to the Dopamine Transporter in Rat Striatal Membranes: Is the Bioactive Form Positively Charged or Neutral?, J. Pharm. Expt. Ther., 278, 1340-1348.

35. Venanzi group. Manuscript in preparation.

36. Venanzi group. Unpublished data.

37. Tripos Inc. Conformational Analysis, op.cit., p. 57.

38. Tripos Inc. Force Field, op.cit., p. 57.

39. Clark, M., Cramer, III, R.D., Van Opdenbosch, N. (1989). Validation of the General Purpose Tripos 5.2 Force Field, J. Comput. Chem., 10, 982-1012.